Site effects characterization in the basin of Ulaanbaatar.

Odonbaatar Chimed

UNIVERSITÉ DE STRASBOURG

Ecole et Observatoire des Sciences de la Terre

THÈSE

présentée par

Chimed Odonbaatar

Caractérisation des effets de sites dans le bassin d'OulanBator

pour l'obtention du grade de

Docteur de l'Université de Strasbourg

Spécialité : Géophysique

Composition du Jury

Directeur de thèse:

L. Rivera	Professeur	Université de Strasbourg

Co-directeur de thèse :

A. Schlupp	Ingénieur de recherche	Université de Strasbourg

Rapporteurs :

M. Cara	Professeur	Université de Strasbourg
P-Y. Bard ,	Professeur	Maison des géosciences – LGIT , Grenoble
H. Yamanaka	Professeur	Tokyo Institute of Technology

Autre(s) membres du jury :

O. Sebe	Ingénieur de Recherche	CEA \ DASE \ LDG

July, 2011

This thesis is dedicated to the memory of my parents who would be astonished and delighted at this unusual undertaking by their son

Acknowledgements

I would like to express my deepest thanks to my supervisors Prof. Luis Rivera and Dr Antoine Schlupp for they continuous support and valuable advises in this thesis. This dissertation could not have been written without Dr. Antoine Schlupp. He not only served as my supervisors but also encouraged and challenged me throughout my academic program. He showed me different ways to approach a research problem and the need to be persistent to accomplish any goal. He also helped me during my stays at Strasbourg.

I am indebted to many of my colleagues and administrative team at RCAG who supported me during all my thesis.

Many thank also go to DASE with whom RCAG has a long and deep collaboration. All the measurements done in the field for my work were possible thanks to DASE instruments. DASE financed also my stay in Strasbourg in May and June in 2010 to complete my thesis. I got a continuous support of DASE team who gave me valuable comment and recommendation. Also many thanks to go Dr. Mariotti, who made possible 2D simulation at DASE with Florent Szitkar.

I would like to express thanks to the French Embassy of Mongolia and EGIDE organization who supported my study and financed me several stays of 3 months in the laboratory of seismology of the EOST. Between these stays, I pursued my thesis works in the department of seismology of RCAG (Mongolia) while participating also actively in various projects.

Finally I would like to thank my wife Tungalag and my sons Tengis and Tselmeg for their support and encouragement.

And to God, who made all things possible.

Résumé

Les principales failles actives près de la capitale de la Mongolie, Ulaanbaatar avec environ 1.2 M d'habitants, sont à moins de 20 km et pourraient produire des séismes avec des magnitudes jusqu'à 7.5. La ville est construite sur un bassin sédimentaire, d'une épaisseur jusqu'à 100 mètres, qui peut générer des effets de site. Pour quantifier leur impact sur l'amplitude et la durée du mouvement du sol, selon la fréquence, j'utilise des mesures de mouvements faibles, à 32sites, et de bruit de fond, à 104 sites. Pour cela, j'ai appliqué les rapports spectraux « horizontal sur vertical » (HV) et « site sédimentaire sur rocher » (SSR). L'analyse de la fiabilité des résultats montre que l'amplitude du rapport HV varie en fonction du niveau du bruit de fond et que lorsqu'on est en présence d'une source de bruit particulière la fréquence amplifiée se polarise perpendiculairement à la direction de cette source.

Une structure de vitesse du bassin, évaluée à partir de 3 mesures en réseaux, et un modèle numérique 3D du bassin m'ont permis de produire des simulations 1D et 2D. La fréquence amplifiée (HV) est bien expliquée par la simulation 1D mais la forme du pic (SSR) se corrèle mieux avec la simulation 2D.

L'extension de la durée de signal induite par le bassin a été étudiée à partir de méthodes basées sur l'Intensité d'Arias et l'analyse fréquence-temps. A certains sites du basin, la durée augmente entre 20 et 160%. L'augmentation principale de la durée du mouvement du sol est due à l'amplification 1D, une partie étant à relier à des effets 2D à 3D. Nous avons cependant besoin de mouvements plus forts pour observer et étudier des effets 2D ou 3D.

Finalement, je propose une carte de la fréquence amplifiée qui est essentielle pour l'évaluation de l'aléa sismique d'Ulaanbaatar.

Abstract

The main active faults near the capital of Mongolia, Ulaanbaatar with about 1.2 M inhabitants, are located at less than 20 km and could produce large earthquakes with magnitude up to 7.5. The city is built on a sedimentary basin, of a thickness up to 100 meters, which may generate site effects. To quantify their impact on the amplitude and the duration of the ground motion, according to the frequency, I used weak motion, at 32 sites, and ambient noise records, at 104 sites. For that, I applied horizontal to vertical (HV) and sedimentary to rock site (SSR) spectral ratio. An analysis of the reliability of the results shows that the HV ratio amplitude varies in relation to the noise level and that when there is a particular local noise source the amplified frequency polarizes itself perpendicularly to the source direction.

A velocity structure of the basin, determined by 3 microtremor array measurements, and a 3D digital model of the basin were used to produce 1D and 2D simulations. The amplified frequency (HV) is well explained by the 1D simulation but the shape of the peak (SSR) fits better with the 2D simulation. The signal duration extension induced by the basin has been studied using methods based on Arias Intensity and time-frequency analysis. At certain sites of the basin, the duration increases between 20 to 160 %. The main increase of the duration of the ground motion is due to the 1D amplifications; a part seems to be related with 2D or 3D effects. Nevertheless, we need stronger ground motion to observe and study 2D and 3D effects.

Finally, I propose a map of the amplified frequency, which is essential for the seismic hazard assessment of Ulaanbaatar

RESUME

Caractérisation des effets de sites dans le bassin d'Oulan-Bator, Mongolie.

Les effets de site peuvent fortement amplifier et augmenter la durée du mouvement du sol pour des sites aux sédiments par rapport à des sites au rocher. Le phénomène physique des effets de site est la perturbation, des ondes sismiques ou de la déformation, due à une configuration locale particulière du site. Les plus importants paramètres caractérisant les effets de site sont l'amplification, la fréquence amplifiée et l'allongement du mouvement du sol.

L'objectif de cette thèse est l'estimation de l'impact des effets de site générés par le basin d'Oulan-Bator, capitale de la Mongolie, sur le mouvement sismique du sol. Pour cela, j'ai utilisé des enregistrements de mouvements faibles et de bruit de fond sismique qui ont été acquises lors d'une campagne de 6 mois antérieure à cette thèse. J'ai réalisé des mesures complémentaires en réseau, en profitant d'une disponibilité temporaire de capteurs sismiques, pour en déduire des profils de vitesses des ondes S en différents points. J'ai utilisé les techniques de rapport spectraux SSR (site sur référence) et HV (composante horizontale sur verticale) pour l'estimation des effets de site. Afin de comparer les résultats obtenus avec des modélisations numériques, j'ai déterminé la géométrie 3D du bassin et de son remplissage en combinant les données disponibles tels que forages et données géophysiques. Aussi, j'ai étudié et estimé la variation de la durée du signal sismique, due au basin d'Oulan-Bator, par diverses méthodes. Le rapport de thèse est composé de 5 chapitres. Une annexe reprend les nombreuses mesures effectuées.

Le premier chapitre présente une synthèse des connaissances sur les effets de sites, sur l'activité sismique dans la région d'Oulan-Bator et sur les caractéristiques géologiques du bassin sédimentaire sur lequel est construit la ville.

Une technique empirique pour estimer les effets de site utilise les rapports spectraux des enregistrements, du même séisme, au sédiment et au rocher [Borcherdt, 1970] appelé le "Standard Spectral Ratio" (SSR).

La principale difficulté de cette méthode est de trouver un bon site de référencé et, dans un milieu urbain, la nécessité de laisser les stations sur le terrain pendant suffisamment longtemps afin d'enregistrer des séismes avec un bon rapport signal sur bruit. C'est pourquoi une méthode

ne nécessitant pas de site de référencé est très largement utilise, le rapport spectral HV. Cette technique a été d'abord introduite par Nogoshi and Igarashi [1971] et rendue populaire par Nakamura [1989].

Pour comparer les observations avec des simulations numériques, les modèles 1D sont souvent utilisés. Les effets de sites sont considérés comme une fonction de transfert au dessus du socle rocheux qui peut être calculée quand les paramètres géologiques et physiques du site ou du bassin sont bien connus. Des études récentes montrent que la géométrie 2D et 3D du bassin peuvent avoir une forte influence sur l'amplification des ondes sismiques et de leur durée. Cependant, la fréquence amplifiée dominante est principalement contrôlée par une réponse à une dimension de la colonne de sol sous le site.

Pour caractériser les effets de sites par modélisation, le profil de vitesse des ondes S doit être connu. Pour cela, une analyse en fréquence-nombre d'onde est fréquemment utilisée (fk). L'analyse fk est une technique standard en réseau [Capon, 1969].

Un autre paramètre qui caractérise le mouvement du sol est sa durée. La variation de la durée du mouvement du sol due aux effets de site est moins étudiée que le phénomène d'amplification des ondes. La plupart des études sur la durée sont concentrées sur l'estimation de la durée du mouvement fort et leur corrélation avec les conditions de site. Mais il n'existe que quelques études estimant la variation de la durée du mouvement du sol pour des sites sur un bassin par rapport à des sites proches au rocher.

Mon objectif est d'estimer les effets de sites à Oulan Bator, Capitale de la Mongolie. La ville est le centre politique, commercial et industriel du pays. La population y est en forte croissance depuis deux décennies avec environ 1,2 million d'habitants ce qui représente la moitié de la population du pays. Oulan-Bator est située dans la vallée de la rivière Tuul et sur un dépôt sédimentaire atteignant localement 120 mètres d'épaisseur. L'aléa sismique pour la ville provient principalement de plusieurs failles actives qui sont situées à moins de 20 km de la zone urbanisée. Une de ces failles actives, qui pourrait produire un séisme de magnitude 7 ou plus, est marquée par une importante microsismicité depuis 2005 (Munkhuu et al., 2010). Pendant les derniers 70 ans, plusieurs séismes ont été ressentis dans la ville (Gobi-Altai 1957, Mw=8.1, distance≈600km; Mogod 1967, Mw=7.2, distance≈230km; Deren 1998, ML=5.8, distance≈180km; Deren 2010, ML=5.4, distance≈180km). L'intensité MSK à Oulan Bator due

au séisme de Mogod varie entre III et V, ce qui montre que le basin sous la ville induit des effets de sites.

Le deuxième chapitre est consacré à l'analyse des rapports spectraux HV et SSR. J'ai utilisé pour cela des mesures de faible mouvement du sol de séismes enregistrées sur 32 sites, et des mesures de bruit de fond enregistrées sur 104 sites au cours d'une campagne de terrain de 6 mois au cours de l'année 2000 en collaboration avec le CEA-DASE (Figure 1). Pour l'analyse de rapport spectraux, afin d'éviter d'utiliser les périodes de temps avec des perturbations locales j'ai sélectionné les données après un contrôle qualité à partir des formes d'onde et des spectres de Fourier. Ensuite, pour calculer les rapports spectraux, j'ai considéré des fenêtres glissantes avec un chevauchement de 90% et un lissage avec une fenêtre Konno-Omachi.

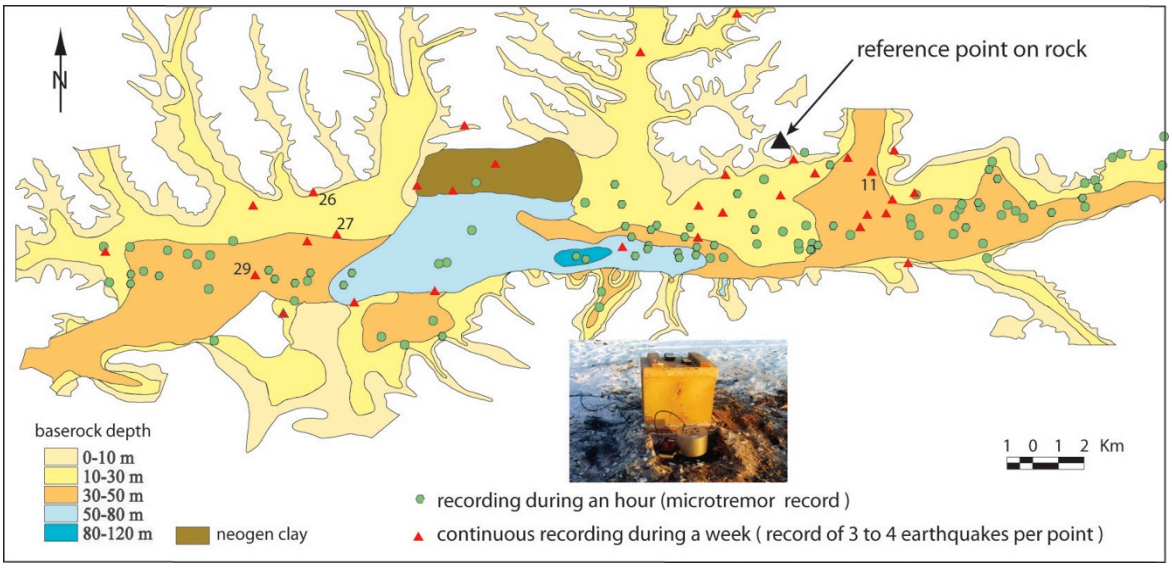

Figure 1. Carte montrant la localisation des stations sismiques déployées dans le basin d'Oulan-Bator.

J'ai comparé les résultats issus des deux méthodes (HV et SSR). Les fréquences amplifiées observées sont identiques quand le rapport spectral montre un pic clair et étroit. Mais le facteur d'amplification issu de la méthode SSR donne toujours une plus forte valeur que par la méthode HV sur bruit de fond. La forme du pic est un des critères de fiabilité du résultat.

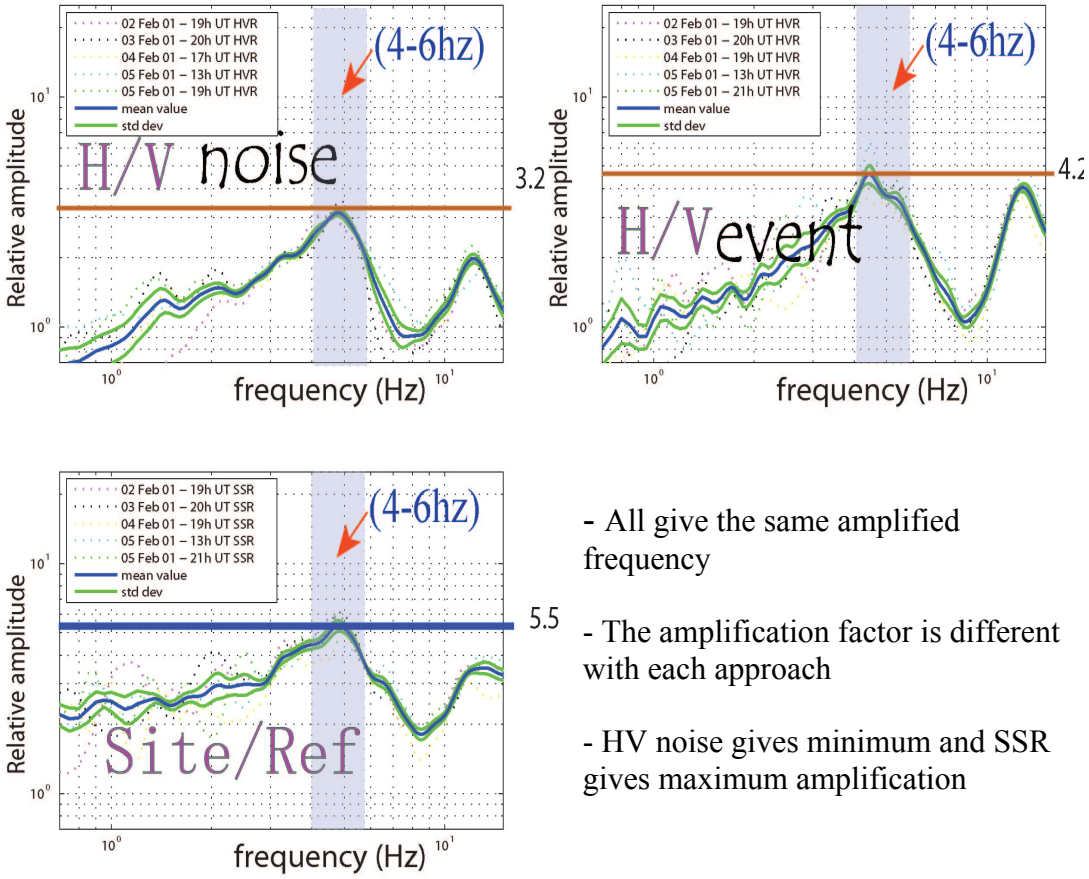

Figure 2. Comparaison des rapports spectraux HV et SSR pour estimer les effets de site en utilisant le bruit de fond et des enregistrements de séismes.

J'ai analysé la variation du rapport spectral HV sur bruit de fond sismique au cours de la journée. J'ai observé que la fréquence amplifiée est stable tout au long de la journée sauf quand il y a des sources locales de bruit particulières et importantes. Dans ce cas, elles ont un impact sur le rapport HV particulièrement en augmentant l'amplitude des basses fréquences. Quand le bruit local augmente, le pic du rapport spectral HV est lissé et l'amplitude décroit fortement. L'amplitude du rapport HV sur bruit de fond dépend fortement du niveau de bruit environnant et ceci démontre l'importance, pour la fiabilité des résultats, de faire une campagne de mesure avec un contrôle stricte des sources de bruit environnantes.

J'ai analysé la variation du rapport spectral HV avec l'azimut de la composante horizontale. Cette analyse montre que les fréquences amplifiées ne dépendent pas de l'azimut mais leur facteur d'amplification varie. L'amplitude maximale, dans une bande de fréquence amplifiée, est selon une orientation particulière ou « polarisée ». Je présente cette polarisation sous forme de « compas ». Je montre que l'azimut de cette polarisation est affecté par les sources de bruit important situées à proximité (central électrique, trieuse de graviers, zone commerciale avec forte circulation de véhicules). Elle prend alors une direction perpendiculaire à l'azimut source-site. Ceci suggère que les ondes sismiques générées dans le basin d'Oulan-Bator par des sources proches sont principalement des ondes SH ou Love.

La comparaison des valeurs des fréquences amplifiées, issues des rapports spectraux, avec l'épaisseur moyenne des dépôts sédimentaires me permet d'estimer une vitesse des ondes S d'environ 500m/s (H=V/4f). Les facteurs d'amplification, mesurés à partir des rapports spectraux SSR sur des mouvements faibles, sont de 3 à 10 entre un site sur le basin et sur le rocher.

Dans le chapitre trois, je présente la base de données géo référencée sous SIG, que j'ai construite, intégrant les propriétés physiques du bassin d'Oulan-Bator (épaisseur, vitesse des ondes S, interfaces géologiques, type de dépôts, niveau d'eau, isolignes gravimétriques) déduites des données gravimétriques, profils sismiques and données de forage. Basé sur ces données, j'ai construit le premier modèle numérique 3D du bassin et de l'interface sédiments – rocher (Figure 3). Pour estimer les profils de vitesses des ondes S avec la profondeur, j'ai appliqué une analyse « fréquence - nombre d'ondes » en trois sites du bassin, avec un réseau de stations. La vitesse moyenne des ondes S dans le bassin est estimée à 550 m/s et les profondeurs des interfaces obtenues sont en bon accord avec les profondeurs issues des forages proches de mes sites de mesure.

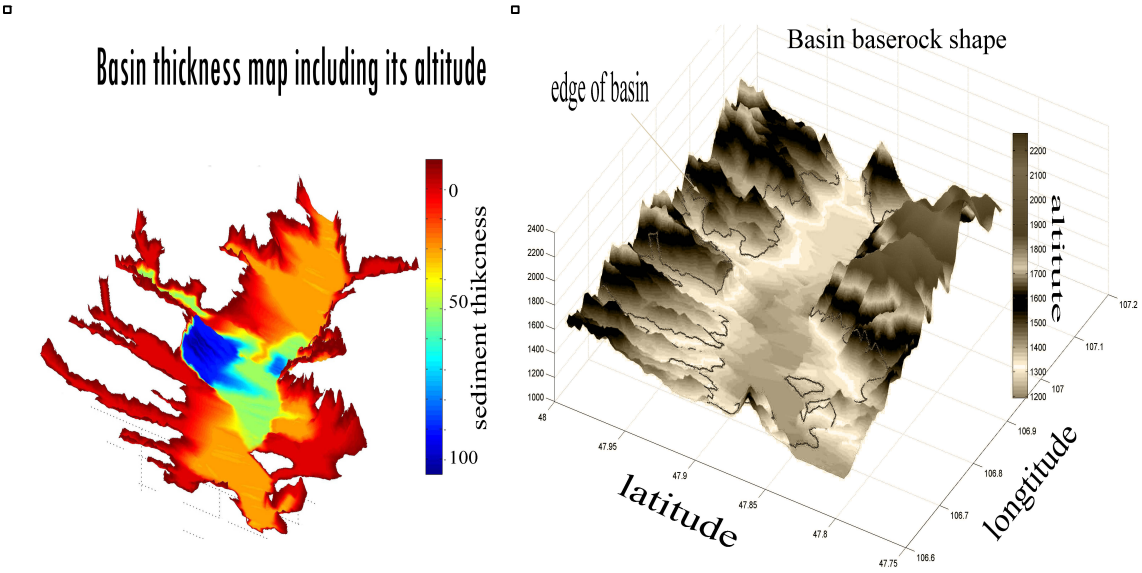

Figure 3. Modèle 3D du bassin d'Oulan-Bator déduit des données géologiques et géophysiques disponibles.

J'ai généré une carte des fréquences amplifiées en utilisant une modélisation 1D, (shake91), pour 16000 points du bassin selon une maille régulière, les caractéristiques 1D étant obtenues à partir du modèle 3D. En dehors des sites à l'aplomb de zones d'argile et de la bordure du bassin, les fréquences amplifiées obtenues à partir de la modélisation 1D sont similaires aux fréquences amplifiées déduites des rapports spectraux sur les données observées. Les différences peuvent être en partie dues à la variation de la vitesse des ondes sous certains sites par rapport à la valeur moyenne utilisée dans la modélisation. Pour améliorer la connaissance des vitesses des ondes S dans le bassin, nous devons multiplier les mesures en réseau. De même, pour préciser la géométrie 3D du basin, il faudra collecter plus d'informations géologiques et géophysiques.

Une modélisation 2D de la propagation des ondes sismiques a été réalisée le long des deux principales directions du bassin. Elle a été réalisée au CEA (Commissariat aux Energies Atomique) en utilisant une version 2D du programme Mak3D développé au CEA-DASE par Mariotti (2007). Cette approche 2D peut expliquer la largeur des pics observée sur des sites à l'aplomb de pente forte de l'interface sédiment-rocher. Les fréquences amplifiées obtenues par cette modélisation sont plus hautes fréquences que celles observées par les rapports spectraux à

partir des données de terrain. Ceci peut être du à : 1) une propagation des ondes dans le bassin actuellement peu contrainte ; 2) des mesures sur le terrain qui ne sont pas exactement à la vertical des profils modélisés ; 3) une connaissance insuffisante de la géométrie du bassin et de l'interface sédiment-rocher ; 4) une résolution (taille des mailles) de la modélisation de 5 mètres pouvant induire un décalage de la fréquence amplifiée.

Cette première étape, 2D, se poursuivra au-delà de la thèse par une modélisation 3D dans le cadre d'une collaboration entre le RCAG, le CEA-DASE et l'EOST.

Au final, j'ai défini une carte du zonage des fréquences amplifiées pour le bassin d'Oulan Bator déduite des observations de fréquences amplifiées, des données topographiques SRTM, des cartes géologiques et des calculs de la réponse 1D du bassin.

Le chapitre 4 présente l'étude de l'impact du bassin sur la durée du mouvement du sol par rapport au rocher à partir d'enregistrements de mouvements faibles. La définition et la mesure de la durée sont étudiées selon plusieurs méthodes

J'ai utilisé une approche basée sur l'enveloppe du signal filtré à diverses fréquences pour estimer la différence de durée du signal entre les sites sur du rocher et du sédiment (durée absolue). Pour cela, après avoir filtré les signaux dans les mêmes bandes de fréquences, j'ai calculé l'évolution de « l'amplitude de l'énergie » avec le temps. La durée est alors mesurée à la même valeur d'amplitude sur les signaux au rocher et au sédiment. Je montre que pour les mouvements faibles enregistrés, la principale source d'allongement de la durée du signal est due à l'amplification 1D des sites. Cette allongement a lieu aux mêmes fréquences que celles amplifiées par le site. Cependant, j'ai observé un allongement plus important dans la direction NS qu'EW dans tous les sites ce qui ne peut être expliqué seulement par un effet 1D (le bassin d'Oulan Bator étant principalement orienté EW).

Pour identifier les autres causes que les effets 1D, j'ai dans un premier temps utilisé l'intensité d'Arias, en quantifiant la durée entre 5 et 95% du maximum de l'intensité d'Arias. Par cette approche, il apparaît un très faible allongement de la durée sur les sites au sédiment. J'ai alors filtré le signal dans différentes bandes de fréquences et mesuré sur chacun la durée via la même procédure. J'observe une faible augmentation de la durée (environ 5 secondes) dans la bande 5-8 Hz pour des sites qui sont sur environ 30m de sédiments. Cette fréquence d'élongation

de la durée n'est pas la fréquence de résonnance 1D du bassin. Ces allongements sont comparés avec ceux déduits par la même méthode sur les signaux générés par la modélisation 2D. Dans la modélisation, nous pouvons aussi observer cet allongement de la durée qui semble être due aux ondes de surface générées par les bords des bassins. Ceci pourrait expliquer mes observations sur les enregistrements en utilisant la méthode basée sur l'intensité d'Aris filtrée.

Avec nos données acquises, des mouvements faibles, il apparaît qu'elles n'ont pas assez d'énergie pour générer des ondes de surfaces que l'on puisse détecter par cette méthode. Avec la durée absolue, nous observons un allongement de 20 à 80 % pour la plupart des sites et jusqu'à 160 % localement. Cette méthode est la plus adaptée à l'étude de mouvements faibles.

Chapitre de conclusion: J'ai recherché à identifier l'origine des effets de sites générés par le basin d'Oulan Bator et à quantifier leur impact sur l'amplitude et la durée du mouvement du sol en fonction de la fréquence. Dans un premier temps, j'ai réalisé un travail sur l'analyse de la qualité des données disponibles et les limites des méthodes.

Les principales concluions de mon études sont les suivantes:

- L'estimation de la fréquence amplifiée est stable quelque soit la méthode de rapport spectral utilisée (HV sur bruit de fond, HV sur évènement or SSR).
- Le facteur d'amplification à partir de HV sur bruit de fond est influencée par le niveau de bruit de fond et l'azimut de la source de bruit local.
- La fréquence amplifiée à partir de HV sur bruit de fond peut être décalée vers les basses fréquences dans des cas particuliers comme par exemple quand le site est près de sources de bruit important.
- SSR donne des facteurs d'amplification plus forts qu'à partir de HV sur bruit de fond. On observe un facteur d'amplification entre 3 et 10 dans le basin d'Oulan Bator avec SSR à partir de l'enregistrement de mouvements faibles.
- Un modèle géométrique 3D a été réalisé à partir des données disponibles. Les vitesses déterminées localement donnent une vitesses des ondes de cisaillement d'environ 550 m/s pour le remplissage sédimentaire.
- Les fréquences amplifiées dans le basin d'Oulan Bator varient entre 2 et 5 Hz. Un zonage des fréquences amplifiées a été déduit des observations et modélisations 1D.

L'étude de la variation de la durée suggère:

- L’allongement de la durée, déduite de la coda, montre un allongement de la durée absolue. Elle est maximale à la même fréquence que la fréquence amplifiée du site. L’allongement observé atteint localement 160%.
- On peut observer un allongement de la durée, due aux effets de site autres que 1D, en utilisant l’intensité d’Arias normalisée. On observe localement, par cette approche, un allongement entre 5 et 13 secondes pour 40 à 80 seconds de signal de mouvement faible. La fréquence allongée est toujours plus haute que la fréquence amplifiée.
- L’allongement de la durée, observée sur des enregistrements de mouvement faibles dans le basin d’Oulan Bator, est principalement du aux amplifications 1D.

L’ensemble de ce travail me permet de proposer un zonage des effets de sites, induits par le bassin d’Oulan Bator, indispensable pour l’évaluation de l’aléa sismique et la réduction du risque sismique dans la capitale de la Mongolie.

SUMMARY

Characterization of the site effects in the Basin of Ulaanbaatar, Mongolia

Site effects can strongly amplify and extend duration of the seismic ground motions at sedimentary sites respect to rock sites. The physical phenomenon of the site effects is the perturbations, of seismic wave or deformation, caused by particular configuration of the local site. The most important parameters characterising the site effects are amplification, amplified frequency and lengthening of the seismic ground motion.

The objective of this thesis is to estimate the impact of the site effects generated by the basin of Ulaanbaatar, capital of Mongolia, on the seismic ground motion. For that I used recordings of weak motion and ambient noise, which were acquired during a previous 6 months survey done before this thesis. I did additional measures with microtremor array, by taking advantage of a temporary availability of seismic sensors, to deduce S waves velocity profile at different sites. I used the techniques of spectral ratio as SSR (site on reference) and H/V (horizontal to vertical) for the estimation of the site effects. In order to compare the obtained results with numeric modelling, I constructed a 3D geometry of the basin and it's filling by combining available data, such as drillings and geophysical studies. Also I studied and estimated the variation of the duration of the ground motion, due to the basin of Ulaanbaatar, by diverse methods. The thesis report consists of 5 chapters. An appendix includes information about the numerous measurements.

The first chapter present a review of the knowledge on the site effects, on the seismic activity in the region of Ulaanbaatar and on the geological characteristics of the sedimentary basin on which is built the city.

One empirical technique for assessment site response uses the spectral ratio, of same earthquake, between records at a sedimentary site and at a rock site [Borcherdt, 1970] that usually refers as the Standard Spectral Ratio (SSR).

The main drawbacks of this method is the difficulty to find a good reference site and, in urban area, the necessity to deploy stations during long time in order to record seismic events

with a good signal noise ratio. Therefore a non-reference site method using horizontal to vertical spectral ratio (HV) is widely used. This HV spectral ratio technique was first introduced by Nogoshi and Igarashi [1971] and popularized by Nakamura [1989].

To compare observation with theoretical calculations, 1D modelling is often used. Local site effect can be considered as a transfer function over the bedrock that can be calculated when the geological and physical parameters of the site or basin are well known. Recent studies shows that 2D and 3D geometry of the basin can have strong influences on seismic wave amplification and duration. Nevertheless, the dominant amplified frequency is mostly controlled by the one-dimensional response of the local sedimentary soil column.

To characterize local site effect by modelling, S wave velocity profile must be known. For that frequency-wavenumber (fk) analysis is widely used. The fk-analysis is a standard array technique, which simultaneously calculates the power distributed among different slowness and directions of approach [Capon, 1969].

Another parameter that determines ground motion is the duration of seismic waves. The change of ground motion duration due to basin characteristics is less studied in comparison to seismic wave amplification phenomena. Most of the duration studies were focused on strong motion duration estimation and their correlation with the site conditions. But it exists only few studies estimating ground motion duration change for sites in a basin respect to nearby bedrock sites.

My purpose is to estimate the site effects at Ulaanbaatar, capital of Mongolia. The city is the political, commercial and industrial centre of the country. The population is in strong growth during the last two decades and reaches approximately 1,2 million inhabitants, which represents half of the population of the country. Ulaanbaatar is located in the valley of the river Tuul where the thickness of the sedimentary deposits reaches locally 120 m. The seismic hazard for the city results mainly from several active faults that are situated at less than 20 km from the urbanized area. One of these active faults, which could produce an earthquake of magnitude 7 or more, is associated since 2005 with an important microseismicity (Munkhuu and al. 2010). During last 70 years, the city felt several earthquakes (Gobi-Altai 1957, Mw=8.1, distance≈600km; Mogod 1967, Mw=7.2, distance≈230km; Deren 1998, ML=5.8, distance≈180km; Deren 2010, ML=5.4,

distance≈180km). The MSK intensity at Ulaanbaatar due to the Mogod earthquake varied between IV to VI, which shows that the basin under the city induces real site effect.

The second chapter is dedicated to the analysis of the spectral ratio HV and SSR. I used for it earthquakes weak motion measurements at 32 sites, and ambient noise measurements at 104 sites during a 6 months field survey done during the 2000 year in association with the CEA-DASE (Figure 1). For the analysis of spectral ratio, to avoid periods of time with local disturbances I selected the data after a quality control using their waveforms and their Fourier Spectrum. Then to calculate the spectral ratios, I used a moving window with a 90 % overlapping and a smoothing with a Konno-Omachi window.

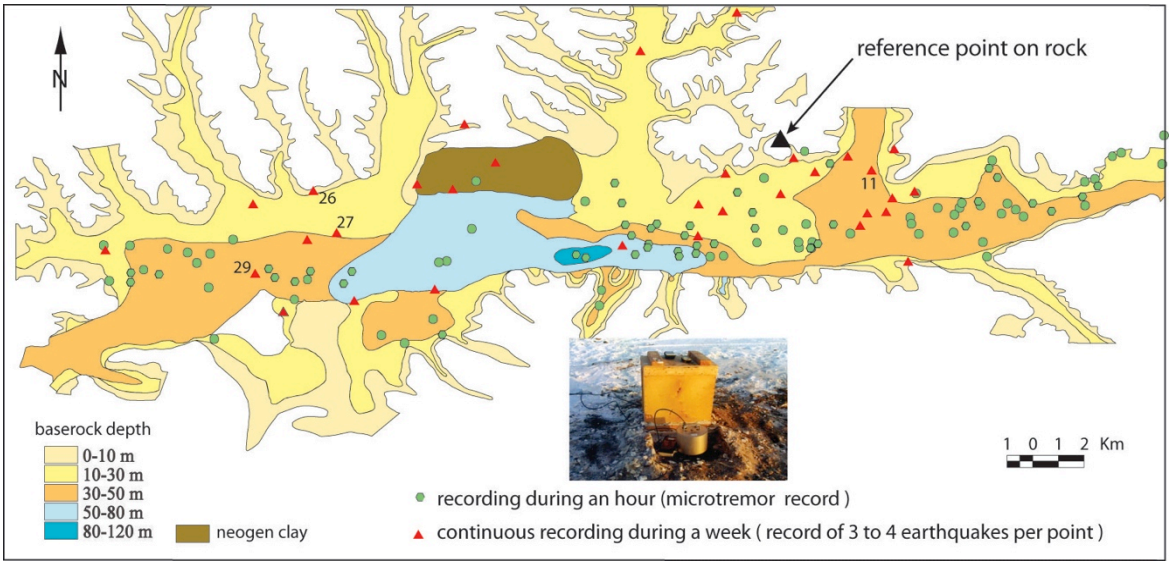

Figure 1. Map with the location of the seismic stations deployed on the Ulaanbaatar basin.

I compared the results obtained from both spectral ratio methods (HV and SSR). The observed amplified frequencies are identical when the spectral ratio shows a clear and narrow peak. But the amplification factor of SSR method gives always higher value than HV ratio using noise either event. The shape of the peak is one criteria of the reliability of the results.

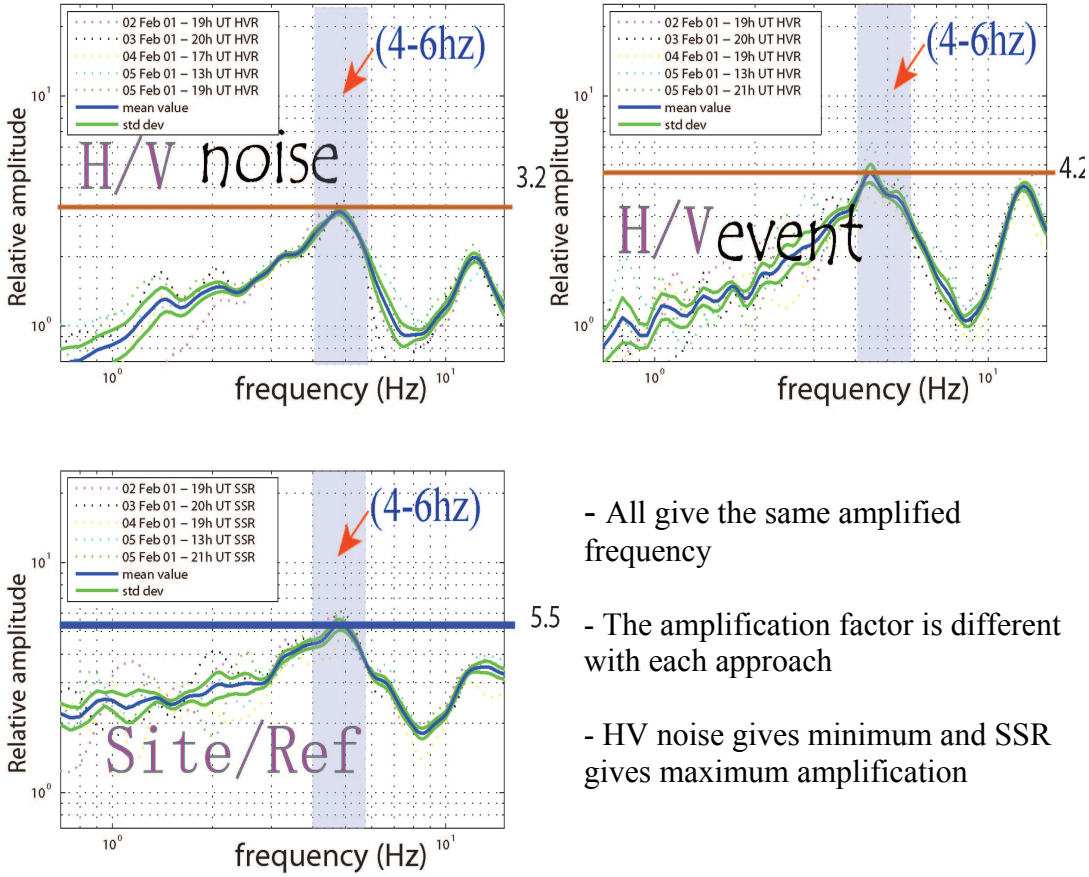

Figure 2. Comparison of spectral ratio HV and SSR for estimating the site effect using microtremor and earthquake records.

I analysed the variation of the spectral ratio HV, on seismic ambient noise, during a day. I observed that the amplified frequency is stable throughout the day except when there are particular and important local noise sources. In case of very local high noise, they have an impact on the HV ratio particularly by increasing the amplitude of low frequencies. When the noise level increases, the HV spectral ratio peak is smoothed and the amplitude is strongly decreasing. The amplitude of the HV noise ratio highly depends from environmental noise level and then demonstrates the importance, for the reliability of the results, to make a survey with a strong control of the sources of surrounding noise.

I analysed the variation of the spectral ratio HV with the azimuth of the horizontal component. This analysis shows that the amplified frequency does not depend of azimuths but its amplifications factors varies. The maximal amplitude, in the amplified frequency band, is along a particular or "polarized" orientation. I present this polarization in the form of "compass". I show that the azimuth of this polarization is affected by near sources of important noise (electric power station, sorter of gravels, shopping district with strong traffic of vehicles). It takes then the perpendicular direction to the source-site azimuth. This suggests that seismic waves generated in the basin of Ulaanbaatar by close sources are mainly SH or Love waves.

The comparison of the amplified frequencies, obtained from spectral ratio, with the average thickness of the sedimentary deposits allows me to estimate an average velocity of the S waves approximately 500m/s (H=V/4f). The amplification factors, measured by the SSR on weak motion, are from 3 to 10 between site on the basin and the rock site.

In the chapter three, I present the database georeferenced, which I built under GIS, integrating the physical properties (thickness, S wave velocity, geological interfaces, sediment type, water level, gravimetric isolines) of the basin of Ulaanbaatar deduced from gravimetric data, seismic profiles and drilling data. Based on these data, I built the first 3D digital model of the basin and of the interface sediments – rock (Figure 3). To estimate the S waves velocity profiles I applied a "frequency - wavenumber" analysis on measurements done at three sites using a seismic array. The average velocity of the S waves in the basin is estimated at 550 m/s and the depths of the obtained interfaces are in good agreement with the depth obtained from drillings close to my sites.

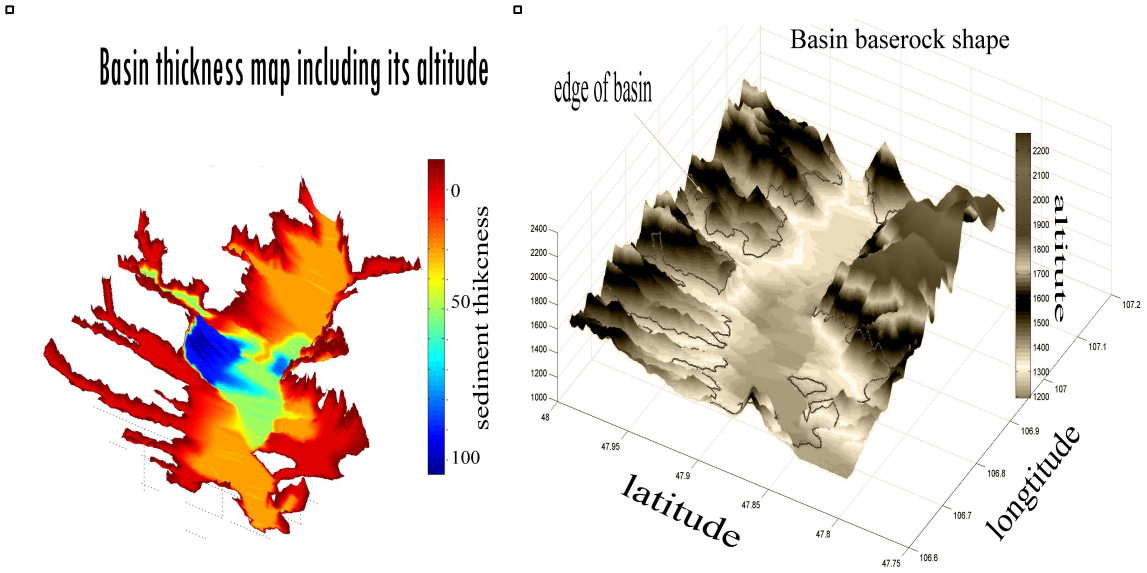

Figure 3. Ulaanbaatar basin 3D model deduced from available geological and geophysical data.

I generated an amplified frequency map using a 1D simulation (shake91) at 16000 sites of the basin, according to a regular grid, the 1D characteristics being obtained from the 3D model. Except sites directly above zones of thick clay deposits or at the border of the basin, the amplified frequencies obtained by the 1D simulation are similar with observed amplified frequencies deducted by spectral ratios. The differences can partially be due to the variation of the S wave velocity under certain sites with regard to the constant mean value used in the simulation. To improve the knowledge of S wave velocity in the basin, we need to multiply array measurements. Also, to precise the 3D geometry of the basin we need to get more geological and reliable geophysical information.

A 2D simulation of seismic waves propagation was done along the two main directions of the basin. It was realized at the CEA (French Atomic Agency) using a 2D version of the program Mak3D that was developed at the CEA-DASE by Mariotti (2007). The width of peaks observed at sites directly above strong slope of the interface sediment-rock are well modelled by this 2D approach. The amplified frequencies obtained by this 2D simulation are at higher frequency than those observed by the spectral ratio from the recorded data. This can be due to: 1) propagation characteristics in the basin, as S wave velocity, are only locally constrained; 2) measured site are not exactly along the modelled profiles; 3) a still insufficient knowledge of the basin geometry;

4) the resolution (vertical size of mesh) used for the simulation, 5 meters, which can lead to a small shift of the amplified frequency.

These first simulations, using a 2D modelling, will continue beyond the thesis by using 3D modelling within the framework of the collaboration between the RCAG (research Center of Astronomy and Geophysics, Ulaanbaatar, Mongolia), the CEA-DASE (Commissariat Energie Atomique, Departement Analyse, Surveillance, Environnement, Arpajon, France) and the EOST (Ecole et Observatoire des Science de la Terre, Strasbourg, France).

At the end I defined an amplified frequency zoning map of the Ulaanbaatar basin deduced from observed amplified frequency, SRTM, geological map and calculated 1D response of the basin.

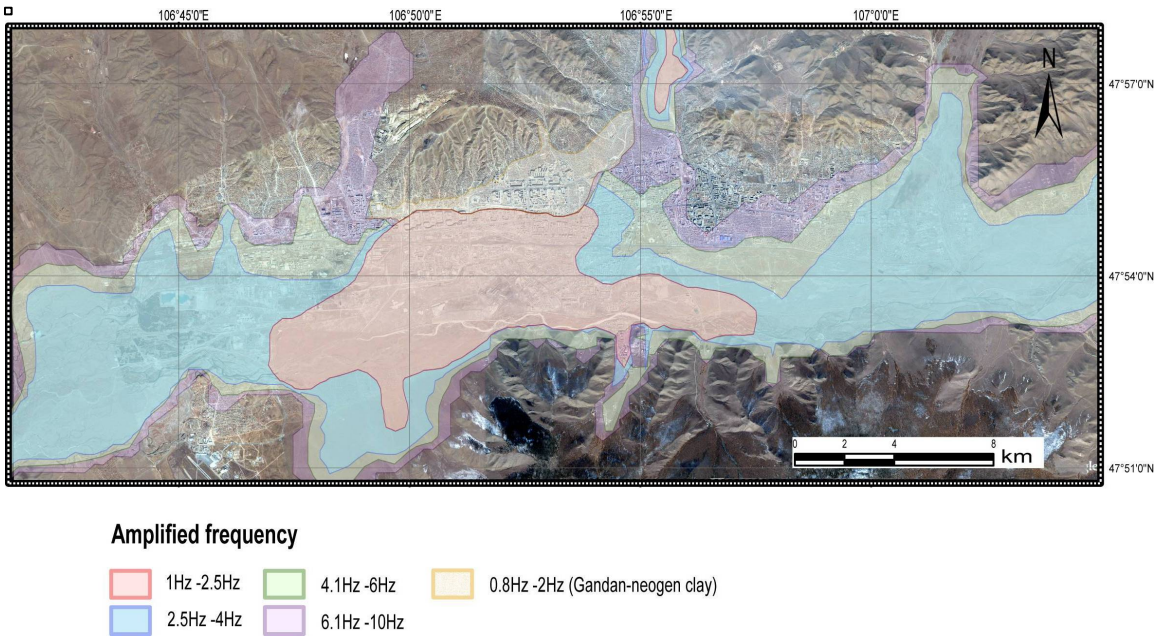

Figure 4. Amplified frequency zoning map for the Ulaanbaatar basin

The chapter 4 presents the impact of the basin on the duration of the ground motion using weak motion recordings. The definition and the measure of duration are studied according to several methods.

I used an approach based on the envelope of filtered signal to estimate the variation, for various frequencies bands, of the ground motion duration between sites on rock and on sediment (absolute duration). For that purpose, after having filtered the signals at rock and sediment in the same frequency bands, I calculated the evolution of "the amplitude of the energy". The duration is then measured at the same amplitude value on the signals recorded at rock and at sediment. I show that for the recorded weak motion, the main source of lengthening of the signal is due to 1D amplification. This lengthening is at specific frequency, which is the same as the amplified frequency of the site. However, I observed a greater signal elongation in the NS direction than EW at most sites that cannot be explained by only a 1D effect (the basin of Ulaanbaatar being mainly directed EW).

To identify other causes than the 1D effects, I calculated the duration as the time interval between 5 to 95 % of the maximum of the Arias intensity. Using this approach, it appears a very small elongation of duration on sites at the sediment. I then filtered the signal in various frequency bands and measured on each the duration through the same procedure. I observed a low increase of duration (approximately 5 seconds) in the band 5-8 Hz for sites that are on about 30m of sediments. This frequency of the elongated duration is not the 1D resonance frequency of the basin. These elongations are then compared with those, deducted by the same method, on the simulated waveforms generated by the 2D modelling. In the modelling, we can also observe this duration lengthening that seems to be due to surface waves generated at the edges of the basins. This process could explain my observations on records using the filtered Arias intensity procedure.

With our acquired weak motion data, it seems that the energy is too low to generate surfaces waves that we can be detected. With absolute duration, we observe a lengthening of 20 to 80% for most of the sites and locally up to 160%. This method is the most adapted for the study based on weak motions.

Chapter of conclusion: I looked to identify the origin of the site effects generated by the basin of Ulaanbaatar and to quantify their impact, according to the frequency, on the amplitude and the duration of the ground motion. At first, I analysed the quality of the available data and the limits of the methods.

The main conclusions of my study are the followings:

- The estimation of the amplified frequency is stable whatever is the spectral ratio method used (HVnoise, HVevent or SSR).
- Amplification factor of HVnoise ratio is influenced by the noise level and local noise source azimuth.
- The amplified frequency of the HVnoise ratio can be shifted to lower frequencies in particular situations such as when the site is near strong noise sources.
- SSR gives higher amplification factor than HV ratio. We observe an amplification factor between 3 and 10 at the Ulaanbaatar basin with SSR on weak motions.
- A 3D geometrical model was produced using available data. Velocity structure determined locally gives a shear wave velocity of ~ 550 m/s for sediments.
- The amplified frequencies at Ulaanbaatar basin vary mainly between 2 and 5 Hz. An amplified frequencies zoning was deduced from observations and 1D modelling.

The study of duration variation suggests:

- The lengthening duration, deduced from the coda wave, shows an absolute duration lengthening. It is the maximum at the same frequency that the amplified frequency of the site. The observed lengthening reached locally 160%.
- We can observe a lengthening duration, using normalized Arias intensity, due to other basin effects then 1D. We observe locally, by this approach, lengthening between 5 to 13 seconds for 40 to 80 seconds weak motion signals. The lengthened frequency is always higher than the amplified frequency.
- The duration lengthening, observed on weak motion records at Ulaanbaatar basin, is mainly due to 1D amplification.

This whole work allows me to propose a zoning of the site effects, induced by the basin of Ulaanbaatar, which is essential for the seismic hazard assessment and its consideration for the risk mitigation of the capital of Mongolia.

Table of Contents

Acknowledgements ..... **iii**

Résumé ..... **iv**

Abstract ..... **v**

RESUME ..... **vi**

SUMMARY ..... **xv**

CHAPTER I: Introduction **2**

1.1 Background **4**

1.2 Methods **5**

1.3 Study area: Ulaanbaatar region **8**

CHAPTER II: Site effect estimation using SSR and HV ratio **14**

2.1 Introduction **16**

2.2 Site survey & Data collection **17**

2.3 Data analysis **22**

2.3.1 Data processing HV and SSR *22*

2.3.2 Characteristics of Reference site. *26*

2.3.3 SSR and HV ratio analysis for long time measured sites *27*

2.3.4 HV ratio analysis on noise recorded during short time measurements *33*

2.4 HV stability in time **37**

2.5 HV ratio variation with the azimuth. **41**

2.6 Result and discussion **48**

CHAPTER III: 3D Model of Ulaanbaatar Basin And 1D, 2D Seismic Waves Simulations **54**

3.1 Introduction **56**

3.2 3D model of the Ulaanbaatar basin 57

3.3 Exploration of Subsurface S-wave velocity by Microtremor Array technique at Ulaanbaatar basin 61

3.3.1 Introduction 61

3.3.2 Field survey 62

3.3.3 Basic principle of frequency wavenumber analysis 66

3.3.4 Frequency-wavenumber analysis 67

3.3.5 Dispersion curve inversion 69

3.4 1D and 2D seismic wave modelling in the Ulaanbaatar basin 71

3.4.1 2D simulation using Mka3D 71

3.4.2 1D simulation SHAKE91 74

3.4.3 Comparison of 1D SHAKE91 and 2D Mka3D simulations with field data. 75

3.4.4 1D calculation for the whole Ulaanbaatar basin 77

***CHAPTER 4 : Duration Variations due to The Ulaanbaatar Basin* 84**

4.1 Introduction 86

4.2 Data used for analysis 88

4.3 Procedure "Arias duration": Frequency independent 90

4.4 Procedure "Arias duration": Frequency dependent 94

4.4.1 Applied method 94

4.4.2 Application to recorded events. 96

***4.5 Procedure to measure the absolute duration ratio* 97**

4.6 Result and discussion 103

4.6.1 Arias duration 103

4.6.2 Arias frequency dependent: 106

4.6.3 Comparison of the duration, using Arias frequency dependent duration, between 2D modelling and field records. 108

4.6.4 Absolute duration ratio 110

***CHAPTER 5: Conclusions* 116**

APPENDIX A 124

APPENDIX B 140

APPENDIX C **144**

BIBLOGRAPHY **147**

CHAPTER I: Introduction

1. INTRODUCTION

1.1 Background

Earthquakes are one of the most powerful natural forces that can cause large-scale loss of life and property. Earthquakes ground motions can damage directly the constructions or indirectly by inducing effects such as liquefaction, slope instability, tsunami and fire. Ground shaking is caused by seismic waves, which depends on the source characteristics, the distance from the source and local geologic conditions. To predict this ground motion, traditionally we separate source propagation path and local site condition. Local site condition is generally called "site effect" which is a major issue in the engineering seismology since last decades. Site effects can strongly amplify and extend duration of the seismic ground motions at sedimentary sites respect to rock sites. The physical phenomenon of the site effects is the perturbations, of seismic wave or deformation, caused by particular configuration of the local site. The most important parameters of site effects are amplification factor, amplified frequency and lengthening of the seismic ground motion.

One of the most outstanding site effect observations was at Mexico during an earthquake in 1985 [Singh et al., 1988]. They concluded that sites located on previous filled lakebed were amplified 8 to 50 times with respect to a hill zone site in Ciudad Universitaria. Moreover, strong amplification, as well as ground motion duration lengthening due to extremely soft clay layers, caused the collapse of many high-rise buildings despite they were locate at more then 350 km from the source. Nowadays we can found many examples of site effect observed during strong and moderate earthquakes like Northridge in 1994 [Hartzell et al., 1996] or Turkey in 1999 [Ozel et al., 2002] increasing the destructions.

1.2 Methods

Site response estimation techniques were summarized and discussed by many authors [Bonilla, 1997; Bard, 1998; Parolai et al., 1999; Satoh et al., 2001; Drouet et al., 2008 and others].

One of the most used empirical technique for site response assessment is the spectral ratio between the spectrum observed at a sedimentary site with the spectrum observed at a rock site [Borcherdt, 1970] usually called the Standard Spectral Ratio (SSR).

The method gives reliable estimates of site response if a sedimentary and rock (reference) sites are close enough in comparison to the hypocenter distance. Then the records differences between each site are due to site conditions [Yu and Haines, 2003]. Another critical assumption of this method is that the reference site record (at the surface) is equivalent to a record that would be observed at the rock at the base of the sediment site. Nevertheless, sometimes the weathered and cracked bedrock can have their owns site effect [Steidl et al., 1996]. Many authors investigated the site response functions from moderate and earthquakes weak motion records using SSR method [Hartzell et al., 1996; Riepl et al., 1998; Lebrun et al., 2004 and others].

Andrew [1996] extended this method to large network. He proposed to separate contributions of the source, the path and the site using an inversion scheme called the generalized inversion technique (GIT). Comparison between GIT and SSR methods gives similar results [e.g. Bindi et al., 2009]. For SSR technique, measurements are mainly available for weak motions and few for strong motions. Therefore, due to nonlinearity, the site effect estimated using SSR technique might be considered as an overestimation or upper limit of the site effect.

The main drawbacks of this method is the difficulty to find a good reference site and, in urban area, the necessity to deploy stations during long time in order to record seismic events with a good signal noise ratio. Therefore a non-reference site method using horizontal to vertical spectral ratio (HV) is widely used. This HV spectral ratio technique was first introduced by Nogoshi and Igarashi [1971] and popularized by Nakamura [1989]. The method assume that the surface layers do not amplify the vertical component of ambient noise, then the site response is the ratio of the horizontal to the vertical motion. Despite the lack of theoretical background, this method is widely used for determining fundamental frequency [Mora et al., 2001.; Molnar et al., 2007; Bonnefoy-Claudet et al., 2009] and

sometimes site amplification factors [e.g. Lermo and Chavez-Garcia, 1994.; Horike et al., 2001]. Also many papers discussed its stability and the theoretical meaning [Bard, 1998; Fah et al., 2001; Pilz, 2009]. This method was also extended to earthquake records and was first applied for S waves in Mexico by Lermo and Chavez-Garcia [1993].

There are many authors comparing different site response evaluation technique. Horike et al. [2001] showed that amplification factor can be inferred from horizontal component ratio using SSR, but that HV does not agree with site amplification factors. Nevertheless, the HV and SSR methods agree to estimate fundamental frequency of site but for the amplification factor observed with HV gives lower amplification than with SSR method [Drouet at al., 2008; Parolai et al., 2004; Pilz et al., 2009 etc].

European project SESAME (http://sesame-fp5.obs.ujf-grenoble.fr/) aimed to study the site response estimation using microtremor. Guidelines prepared within the framework of this project included the experimental factors affecting the HV ratio results [Chatelain et al., 2007], the standardized processing software and the recommendations in regard to the experimental evaluation. In a comprehensive study of Nakamura's method [SESAME participants, 2004] it has been concluded that the microtremor HV allows identifying the site fundamental frequency. However, they pointed that the microtremor HV peak amplitude is smaller than SSR amplification factor. It is farther concluded that the HV amplitude at that fundamental frequency may serve as a lower bound of the real amplification level.

In this thesis I consider the traditional spectral ratio technique (SSR) for estimating site response using event measurements. Then HV ratio on noise and HV ratio on weak motion will be compared with the obtained site response using SSR technique.

When the geological parameters of the site or basin are known then local site effect can be considered as a transfer function over the bedrock. To characterize such local site effect, S wave velocity profile must be known. Recent studies shows that 2D and 3D geometry of the basin has strong influence on seismic wave amplification and duration [Semblat et al., 2005]. Nevertheless, the dominant frequency corresponding to the peaks of experimental amplification is mostly controlled by the one-dimensional response of the local sedimentary soil column [Faccioli et al., 2002]. I applied then in the Ulaanbaatar basin 1D simulation

using Shake91, which is a program for conducting equivalent linear seismic response analyses of horizontal layered soil deposit.

We applied 2D simulation along to main trend of the basin using Mak3D script that was developed by Mariotti [2007], which uses discrete element method. Obtained simulations were compared with site response retrieved from observation data. To constrain input parameter of this simulation, I have to determine S wave velocity profile of the basin. Nowadays microtremor array technique became very popular to retrieve S save velocity for shallow depth. The main assumptions of this microtremor array analysis are that ambient noise is mostly composed of surface waves and that ground structure is horizontally stratified [Tokimatsu, 1997]. The fk-analysis is a standard array technique, which simultaneously calculates the power distributed among different slowness and directions of approach [Capon, 1969]. There is several different ways to estimate fk spectrum, such as Beam forming (BF) and Maximum likelihood method (MLM). Horike [1985] investigated the differences between the two methods and concluded that MLM has a higher resolution than BF method. Wathelet et al. [2008] also concluded that the high-resolution f-k method is more efficient for some arrays than the standard f-k approach in defining the dispersion curve, particularly in the low frequency range. Finally, I used for estimating S wave velocity profile of the basin a frequency -wave number analysis at 3 different sites uses.

Another parameter that determines ground motion is the duration of seismic waves. The change of ground motion duration due to basin characteristics is less studied in comparison to seismic wave amplification phenomena. This probably happens because of the lack of data, the difficulty to use reliable existing methods and the stability of the duration due to 3D basin characteristics. Most of the duration studies were focused on strong motion duration estimation and their correlation with the site conditions [Trifunac and Brandy, 1975; Boomer, and Martinez-Pereira, 1999; Novikova and Trifunac, 1993; Montejo and Kowalsky, 2008]. But it exists only few studies estimating ground motion duration change for sites in a basin respect to nearby bedrock sites [Beauval et al., 2003; Parolai and Bard, 2003].

My work is focused mainly on site effect estimation at Ulaanbaatar city using weak motion and ambient noise records. Ulaanbaatar is located in the basin on the southwestern edge of the Hentiy Range in Mongolia along to Tuul river (figure 1.1.).

1.3 Study area: Ulaanbaatar region

The Ulaanbaatar city, the capital of Mongolia, is the political, commercial and industrial centre of the country that is located in the heart of the central Asia. The city was first established in the year 1639. The population of the city rapidly increased during the last 2 decades from 500 000 peoples in 1990 to 1.200,000 in 2010. The city and its close surroundings have the highest population density in the nation with more almost one-half of the total population of Mongolia (figure 1.1). Most industries, including textile, tanning, food processing, energy production, communication and construction, are primarily concentrated in Ulaanbaatar. Due to this economical and population growth, the number of building and construction increases very rapidly.

On other hand, in history, Ulaanbaatar city felt with moderate intensity several earthquakes (1967 Mogod earthquake Ms=7.2, distance 260 km; 1998 Deren earthquake ML=5.3, distance 190 km; 2010 Deren earthquake ML=5.1). After the Modog earthquake in 1967, Mongolian and Russian joint scientific group made a study for the seismic zoning of Ulaanbaatar and published a book with a seismic zoning of Ulaanbaatar city [Medvedeva 1971] (figure 1.2). This time the city area was smaller than today, therefore the limit of the map does not cover the total actual city. According to Mogod earthquake macro seismic map at Ulaanbaatar, the city felt the earthquake with various Intensities from IV to VI (Intensity MSK was determined by Medvedeva from *Institute* of *Physics* of the *Earth*, *Russian* Academy of Sciense [1962]). Considering the epicenter distance (260 km), it is clear that this intensity variation is related to the local geology that has a real impact on the ground motions.

In years 2000 to 2005, RCAG team implemented a “Seismic hazard assessment of the Ulaanbaatar” project with French (LDG-EOST) collaboration. The study was mainly focused on several specific topics for the seismic hazard assessment of Ulaanbaatar (active tectonic, seismicity, attenuation) and a part of the study included preliminary Site effect estimation using HV ratio and SSR. As an engineer at RCAG, I was involving in this project and handled the Site effect estimation part of this work. During this project, we collected

numerous weak motion and ambient noise records. The important collected dataset was the base for a detailed analysis of the site effect at the Ulaanbaatar basin, which was undertaken in my PhD work.

The seismic activity near the city is directly connected with the main seismic activity of Mongolia. In the last century, Mongolia has experienced four major earthquakes with magnitude more than 8 (Tsetserleg 1905; Bolnay 1905; Fu Yun 1931 and Gobi-Altaï 1957) and many more moderate earthquakes. This seismic activity in Mongolia is related to its location between the compressive structures associated with India-Asia collision and extensive structures localized in north of the country (Huvsgol area) and Baikal rift [Tapponnier et Molnar, 1979]. Active faults are numerous and large but the occurrence of these four large earthquakes, in less than one century, are unusually high [Baljinnyamet al. 1993; Schlupp, 1996]. The capital Ulaanbaatar is located at the central east part of the county that is about 260 km from Mogod, about 600 km away 1905 and 1957 ruptures and about 1000 km from the well-known main active faults in Altay range (west of Mongolia). As précised before, the city felt several earthquakes last decades. Moreover, thanks to new modern seismic network installed around Ulaanbaatar, in collaboration with DASE (CEA, France) since 1994 and CTBTO (Vienna) since 2000, the RCAG is able to observe and locate even small events around Ulaanbaatar (Figure 1.3). With that network we observed a strong increase of the seismic activity since 2005 just 10 to 50 km from the urban area of Ulaanbaatar. This seismicity is associated with active faults that might produce earthquake with magnitude 6.5 to 7.5 at short distance from the capital as the well-known Hustay fault and the Emeelt fault discovered in 2008 [Munkhuu et al., 2010].

Geological context of Ulaanbaatar area: Ulaanbaatar is located on the bank of Tuul River and in the valley of four foothills of the Khangai Mountains, between geographical coordinates: South 47.88, North 48.00, West 106.67, East 107.16. It covers an area of about 136,000 square kilometres, located at an average altitude of 1,350 meters above sea level (Figure 1.2). The basin of Ulaanbaatar is 30 km long, 4-10 km wide and filled with alluvial deposit. According to cross section based on drilling information, the sediments thickness is mainly between 10 to 80 meters and the thickest (deepest) part reaches 120m in the south middle of the basin [G.Tserenjab and D.Unurjargal, 2000]. An overview of the geology of the Ulaanbaatar area is given in figure 1.4 (after Magicnet project, 2000). The geology of base

rock under Ulaanbaatar and its surroundings consists mainly of Cambrian, Devonian, Carboniferous rocks, which are intruded by granite rocks of Jurassic to Triassic age. Most of the area is covered by sandstone and mudstone rocks of Cretaceous period. Noegen deposits are widespread in the basin, especially at border areas and it reaches locally 100 meters thickness at the central north border of the basin. The deposits of the Quaternary period are fairly widespread in Ulaanbaatar area. They are commonly found under the valleys of the Tuul River and in the central part of their tributaries. These deposits are also found on mountain slopes and at their foot. The age of the deposits is from Early Pleistocene to Recent age.

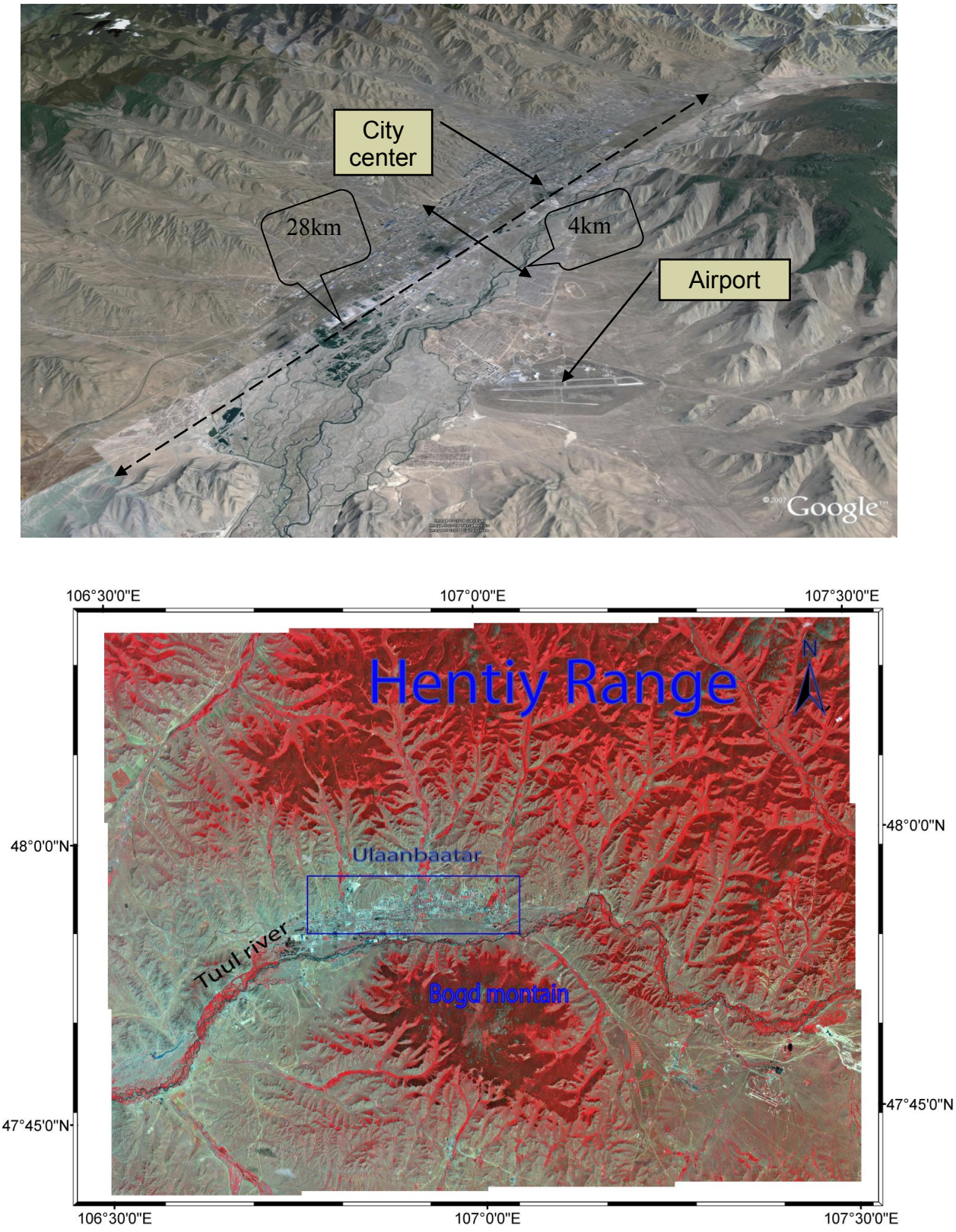

Figure 1.1: Ulaanbaatar city general views. (upper: size of the urban area, background image after Google earth, bottom: location of Ulaanbaatar basin at the regional scale, background SPOT satellite image).

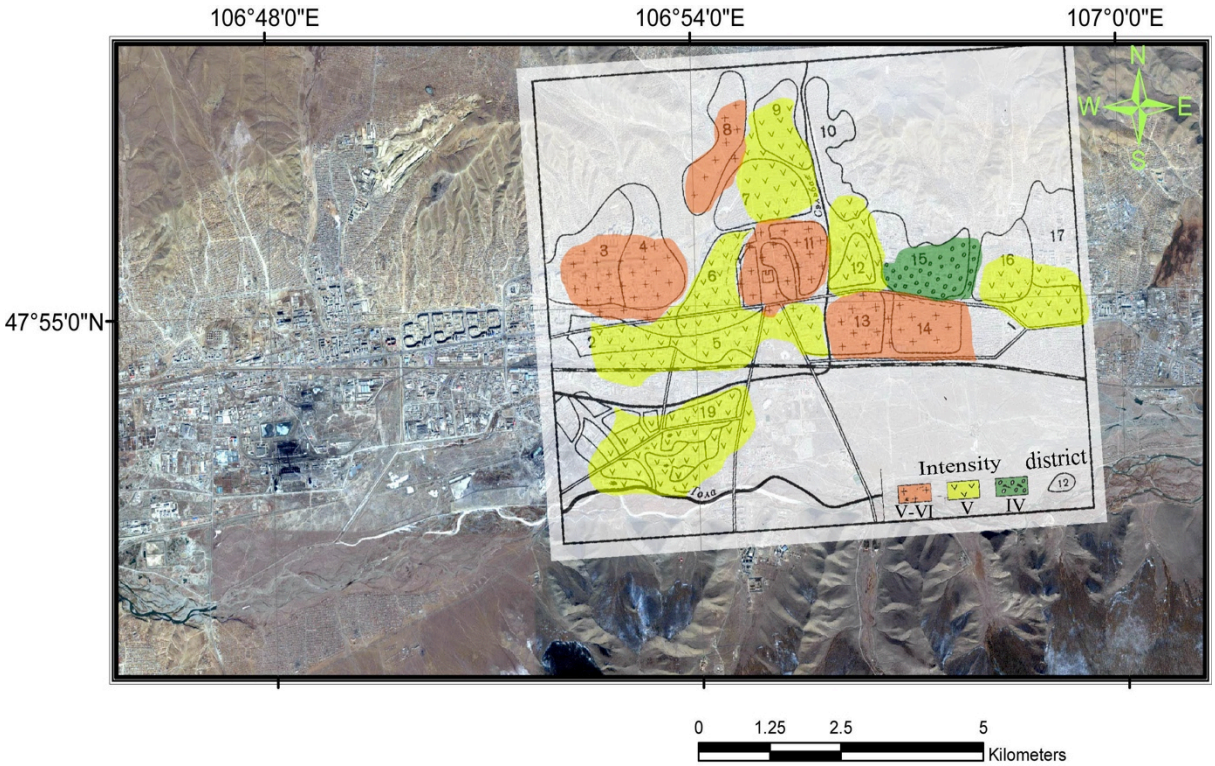

Figure 1.2: Mogod earthquakes MSK Intensity map of Ulaanbaatar city (after Medvedeva C. V. 1971) overlying the actual city urban area observed from Google images.

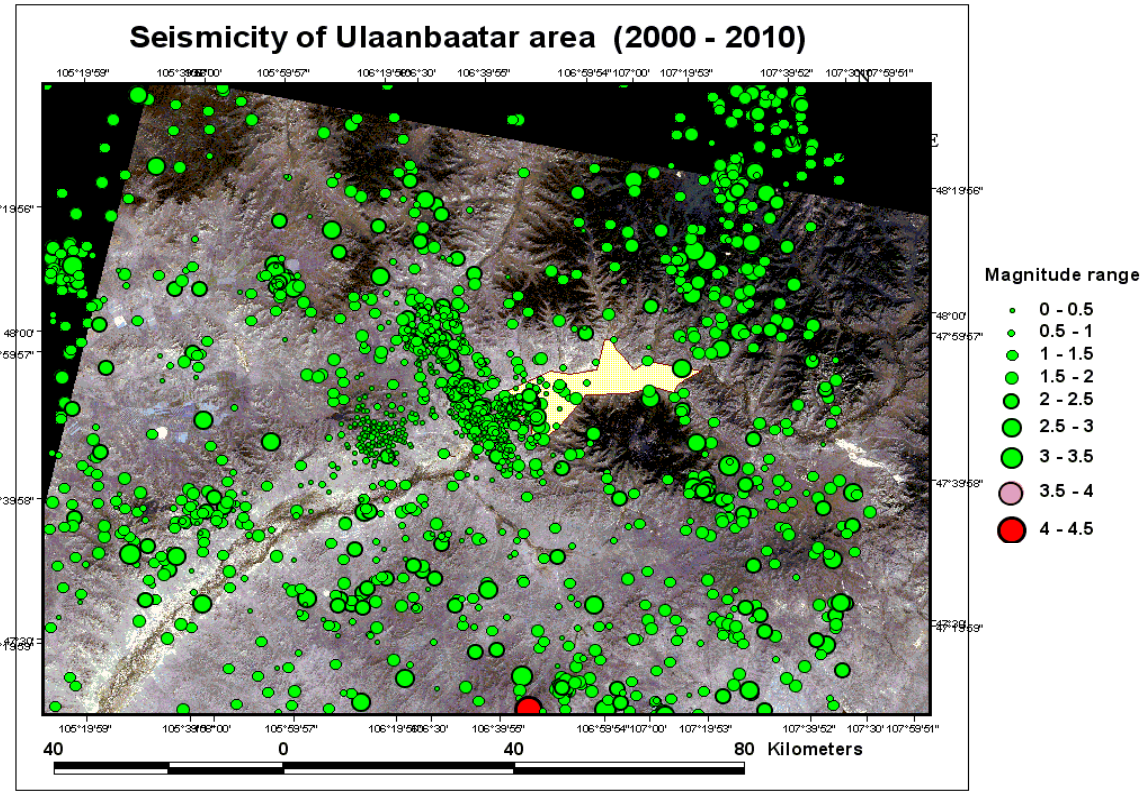

Figure 1.3: Seismic activities around Ulaanbaatar area from 2000 to 2010 (RCAG catalog). Yellow polygon represents Ulaanbaatar urban area.

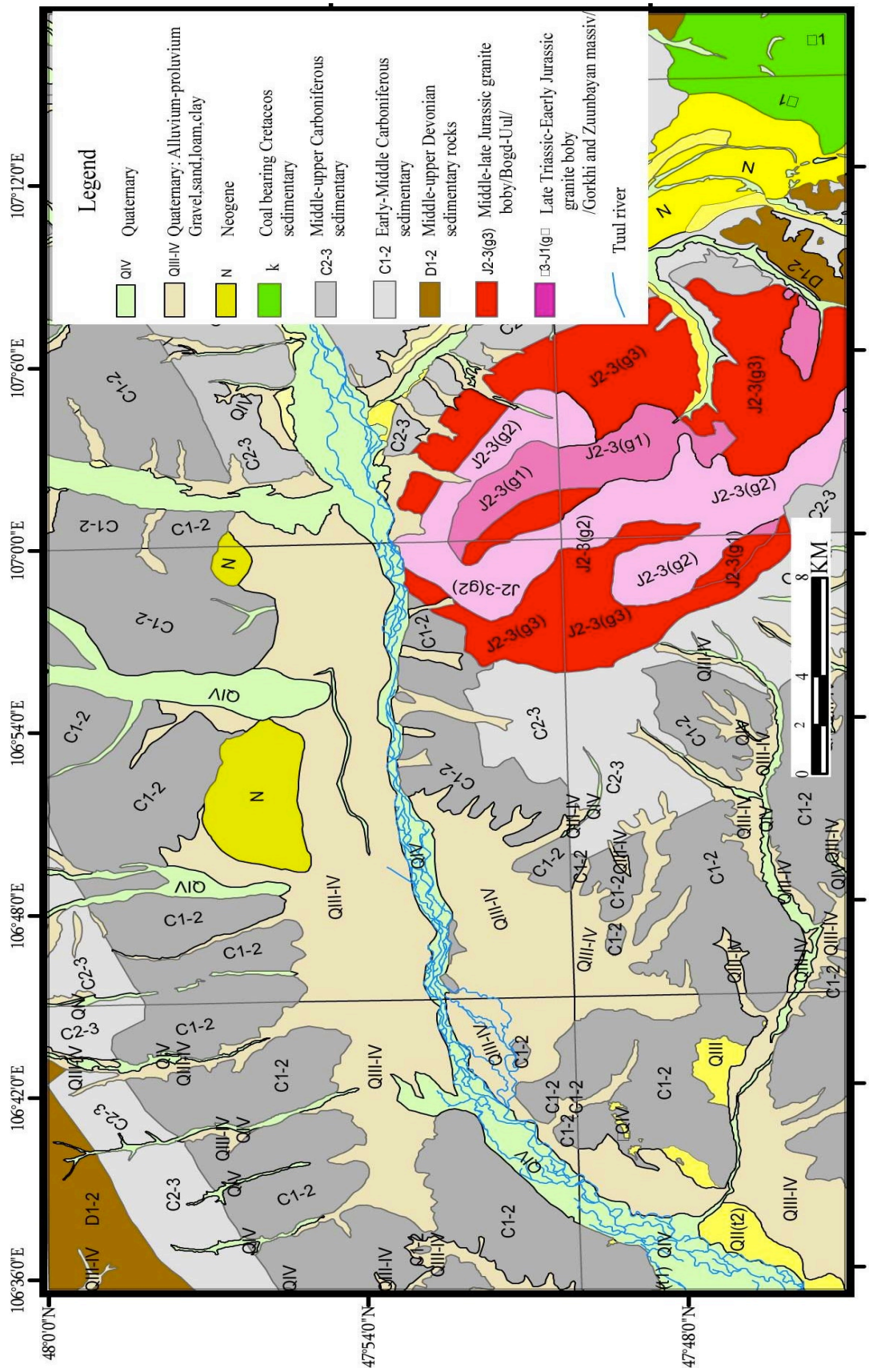

Figure 1.4: Geological map of the Ulaanbaatar area and its surroundings (after Magicnet 2000)

CHAPTER II: Site effect estimation using SSR and HV ratio

2. SITE EFFECT ESTIMATION USING SSR AND HV RATIO

2.1 Introduction

This chapter is dedicated to estimate site effect of Ulaanbaatar basin based on spectral ratio methods. There are many different methods to estimate local site effect, either direct approaches, which use seismic wave records and its spectral ratios, or indirect approaches which use synthetic data and simulation or based on geological information. One of the most traditional methods is to use an earthquake spectrum as SSR. The disadvantages of these methods are the necessity to deploy stations for long time at each site in order to record events, which is difficult to apply in urban areas, and the need to install at the same time many stations to compare effects at different sites. There are also several studies showing that "reference" site can be biased by their own local structure, which can induce to underestimate site effects [Steidlet al., 1996]. In case of Ulaanbaatar, the basin is between 4 mountains that makes easy to find outcropping rock sites.

Another well know method is HV ratio to derive fundamental frequencies of the site. The technique is easy to apply in urban areas and the calculation is simple. The method was initially proposed by Nogoshi and Igarashi [1971] and popularized by Nakamura [1989].

Here in this chapter I will discuss and apply HV and SSR methods at Ulaanbaatar basin. I will also analyse and verify the stability of HV with time and with the azimuth of horizontal component. In the last part of this chapter the agreement between the results of the methods, applied for Ulaanbaatar basin, are considered.

2.2 Site survey & Data collection

The RCAG (with CEA/DASE support) team carried out a site measurement survey on Ulaanbaatar basin from November 2000 until May 2001, with 8 short period seismometers (Figure 2.1.). Each seismic station was equipped with 24 bits digitizer with a recording frequency of 50 Hz. Sensors were short period 3 component Mark-4L with, between 0.7 Hz and 10 Hz, a flat velocity response. Additionally, during the years 2008 and 2009 while I did the array measurement, I recorded microtremor noise at 13 sites using BB Guralp seismometers. At each site, geographical coordinates were measured by hand GPS, with an accuracy of about 5 meters, and the orientation of sensor was adjusted using hand compass. The main purpose of the 2000-2001 survey was to measure local geological site effect of the basin using SSR and HV spectral ratio. With this survey, 104 sites were measured during short period of time (between 30 minutes until 2 hours) in order to record ambient noise. For another 32 sites, we deployed seismic stations during 1 or 2 weeks in order to record seismic events. At each “long time measured site”, we recorded 1 to 3 events and altogether we recorded 64 events (Figure 2.2.) During the whole period of the survey, one station was permanently deployed on the outcropping rock, considered as reference rock site, at the northeast part of the basin (black triangle on the Figure 2.1.).

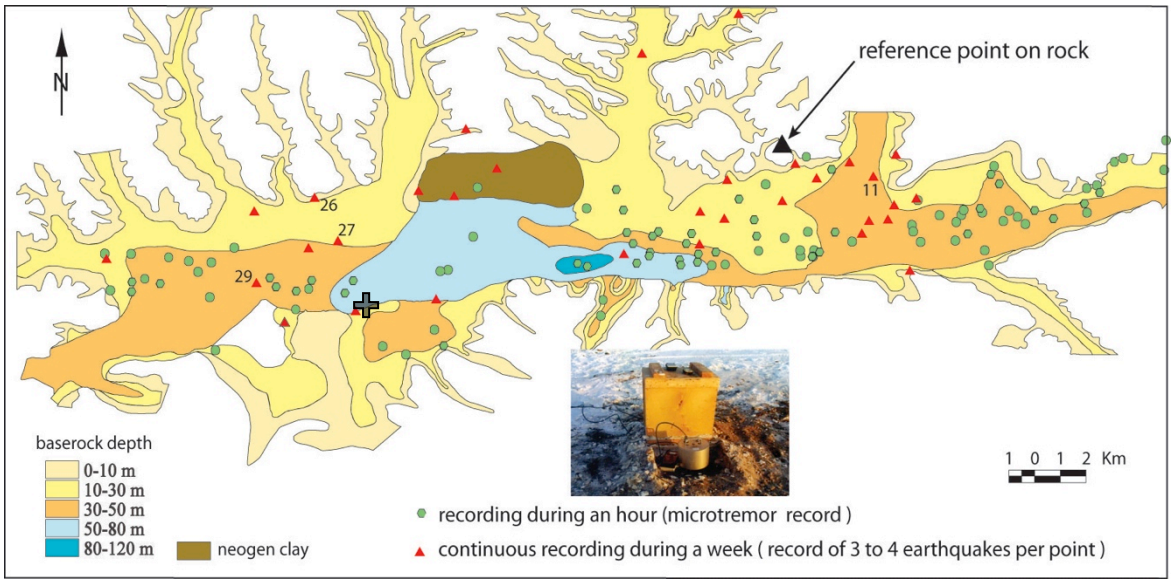

Figure 2.1: Map with the location of the seismic stations deployed on the Ulaanbaatar basin during 2000-2001 field survey. The numbers are example of site names. Colour polygons are related to extend and the thickness of the quaternary sedimentary deposits. Grey cross represents the position of the power plant 4.

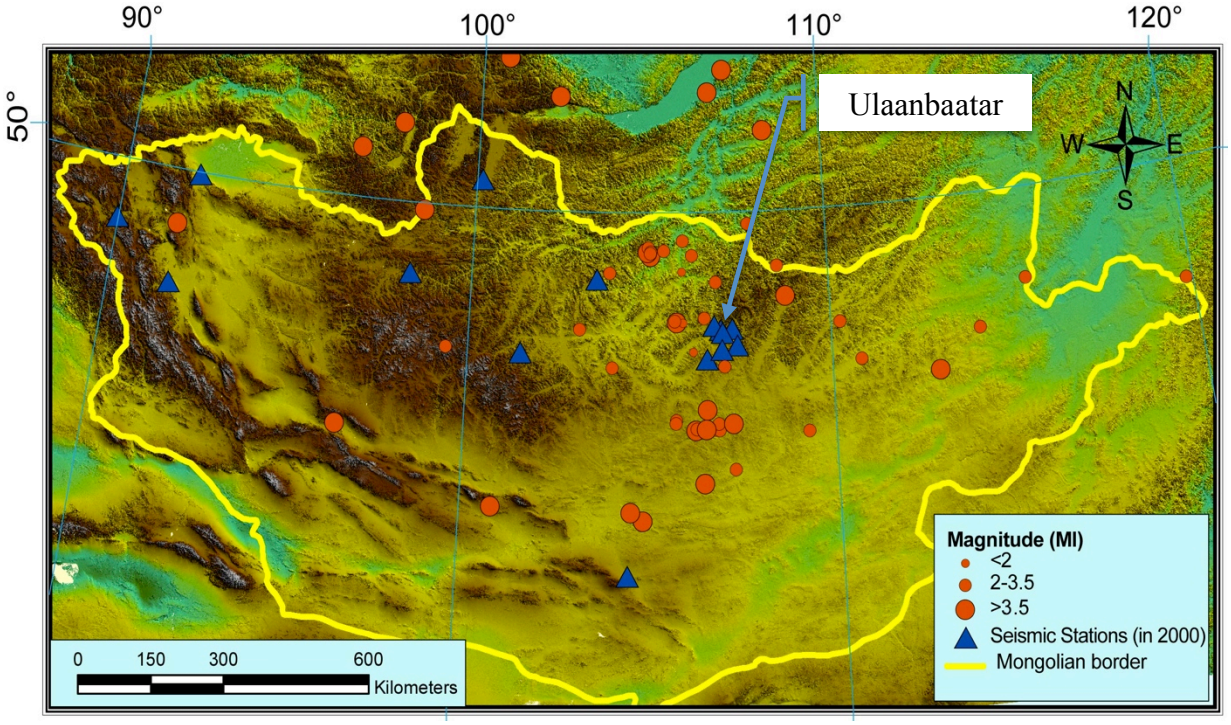

Figure 2.2: Distribution of the earthquakes recorded during field survey in 2000-2001 and used in this study. Blue triangles are permanent stations, RCAG network, that were used to determine the event parameters.

The magnitude and location of recorded events were determined using Mongolian seismic network (Figure 2.2). The recorded events have a magnitude ML between 1.5 and 5.8 and an epicentre distance between 40 to 1000 km, all are in the crust. At the reference site, the associated amplitudes range from 25 to 2500 nm (Figure 2.3).

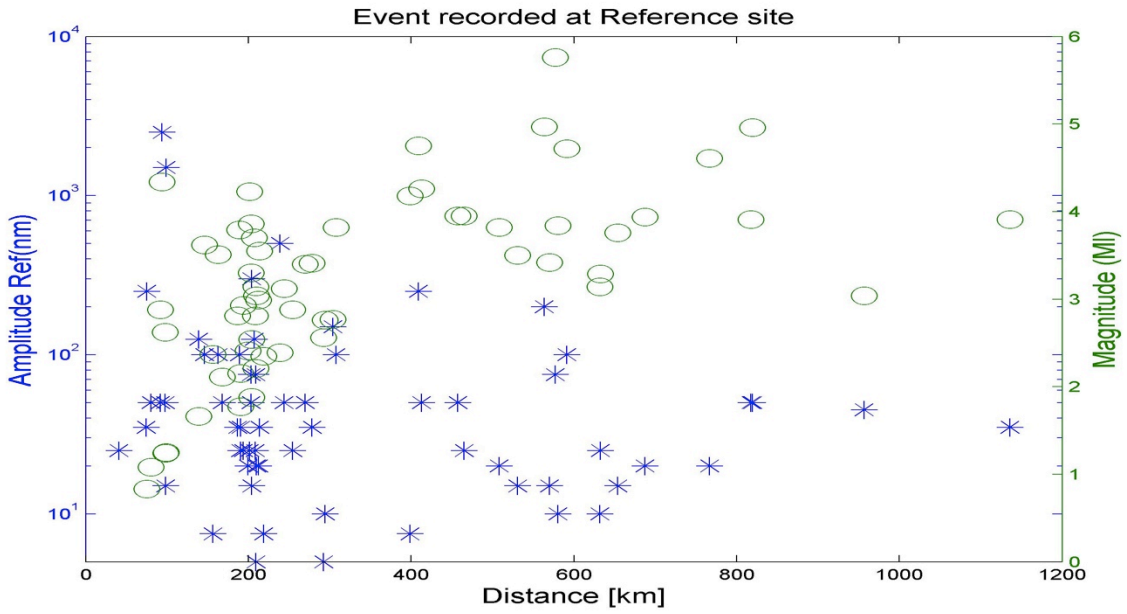

Figure 2.3: Characteristics of the event recorded at the Reference site. The amplitude axis presents the Z component amplitude of events (blue stars). The magnitude axis presents magnitude ML of recorded event (green circles). Horizontal axis presents the epicentre distance.

Mongolia is mainly a plateau and steppe with a strong intra-continental position inducing a big variation of temperature between day and night times with frequent strong winds. At sites, where measurements were done over long time, we made small hole in which we installed the sensor and covered it with wooden cap covered with ground soil in order to avoid a direct contact with humans and animals and also protect them from wind noise. For longer measurements, stations were deployed for security reasons at a local family property or inside an organization fence and those locations were mostly distributed around the basin (Figure 2.1.).

Comparison of weak motion records time sequence between reference and sedimentary sites clearly shows site amplifications. Examples of a waveform recorded at the site 29 (west part of the Ulaanbaatar basin, see Figure 2.1) and at reference site are shown in figure 2.4.

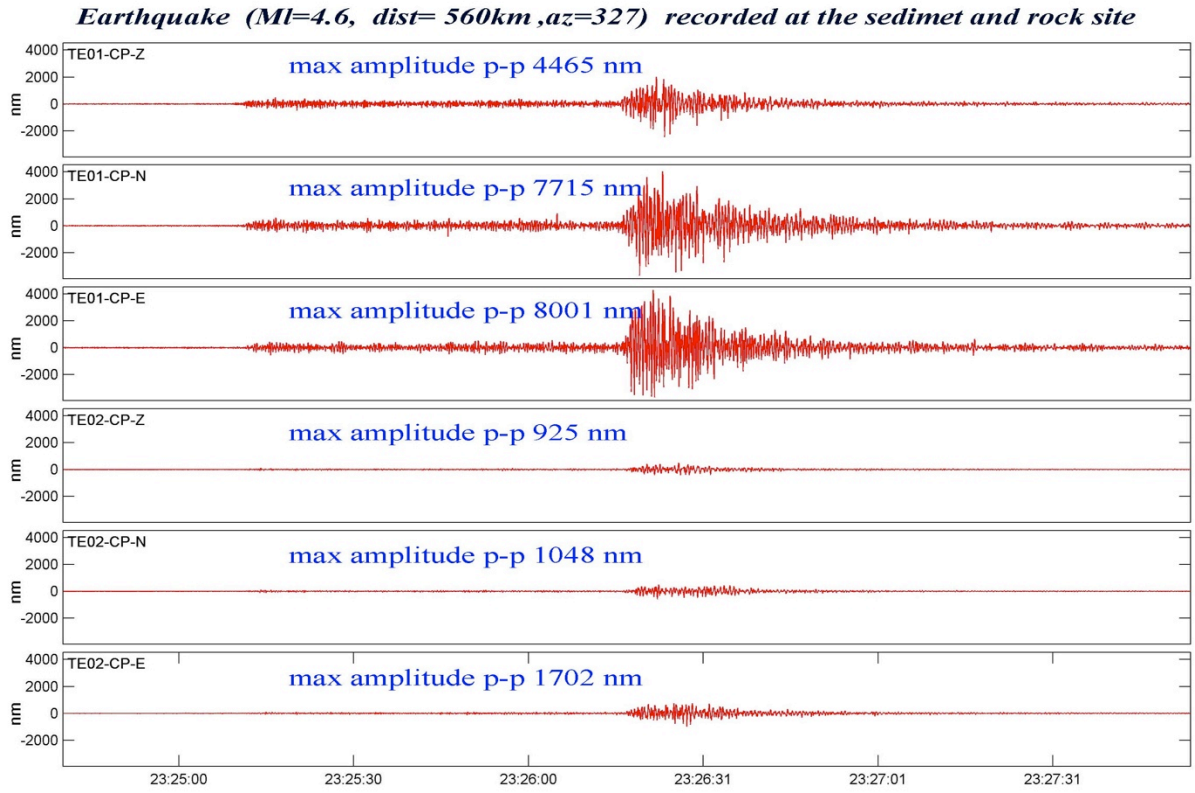

Figure 2.4: Example of an earthquake recorded at the Ulaanbaatar basin. TE01 record corresponds to the Site 29 and TE02 record to the reference site for event numbered 61 (see table in appendix A). Amplitude scales are the same for all records.

The basin's along Tuul river host many activities that produce a high seismic noise, which made us difficulties to find a sufficient low noise site to record weak motions. For example, on the east part of the basin, the Tuul River is bordered by many water supply systems; the central and western parts contain many factories of heavy industry as well as 3 power plants.

During the field survey, many recorded events were disturbed by noise from human and industrial activities. Moreover, we observed a constant noise at 10Hz at most of the sites. The noise level at 10 Hz increased when the station was closer to the power plant IV (figure 2.1 and 2.5). The figure 2.5 represents the records at sites 27, 26 and rock, and the spectrum of the noise before the event and of the event. The sites 27, 26 and 29 were located 1km, 2km and 4km away, respectively, from power plant IV.

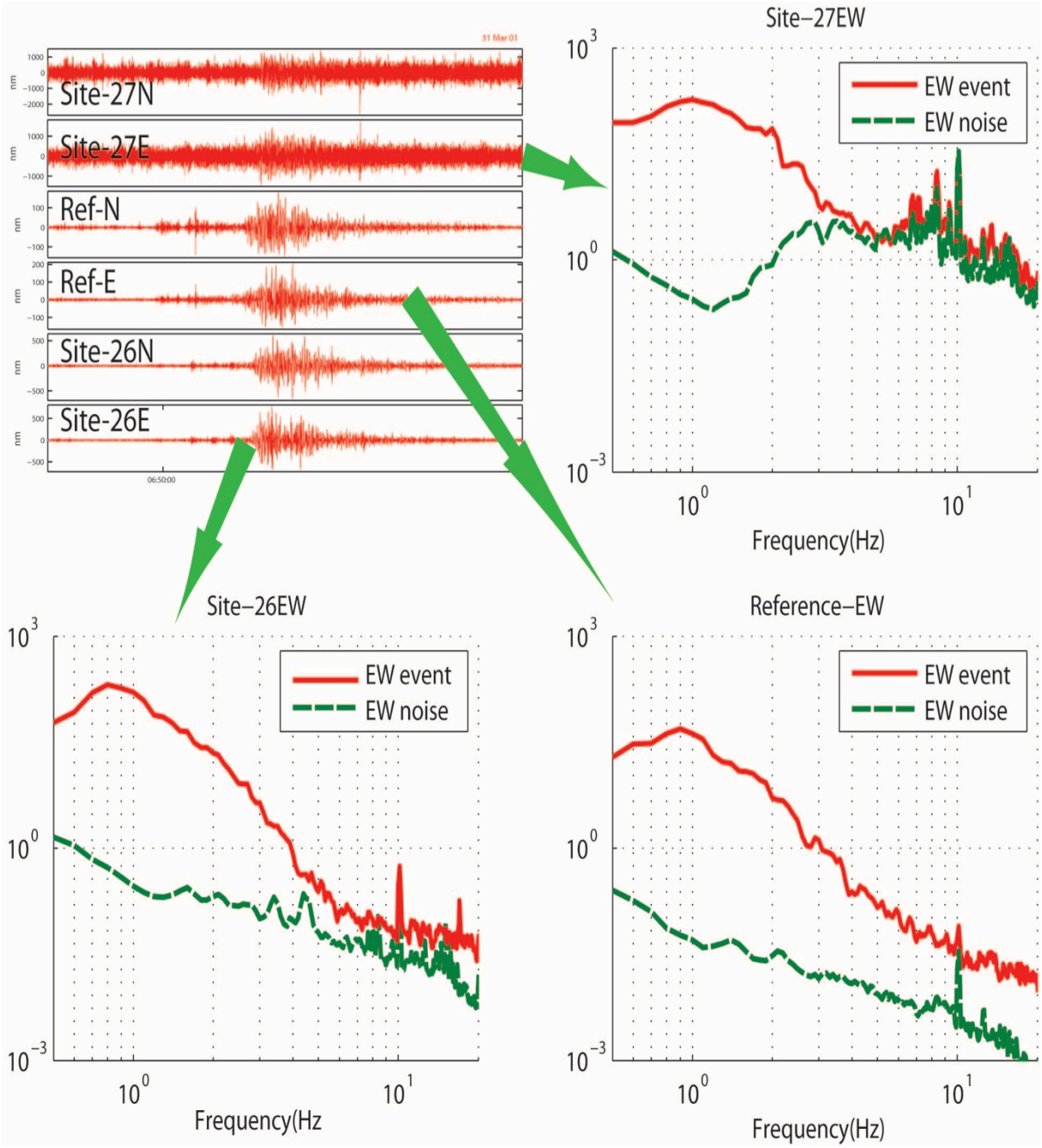

Figure 2.5: An example of an event recorded at a noisy site (signal and spectrum). The vertical scales are normalized to the maximum amplitude (top left). The sites 27 and 26 are located at 1 and 2 km respectively from electric power plant IV. The peak at 10 Hz, observed at many stations, is increasing when the station is closer to the electric power plant.

2.3 Data analysis

2.3.1 Data processing HV and SSR

Since SSR (Standard Spectral Ratio) and HV (Horizontal to Vertical spectral ratio) are both spectral ratio, I performed similar procedure for all spectrum ratio. No instrumental correction was carried out for the ambient noise spectral ratio analysis, as the sensor components employed (Mark4L 3-D) have the same response characteristics in the frequency range of 0.7–20 Hz. Anyway, with convolution theorem, after spectral ratio the response of instrument can be neglected. The parameters of calculation I considered follow the recommendations of the SESAME guideline [SESAME., 2004] to come up reliable HV curves.

1) $f_o > 10/l_w$: The length of windows (l_w) is at least 10 times larger than the period of interest, f_o- HV peak frequency
2) $n_c(fo) > 200$: The number of significant cycles $n_c = l_w * n_w * f_o > 200$; n_w - number of analysis window.
3) $\sigma_a(f) < 2$ for $0.5f_o < f < 2f_o$; f is current frequency ,σ_a -standard deviation. The meaning of this criterion is required for all windows within certain level of scattering.

The SESAME project also provides the free software (GEOPSY) to calculate the HV ratio for ambient noise, which makes it easy to check the above criteria.

In my analysis, I developed scripts in MATLAB environment (script named site effect), initially based on infrasound analysis software developed by Alexis le Pichon (CEA/DASE), to perform most of analysis. The usage of my own script allowed me to test several ideas like one day plot of SSR or HV as well as duration analysis with much more freedom than using GEOPSY or some other existing compiled software (APPENDIX C, Figure C.1). Nevertheless, when the process is possible using GEOPSY, I always compared and checked the results with GEOPSY (APPENDIX C, Figure C.1).

Shear waves typically show large amplification in sediment and usually cause damage in man-made structures. Many previous studies have used S wave (and compared S with coda wave) for estimating site amplification factor. However the S wave signal must be long enough so that any resonant peaks in the spectral ratio can be adequate resolved. Therefore it is necessary to use as long signal as possible in order to achieve better the spectral resolution.

Parolai et al. (2004) studied the impact on the result of using different signal lengths, 5, 10 and 20 sec, around the S wave arrival for GIT and EHV (Earthquake HV ratio) techniques. Both EHV and GIT result shows negligible dependence on chosen window length.

For spectral ratio, first I filtered a raw signal using Butterworth second order band pass filter between 0.7 to 20Hz, in order to remove trend and long period signals. Fourier spectrum were calculated for 10 to 20 second moving window with 90% overlapping which is sufficient for the SESAME criteria 1 for our interested frequencies ranges. Obtained Fourier amplitude spectrum for each analysis is smoothed using Konno-Omachi log scale window [Konno and Omachi, 1998].

$$W(f, f_c) = [\sin(\log_{10}(f / f_c)^b / \log_{10}(f / f_c)^b]^4 \qquad (2.1)$$

where b – is an adjustable factor to control smoothing. I used b=40 which corresponds to a "small" smoothing (smaller b will induce more smoothing).

Horizontal component of HV ratio has been calculated using the following formula

$$H = \sqrt{\frac{(NS^2 + EW^2)}{2}} \qquad (2.2)$$

For analysis of SSR ratio, I used an analysis window starting from S phase with a length between 10 to 30 seconds depending of the signal duration and signal noise ratio parameters. When a single site recorded several events, the final SSR and the associated standard deviation were calculated by averaging all spectral ratios. Figure 2.6 represents an example of SSR procedure.

Similar procedure was performed for HV spectral ratio calculation. The mean value and standard deviation for each site have been calculated using numerous windows.

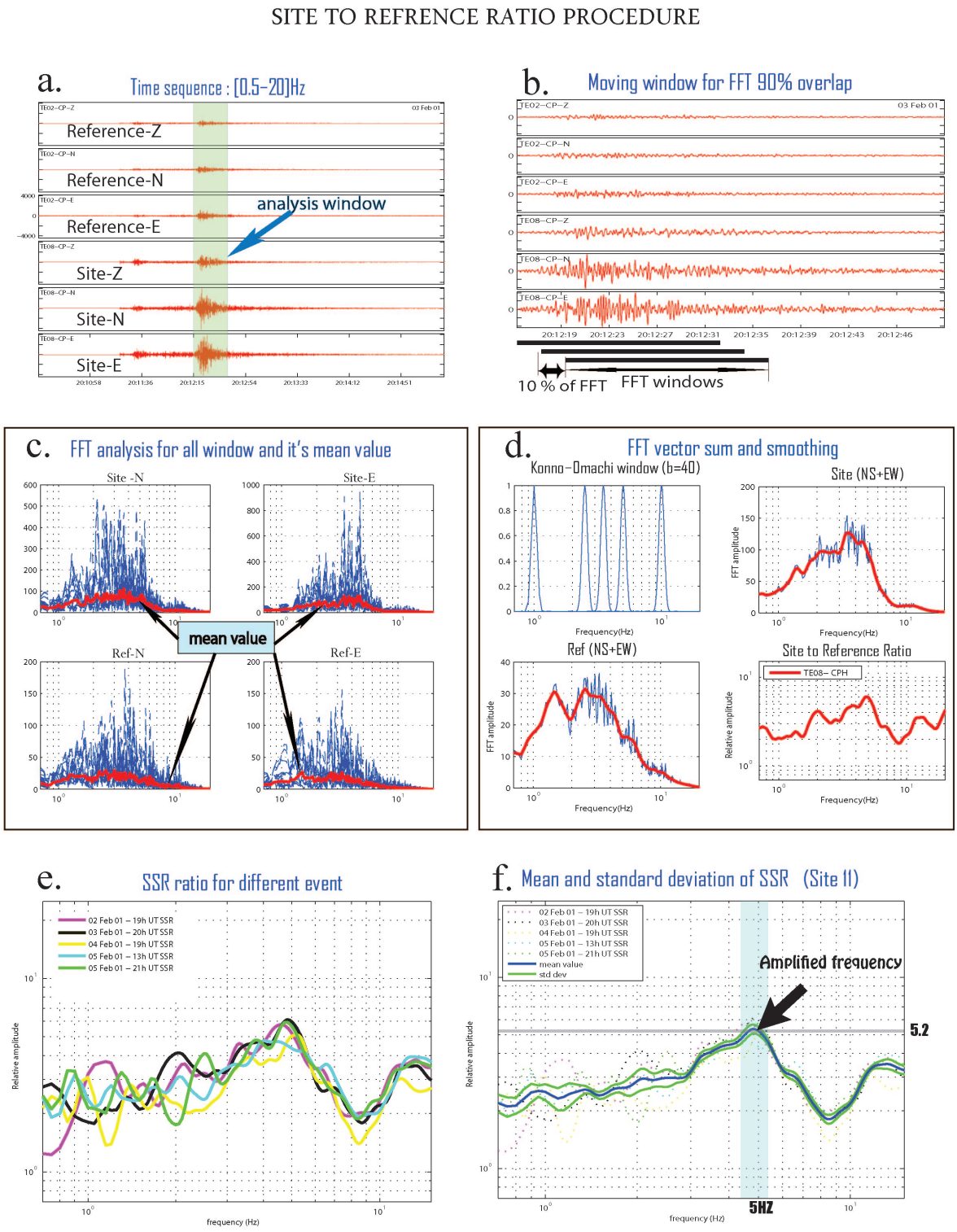

Figure 2.6: SSR procedure: a.) Selection of the S wave window used for SSR. b.) Selection window for FFT and it's overlapping windows. c.) FFT results of all windows and its mean value (red). d.) Konno-Omachi smoothing window (top left), smoothing of vector sum of NS and EW components (top right and bottom left) and SSR (bottom right). e.) SSR for different events. f.) mean and standard deviation values of SSR.

After calculation of all SSR and HV ratio, I classified the obtained HV ratio curves and peak with quality level of A, B, C following the SESAME guidelines criteria.

The criteria are:

For amplitude condition

1. there exist one frequency f', lying between $f_o/4$ and f_o, such that $A_o/A_{HV}(f') > 2$
   f_o is the HV peak frequency, A_o is the HV peak amplitude for f_0,
2. there exist another frequency f', lying between f_o and $4f_o$, such that $A_o/A_{HV}(f') > 2$
3. $A_0>2$

The stability condition

4. the peak should appear at the same frequency (within a percentage 5% limit) on the HV curves corresponding to mean + and – one standard deviation.
5. σ_f lower than a frequency dependent threshold $\varepsilon(f)$, see detailed table 2.1
6. $\sigma_A(f_0)$ lower than a frequency dependent threshold $\theta(f)$, see detailed table 2.1.

here σ_f is the standard deviation of HV peak frequency ($f_0 \pm \sigma_f$), $\sigma_A(f_0)$ is the "standard deviation" of $A_{HV}(f)$, $\sigma_A(f)$ is the factor by which the mean $A_{HV}(f)$ curve should be multiplied or divided

Table 2.1. Threshold Values for σ_f and $\sigma_A(f_0)$

Frequency range [Hz]	< 0.2	0.2 – 0.5	0.5 – 1.0	1.0 – 2.0	> 2.0
$\varepsilon(f_0)$ [Hz]	0.25 f_0	0.20 f_0	0.15 f_0	0.10 f_0	0.05 f_0
$\theta(f_0)$ for $\sigma_A(f_0)$	3.0	2.5	2.0	1.78	1.58
log $\theta(f_0)$ for $\sigma_{logHV}(f_0)$	0.48	0.40	0.30	0.25	0.20

For Ulaanbaatar basin analysis, I applied these amplitude criteria for SSR and HV ratio. The stability conditions were considered just for HV ratio, when the number of analysis window has been sufficient.

Class A corresponds to ratio that fulfils the above condition.

Class B corresponds to the spectral ratio curve that does not fulfil the above conditions generally with a very wide or small peak.

Class C is for ratio curve considered flat, meaning site that does not have amplification frequency, using HV or SSR ratio, in the instrumental response frequency range.

2.3.2 Characteristics of Reference site.

The first survey was dedicated on getting a point qualified as rock and on which could stay a station during the whole survey with continuous recording. This was important to allow us to compare the numerous sites (more than 100) with one permanent site as we had only 8 mobile seismic stations. The reference point station was deployed at a rocky site at northern part of Ulaanbaatar basin. The SSR method assumption is that the reference point does not amplify the signal. In order to check this attribute, I compared event spectrum recorded at reference points, with the permanent station ALFM. The ALFM (47.991N 106.776E) station is one of the Ulaanbaatar surrounding network, which is located at 15 km west from the Reference site. The ALFM station is installed on hard rock in a "vault". It contains short period 3 component seismometers, similar to the station used for our survey. The distance between ALFM station and Reference site (15 km) is small compared to epicentral distance (figure 2.7). For that I used 2 events (*Event 1*: 19.Apr.2001; t0=23h23m39sec; 102.30W, 52.03N; Ml= 4.9 distance to Alf=560 km; *Event 2*: 03.Feb.2001; t0=20h10m22sec; 104.5W, 44.7N; Ml=4.7 distance to Alf=408 km).

Also I calculated the HV ratio of the reference point at different time (figure 2.7). From SSR with ALFM stations and HV noise ratio at the reference site, the both spectral analyses show us that the selected reference site does not have any specified amplification in the range of 1 to 10 Hz. Therefore the site is assumed appropriate to be used as a reference rock site.

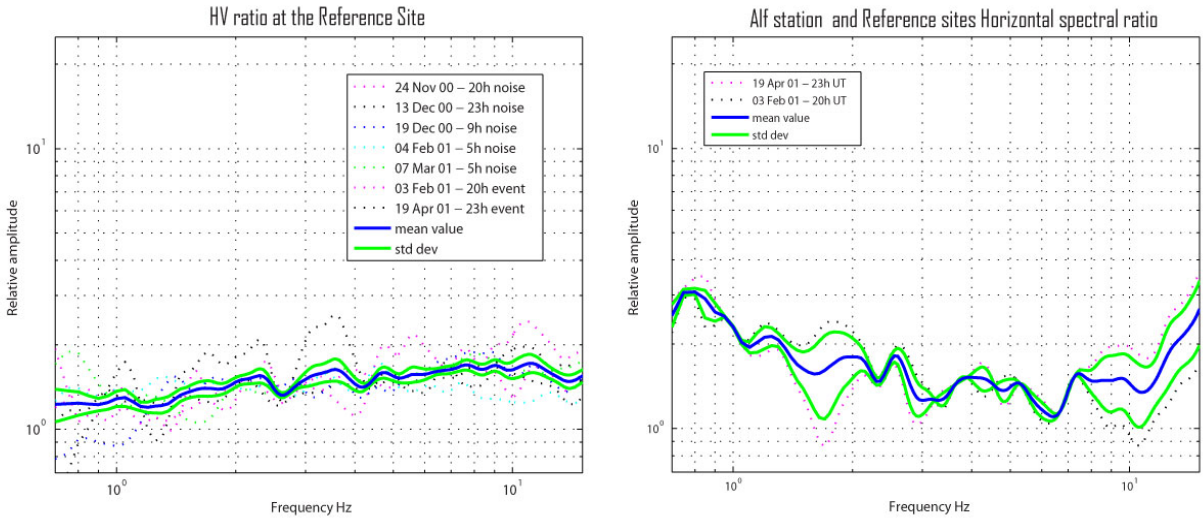

Figure 2.7: Reference rock site quality check. Left: HV ratio at different time on noise and for two events. Right: SSR at ALFM and Reference Sites for two events at a distance of 400 and 500 km .

2.3.3 SSR and HV ratio analysis for long time measured sites

Totally, 64 earthquakes were recorded at the 32 sites deployed during long time. Sites 27 and 24 were deployed near power plant IV, 14 and 16 were deployed near the main black market, which is the highest noise part of the city (appendix A, figure A.1). Therefore these sites have too low Signal Noise Ratio (SNR) to execute the analysis of SSR using our recorded weak motions (see example at figure 2.5). Nevertheless, SSR, HV on event and HV on noise ratio were calculated for the other 27 sites in order to estimate amplified frequency and amplification factor and to compare the obtained results. I show examples of calculated HV noise, HV event and SSR ratio for 3 different sites along to main trend of the basin (figure 2.8.). In addition long time measurements give possibility to apply HV ratio at different time.

After obtaining the spectral ratios, I classified them by the "topology" of the spectral curves. Class A is when the curves show clear peak, Class B corresponds wider or small peaks and Class C is when the curve is near to be flat. I present examples of classified HV and SSR curves (figure 2.9.). The HV and SSR comparison, using events, are presented in APPENDIX A. After plotting the average value of the spectral ratios for HV noise, HV event and SSR, I calculated the correlation coefficient between the spectral ratio curves, for 1Hz to 10 Hz frequency range (figure 2.8). The peak frequencies determined with SSR and HV and the correlation coefficients are shown in table 2.2

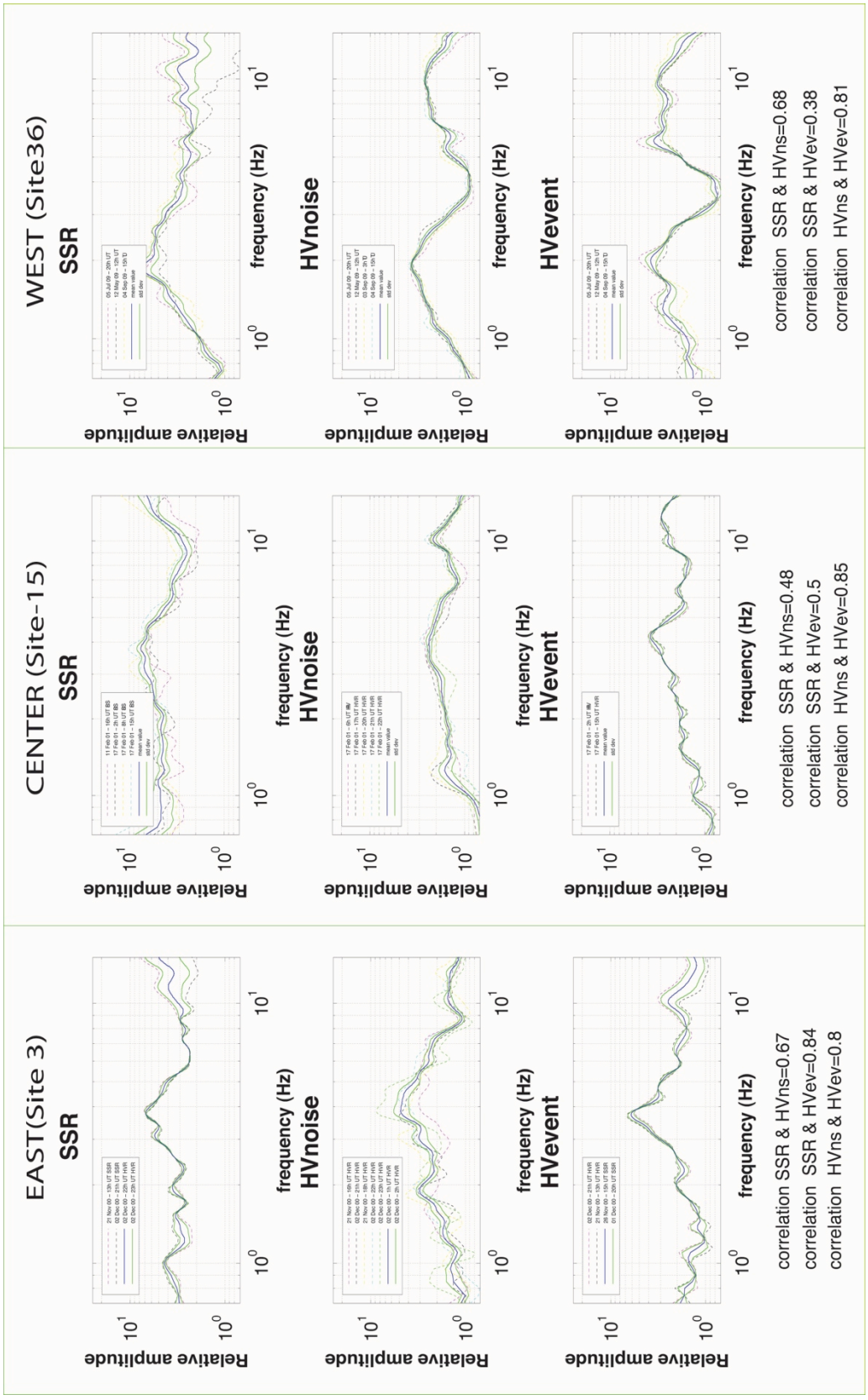

Figure 2.8: Example of the SSR , HV noise and HV event and their comparison of different site along to the main basin. "Correlation AAA & YYY=0. 67" is the correlation coefficient between curve AAA and curve YYY.

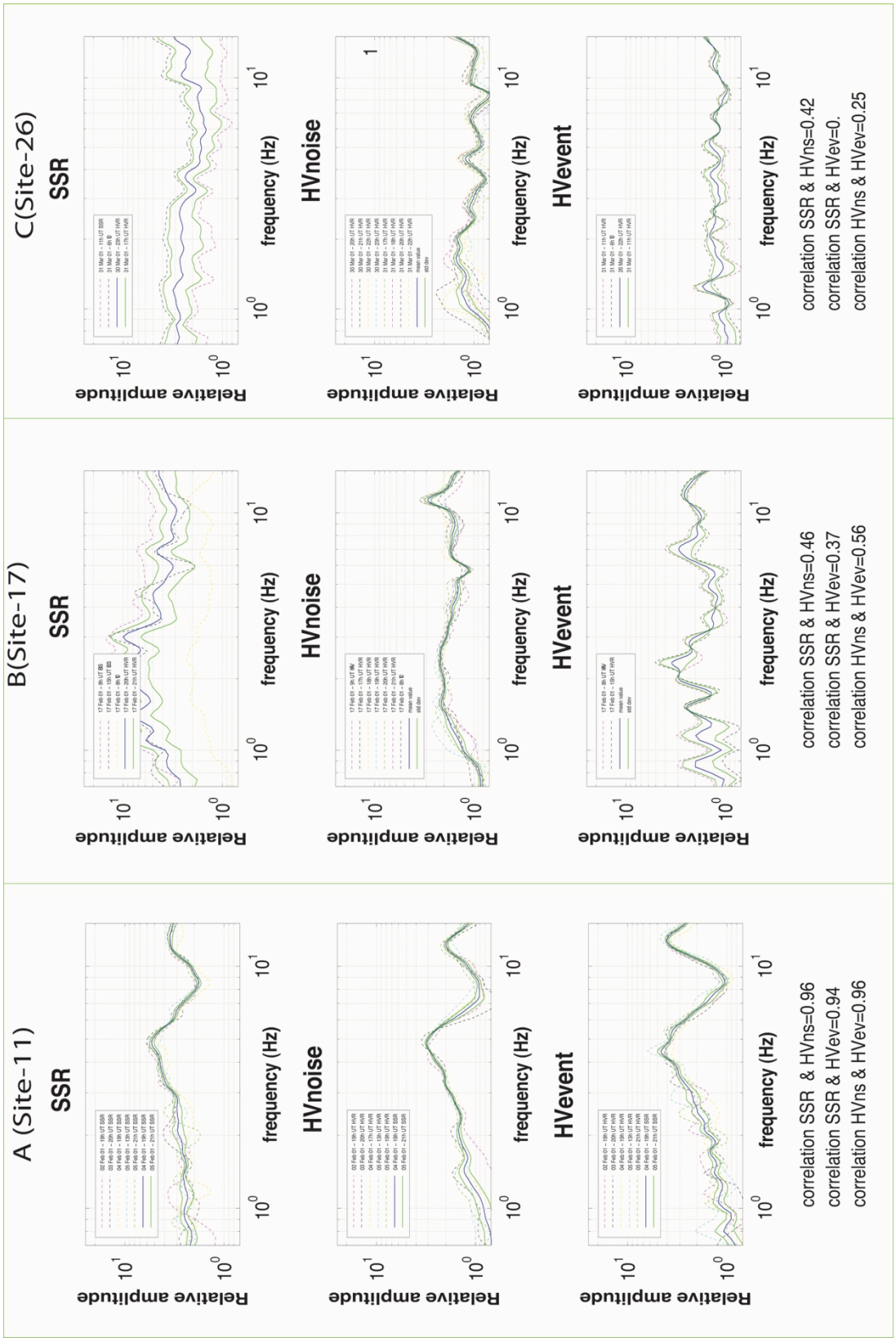

Figure 2.9: Example of the SSR , HV noise and HV event comparison. Example of classification :A- Clear peak, B- wide or small peak , C-flat peak

Table 2.2. Result of SSR and HV event (HV2) and HV noise (HV) and their correlation coefficients

NB	LAT	LON	HV [Hz]	QH-V	HV2 [Hz]	QHV2	SSR [Hz]	Q-SSRI	HV AMP	SSR AMP	Corr SSR_HV	Corr_SSR_HV2	Corr_HV HV2
REF	47.9420	106.9898	--	--	--	--	--	--	--	--	--	--	--
1	47.9199	107.0009	1.0	B	1.00	B	1.0	B	2.5	5.0	0.85	0.90	0.95
2	47.9334	106.9956	6.0	B	6.00	B	7.0	B	2.4	7.0	0.90	0.85	0.89
3	47.9037	107.0254	3.9	A	3.80	A	3.8	A	4.8	7.0	0.67	0.83	0.81
4	47.9187	107.0500	4.0	A	4.00	A	4.0	A	3.8	10.0	0.88	0.96	0.86
5	47.9097	107.0372	-	C	-	C	-	C	1.5	2.0	0.64	0.73	0.75
6	47.8879	107.0471	-	C	-	C	-	C	1.9	3.0	0.06	0.22	0.74
7	47.9092	107.0287	4.5	A	4.00	A	4.5	A	3.8	5.0	0.73	0.76	0.92
8	47.9273	107.0052	-	C	-	C	2.0	B	2.1	4.0	0.19	0.11	0.75
9	47.9177	106.9897	9.0	B	8.00	B	-	C	2.4	3.0	0.61	0.45	0.81
10	47.9342	107.0199	9.5	C	8.00	B	0	C	2.3	3.0	0.68	0.80	0.85
11	47.9281	107.0307	4.8	A	4.50	A	4.9	A	3.1	5.0	0.96	0.94	0.96
12	47.9374	107.0408	11.0	B	11.0	B	11.0	B	2.2	3.0	0.73	0.88	0.93
13	47.9267	106.9651	8.5	A	9.00	A	8.5	A	2.6	7.0	0.82	0.88	0.92
14	47.9130	106.9529	4.5	A	-		-	-	6.2	-	-	-	-
15	47.8992	106.9526	4.0	A	4.10	A	3.8	A	1.8	7.5	0.48	0.5	0.88
16	47.9101	106.9638	5.5	A	-	-	-	-	6.5	-	-	-	-
17	47.8949	106.9187	2.5	B	2.20	AB	2.5	A	2.2	8.0	0.46	0.37	0.68
18	47.9197	106.8425	10	C	-	C	-	C	1.5	3.0	0.45	0.06	0.47
19	47.9315	106.8616	10.0	C	-	C	1.0	B	1.5	6.0	0.65	0.49	0.64
20	47.8756	106.8344	1.7	A	2.00	A	2.0	A	3.6	7.0	0.73	0.84	0.67
21	47.9220	106.8265	1.1	B	1.10	B	1.1	B	2.1	10.0	0.74	0.61	0.66
22	47.8707	106.7983	2.5	C	-	C	-	C	2.1	3.0	0.01	0.43	0.08
23	47.9518	106.8478	0	C	6.00	B	2.0	B	1.3	4.0	0.61	0.65	0.61
24	47.8975	106.7771	2.7	A	-	-	-	-	4.9	-	-	-	-
25	47.8659	106.7664	-	C	-	C	9.0	B	1.8	4.0	0.21	0.17	0.16

26	47.9230	106.7793	-	C	-	C	0.0	C	1.5	1.0	0.11	0.05	0.07
27	47.9006	106.7903	2.8	A	-	-	-	-	4.0	-	-	-	-
28	47.9131	106.7528	7.0	A	7.0	A	7.5	A	2.6	8.0	0.71	0.75	0.88
29	47.8826	106.7537	2.0	B	2.0	B	2.0	B	2.9	7.0	0.59	0.84	0.82
30	47.8928	106.6864	10.0	C	4.0	B	3.0	B	1.4	10.0	0.24	0.71	0.24
UB9	48.0001	106.8265	2.0	A	2.0	A	1.8	A	5.2	6.5	0.68	0.38	0.80

Whereas:

NB=the number of sites,

LAT LON=location of the site,

HV=peak frequency of HV ratio on noise,

QHV= classification of the peak of the HV noise curve,

HV2=peak frequency of HV ratio on event,

QHV2= classification of the peak of the HV event curve,

SSR=peak frequency of Standard Spectral ratio,

QSSR= classification of the peak of the SSR curve,

SSR-AMP= SSR amplification,

HV-AMP=HV noise amplitude

corr-SSR_HV, corr-SSR_HV2, corr-HV_HV2=correlation coefficient.

For QHV, QHV2 and Q-SSR: A=Clear peak, B= wide or small peak, C=flat curve,

"-" = no result

Grey colour = sites with no event recorded or SNR of recorded event is too low.

We can see from the table 2.2 that, for the SSR classification, 7 sites are associated with almost flat response (C), 10 sites with clear peak (A) and 10 sites with small or wide peak (B).

When we observe flat curve of SSR or HV (classified-C) the correlation was small at most sites, it shows probably that the small variation of the curve amplitude do not have significant meaning. (Figure 2.10) But when the curve shows clear peak (Sites has a clear amplification at a certain frequency, classified A or B) the correlation coefficient was relatively high. Beside, the spectral ratio SSR, HVnoise and HVevents classified A or B gives

similar amplified frequency but also similar curves. In most sites the SSR shows peak with higher amplitude than HV event or HV noise.

For almost each site, when the class is A or B for HV noise, it is the same (respectively A or B) for HV event and SSR. Then, the correlation coefficient between "HV noise and HV event" or between "HV noise and SSR" is high, most of time more than 0.6 and with some correlation coefficient higher than 0.9 (table 2.2 and figure 2.10). In that case, the frequency of the peak is similar with the three methods (figure 2.11).

When the peak is not clear (class C) then the correlation coefficient became smaller, less than 0.4. When we are able to estimate this peak, is at a frequency, which differ when using the various methods (figure 2.11).

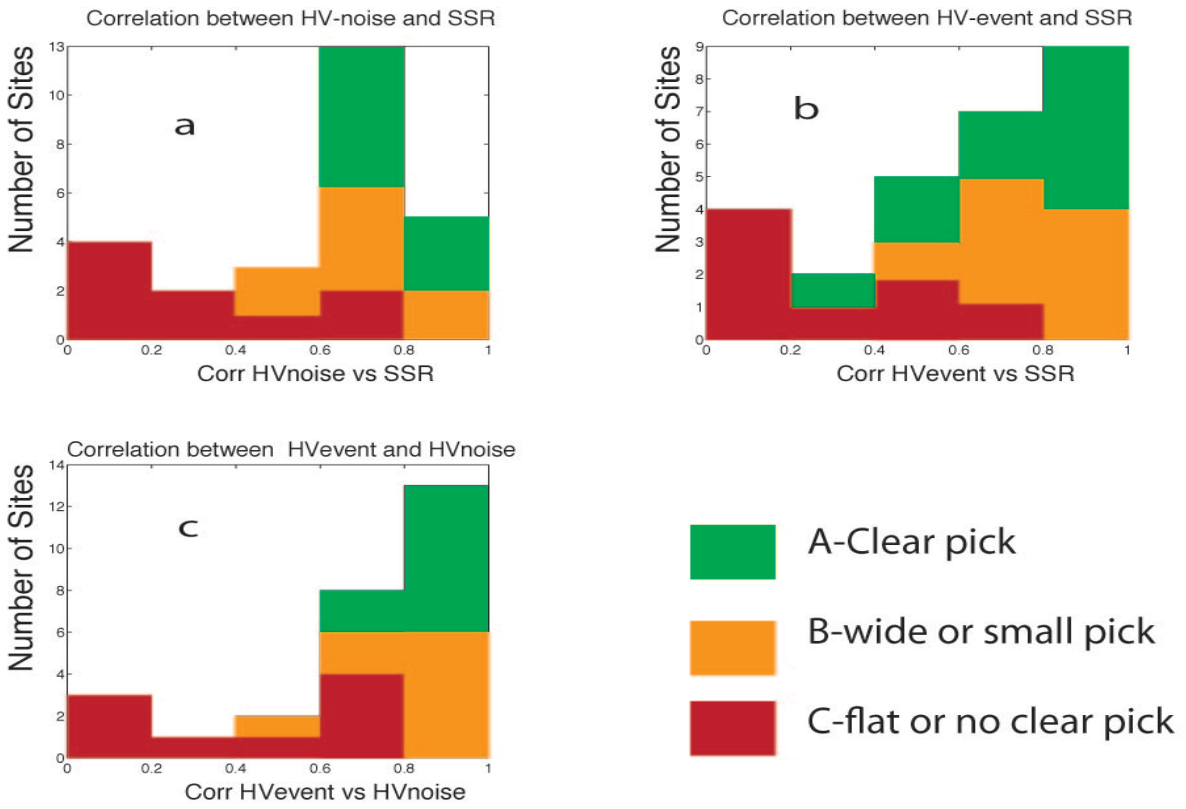

Figure 2.10: Correlation coefficient histogram. a) between HV noise and SSR; b) between HV event and SSR; c) between HV event and HV noise. The class of the peak indicated corresponds always to the HV noise peak.

I plotted obtained peak frequency value with SSR against HV noise or HV event (Figure 2.11). The graph shows that, when site has clear peak (A and B) then estimated amplified peak frequency are in very good agreement.

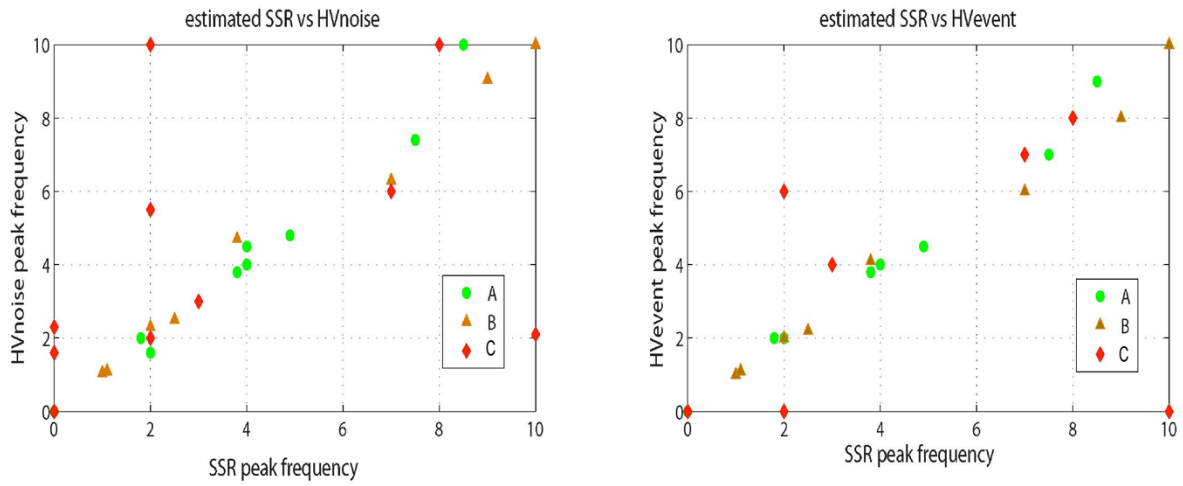

Figure. 2.11: Peak frequency estimated by HV-noise, HV-event, and SSR gives same results when the peaks are classified A or B.

In conclusion, when the peaks are clear, even small or wide (class A or B), we observe with that the ratio curve and the amplified peak frequency values obtained either from HV noise, HV event or SSR (for weak motion events) are similar. The site effect amplified frequency can be studied and give similar results with different methods at least when they are based on weak motion.

These obtained results suggest that we can infer the HV pick as a fundamental frequency when HV ratio has clear or wide peak.

2.3.4 HV ratio analysis on noise recorded during short time measurements

In previous part, I concluded that SSR, HV event and HV noise procedures give the same result for the amplified frequency. Then, I can consider that we can use the HV noise ratio to estimate the amplified frequency at a site where we could only install the station for short time and then record only noise. This will highly increase the number of site to attempt to make a zoning of amplified frequency for the Ulaanbaatar basin.

The HV noise ratios for short time microtremor measurements were done for 104 sites in the Ulaanbaatar area. At all sites, where microtremor were recorded, I give in the appendix Table A.1 the site location, duration of measurement, average amplitude of microtremor, classification of noise levels stability and distortion, classification of the HV noise peak and amplified frequencies.

Observed HV noise spectral ratios give at most sites expected amplified frequencies considering the thickness of the sediments (see chapter 1, figure 2.1) and using the simple relationship $f0=Vs/4h$.[SESAME, 2004] except at few points (3-16, 3-17, 3-18, 3-19 etc. see table A1). For this relationship, I used an average shear wave velocity of 550m/s (See chapter 3 for its estimation).

At some sites, HV noise spectral ratios show a more or less flat curve but the amplitude of the curve is high at all frequencies, which means that the horizontal component noise is always bigger than vertical. Back to the noise records we see that, at these sites, microtremor has higher amplitude than at other measured sites. Those high noise sources might be water pipeline, water Stream of Tuul River or most probably wind noise.

For the impact of the noise level on the results, as an example I show the analysis on noise recorded at the site 14 (figure 2.12). The upper part shows 3 different times: 6h, 8h and 20h by UTC time which is equal to (+6h for local time at 11.Feb.01) 12h, 14h and 02h (12 Feb.) local time. I show the microtremor records and at its right the HV spectral ratio. We compare HV for low noise period with HV for higher noise period. When noise average amplitude is increasing up to 4000 nm, HV spectral ratio peak is shifted to higher frequency, HV ratio amplitude decreases from 7 to 1.2 and wider frequency peak. When noise maximum amplitude level is about 1000 nm, then HV ratio is similar then for low noise data, but with a lower amplitude factor, about 2.5. This example shows that when the noise level is too high and the signal is distorted by local noise (many peaks at high frequency) HV ratio gives wider frequency peak and a shift in frequency that could induce unreliable conclusions. Therefore to consider the quality of the dataset, I made a classification of the microtremor relative to its amplitude and distortion level (Appendix A.1).

Nevertheless, at few sites located over the thickest part of the basin and with high noise level (> 1000 nm), the HV ratio gives clear peak with a frequency in good agreement with the sediment thickness and the shear wave velocity. (Shear wave velocity is obtained by FK analysis that will be detailed in the chapter 3). Perhaps, in that case, the noise source

could have other characteristics less unfavourable. These observations show the importance to observe, detect and search possible noise sources during the measurement time and to note them carefully in the field book. If noisy sources are detected, we should delay and/or prolongate the measurements.

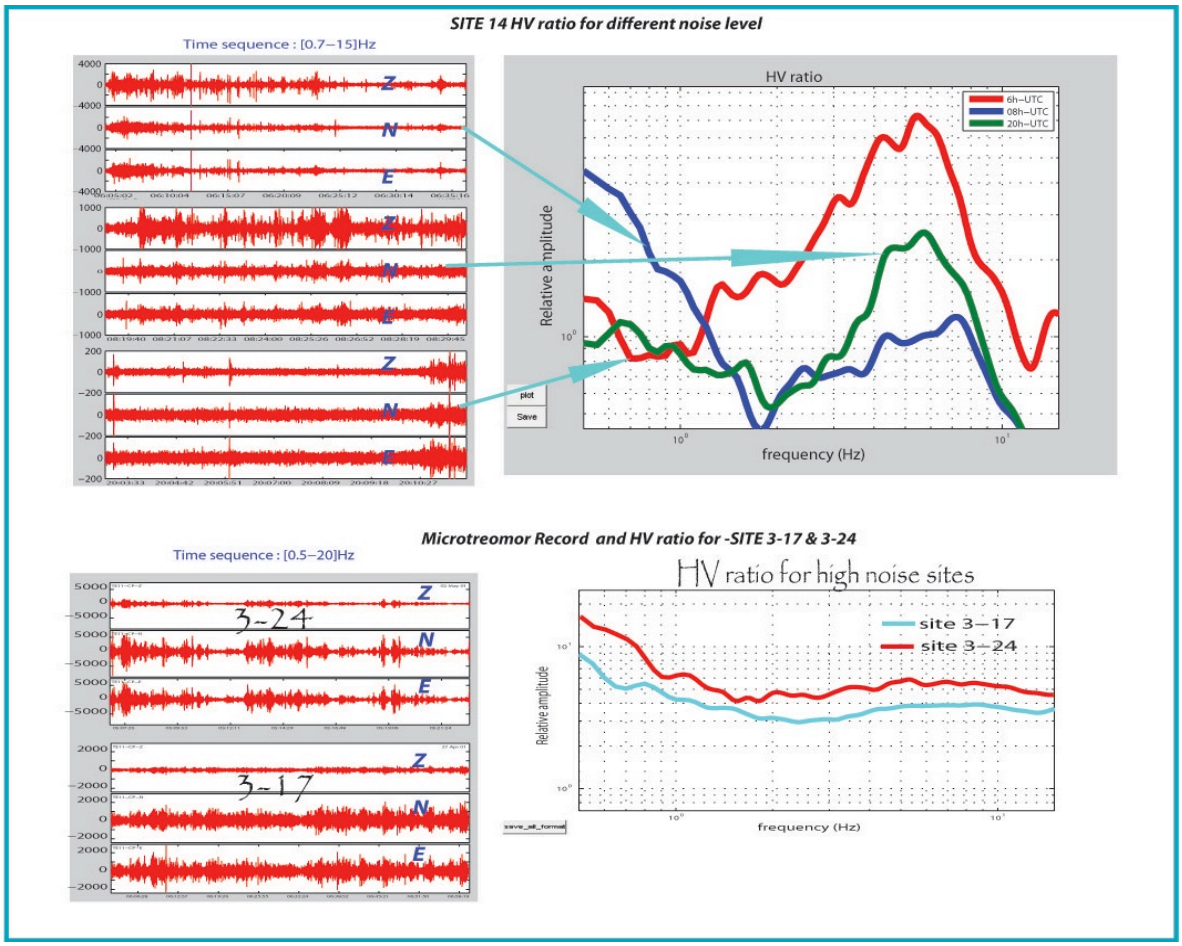

Figure 2.12: An example of the HV ratios for site 14. Upper: the HV ratio of the site 14 for low (red), high (green) and very high (blue) noisy time. Down: the HV result of some sites, which have high noise level.

Data qualification of HV noise record: We lost 5 sites, on the 104 sites, where data have not been recorded or where the sensors device was not correctly connected. For the remaining 99 points, I made a classification using the distortion level and the average amplitude of microtremor that were used for HV ratio analysis. The HV ratio curves are then classified by their topology of the spectral curves (see previous part): A, B and C. (appendix A Table A.1.). From it, I selected which signals, and then related site, I will use for the HV

amplified frequency. Finally, from the total microtremor, 50 % of sites were classified as Low, 35% as middle and 15% as high noise level. This 15% of sites have very high amplitude (more than 1000nm) and their HV ratio gives a more or less flat response. Those points were not used.

Also, in addition to HV analysis, I calculated the Fourier spectrum of each component in order to identify potential artificial noise picks. At most of the sites, I observed a very narrow pick at 10 Hz. This 10 Hz pick, observed over a large part of the Ulaanbaatar basin, is increasing when station is located closer to the power plant IV. Another example: at site 29, HV noise ratio shows amplification at 2, 8 and 10 Hz. After plotting the Fourier spectrum I discovered that 8 and 10 Hz frequencies are due to some artificial noise (figure 2.13). These peaks disappeared or decreased when I applied SSR analysis on weak motion records.

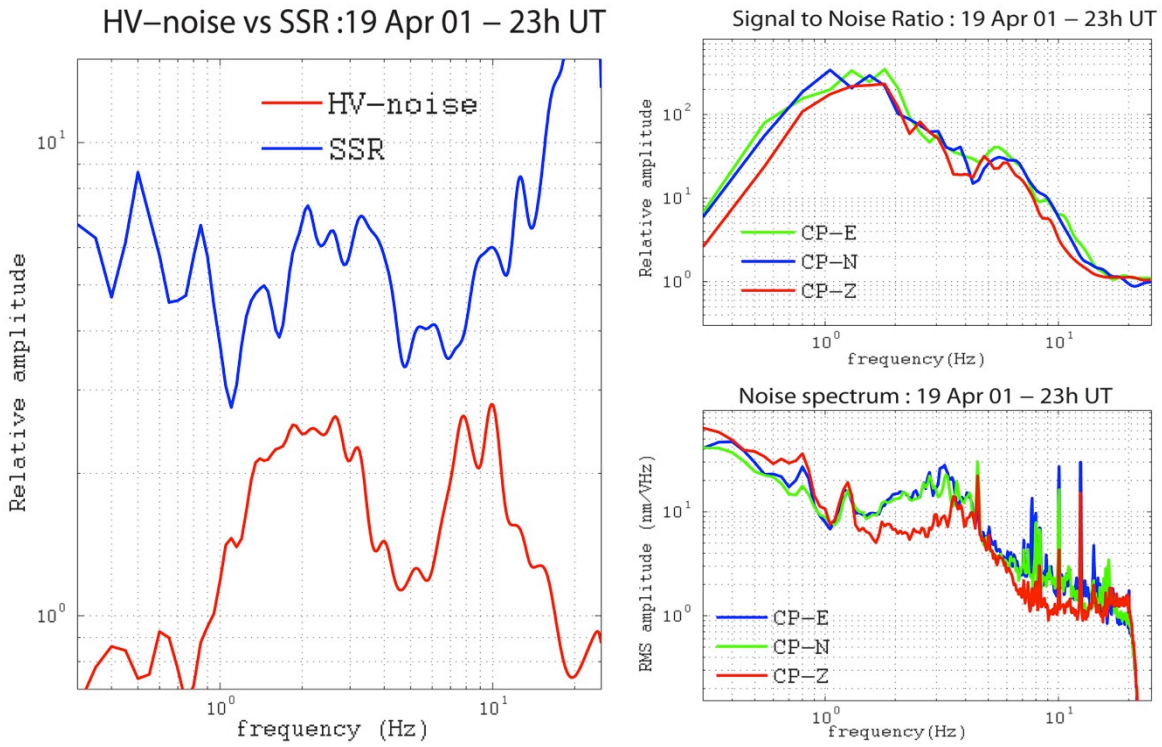

Figure 2.13: Example SSR and HV-noise at the site 29 with it's SNR and noise Fourier spectrum.

2.4 HV stability in time

In most analysis of HV ratio, we did microtremor records of 30 minutes during daytime. The short record duration make these measurements easy to do in an urban area but it does not allow identifying disturbance along time. Therefore, in order to study the possible impact of the time period of measurements to the HV ratio, I selected 24 hours of recording from long time measured sites.

The figure 2.14 shows five selected sites for the analysis of the variation of the HV ratio with time (24 hours). Site 3 was located at the east part of the city and 50 meter away from main road. Site 11 was located in the eastern part of the basin, where the human activity is low. Site 14 was located 150 m away from main market of Ulaanbaatar city, where there is a very high human activity during daytime (Market for food, clothes with many heavy car or truck traffic). Site 29 was located 150 m from a heavy gravel sorter machine that is working only during daytime. Site 27 was located 800 m away from main power plant IV.

Figure 2.14: Sites locations and their closest noise sources. Green rectangles are zoom on the site area.

After the selection of one-day record, I calculated the HV ratio at each hour by using the lowest noise part of the microtremor record. Then I plot the results on a graph showing frequency versus time, and with colour for the HV ratio amplitudes (figure 2.15).

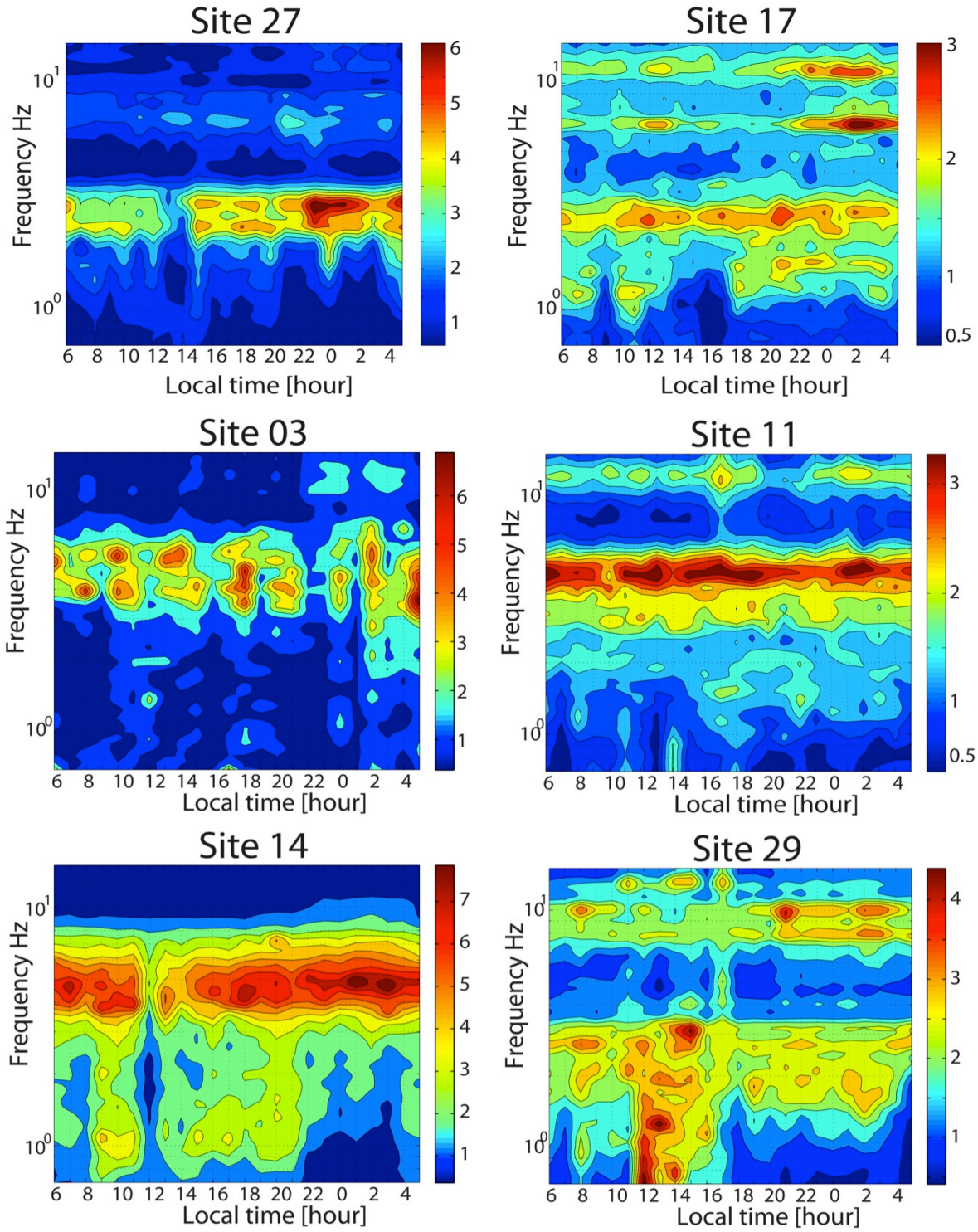

Figure 2.15: HV ratio variation along a day (ratio calculated at each hour): Colour bar indicates amplitude of HV ratio.

Amplified frequency:

At most studied sites, the main amplified frequencies were observed over all the day, including sites located near main road, power plant and market places (site 3, site 27, site 14). The HV ratio main amplified frequencies in this area are independent from the time of records in the day.

On site 14 (close to market area) during market's working time, the HV ratio peak is lower and wider and new small amplifications peaks appear at lower frequencies. In that case, the main peak, very clear, is not affected. The very low amplification value, at any frequency at 12h local time, is unexplained. In case of lower amplitude for the main peak, this others peaks could make difficult to estimate the amplified frequency.

In case of site 29, HV ratio peaks are wide in general and, when gravel sorter machinery is working (between 11h-17 h local time), amplified frequency peaks are extended to the lower frequency with high amplitude. During this time, 11 to 16 h local time, the most amplified frequency appears to be at lower frequency than at quiet time. At some specific hours (22 to 4 h local time), an important peak appears at about 10Hz. In that case, the environment around the site (power plant) influences directly the value of the observed main peak.

Amplification factor:

We see quite always that the amplitude of HV noise ratio varies over the time. As example for the site 3 (at 22h local time) and site 27 (at 13h local time) the amplitude of the main amplified frequency decreased strongly down to 2-3 and then the frequency of the peak is more difficult to identify. For site 27, the HV ratio amplitude peak is increasing up to 6 during night time and is decreasing during day time down to 4 or even 2. The amplification value deduced from HV noise ratio varies strongly along the day. If we compare maximum HV ratio amplitude during quite time with SSR, HV ratio always gives smaller amplification (Figure 2.23).

Ulaanbaatar specific noise at 10Hz:

The noise observed at 10 Hz influences the HV ratio curve of sites with low noise or with small HV ratio peak amplitude (site 17, site 11, site 29). But when HV ratio peak is

high or when the site has globally a high noise; this 10Hz frequency peak is hided by the value of the HV ratio main peaks. On the power spectrum of site 29 and 14 (figure 2.16), for night time, we can see the peak at 10Hz (important at site 29 and lower at site 14) and 8Hz (site 29) but they "disappear" at daytime when the noise level is higher. Nevertheless, this 10 Hz frequency induces a peak on HV ratio all over the day but with lower amplitude during daytime (figure 2.15).

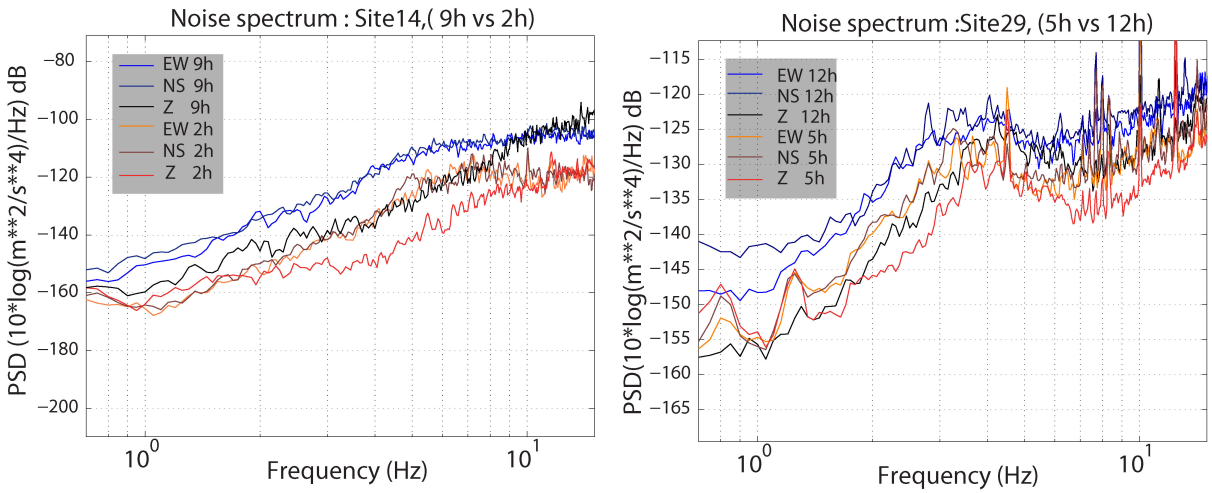

Figure 2.16: Day and night time Power spectrum at site 14 and site 29.

The site 27 was closer than site 29 to Power plant but the amplitude of the amplified frequency peak was always higher than this 8 to 10Hz peak.

Consequently, HV ratios main amplified frequencies are most of the time clearly observable during all the day except if the site is very close to high level noise sources (up to few hundred meters).

Conclusions:

- The main amplified frequencies deduced from HV noise ratio are independent from the time of records in the day.
- New amplified frequencies can appear due to local disturbances, which could influence the result or make difficult to see the main amplified frequency.
- The environment around the site can directly influence the frequency of the observed main peak (with the higher amplification factor).

- The amplification value deduced from HV noise ratio cannot be considered as a permanent characteristic of the studied site.
- The noise influences mainly the HV noise ratio curve for sites characterised by low noise or by small HV ratio peak amplitude.
- Noise generated by human activity, like market, car parking, etc. could widen HV ratio peaks.

2.5 HV ratio variation with the azimuth.

Due to basin shape, the noise wave field could vary with the azimuth and then influence the HV spectral ratio. To check it, I analysed the variation of HV ratio with azimuth. For this analysis, horizontal components were constructed each 10-degree step (only from 0 to 180 degree, the 180 to 360 is symmetric) from the original EW and NS components. Then HV ratio results are plotted on a graph azimuth versus frequency with a colour scale for the amplitude of HV ratio (figure 2.17). In the graph, 0 degree corresponds to the North-South direction and 90 degree corresponds to the East-West direction.

At the site 11, plotted as example in figure 2.17, the HV ratio for different azimuth shows the same main frequencies but with different amplitude. This is observed at most sites.

If we look at the main amplified frequency in this figure, its amplitude factor varies with azimuths (around 3.4 for 160 degree but only 2.8 for 40 degree). This means that the amplified frequency signal is maximum at a particular direction and then polarized. This amplified frequency polarization might occurred due to basin structure or noise source itself. But the polarization direction was variable site-to-site therefore they are no simple relation with the main trend of the basin.

We see that some secondary amplified frequency appears and disappears with azimuth as at 50 degrees (small peak at 2Hz) or as at 0 degree (clear peak at about 12 Hz). On the other hand, if we look at 40 degrees, the main amplified frequency has an amplitude of 2.8 at 5 Hz and 2.2 at 12 Hz.

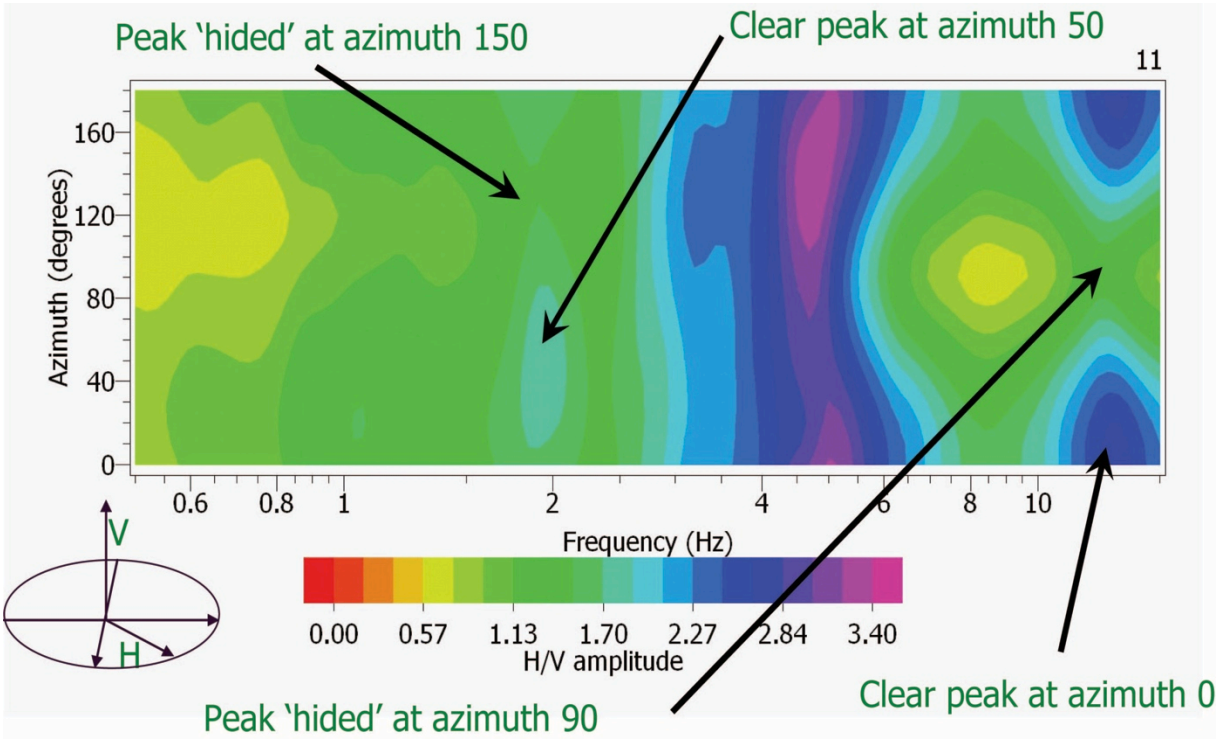

Figure 2.17: HV azimuth calculation. H- is constructed horizontal component from EW and NS direction noise record.

We saw previously that the amplitude of the amplified frequency vary during the day but also with the azimuth. Now I will analyse the variation of this polarization azimuth during the day. To check this polarization stability in time, I constructed HV polarizations compass graph that is shown in figure 2.18 for the case of the site 29.

In the graph (figure 2.18), red dot lines are indicating the polarization of the maximum amplification factor at the amplified frequency of HV ratio. Polarization compass of amplified frequency is calculated using ±0.5 Hz range from maximum amplified frequency (between A and B). HV ratio maximum is, in this case, polarized in 135 degrees azimuth at 2.7 Hz. This polarization direction was close to the 10 Hz noise polarization which was generated by the Power plant IV. I observed that this polarization was variable site to site.

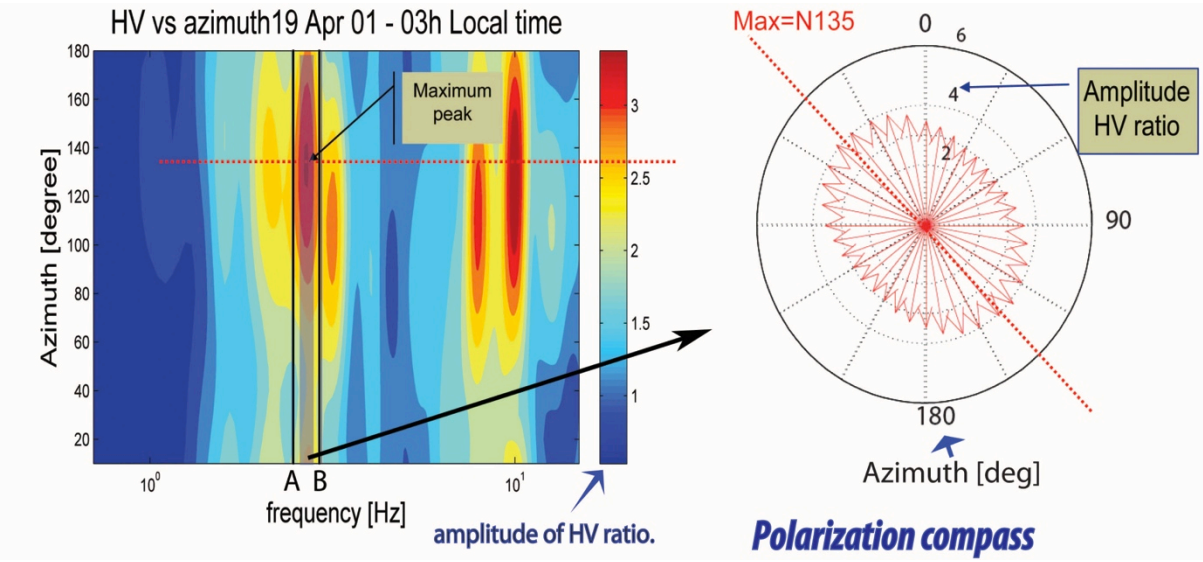

Figure 2.18: Polarization compass of amplified frequency at the site 29. Maximum amplitude of amplified frequency is indicated by red dashed line on both figures. Shadow zones indicate the frequency range on which the azimuth of the maximum amplification is calculated.

I observed at several sites that this polarization direction is stable during daytime but that this polarization varies during the night time. At other sites, this polarization seems to be stable during night time but varies, apparently randomly, in day time. These observations suggest me that the observed polarization depends on noise source itself rather than basin structure. For example, at sites 15, 14, 16 and 17, polarization of amplified frequency was stable during daytime. These sites were close to the "black market", which operates only during daytime. This market is the biggest one in the country, the place is highly congested and there are many trucks coming from and leaving to the countryside. There is also a car spare parts market next to this black market. As an example, 24 hours polarization analysis of sites 14 and 15 are shown in figure 2.19. In polarization figures, UTC hours were converted to local time, which is UTC time + 8 hours in winter. In the figure 2.19, blue colour compasses correspond to operating time of the black market which is located approximately 250 m from site 14 and 1 km from site 15 (see figure 2.20). The polarization at each site was stable for day time (blue compasses).

Then I apply the same procedure for sites around Power plant IV (biggest Power plant in the city with 3x100 MW steam turbine generators) and gravel machinery, respectively site 27 and 29, (see location in figure 2.2).

It is clearly observed at site 27 that polarization was stable during whole day and its direction was approximately perpendicular to the Power plant IV direction.

For site 29, we know that the local noise source (gravel sorter machine) is located at 150 meters and that the machinery was working only during short time (12h-15h local time). It is also observed at the site 29, during operation of this heavy machinery, that the polarization was directed perpendicular to the machine direction (100 degrees) despite during night time (23h-10h local time) the polarization was stable but approximately directed to the azimuth of 135 degree. This amplified frequency polarization (135 degree) direction is nearly perpendicular to Power plant IV direction. Notice that at 10 Hz, we can detect in the entire basin the noise from power plant IV. This 10 Hz is very clearly observed at site 29 and its polarization direction (135 degrees) is almost the same as the polarization direction of the main amplified frequency of the site (at 2 to 3 Hz) that we can observed during night time (Figure 2.20).

For the market, as its area occupied a large territory, it is difficult to consider a precise direction. For example, the azimuth between the site 14, located 250 meter away from market, and the market varies from 120 to 250 degrees. (Figure 2.21)

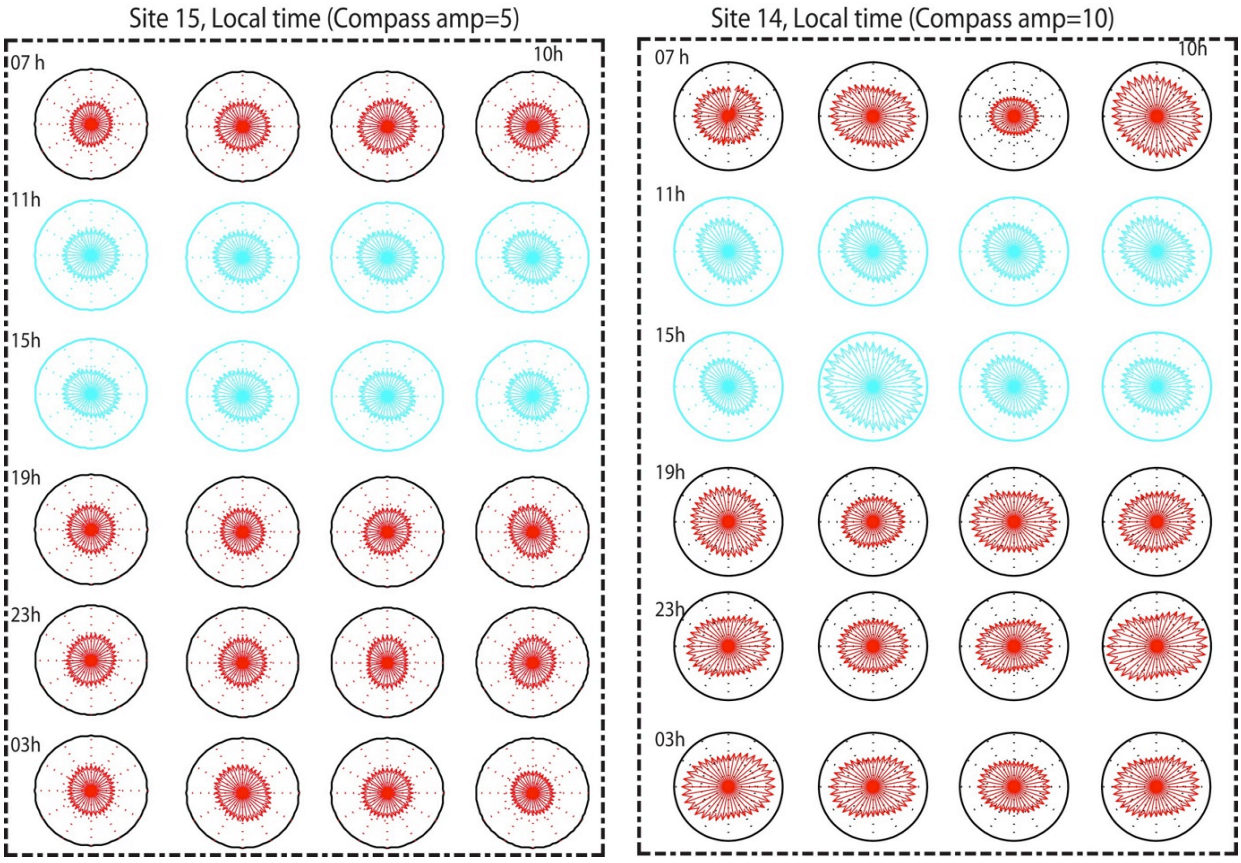

Figure 2.19: Amplified frequencies HV polarization calculated each hour during 24 hours for sites 14 and 15. For site 14, circles radius represents HV amplitude of 10 despite for site15 circle radius indicates amplitude of 5.

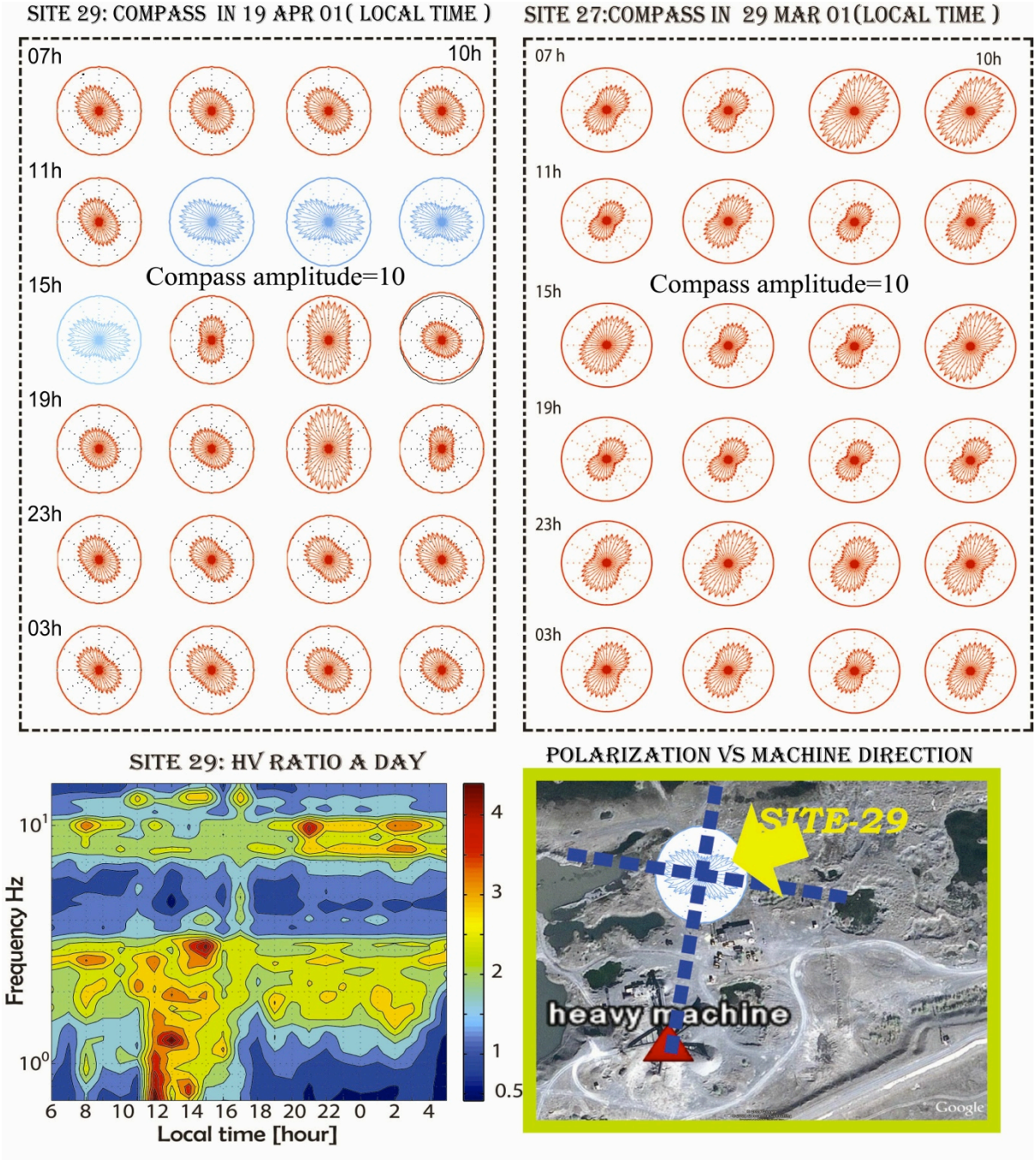

Figure 2.20: HV frequencies polarization analysis for site 29 and site 27. Down left: 24 hour HV ratio analysis for site 29. Down right: location of heavy machinery and Site 29. Blue dashed line represents polarization during machinery working time.

A synthesis of the polarization compasses are represented in the figure 2.21, which includes Power plant IV and black market area. Estimated azimuth, distances between site and assumed main noise sources are presented in table 2.3. I must mention here, that during the temporary seismic station survey, the direction of seismometer was adjusted using hand compass and it might be associated with an uncertainty of few degrees.

Power plant generated a noise during whole day, and it dominates during nighttime. The black market is operating only during day time. Therefore in the map, amplified frequency polarization of stations deployed around Market area is drawn for daytime (14 h local time), and near Power plant IV the sites polarization compass is drawn as night time (2h local time). In the figure 2.21, grey colour compasses represent daytime polarizations and red colour compasses represent night time polarization. Around market place, at sites 14, 15 and 16, the azimuth of the polarizations is stable during daytime. Notice that the 2-17, 2-21 and 4-14 sites were measured only for short time during day. For sites 24 and 27, near the power plant IV, the polarization is always in the same direction.

Polarization directions at all these sites are approximately perpendicular to the local high source noise directions. Consequently, HV azimuth analysis shows that HV ratio's amplified frequencies are not depending from azimuth but their amplification factors varies with the azimuth. I did not observe a clear correlation between HV ratio azimuths and the basin main trends. But near to strong noise source, the HV ratio's polarization azimuth is pointing to specific directions; its direction is perpendicular to the source directions.

If we assume that most of the noise is mainly generated by the power plant or the market place in the Ulaanbaatar basin, then the noise source is inside the basin and the highest pick of HV ratio are related to horizontal waves. Therefore, in Ulaanbaatar basin, the SH wave or/and Love wave are dominating in the wave field near particular sources. Moreover recent studies show that most energy, at least 50%, in noise wave field is propagated by Love waves [Bonnefoy et al., 2006]. But to answer the question of the origin of HV noise ratio peak frequency, we need a careful and precise study using 3C sensor array in order to derive the proportion between Rayleigh and Love waves.

Table 2.3. Most known Noise source azimuth and distance from studied sites

Site number	Power plant			Site number	Market		
	Θ	Δ	Ω		Θ	Δ	Ω
Site-29	60	3.9	50	Site-14	200	0.25	220
Site-20	-55	3.1	-60	Site-16	-90	0.5	-30
Site-27	120	0.8	120	Site-15	0	1	25

Site-4-14	23	1.4	25	Site-2-17	60	0.55	55
Site-24	100	2.0	125	Site-2-21	-175	0.9	165

Θ – Azimuth site to source, Δ-distance between site to source in km, Ω – azimuth (perpendicular to polarization direction). Notice that site 29 is also near to the gravel sorter machine, (distance = 150m , Θ= 200 , Ω=200).

Figure 2.21: HV ratio polarization and known noise sources. Red polarization represents the night time and grey polarization indicates day time polarization. Down side zoomed area for blue and red squares.

2.6 Result and discussion

I applied SSR and HV ratio at 32 sites, deployed across Ulaanbaatar basin during long time, using weak motion and ambient noise records. With the event recorded simultaneously at rock and sediment sites, the spectral ratio analysis shows that, on the Ulaanbaatar basin, certain frequencies are clearly amplified.

I found that there is no significant difference to estimate amplified frequencies using either SSR or HV noise or HV event spectral ratio techniques (Figure 2.9 - correlation analysis; figure-2.10 comparison of amplified frequencies obtained with different methods; appendix –A: SSR, HV event and HV noise comparison results). The correlation coefficients between HV noise and HV event curves are higher than between SSR and HV. The reason might be that HV ratio mainly incorporates 1D amplification beside site-to-bedrock (SSR) spectral ratio incorporates 1D and all the 2D/3D site effects [Cornou and Bard, 2003].

In the spectral ratio analysis, I observed an important difference between HV and SSR ratio amplitude factor values (Figure 2.23). At most of the sites, SSR method gives higher value than HV ratio's amplitude. I demonstrated or confirmed that the HV ratio amplitude factor is dependent of many parameters such as global noise level, azimuth with local strong noise source inducing variation between day and night time. The HV noise ratio should not be used for estimating amplification factor.

With weak motion records and using SSR, the amplification at sediment is between 2 to 10 (Table 2.2, Figure 2.24). Nevertheless, the site amplification is correlated not only with the soil thickness but also soil conditions, such as shear modules, damping and density. Moreover, it is highly dependent on nonlinearity of soil properties at soft soil sites, thereby; during strong earthquake the amplification factors can be very different than what we observe with weak motion. Therefore, to estimate the potential amplification factor for strong motion due to Ulaanbaatar basin, which is a complicated problem, we need other specific studies. One way is to model stronger motion, which I will apply in the next chapter, for example by estimating the PGA by shake91 using 0.1g normalized seismic waves.

Prior to my estimation of HV ratio's amplified frequencies, I had attempted to qualify the quality of the recorded data and check the HV ratio stability for Ulaanbaatar basin. I found that HV ratio curve is not stable, when noise level is more than 1000 nm for Ulaanbaatar basin case. Therefore for final HV analysis, I used ambient noise that has amplitude less than 1000 nm. A histogram of amplified frequencies, estimated at the site used in this study, shows mainly frequencies in the range 2 to 4 Hz. This histogram is of

course highly dependent on the spatial distribution of the sites (figure 2.25) and do not represent the distribution along Ulaanbaatar.

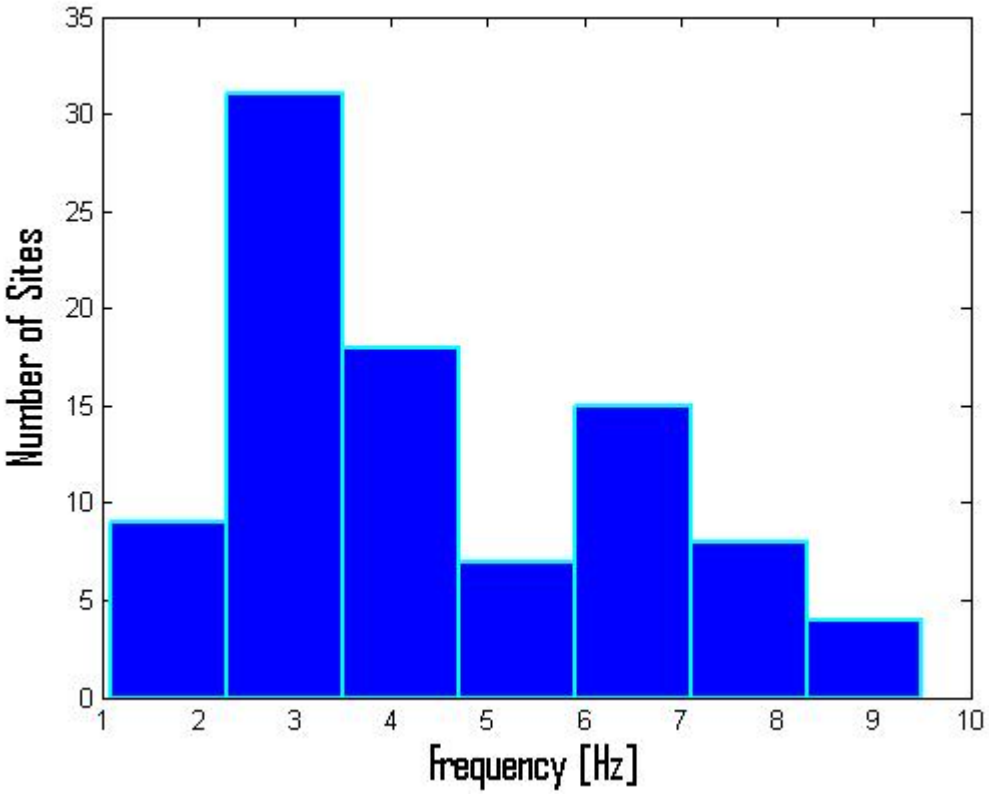

Figure 2.22: Ulaanbaatar basin amplified frequency distribution at our measured sites.

For long time measured sites, I applied HV ratio each hour over 24 hours in order to verify the stability of HV ratio with time. This analysis shows that HV ratio amplified frequency on noise is stable during day and during night time for most sites. But HV ratio was not stable when the site is located very close to strong sources, like heavy machinery or power plant or high human activity. Then I observed that the amplified peak is shifted to the low frequencies in our case. Also when noise level increased, the HV ratio peak is widening (figure 2.15).

I analysed the impact of the azimuth variation of the horizontal component on the HV noise ratio curve. It shows that HV ratio amplified frequencies does not depend on the horizontal component azimuth but the amplitude of the peak varies. Thus, the azimuth of the maximum amplitude of the peak characterizes a “sites polarization” of the amplitude of the

amplified frequency. To detect if this polarization is stable and related to a site or basin, characteristics, long-term measurement were used to observe its stability over a full day. I observed several periods of time with different polarization but during which the polarization was stable. This amplified frequencies HV ratio is polarized perpendicular to the direction from station to the main source of noise. Therefore, we can conclude that mainly Love or SH waves are dominating in the noise wave field at Ulaanbaatar basin. This shows that the very common assumption that almost all the ambient noise energy would be carried by the fundamental-mode Rayleigh waves is not in agreement with our observation for the Ulaanbaatar basin case [Fah et al., 2001].

Consequently, estimated amplified frequency map has been produced and is illustrated in the figure 2.25. Estimated amplified frequency based on recordings has a quite good agreement with sediment thickness distribution map.

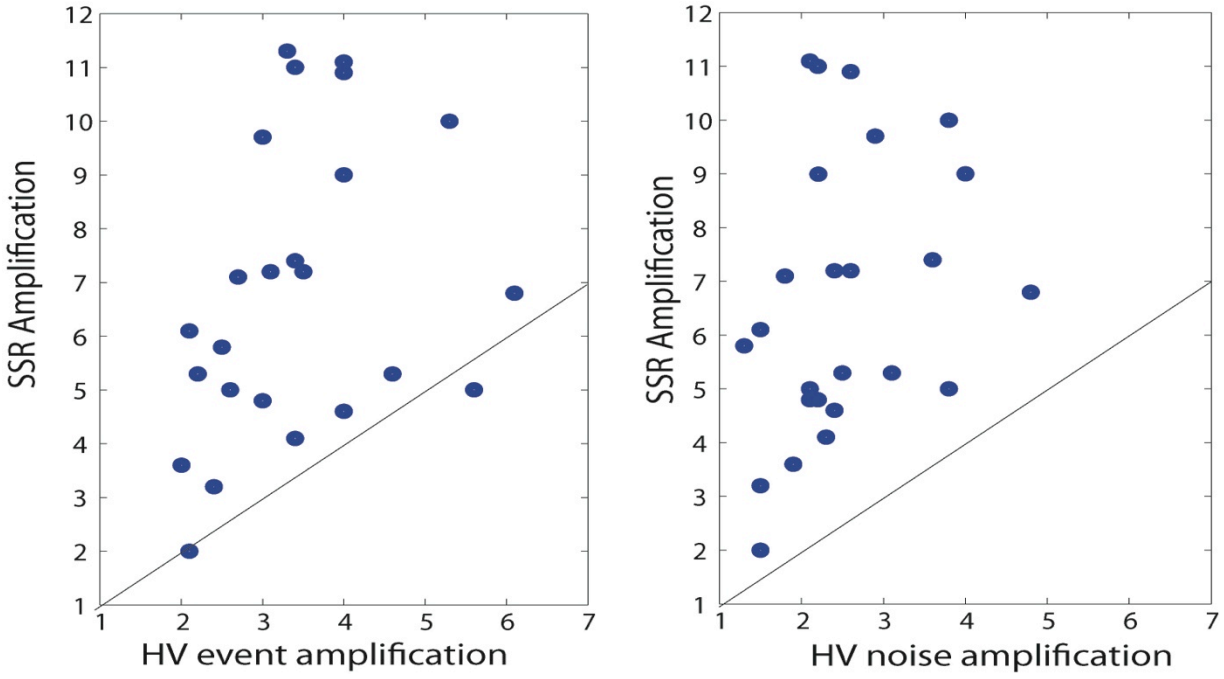

Figure 2.23: Comparison amplification factor estimated by different spectral ratio techniques

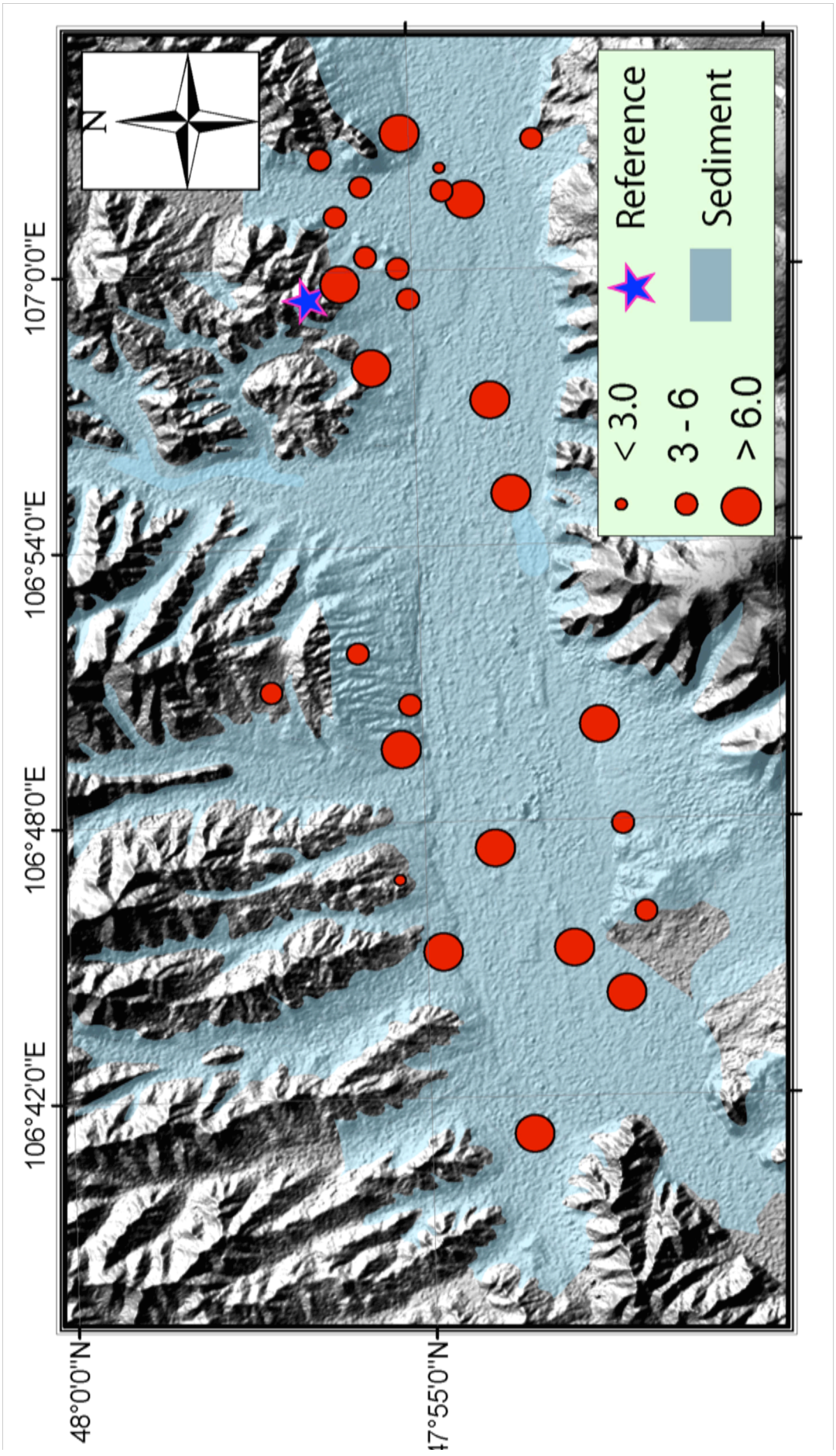

Figure 2.24: Amplification factor estimated from SSR technique.

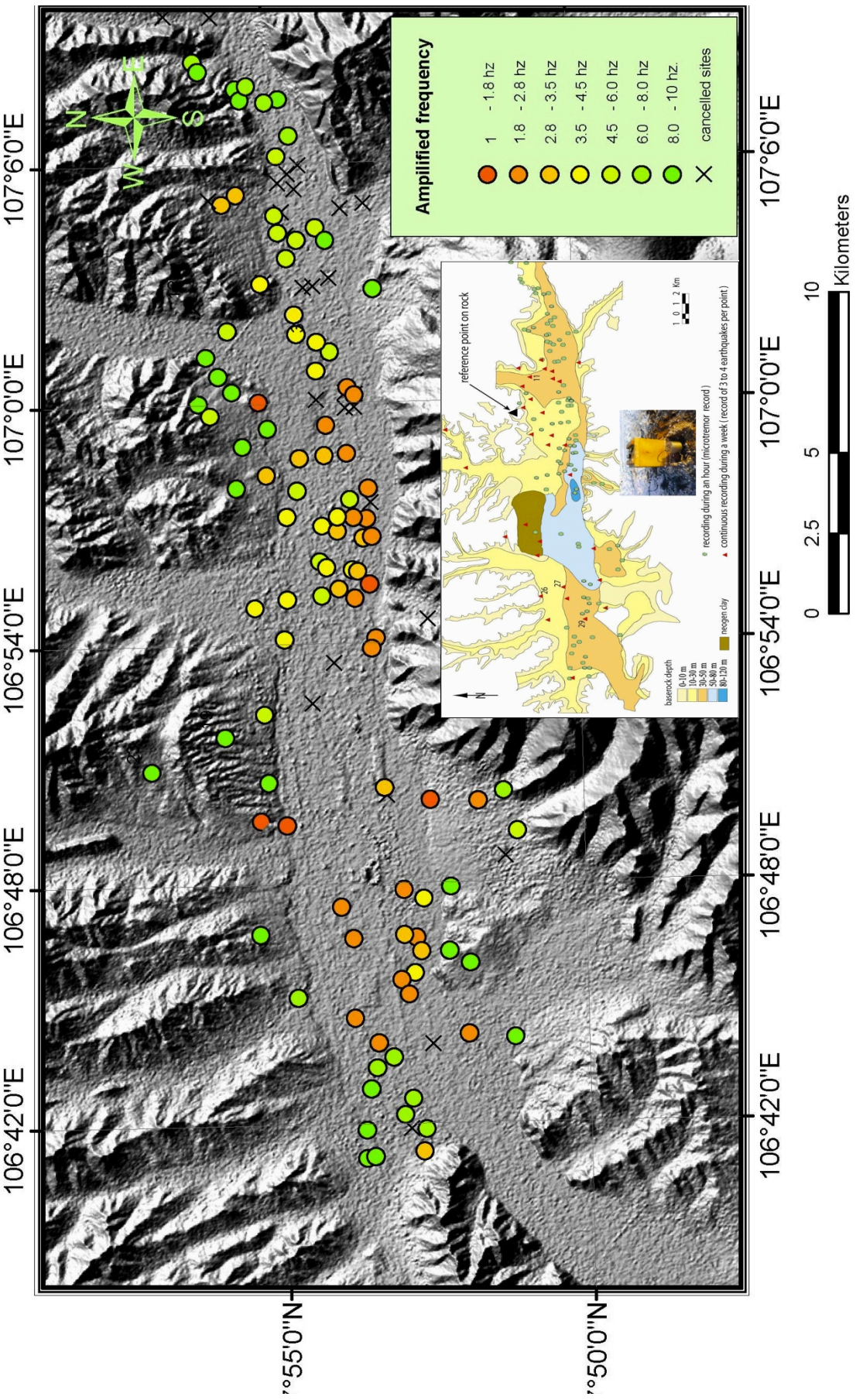

Figure 2.25: HV peak frequency distribution across Ulaanbaatar basin

CHAPTER III:

3D Model of Ulaanbaatar Basin

And

1D, 2D Seismic Waves Simulations

3. 3D ULAANBAATAR BASIN MODEL AND 1D, 2D SEISMIC WAVES SIMULATIONS

3.1 Introduction

The fast development of computer science brings a possibility to numerically simulate the environment, as well as a great opportunity, for geophysical scientists, to better understand complicated physical processes of earth. In last years, many numerical codes have been developed for seismic wave propagation in 2D and 3D basin. The simulated ground motions helps to better understand the waves propagation phenomena through a basin and better predict the ground motion in a region [Bard and Bouchon, 1980 a,b]. Many basins have been modelled as for example: Volvi basin in Greece [Semblat et al., 2005], Greate Kanto basin [Koketsu et al., 2009], Santa Clara Valley [Hartzell et al., 2006]. They conclude that the response of a basin strongly depends on its properties, such as impedance contrast, wave velocities and geometry.

In the previous chapter I discussed the seismic wave response of the Ulaanbaatar basin based on microtremor and weak motion records. We will now process simulations in order to estimate the site effects all over the Ulaanbaatar basin and to improve our understanding of the origin of these site effects at Ulaanbaatar. For that, first I need to

characterize the physical parameters of the basin necessary for the simulations such as its 3D geometry and its S wave velocity.

I created a database in a GIS (Geographical Information System) to combine available information from the Ulaanbaatar basin, including existing geophysical and geological investigations and studies, basin thickness, gravity map and drilling information. I compiled all available data collected by various organizations at Ulaanbaatar. Based on obtained data, I built a preliminary 3D geometry model of the Ulaanbaatar sedimentary basin for the ground surface and the sediment - base-rock interface. I also attempted to determine the seismic shear wave velocity at 3 different sites in the basin using microtremor array analysis. Then I estimated 1D and 2D seismic wave response of basin using respectively shake91 [IDRISS and SUN, 1992] and Mak2D [Mariotti C., 2007] scripts. At the end of the chapter, I compare the obtained results with the SSR and HV ratio calculated using field records.

3.2 3D model of the Ulaanbaatar basin

GIS database and data selection for the interpolation:

To build a 3D digital model of Ulaanbaatar basin, I included following information into a GIS database system with WGS 84 projection system:

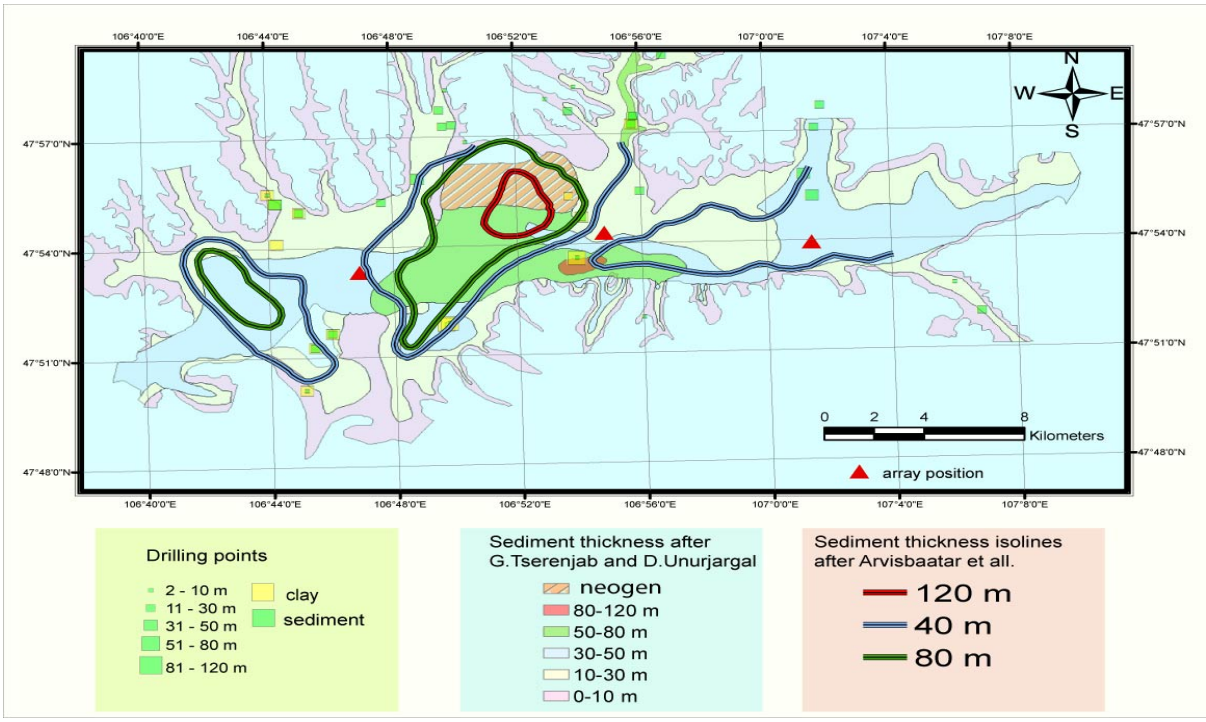

Figure 3.1: Map of compiled available information for estimating the sedimentary thickness of the Ulaanbaatar basin.

Sediment thickness: For a previous seismic hazard analysis of Ulaanbaatar (Dugarmaa et al., 2006), two hydrogeologists, G. Tserenjab and D. Unurjargal, give a general view of the sediment thickness for the Ulaanbaatar basin using existing drilling information. They divided the basin into 6 different sediment thickness classes (0-10m, 10-30m, 30-50m, 50-80m, 80-120m, and additionally a Neogene-clay class). According to this map, the thickest part is 120 m and is located at the southern part of the basin and the central north part where are thick Neogene deposits.

If we compare the depth obtained by the HV or SSR resonance frequency, deduced from field measurements, and the following simplified expression,

$$H=V/4*f \qquad (3.1)$$

with the thickness map, we see that at mots of the sites, they are in good agreement.

H - thickness of sediment,
V - average velocity (obtained by array measurements)
f – amplified frequency.

According to the map, the thickness of Noegene clay is unknown (no thickness specified) but Medvedev [1971] wrote that it is between 170 to 200 meters by using only one drilling. From gravity measurement, this area would have only 120 meters of sediment [Arvisbaatar et al., 1991]. It is difficult to understand how this thick clay was accumulated locally at the north part of the basin. With the data recorded at the clay sites and using SSR ratio, I obtained a wide range amplification around 1 Hz (sites 18, 19 and 21).

Seismic amplification frequency*:* They were obtained by HV and SSR methods (Chapter 2). The amplified frequencies could be used as depth information considering a average velocity and the formula 3.1. We did not use the deduced depth directly for the interpolation to build the 3D basin model itself due to the uncertainty on the velocity, but the information was used to control the result.

SRTM data of Ulaanbaatar: SRTM (Shuttle Radar Topography Mission) data has been used to get the topography. The ground resolution is 3” arc, which is approximately at

Ulaanbaatar 30 meters in latitude and 60 meters in longitude. Then, I converted depth (or thickness) into altitude for the sediment-rock interface.

Geological map: I used the geological map of Ulaanbaatar area, produced through "MAGICNET project" (2000) to introduce precise limits of the sedimentary basin (figure 1.3, chapter 1).

Drilling data. A total of 300 drillings were collected and included in the GIS. Most of them were "old" (1930-1990) and the associated geographical locations were some times dubious. Several name of the drilling site were totally incoherent with coordinates. Also hydrological companies, for the purpose of water level study, made most of drillings, therefore those drillings were superficial and most of them did not reach the base rock. Finally, for the interpolation, I selected only 54 drillings precisely located and associated with clear information ([JICA, 1995], and other resources).

Shear wave velocity model: The shear wave velocity profiles were determined by ambient noise array at 3 different sites in the basin. Details will be explained in the next part of this chapter.

Gravimetric data: Three different sediment thickness isolines (40 m, 80 m and 120 m) have been deduced from Gravity measurements at 128 points and mapped at 1/100000 scale [Arvisbaatar et al., 1991]. The thickest isoline, 120 m, is located at the north-central parts of the basin (Figure 3.1). These data are in agreement with the general trend of the sedimentary map [G.Tserenjab and D.Unurjargal, 2000] but with much less details. Comparing with the observed HV resonance frequency, I saw several incoherencies, therefore I decided to not include directly these thickness isolines for my interpretation.

Using these available data, 3D simplified basin geometry was derived in MATLAB environment by interpolating between the observations. The area covered is between latitude 47.8 N to 48.0 N and longitude 106.6275 E to 107.1685 E degrees, which cover about 900 square kilometres. The area is divided in 60x40 meter size grid, which represent 401x1131= nodes. The calculation is made at each node using a linear interpolation. The limit between sediment and rock was converted form "shape file" (ArcGis format) to "mat file" (Matlab)

and sampled with the same grid size. The interfaces inside the sedimentary deposit were not precise enough to consider them in the 3D model. Therefore, the 3D model includes the surface topography and the 3D geometry of the sediment-rock contact, representing 2 layers. (figure 3.2).

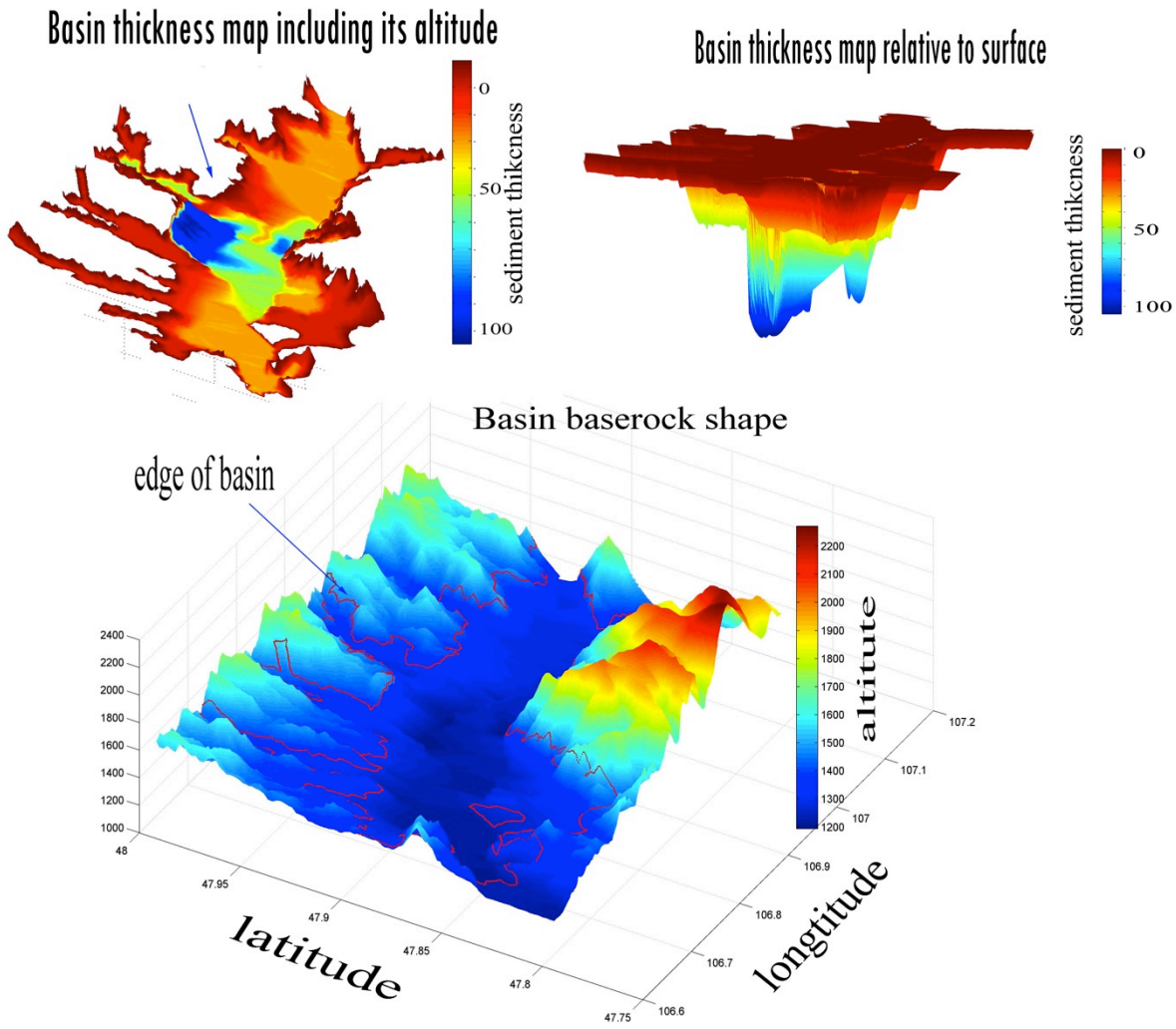

Figure 3.2: 3D geometry of Ulaanbaatar basin and its bedrock shape.

3.3 Exploration of Subsurface S-wave velocity by Microtremor Array technique at Ulaanbaatar basin

3.3.1 Introduction

The knowledge of the Shear wave velocity profile at a given site is a major issue in earthquake engineering and for the ground motion assessment. There are several kinds of geophysical techniques, such as logging, seismic refraction or reflection, microtremor array, which can be applied to estimate seismic velocity profiles. Among these methods, the velocity structure inversion, through microtremor array observation, is a cost effective method compared with other geophysical methods. The reasons are that it does not use any specific tools to generate a source necessary for reflection and refraction, any logging like for VSP (Vertical Seismic Profiling) exploration or for a simple S-P logging. On the other hand, this method is not sensitive to ambient noise perturbation, which is then appropriate for application in urbanized area. [Yamanaka, 1998]

To determine S-wave velocity structure, I applied the frequency-wavenumber (fk) array technique at 3 different sites on the basin. The method can be divided into 2 parts: the procedure deriving phase velocity dispersion curve from ambient vibration (or autocorrelation curve), and inversion of a dispersion curve to derive soil velocity profile.

The Frequency wavenumber Spectrum analysis was developed to detect earthquake with data contaminated by noise [Capon, 1969]. The method simultaneously calculates the power distributed among different wavenumbers and directions. Capon added a weighted factor for the contribution of each sensor used for the computation, which is called now “high-resolution fk array method” or just “Capon method”.

In general, the inversion of the dispersion curve is based on the numerical simulation of the surface wave propagation in a layered media. One of the common methods to calculate this dispersion curve is by using a propagation matrix technique [Haskell, 1954]. Then the S wave velocity profile is obtained by minimizing the misfit function between simulated and observed dispersion curves. In this study, I applied high-resolution fk analysis, implemented in “Geopsy” software, which was developed for site effect assessment using ambient excitations (SESAME project) [Wathelet et al, 2005; Ohrnberger, 2004].

3.3.2 Field survey

In 2008 May and 2009 July, I conducted field measurements at 3 different sites along the Ulaanbaatar basin. The central array was deployed at a site where new constructions are planed. At that place, a company did a drilling, which shows 29 meters of gravel and clay deposits.

For the first experiment I used ten STS2 stations with 24 bits digitizer. On the other two sites, I used two short period and 5 broadband stations. All the equipment's for the field surveys were provided by CEA/DASE.

Up to now, there are no general agreement on the optimum size of array and design for analysis using ambient noise records. There are several propositions for the selection of the array aperture. Tokimatsu [1997] proposed the following relationship, between minimum or maximum spacing sensor (D_{min}, D_{max}) and wave lengths studied (λ_{min}, λ_{max}), in order to get reliable results.

$$\lambda_{max} < 3D_{max} \qquad (3.2)$$

$$\lambda_{min} > 2D_{min} \qquad (3.3)$$

Considering these criteria and Ulaanbaatar basin sediment thickness, I have deployed a 100 m and a 50 m aperture array that allows studying wavelength between 28 to 300 meters and 14 to 150 meters respectively. The precise absolute time was based on a GPS receiver. The geographical positions of the sensors were determined with a differential GPS with a horizontal accuracy of about 20 cm. Before deploying the stations in the field, I made for each station a huddle test at the RCAG office in order to check the stations operating and characteristics. At the first experiment site (Amgalan) the geometry of the array consisted of 3 triangles, into each other, of a size of 100 m, 50 m and 25 m plus a central station. At the two other arrays, I deployed the stations with geometry of 3 triangles of 50, 25 and 12.5 m (figure 3.3). At the site 2 and 3, due to limited number of stations available, I built first an array with aperture of 25, 12.5 m + central station, which recorded microtremor during one day and then I change the geometry, keeping the 25 meters aperture stations and the central station at their positions and moving the stations from the small triangle (12.5m) to the 50 m

aperture triangle (in red in the table 3.1). This new geometry recorded again microtremor during one day.

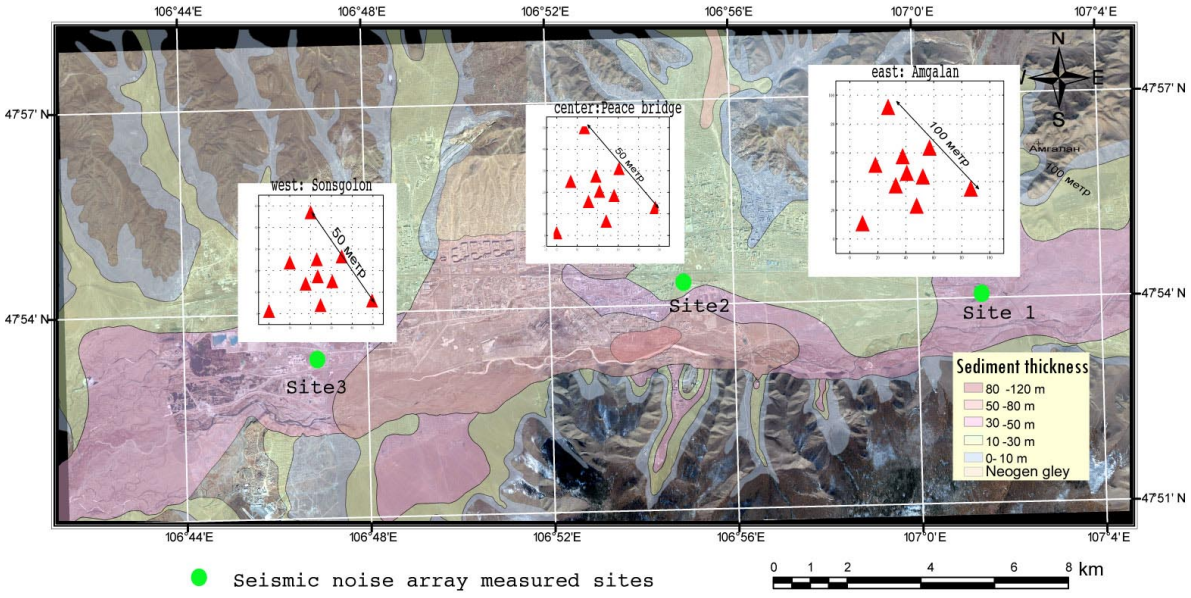

Figure 3.3: Sites of microtremor array measurements. The red triangles represent the stations and the arrays configuration. The green circles represent arrays positions.

The coordinates of each station in the array are presented in the table 3.1. Due to instabilities of the sensors and their sensitivity to humidity and temperature, I deployed the sensors and recorded the microtremor during a full day.

TABLE 3.1 array stations coordinates.

East: Amgalan area

point number	Lat N	Lon E	Alt (m)	Sta name	Start time (UT)	Stop time (UT)
p1-100	47.89934398	107.023712	1271	S100	2008.06.25 01h	2008.06.26 05h
p2-101	47.90022022	107.0240145	1272	S200	2008.06.25 01h	2008.06.26 05h
p3-104	47.89960531	107.0249925	1273	S300	2008.06.25 01h	2008.06.26 05h
p1-52	47.89991363	107.0245049	1273	ST50	2008.06.25 01h	2008.06.26 05h
p2-53	47.89978402	107.0238644	1271	S250	2008.06.25 01h	2008.06.26 05h
p3-52	47.8994763	107.0243522	1273	S350	2008.06.25 01h	2008.06.26 05h
p1-25	47.8996295	107.0241048	1273	S125	2008.06.25 01h	2008.06.26 05h

p2-26	47.89984853	107.0241863	1273	S225	2008.06.25 01h	2008.06.26 05h
p3-27	47.89969675	107.0244253	1273	S325	2008.06.25 01h	2008.06.26 05h
Center	47.8997228	107.0242357	1273	STTV	2008.06.25 01h	2008.06.26 05h

West: Sonsgolon area

point number	Lat N	Long E	Alt (meter)	Sta name	start time (UT)	stop time (UT)
2	47.88903896	106.781624	1263	UB6	2009.06.09 08h	2009.06.10 02h
3	47.88862745	106.7813554	1263	UB3	2009.06.09 08h	2009.06.10 02h
4	47.88867075	106.7820203	1263	UB9	2009.06.09 08h	2009.06.10 02h
5	47.88885487	106.7818242	1263	UB4	2009.06.08 08h	2009.06.10 02h
6	47.88882973	106.7814895	1263	UB8	2009.06.08 08h	2009.06.10 02h
7	47.88865173	106.7816879	1263	UB5	2009.06.08 08h	2009.06.10 02h
8	47.88875125	106.7817633	1263	UB9	2009.06.08 08h	2009.06.09 08h
9	47.88884314	106.7816636	1263	UB6	2009.06.08 08h	2009.06.09 08h
10	47.88874131	106.7815918	1263	UB3	2009.06.08 08h	2009.06.09 08h
11	47.88877189	106.7816697	1263	UB2	2009.06.08 08h	2009.06.10 02h

Central: Peace bridge

point number	Lat N	Long E	Alt (meter)	Sta name	start time (UT)	stop time (UT)
1	47.90517592	106.9132072	1288	UB6	2009.06.06 03h	2009.06.07 02h
2	47.9056141	106.9130259	1288	UB3	2009.06.06 03h	2009.06.07 02h
3	47.90550863	106.9136709	1288	UB9	2009.06.06 03h	2009.06.07 02h
4	47.90534631	106.9134338	1288	UB8	2009.06.05 08h	2009.06.07 02h
5	47.90539974	106.9131176	1288	UB5	2009.06.05 08h	2009.06.07 02h
6	47.90556551	106.9133499	1288	UB4	2009.06.05 08h	2009.06.07 02h
7	47.90545874	106.9134015	1288	UB9	2009.06.05 08h	2009.06.06 03h
8	47.90537757	106.9132822	1288	UB6	2009.06.05 08h	2009.06.06 03h
9	47.9054833	106.9132342	1288	UB3	2009.06.05 08h	2009.06.06 03h
10	47.90544101	106.9133062	1288	UB2	2009.06.05 08h	2009.06.07 02h

After having recorded the noise in time domain, I selected the segment of data for the fk analysis using its time sequence, noise distortion level and noise spectrum. An example of simultaneously recorded data at the site Amgalan area and its power spectrum is shown in the figure 3.4

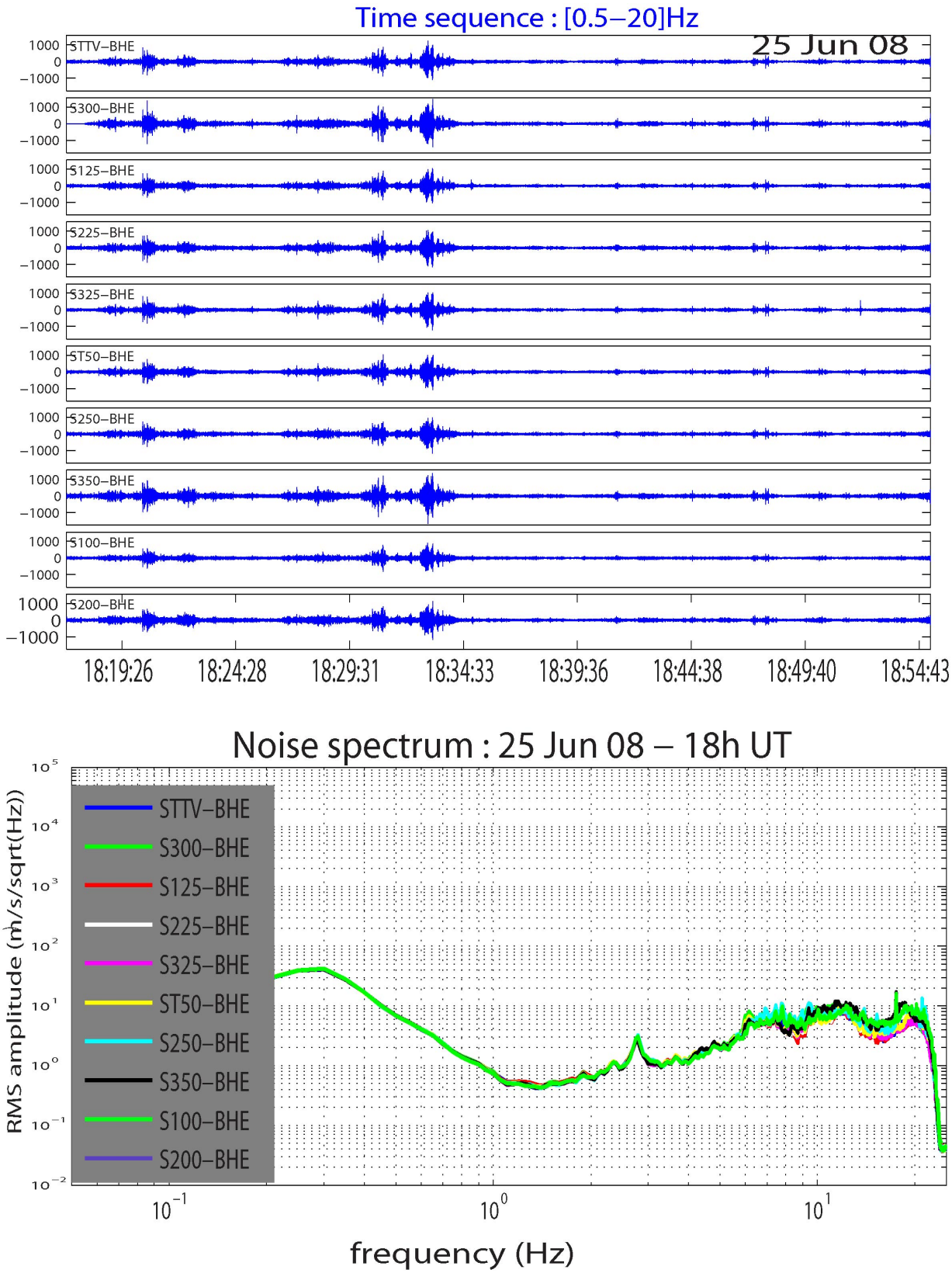

Figure 3.4: Example of data recorded at the Amgalan site and its power spectrum.

3.3.3 Basic principle of frequency wavenumber analysis

The fk-analysis is a standard array technique, which simultaneously calculates the power distributed among different wavenumbers and directions. There are several ways to estimate fk analysis such as Bean forming Method and Maximum Likelihood Method – MLM [Capon, 1969].

The estimation of fk spectra P(f,k) by MLM is given by [Yamanaka, 2003]

$$\bar{P}(f,k) = [E(k)^{*} S(f)^{-1} E(k)]^{-1} \qquad (3.4)$$

Namely

$$\bar{p}(f,k) = \left\{ \sum_{i=1}^{N} \sum_{j=1}^{N} q_{ij}(f) \exp\left[ik(r_i - r_j) \right] \right\}^{-1} \qquad (3.5)$$

q_{jl} is the ij-th element of $S(f)^{-1}$,

S(f) is the coherency of microtremor between sites i and j, and can be obtained by

$$S_{ij}(f) = \frac{C_{ij}(f)}{\sqrt{C_{ii} \cdot C_{jj}}} \qquad (3.6)$$

where

$C_{ij}(f)$ is the cross spectrum which is derived from the Fourier spectra of the recorded microtremor at sites i and j using

$$C_{ij}(f) = U_i(f)\ U^{*}_j(f) \qquad (3.7)$$

where

$U_i(f)$ is Fourier spectrum at sites i

$U^{*}_j(f)$ denotes complex conjugate of Fourier spectra at site j.

As a result of fk analysis, we obtain the amplitude spectrum of the wavenumber. Once we estimate the fk spectrum at a frequency, from array records, phase velocity and back azimuth can be estimated from the wavenumber (k_{mx}, k_{my}) by

$$Vph = \frac{2\pi f}{\sqrt{k_{mx}^2 + k_{my}^2}} \quad , \quad \theta = \tan^{-1}\left(\frac{k_{my}}{k_{mx}} \right) \qquad (3.8)$$

By repeating the above procedure at different frequencies, we can get the phase velocity dispersion curve.

3.3.4 Frequency-wavenumber analysis

Array geometry is very important to obtain a reasonable surface wave dispersion curve that corresponds to the velocity structure of the deposits. Therefore I calculated the array responses to determine the resolution and the aliasing limits ($k_{min}/2$ and k_{max}) as defined by Wathelet et al. [2008]. The figure 3.5 presents the array responses for the two different arrays geometry I used. Amgalan array response is shown in the figure 3.5 a and c. The array response of the sites Bridge and Sonsogolon, which were deployed with the same configuration, is represented in the figure 3.5 b and d.

Te resolution of the deployed arrays (distance between stations) and their aliasing limits ($k_{min}/2$ and k_{max}) are summarized in the table 3.2:

Table3.2.

Array name	Min dist (meter).	Max dist (meter).	$k_{min}/2$ [rad/m]	k_{max} [rad/m]
Amgalan	14.4	100	0.033	0.268
Bridge	7.2	50	0.06	0.525
Sonsgolon	7.2	50	0.06	0.525

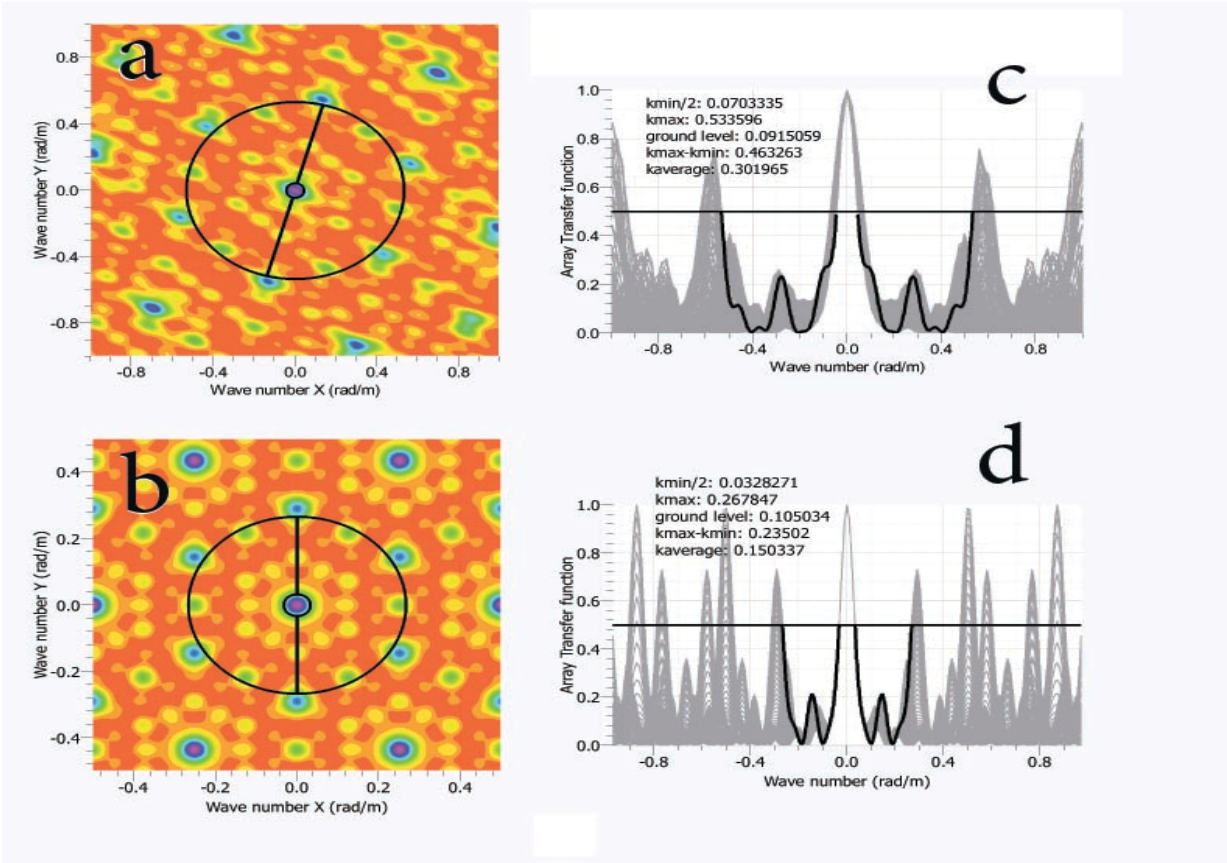

Figure 3.5: a- theoretical frequency-wavenumber response of Amgalan array ; b-theoretical frequency-wavenumber response of Bridge and Sonsgolon arrays; c and d are, across several azimuths, the theoretical fk grids of array a and b respectively. Black curves correspond to the orientation of the lines drawn in a and b.

For calculating frequency-wavenumber spectrum, I used signal windows of 60 to 120 seconds. The wavenumber spectrum is plotted as a contour map for each frequency for each time window. The highest peaks are taken to calculate the dispersion curve. The peak was selected using the wavenumber grid for each frequency. The grid step was 0.0025 rad/m and the size was 0.8 rad/m. For the phase velocity calculation, I used the average of the peaks for each fk power window and its standard deviations for each frequency.

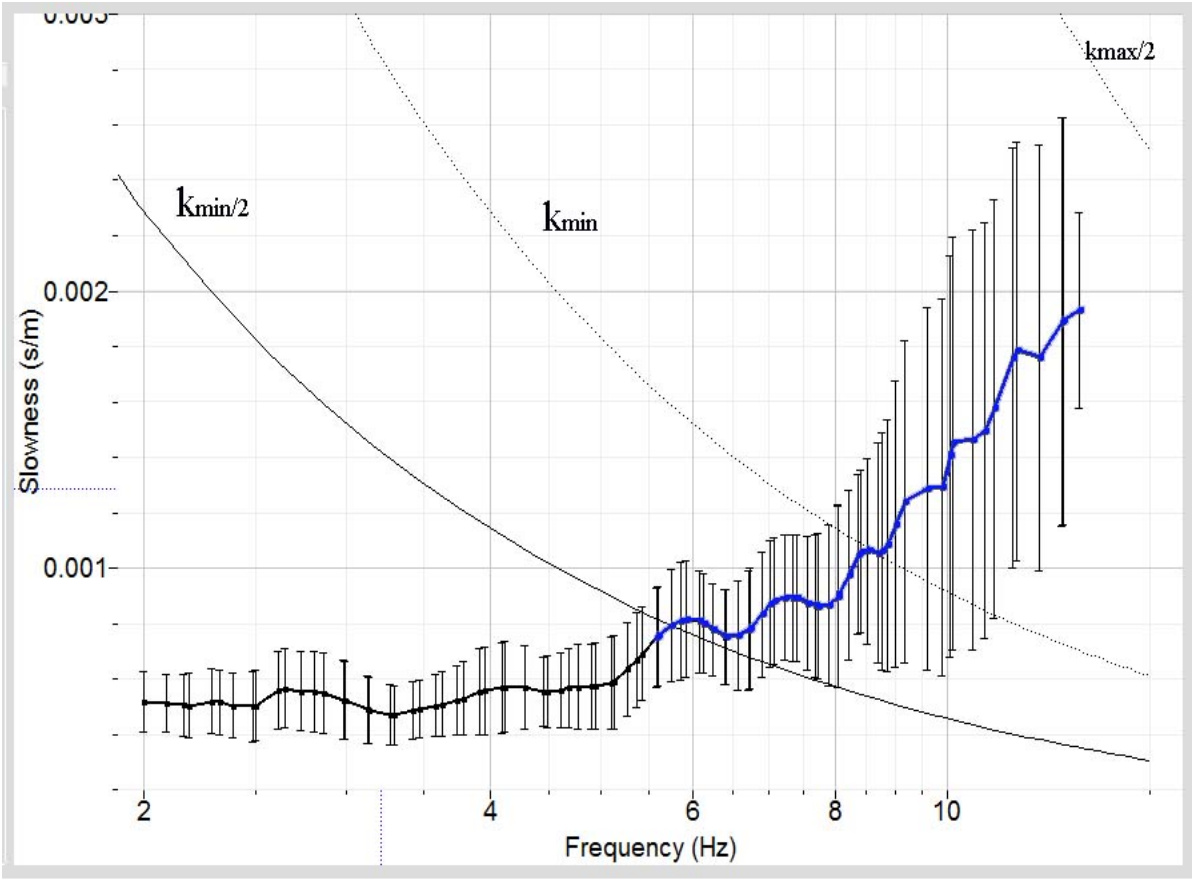

Figure 3.6. Dispersion curve obtained using high-resolution fk analysis at the Amgalan site. Exponential curves represent constant wavenumber values ($k_{min}/2$, k_{min}, $k_{max}/2$). Blue curves represent the part of dispersion curve that are used for the inversion.

The obtained dispersion curves are plotted, with wavenumber resolution and aliasing filter (k_{min} and k_{max}), to determine the dispersion curve part that is used for the inversion (figure 3.6).

3.3.5 Dispersion curve inversion

The phase velocity of Rayleigh wave is function of the frequency and the wavelength. To obtain the S wave velocity profile beneath the site, we can invert the phase velocity using the misfit function between the theoretical calculation and the estimated dispersion curves. The main assumption of this method is that vertical component of microtremor mainly consists of Rayleigh waves.

I inverted the S wave velocity structure beneath the arrays using the code DINVER, which is included in the GEOPSY software. In this inversion code, a neighbourhood algorithm is used, which is a probabilistic searching method for finding the global minimum of misfit functions based on Voronoi geometry [Wathelet, 2005].

The HV ratio measured on the array sites are presented in appendix A, Figure A.7 (sites 5-36, 5-37 and 5-39 correspond to Sonsoglon, Amgalan and Bridge array respectively). From HV ratio, we observe that Amgalan and Bridge sites have clear peaks at 4 and 4.5 Hz, and that Sonsgolon site has a wide peak at 2 to 3.5 Hz. Considering the estimated sediment thickness under the array sites, the observed peak frequency gives us a first idea of the potential shear wave velocity. For the Bridge array, we know, thanks to a drilling, that they are 29 to 30 meters of deposits directly over stiff rock. Then we can deduce that the share wave velocity is around 520 m/s.

The inversions were applied using different input layers (from 2 to 4 layered model). The different trails show that the upper sediment layer's velocity and the total thickness is stable for the different inversion models used. The figure 3.7 shows the result of the dispersion curves, obtained through high-resolution fk analysis, and the resulting inverted velocity profiles.

I obtained an average S wave velocity of 500 to 550 m/s and 28 meters of sediments at the Amgalan site, 550 to 600m/s with 30 meters of sediments at Bridge site and 600 to 650 m/s and 37 meters of sediments for Sonsoglon site. These three sites are widespread along the longitudinal axis of the Ulaanbaatar basin and the estimated S wave velocity (average velocity from surface to bedrock) are increasing when the sediment thickness increases. The bedrock shear wave velocity is about 1600 m/s. This value is close to the velocity determined at 5 different building sites using seismic refraction (Dzurick et al., 2009).

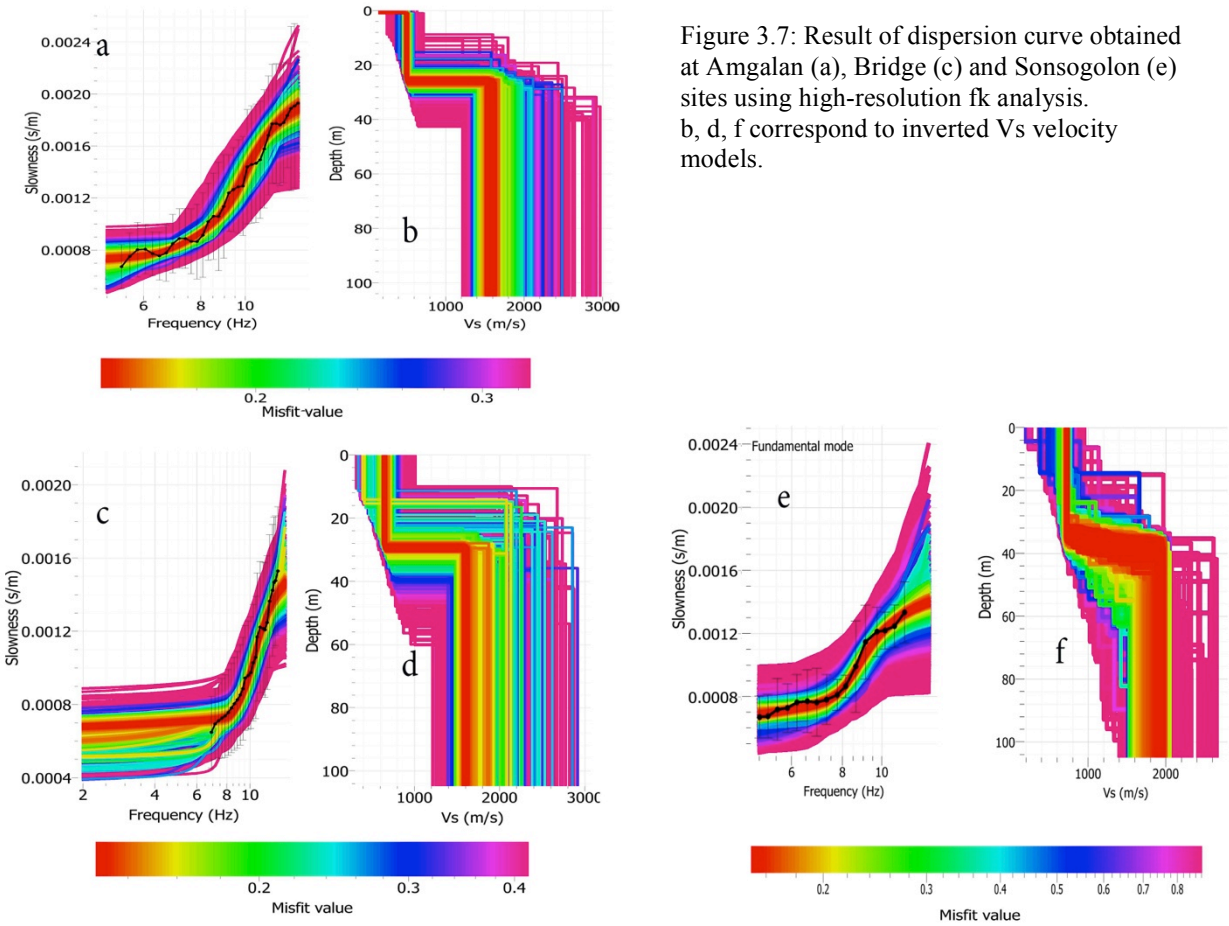

Figure 3.7: Result of dispersion curve obtained at Amgalan (a), Bridge (c) and Sonsogolon (e) sites using high-resolution fk analysis.
b, d, f correspond to inverted Vs velocity models.

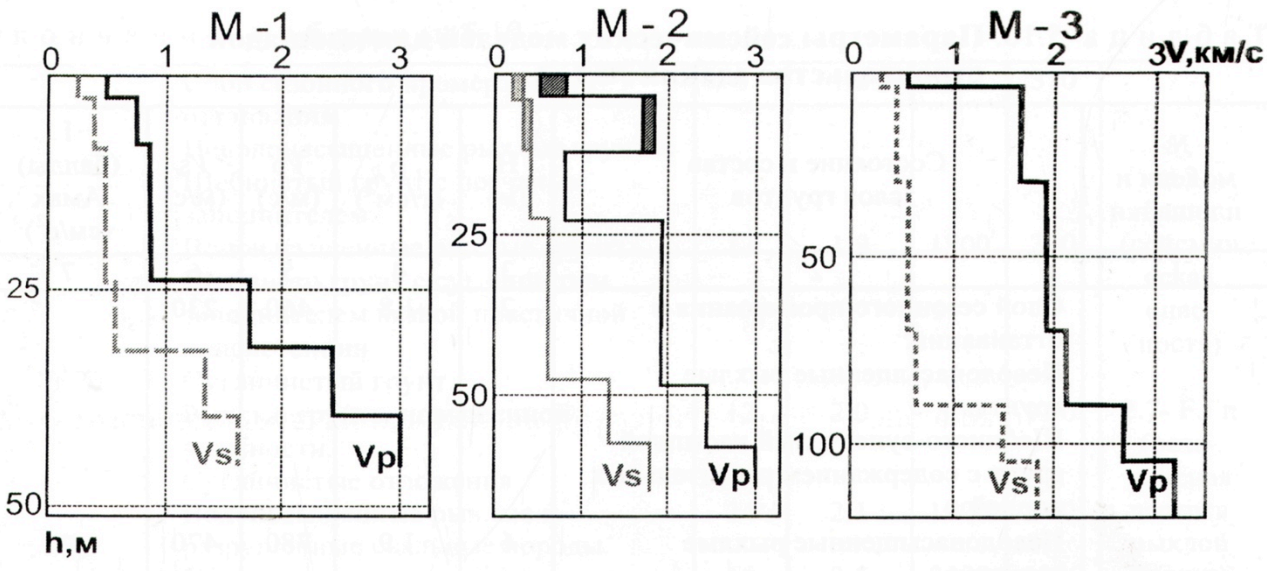

Figure 3.8: S and P wave velocity profile at 3 different building sites in the Ulaanbaatar basin using Seismic refraction profile (Dzurick et al., 2009).

3.4 1D and 2D seismic wave modelling in the Ulaanbaatar basin

3.4.1 2D simulation using Mka3D

2D seismic waves simulations in the Ulaanbaatar basin were made in relation with Szitkar (Szitkar, 2009) using the Mka3D program developed at CEA/DASE. The Mka3D (M- for mechanic, k- for stiffness between particle, a- acceleration, 3D- for 3 dimensions) code is developed by Christian Mariotti, from CEA/DASE [Mariotti, 2007] and uses discrete element technique. In the simulation of the seismic waves in the Ulaanbaatar basin, we applied a 2D version of the Mka3D code. The aim was to start with a simple geometry of the basin and to improve it step by step. The 3D modelling will be done as a prolongation of this PhD study (Collaboration DASE, RCAG, EOST).

We decided to focus the 2D simulation along the main trend of the basin (figure 3.9). Near this cross section are four sites that recorded weak motions events (see chapter 2). For the simulation process, we built a grid of 30m (horizontal) x 5m (vertical) for the sedimentary deposit and a grid of 20x20m for bedrock. In the simulation, the input wave consists of a plane wave, of 2.5 seconds length, with a vertical incidence. It was numerically generated by a line of sources under the rock with an infinite fault rupture velocity. We deployed 32 virtual velocity stations at the surface, with 1 km distance between them, 30 are on the sediment and 2 are on rock. At figure 3.10, blue and red colours represent respectively sediment and rock, green circles are the virtual stations and pink triangles are real stations that were deployed near the cross section for recording weak motions. We observed the generation of surface waves and their propagation in the basin at various time (figure 3.11. We can clearly observe how the waves are trapped in the sedimentary basin. These surface waves are also clearly observed on simulated waveforms (figure 3.10). At the central part of the basin, the thickest sedimentary part, the frequencies of the waves are lower than near its borders, where the sedimentary deposits are thinner.

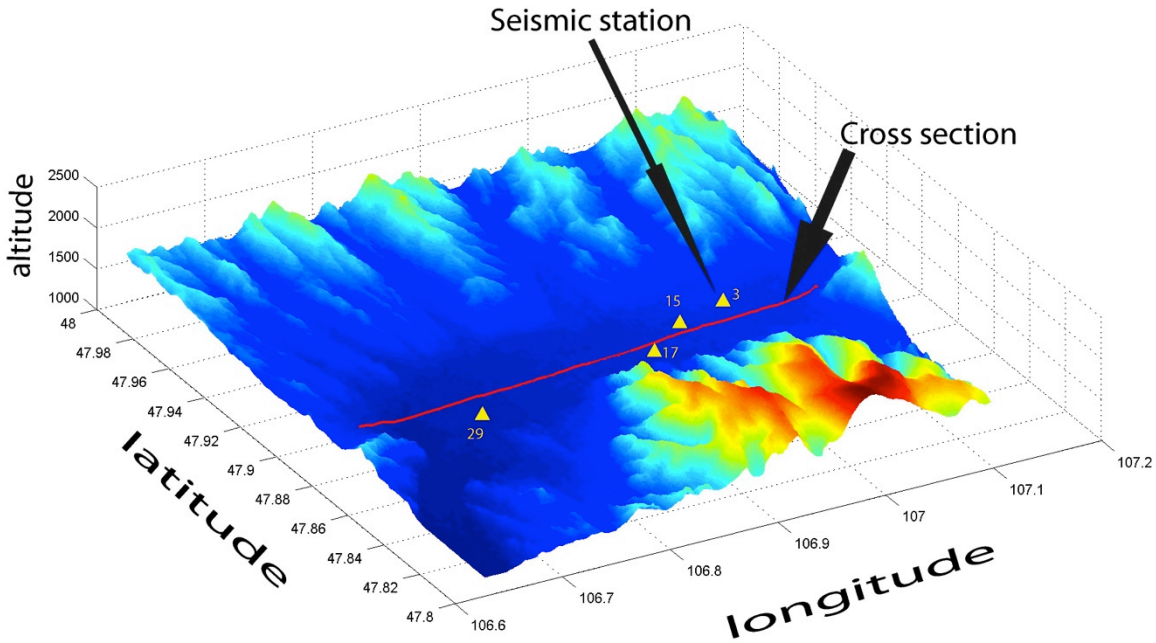

Figure 3.9: Location of the cross section in Ulaanbaatar basin used for the 2D simulation. Yellow triangles are the position of the nearest stations that recorded weak motions.

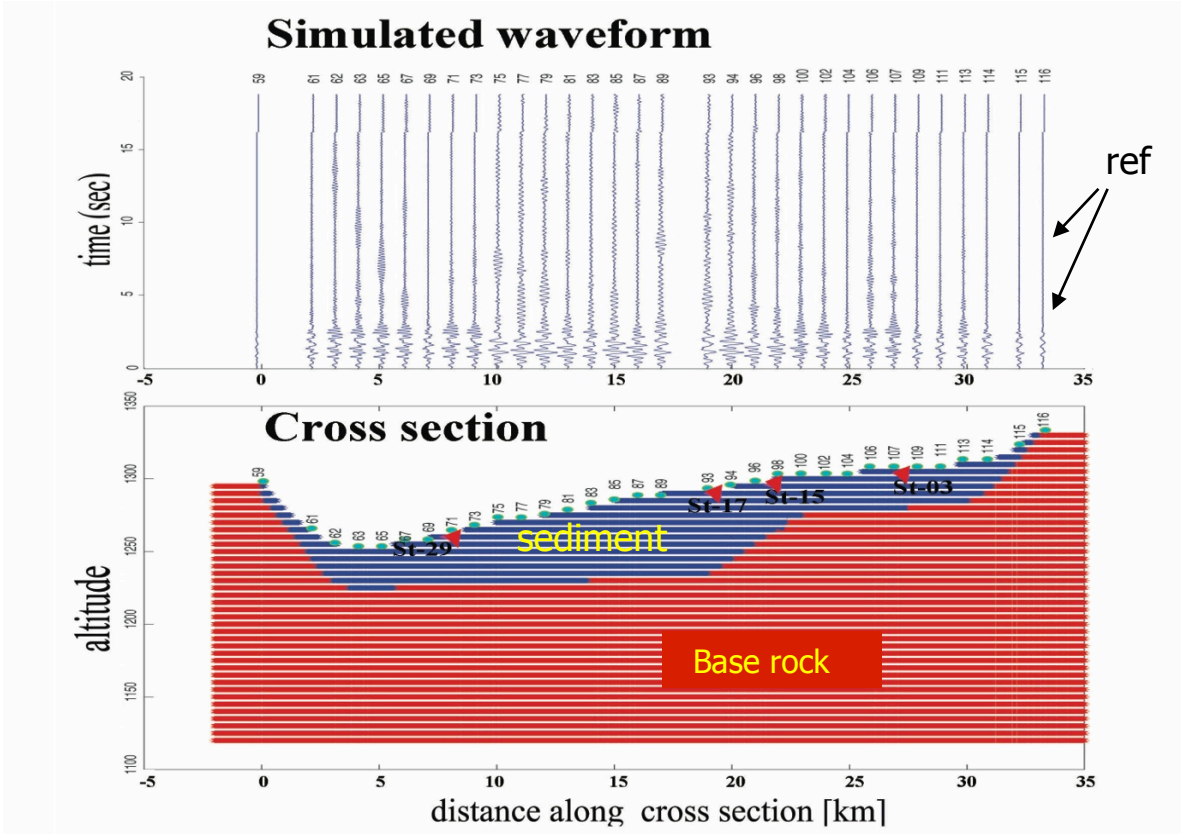

Figure 3.10: Cross section and simulated waveform at the Ulaanbaatar basin: top picture shows simulated waveforms at the virtual stations along the cross section using Mka3D, bottom picture shows the cross section of the basin and the stations positions (green circles are virtual stations, red triangles are stations deployed near

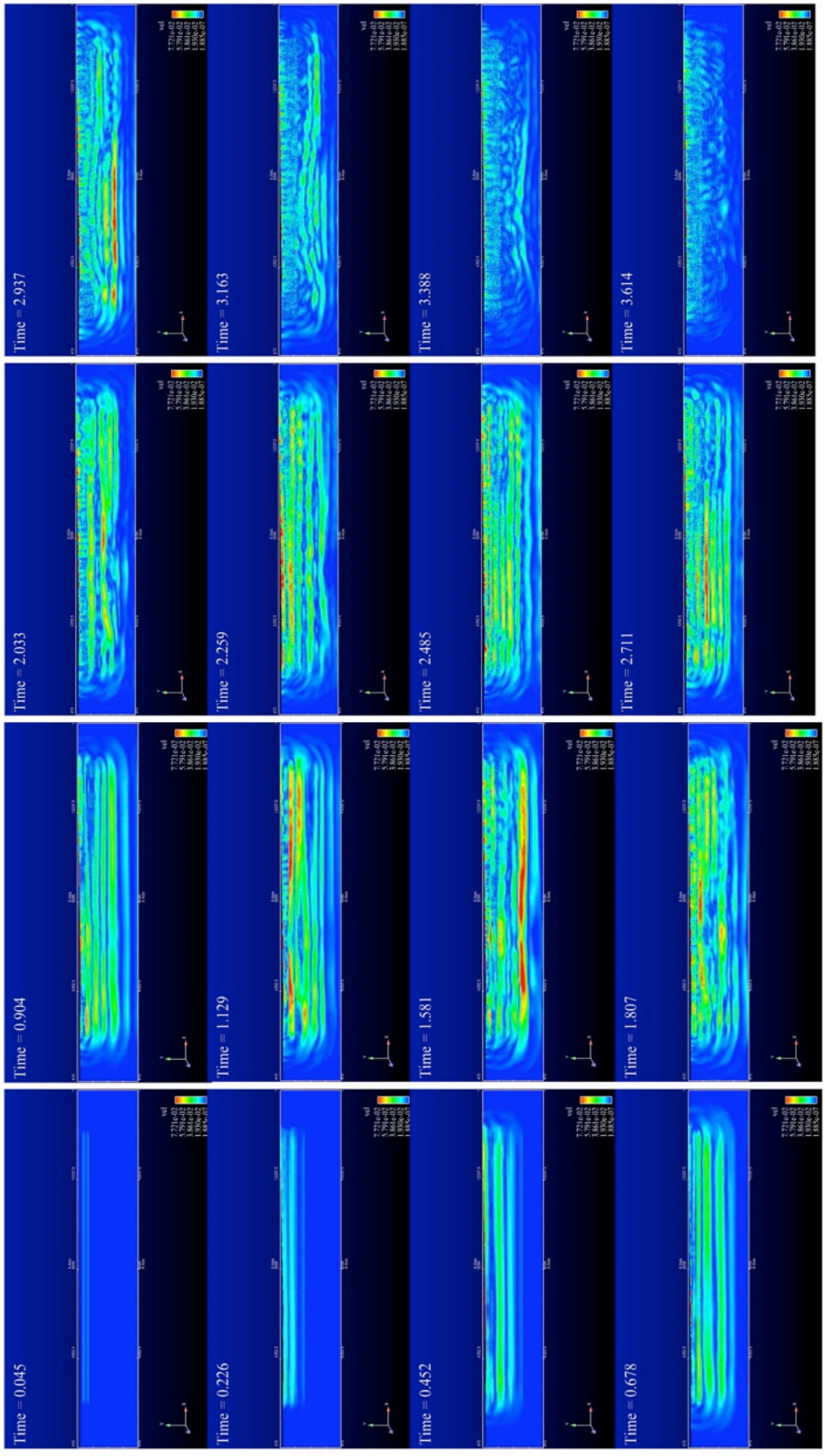

Figure 3.11: Snap shots at various time (in seconds) of the 2D simulation at Ulaanbaatar basin

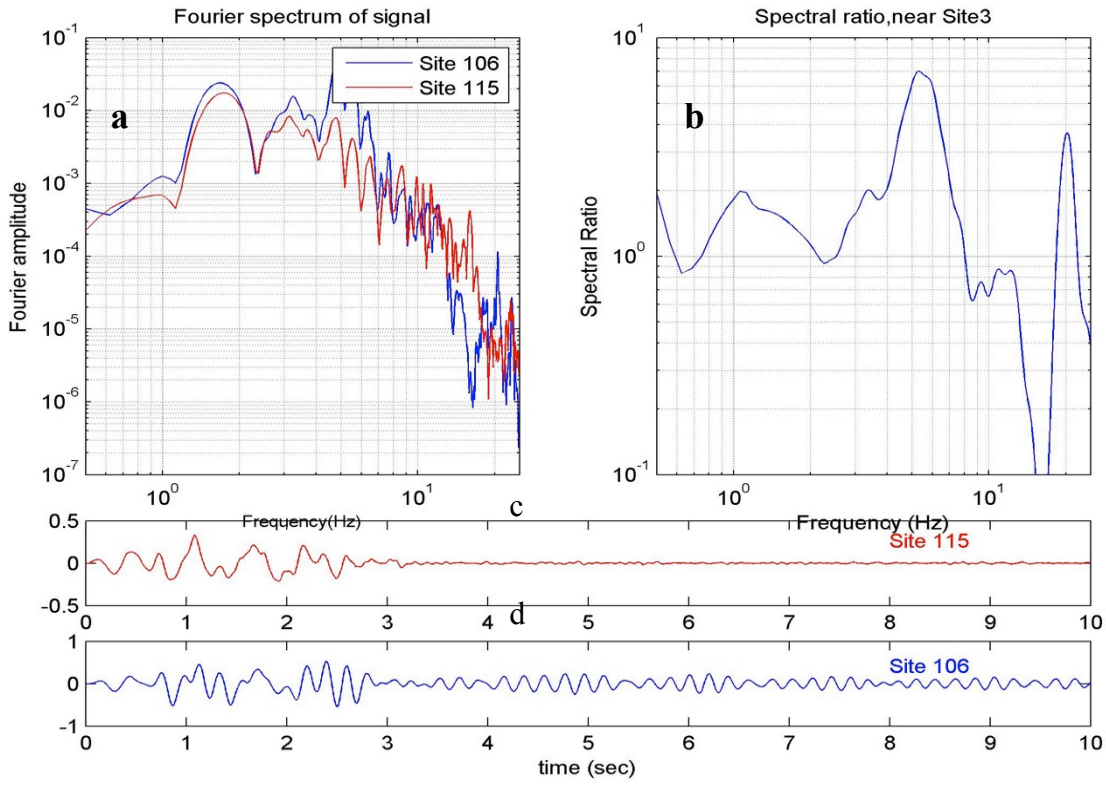

Figure 3.12: SSR applied at two virtual stations near the observed site 3 on the field.
red line = outcropping rock site; blue = site on the sediment; a = Fourier amplitude spectrum of waveforms; b = standard spectral ratio between the two virtual stations (sediment and rock sites); c, d = recorded waveforms.

With the obtained simulated waveforms, I calculated the SSR using 10 seconds of the horizontal components. I applied for the SSR, calculated between virtual sites at sediment and rock, the same procedure that I used in chapter 2. One example of SSR between stations 106 and 115 is shown in the figure 3.12. All obtained SSR with simulated waves show clear site amplification at various frequencies depending on the thickness of the sedimentary deposits. This obtained amplified frequency are in agreement with the depth and the S wave velocity using f=H/4V formula. (figure 3.10 and figure 3.12)

3.4.2 1D simulation SHAKE91

I calculated the 1D transfer function of sediments using SHAKE91 program. Shake91 is a program for conducting equivalent linear seismic response analyses of horizontal layered soil deposit. The software was written in 1970 -1971 by P. Schnabel and modified by Idriss and Sun [1992]. The program computes the response of a semi-infinite horizontal layered soil (sedimentary deposit) overlying to a uniform half-space (rock) that undergoes a vertical

propagating shear waves. In my calculation, for the input soil parameters, I selected them directly from predetermined values in shake91. I selected the shear wave velocity from the closest site where I applied a frequency wavenumber analysis. Nevertheless, I have to give a velocity profile at each point of the grid, even far from fk analysis sites. For that, I considered that the thickness proportion between the two sedimentary layers are constant, whatever is the total thickness of the sedimentary deposit. The velocity value for each layer is taken as equal to the velocity measured on each layer on the nearest site with fk analysis. The layer thickness is extracted from my 3D basin model (see chapter 2). For the input ground motion in the Shake91, I used a 0.1g normalized signal, which has been chosen from the weak motion recorded at the Ulaanbaatar basin. I considered the ground motion input signal as an "outcropping rock record" in Shake91.

3.4.3 Comparison of 1D SHAKE91 and 2D Mka3D simulations with field data.

I selected 4 sites, used for weak motion records, which were deployed near the cross section used for the simulations (sites 3, 15, 17 and 29) and I compared them with the nearest virtual stations (104, 98, 93, 71 respectively). Notice that the selected stations were not exactly on the cross section (see figure 3.9). I compared SSR and HV results processed on real and simulated signals (3/104, 15/98, 17/93, 29/71) (figure 3.13). I note SSR(sim) when it is calculated from simulated signals and SSR(obs) when it is calculated from observed signals .

The resulting amplified frequencies, from **1D simulation**, are in good agreement with the observed amplified frequencies using weak motions SSR(obs) and microtremor HV(obs) ratios. For the sites 15, 17 and 29, the SSR(sim) is closer to the HV(obs) noise ratios than to the SSR(obs). For site 3, they are all in agreement.

When I use the **2D simulations**, most of the main amplified frequencies were lightly shifted to higher frequencies in comparison to observed amplified frequencies. They are various possible explanations. One is that, in the simulation, we used a 5 m grid sampling in the vertical directions. Therefore, there is a 5 m uncertainty for the layer thickness that induce an amplified frequency shift up to 1 Hz considering the velocity profile. Another is that, according to the cross section, the site 17 is located at the vertical of the bedrock slope. At this site, the SSR(sim) (2D simulation) shows a wide amplified peak that is in good agreement with the SSR(obs) amplified peak shapes at site 17.

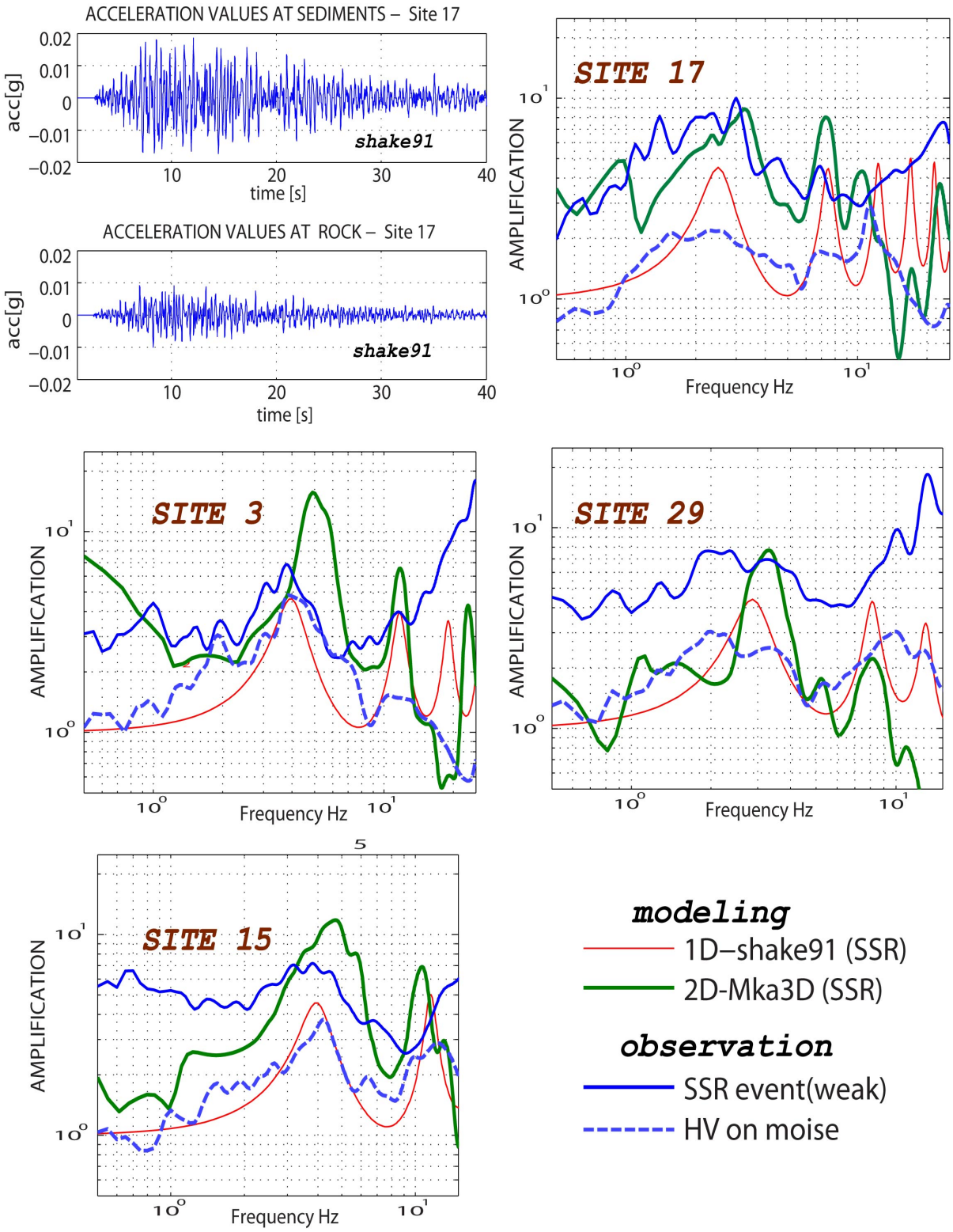

Figure 3.13: Comparison of SSR calculated from theoretical 1D and 2D simulations with observed weak motions SSR and HV noise ratios.

3.4.4 1D calculation for the whole Ulaanbaatar basin

In general, the amplified frequencies obtained by Shake91, 1D approach, were in good agreement with observed amplified frequencies. Therefore, I estimated the amplified frequency overall the Ulaanbaatar basin using shake91. For that, I first built a grid of 100x160 lines (EW x NS) covering a large geographic area (coordinates of its corners are 47.8°N/106.63°E and 48°N/107.169°E). Then I calculated the amplified frequency at each grid node using the shake91 program when the sediment thickness is more than 5m. The share waves velocity considered in the model at each grid node corresponds to the value obtained from the closest array used for fk analysis. As explained before, I considered the impact of thickness variation to the velocity profile. For that, I considered that the thickness proportion between the two sedimentary layers are constant, whatever is the total thickness of the sedimentary deposit, Then the velocity value for each layer is taken as equal to the velocity measured on each layer on the nearest site with fk analysis. The depth for each sites is deduced from the 3D basin model. Results are shown in the figure 3.14.

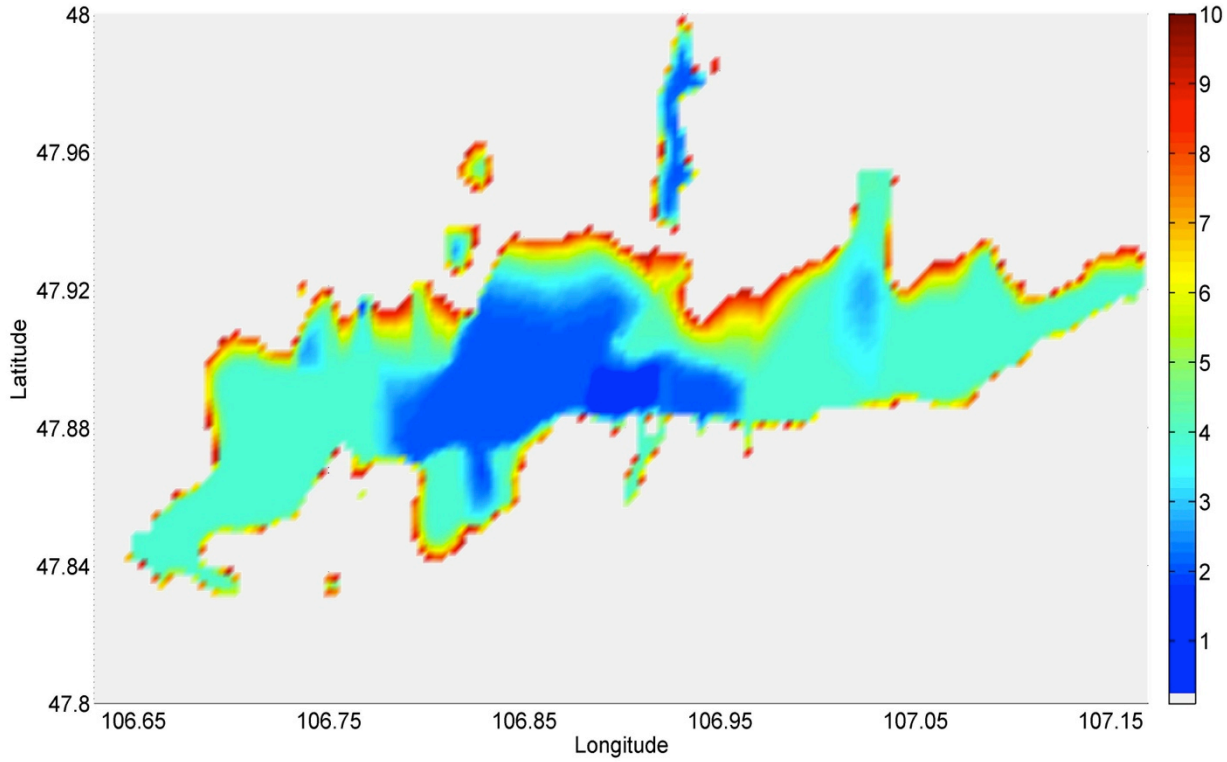

Figure 3.14: Amplified frequencies map, at the Ulaanbaatar basin, calculated by shake91 with parameters obtained from my studies.

After that, I compared the amplified frequencies, obtained with shake91, with those obtained with HV ratio using field records. I firstly removed sites with high noise and for which HV ratio was flat then 94 sites remained. In the figure 3.15, the amplified frequencies obtained from 1D simulation are represented in colour. The measured amplified frequencies using field records, are represented either by a colour circle or a "+" or a "-". When the observed "HV(obs) peak frequency" and "1D simulation peak frequency" are in agreement within 1.5 Hz range, I marked them by a red circle filled by green colour. When "HV(obs) peak frequency" is at lower frequency than "1D simulation peak frequency" then the site is marked by "-" (minus sign). When "HV(obs) peak frequency" is greater than "1D simulation peak frequency" then the site is marked by "+" (plus sign). From the 94 sites, 5% had lower frequencies than those obtained from the SHAKE91 simulation, 20% had higher frequencies and 75% were in good agreement.

From the figure 3.15 it is clearly observed that, using SHAKE91, the simulation gives a lower amplified frequency (plus sign) at sites mainly concentrated at three areas: west, east border and at the north-central part of the basin. One of the reasons could be due to the simplified 3D model itself and locally poorly constrained data. To construct the 3D basin model, I used only 5 isolines, which correspond of 10 to 30 meters steps that simplify strongly the shape at the border sites.

For central north part where are the Neogen clay, I observed very wide amplified frequency at 3-5 Hz by HV(obs) ratio, but the 1D simulation gives a peak at 1-2 Hz. This shows that we need to improve the geometry and the velocity of the 3D model for the basin.

Finally, we obtain an amplified frequency map for Ulaanbaatar basin based on geological and topographical map of Ulaanbaatar added with 1D simulations constrained by velocity profiles using fk analysis. The reliability of the results is based on the comparison of the calculated amplified frequencies and the observed one using HV or SSR on the data recorded on the field. The figure 3.16 presents the data layers used to build this resonance frequency map. The final resonance frequency map is presented in the conclusion part.

Consequently, in this chapter I obtained for the Ulaanbaatar basins a preliminary 3D model using available geological or geophysical information. Shear wave velocity information were extracted at 3 sites using FK analysis. Amplified frequencies of the basin are calculated by equivalent linear seismic response analyses. The results obtained are

compared with the observed amplified frequencies determined by HV ratio. Their comparisons show that it is necessary to improve the 3D model for the border of the basin and the area with Neogen clay. The good agreement between amplified frequencies using 1D simulation and observed amplified frequencies using field records indicates that they are mainly resulting from 1D effect. The differences remain mainly within 1.5Hz; values that are small but not negligible for seismic risk mitigation.

For the 2D simulation, it does not bring clear benefit for the amplified frequency in our case, in comparison to 1D simulation. Nevertheless, the simple model used give quite reliable information in comparison to observed data.

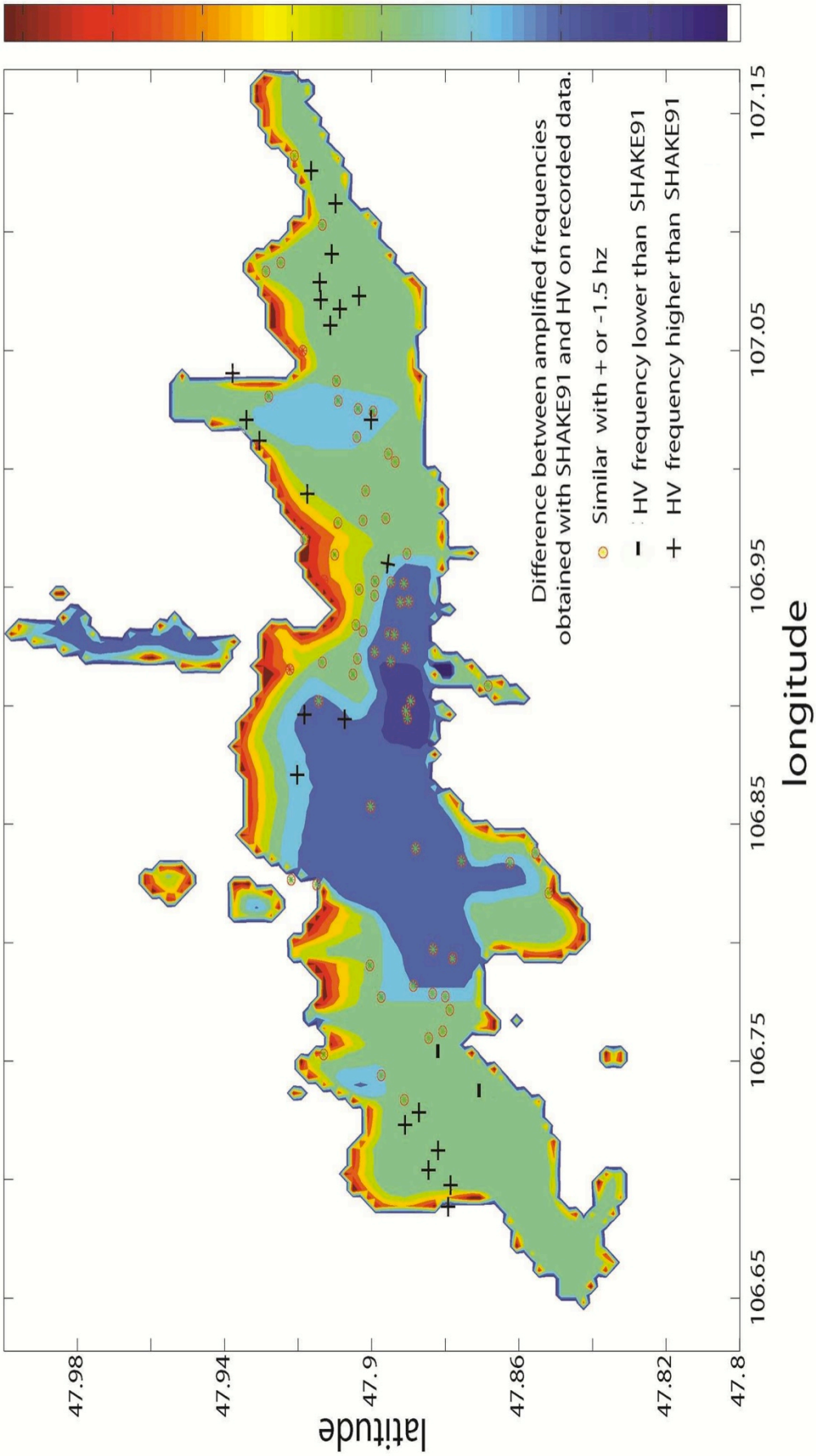

Figure 3.15: Amplified frequencies estimated with shake91 are compared with amplified frequencies deduced from HV ratio done on recorded data.

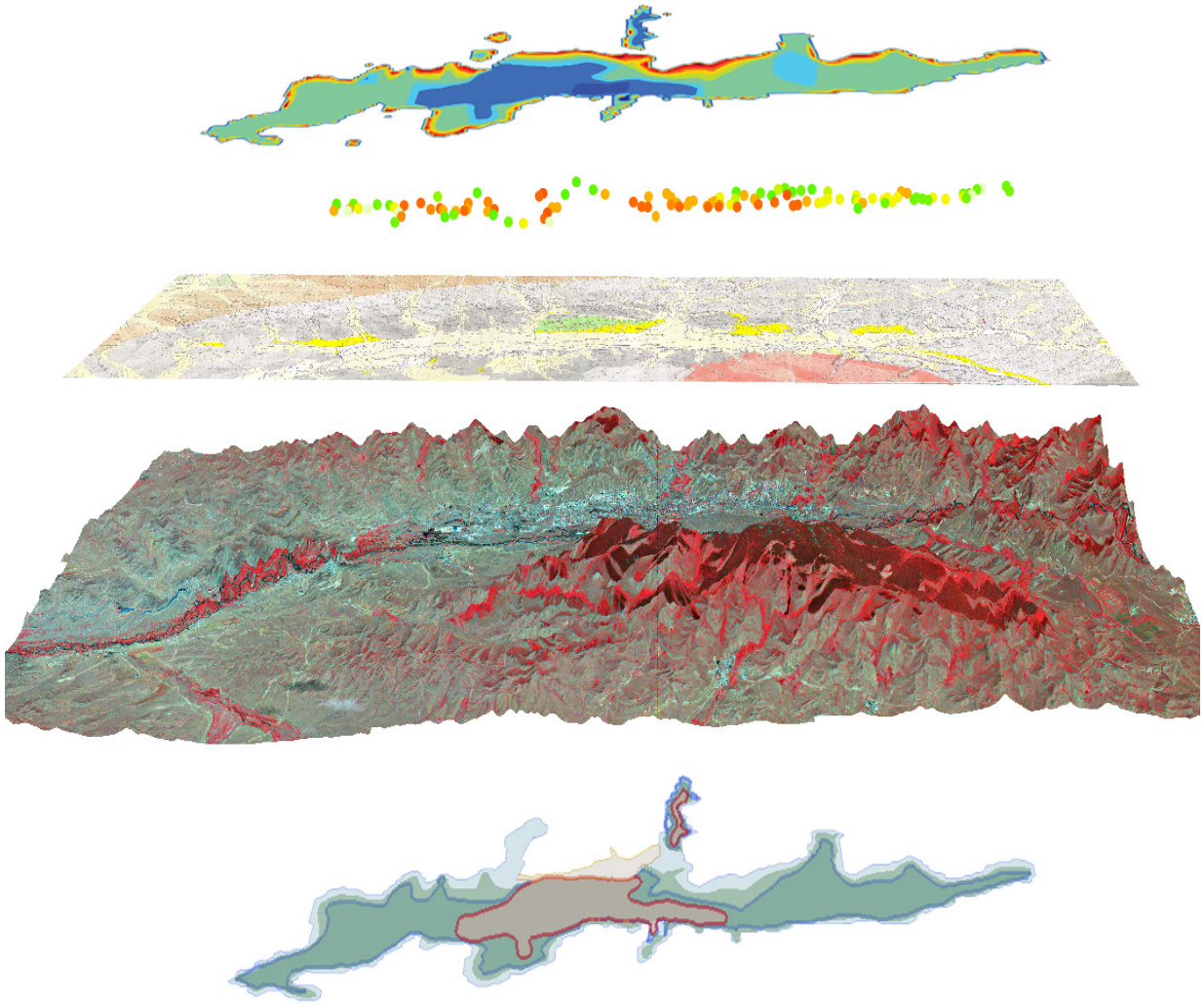

Shake91- amplified frequency

+

HV observation result

+

Geological Map

+

Topographic and Landsat map

=

Amplified frequency Zoning Ulaanbaatar

Figure 3.16: Data "layers" used to build resonance frequency map for Ulaanbaatar basin

CHAPTER 4 : Duration Variations due to The Ulaanbaatar Basin

4. DURATION VARIATIONS DUE TO THE ULAANBAATAR BASIN

4.1 Introduction

It is well known that local site conditions may increase significantly the amplitude and the duration of ground motion and it's playing a major role for the destruction of buildings [Boomer, 1999]. Then, the aim of this chapter is to estimate the duration difference between a site on sediment, and a site on rock at the Ulaanbaatar area.

In general, many authors consider the duration lengthening due to a sedimentary basin. Nevertheless, there are many studies to estimate the site amplification characteristics [Borcherdt, 1970; Nakamura, 1989; Field and Jacob, 1995] but there are only few studies investigating the variation of the duration of the ground motion and its relationship with site conditions.

One of the major difficulties to study the duration is how to define and determine the duration itself. There is a large variety of definition of strong ground motion duration [Husid, 1969; Trifunac, 1975; Montejo and Kowalsky, 2008; etc.]. Boomer and Martinez-Pereira [1999] reviewed more than 30 definitions and classified them into three generic groups. First 2 classifications of duration (bracketed and uniform) were based on the threshold of a level of ground motion (acceleration or velocity). The third group is called "significant duration", and is based on the accumulated energy in the accelerogram. It is represented by the integral of the square of the ground acceleration or velocity. This integral of the acceleration is related to the

Arias intensity [Arias, 1970], and the significant duration (or significant duration of strong motion) is defined by the duration between 5% and 95% of Husid plot [Husid, 1969].

It is also very important to know if the lengthening of the duration of the ground motion is at particular frequencies [Trifunac and Brady, 1975; Beauval et al., 2003; Parolai and Bard, 2003; Montejo and Kowalsky, 2008]. The frequency dependence of the significant duration definition was introduced at University of Southern California [Trifunac and Brady, 1975; Novikova and Trifunac, 1993 and 1995] and was based on the first calculation of Arias intensity [Arias, 1970] for strong ground motion. They used a narrow band Ormsby filters to obtain a seismic signals reduced into the interested narrow band of frequency. Then they calculated the significant duration of the filtered signal using the Husid plot.

Another method to study this frequency dependence was introduced by Beauval et al. [2003] who used the mean group delay. This group delay duration idea was first proposed by Sawada [1998], who basically measured, for each frequency, the arrival time of the central wavelet, obtained from the frequency derivative of the unwrapped phase. I applied this method on the weak motion recorded at the Ulaanbaatar basin [see APPENDIX B]. Nevertheless for recorded weak motion at Ulaanbaatar basin, this method did not show clear duration variation.

As for the study of the amplification factor and the amplified frequency, the analysis of the duration variation of the ground motion between a reference site and the studied site have to be in agreement with the following hypothesis. The distance between the epicentre of the recorded event and the stations (site and reference) is much longer than the distance between reference and site. Then we assume that the source and the path effects are the same for both records at site and reference. In this case, the ground motion duration difference between site and reference can be associated to local effect (as the geology under the site).

In general, the horizontal component of the seismic waves at a sedimentary site has higher amplitudes than vertical component. This is due to particular frequency amplification that has an important role in the destructions. Therefore, I mainly focus my study on the horizontal component of the seismic waves.

To estimate the ground motion duration difference between site and reference, I applied several methods. For all of them, I used weak motion records.

First I applied Arias intensity duration on the original recorded signal. After, in order to check duration lengthening at specific frequency, I applied filtered Arias intensity duration methods. I applied the same procedure on the seismic wave resulting from 2D simulation (see chapter 3). The results, obtained from records and simulations, are compared.

On another hand, the duration estimated by Arias intensity is a "significant duration" or "relative duration", which does not depend on the amplitude of the signal. But for engineering purposes, it is more important to estimate the absolute duration of the ground motion at a site. Therefore, last part of this chapter I estimated the absolute duration difference between sedimentary and rock site using the waveform.

4.2 Data used for analysis

In this duration study, I used the data recorded during our survey in 2000. The basin geology and sediment thickness information are presented in the Chapter 2. The main purpose of this field survey was to measure the local geological effect, at the basin of Ulaanbaatar, to the seismic signal. We deployed at each site the same station which consist of a 24 bits Aorai digitizer (developed at CEA/DASE) with 50 Hz recording frequency and a short period 3 component Mark-4L sensor that has a flat velocity response between 0.7 Hz and 10 Hz. During the survey, we deployed stations at 32 sites for a duration of 1 to 2 weeks in order to record events (see Chapter 2 figure 2.1). One station was deployed in the north part of the Ulaanbaatar basin, on the rock, as a reference point.

I assumed that, to estimate a reliable duration using Arias intensity and weak motion records, it is required a signal-noise ratio of at least 3. Therefore, I determined the signal noise ratio for each component of all records. The noise was taken before the event and the signal was taken starting at S-wave arrival phase (figure 4.1). Finally, 22 events recorded at 15 sites satisfied the criteria. All these sites were on sediments with a thickness of up to 35 meters. Additionally, in June 2009, several broadband "Guralp" stations were deployed around Emeelt fault (west border of the basin) in order to study the activity of the fault source zones. One of those stations was located on the sediment (UB9) and the others (UB4 selected as reference) were at outcropping rock sites (figure 4.2). I selected 30 events recorded there since 2009 and 12

of them fulfilled the signal-noise ratio criteria (figure 4.1). The figure 4.2 presents the locations of sites that were selected for this analysis.

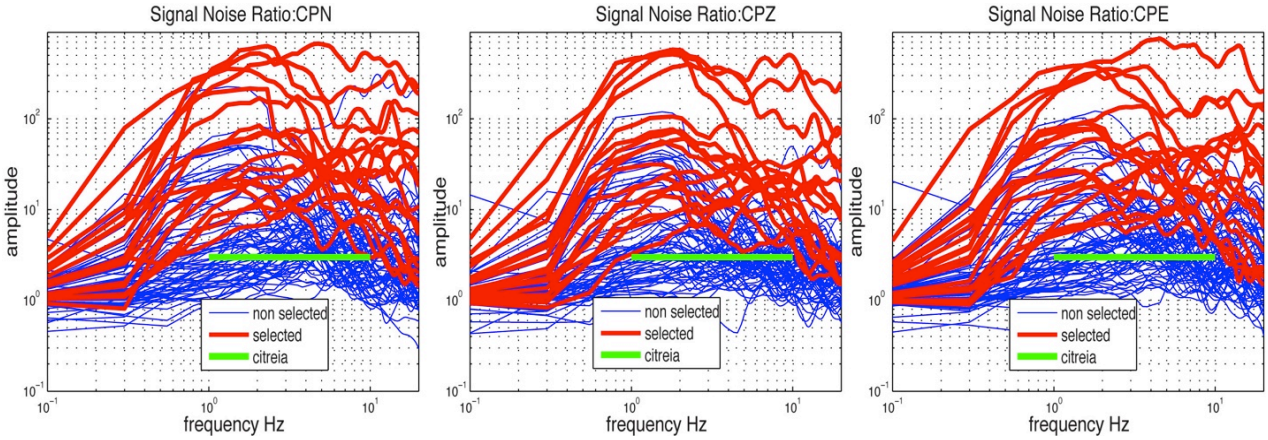

Figure 4.1: Signal noise ratio analysis for all recorded events. The red curves correspond to the events selected for duration analysis, blue curves are rejected events and green line represents signal-noise ratio criteria.

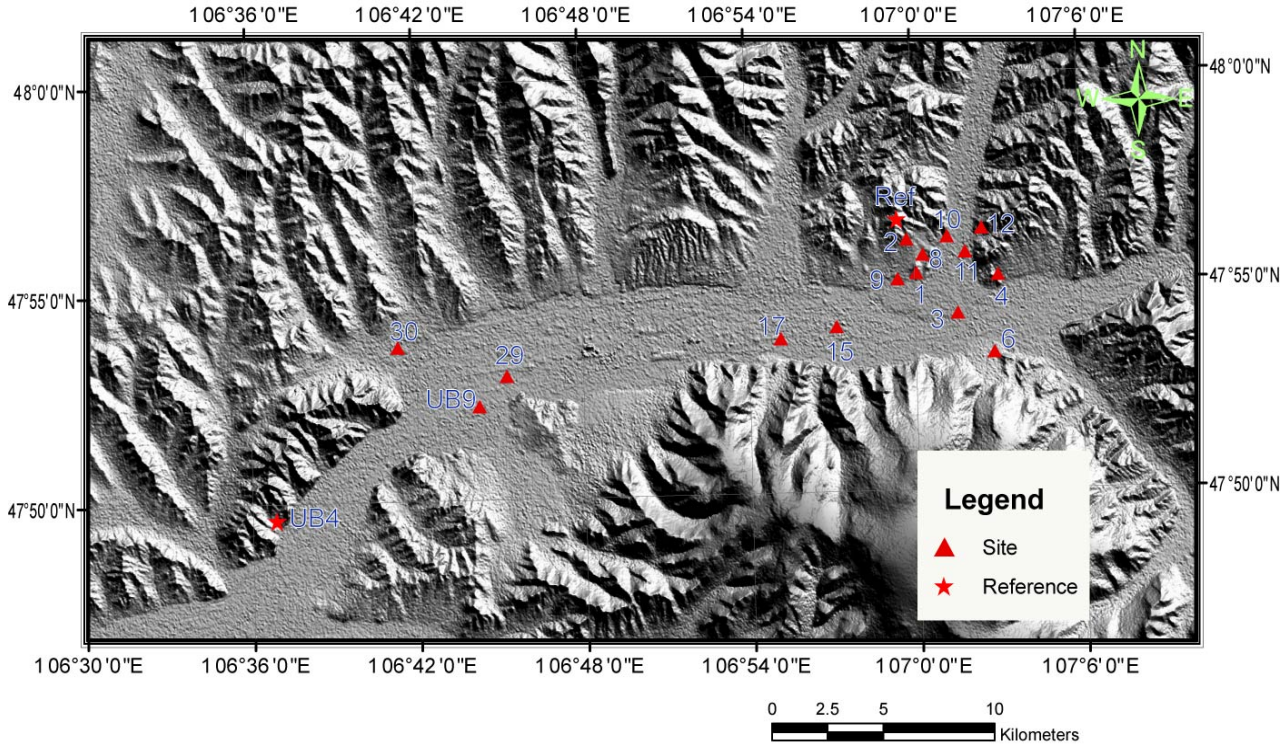

Figure 4.2: Location of the two reference sites (red stars - survey 2000 and 2009) and the studied sites (red triangles) for the duration plotted on a DEM of the region.

4.3 Procedure "Arias duration": Frequency independent

One of the most common procedures for estimating the duration of the significant ground motion is based on the accumulation, with time, of the energy in the accelerogram. It is represented by the integral of the square of the ground acceleration. This integral of the ground motion was first used for Arias Intensity (Ia) [Arias, 1970].

$$I_a(t) = \frac{\pi}{2g}\int_0^t a_i^2(\tau)d\tau \qquad 3.1$$

Where

a(τ) - the acceleration at time "τ",

t - the total duration of the accelerogram (signal)

g- the acceleration gravity.

The "build up" energy versus time plot is also called Husid plot [Husid, 1969]. Then the definition of the duration of significant ground motion is the time difference between 5 and 95 percent of the total Arias intensity of the record. This Arias duration is based on a percentage of the total energy duration of a seismogram; therefore it does not include any information about the absolute amplitude value of the waveform.

For the two horizontal components, the Arias intensity, I_h, is calculated as the sum of each components of the Husid plot. Then a duration variation of the sedimentary site respect to reference site is defined:

$$D_{diff}=D_{site}-D_{ref} \qquad (3.2)$$

where

D_{site}- duration evaluated on sedimentary site (deduced from Arias intensity)

D_{ref} – Duration evaluated at reference site (deduced from Arias intensity)

An example of this process is illustrated in the figure 4.3 for the case of an event (Ml=4.6, distance=560 km, azimuth=327) recorded at the site 29. For it, I applied the following steps.

a) I filtered the raw signals (site and reference) between 0.7 to 10 Hz with a Butterworth filter to remove the signal trend as well as the long period and the very high frequencies noise.
b) I calculated the arrival time difference between sedimentary site and reference site. This allows estimating the Arias duration using the length of the signal starting from S phase arrival time for both site and reference signals.
c) For horizontal component, I used the summation of EW and NS components. This means that this duration is related to the total energy of the horizontal component of the waves.
d) The obtained Husid plot is smoothed with a moving average window in order to avoid that very local noise influences in the duration estimation.
e) Calculation of the duration difference between sediment and reference sites measured on Arias intensities between 5 and 95% of maximum level.

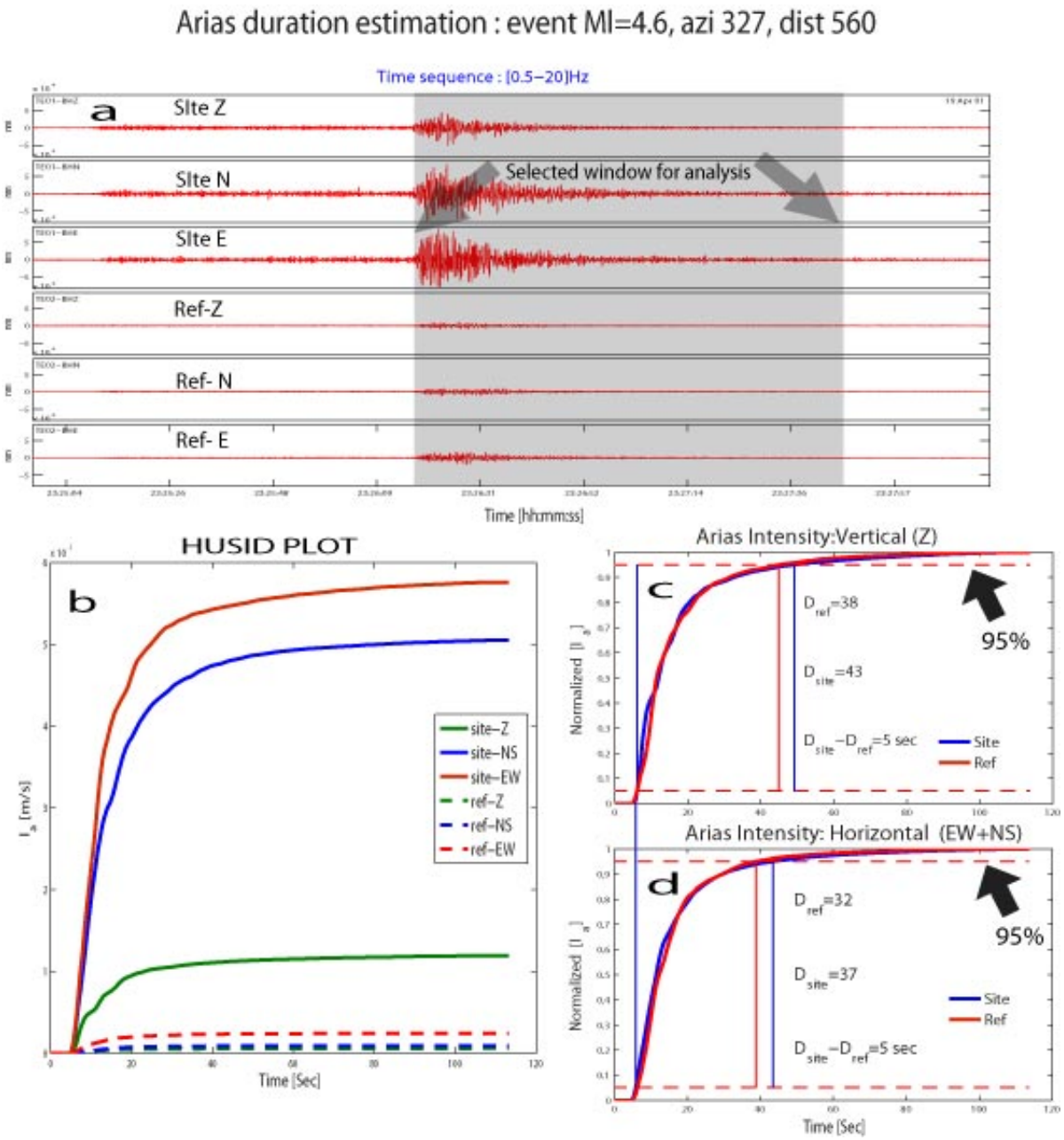

Figure 4.3: Arias duration calculation procedure. a – the event record at site and reference and widow selection. b -Husid plot of the event. c and d are duration estimation process

Following this procedure, I estimated the Arias duration difference for 35 events, 12 of them were recorded at site UB9. The results are summarized in table. 4.1.

Table 4.1 Arias duration estimation

St	event num	Sta	year	jjj	Hh	window length (s)	dura_H (s)		dura_Z (s)		**Dura. diff-H (s)**	**Dura. diff-Z (s)**	D (m)
							ref	site	ref	site			
1	2	1	2000	326	13	139	35	40	42	45	**2**	**1.7**	10
1	8	1	2000	336	20	83	27	28	30	29			
1	10	1	2000	337	21	72	43	43	40	43			
2	4	7	2000	330	23	47	20	21	22	25	**1**	**3**	8
2	2	1	2000	326	13	131	28	29	33	37			
2	10	7	2000	337	21	51	32	32	30	32			
3	10	10	2000	337	21	51	31	31	29	30	**0**	**1**	15
4	14	11	2000	345	21	68	16	22	21	24	**6**	**3**	20
5	14	8	2000	345	21	65	16	17	20	22	**1**	**2**	30
6	14	7	2000	345	21	59	19	24	23	27	**2**	**11**	10
6	18	7	2000	349	20	122	47	46	42	61			
9	23	1	2001	23	23	58	28	28	28	34	**2**	**7.5**	24
9	31	1	2001	34	20	106	37	42	37	46			
10	23	7	2001	23	23	55	24	23	24	24	**1**	**1**	15
10	28	7	2001	32	15	48	20	21	21	22			
10	31	7	2001	34	20	111	42	43	42	44			
11	31	8	2001	34	20	127	44	47	45	45	**3**	**0**	31
12	28	6	2001	32	15	59	22	22	23	23	**2**	**2**	1
12	31	6	2001	34	20	120	43	47	43	47			
15	40	1	2001	48	8								
17	40	6	2001	48	8	53	30	38	32	42	**8**	**10**	51
29	61	1	2001	109	23	134	33	41	41	49	**8**	**8**	30
30	61	8	2001	109	23	117	32	34	39	47	**2**	**8**	15
UB9	1	UB9	2009	161	18	143	0	0	0	0			30
UB9	2	UB9	2009	173	20	42	24	25	24	26	**1**	**2**	30
UB9	4	UB9	2009	179	8	46	20	20	22	25	**0**	**3**	30
UB9	5	UB9	2009	186	20	58	37	40	36	42	**3**	**6**	30
UB9	6	UB9	2009	188	1	55	29	33	36	44	**4**	**8**	30
UB9	13	UB9	2009	246	3	122	38	37	38	41	**-2**	**3**	30
UB9	14	UB9	2009	247	15	84	37	38	38	38	**1**	**0**	30
UB9	16	UB9	2009	261	7	61	19	23	22	28	**4**	**6**	30
UB9	18	UB9	2009	273	14	75	18	17	19	18	**-2**	**-1**	30
UB9	20	UB9	2009	283	21	64	41	41	40	43	**0**	**3**	30
UB9	21	UB9	2009	285	0	64	34	35	36	47	**1**	**11**	30
UB9	25	UB9	2009	333	8	126	40	42	40	46	**2**	**6**	30
UB9 mean											**1.2**	**4.2**	30

Dura.diff-H - duration difference (site – reference) for horizontal components in seconds,

Dura.diff-Z - duration difference (site – reference) for vertical component in seconds,

D - sediment thickness of the site, in meters, deduced from the 3D basin model.

St- site number,

eventnum - event number,

jjj – julian date,

hh-hour (event is within hh and hh+1).

window length -> signal window length used for the analysis in seconds;

dur_H- duration estimated from horizontal component in seconds,

dur_Z –duration estimated from vertical component in seconds,

4.4 Procedure "Arias duration": Frequency dependent

4.4.1 Applied method

In this part of the chapter, I will explain the procedure proposed by Novikova and Trifunac [1995] to estimate the duration of the significant ground motion according to the frequency.

Considering the thickness (0 to 100 m), velocity (400 to 600 m/s) of the basin and the response of the deployed instruments (Short period 1Hz Mark 4L), the frequency range that interests us is between 0.7 Hz and 11 Hz. To get narrow band signals, I used zero phase Butterwort filter with a bandwidth of 1Hz. Then, using a 0.25 Hz I got 38 "windows band" for each signal. Then I applied the same procedure as for the "arias duration" estimation explained in part 4.3. The estimated duration for each band is associated to the central frequency of that band. Then the duration variations of the studied site in respect to the reference site is define by:

$$D_{var}(f)=D_{site}(f)- D_{ref}(f) \qquad (3.3)$$

In the analysis, I selected exactly the same length window for the reference and studied sites, starting from S arrival.

To check the reliability of the procedure, I tested the method on a simple signal generated by the summation of sinusoid. First sinusoids have frequencies of 1, 5 and 9 Hz and with durations of 25, 15 and 20 seconds respectively. Second sinusoids have the same frequencies but with durations of 25 seconds for each frequency (Figure 4.4.). I applied then the

process of Arias duration (script that I developed in MATLAB) on this signal and I could successfully determine the variation of duration for each frequency.

I also tested various signal-noise ratios (S/N ratio) for the procedure to estimate the duration. For that, I added noise, to the previously generated signal, which we recorded at the Ulaanbaatar basin during our noise survey. Then I changed the noise level, using normalized factor N, until the estimation process failed. In this case all sinusoids amplitude was 1. In the formula 3.4 represents the equation that generated sinusoids with noise.

Signal1=1Hz[25sec]+5Hz[15sec]+9Hz[20sec]+noise /max(noise) *N (3.4)

The S/N ratios were calculated at the middle of the 1 Hz band for each frequency. I show (figure 4.4) that the duration is perfectly determined with the Arias filtered procedure, at the real frequencies present in the signals, when S/N ratio is equal or greater than 3 for the corresponding frequencies. The calculated duration outside the frequencies 1, 5 and 9 Hz have no significant meaning in this test case.

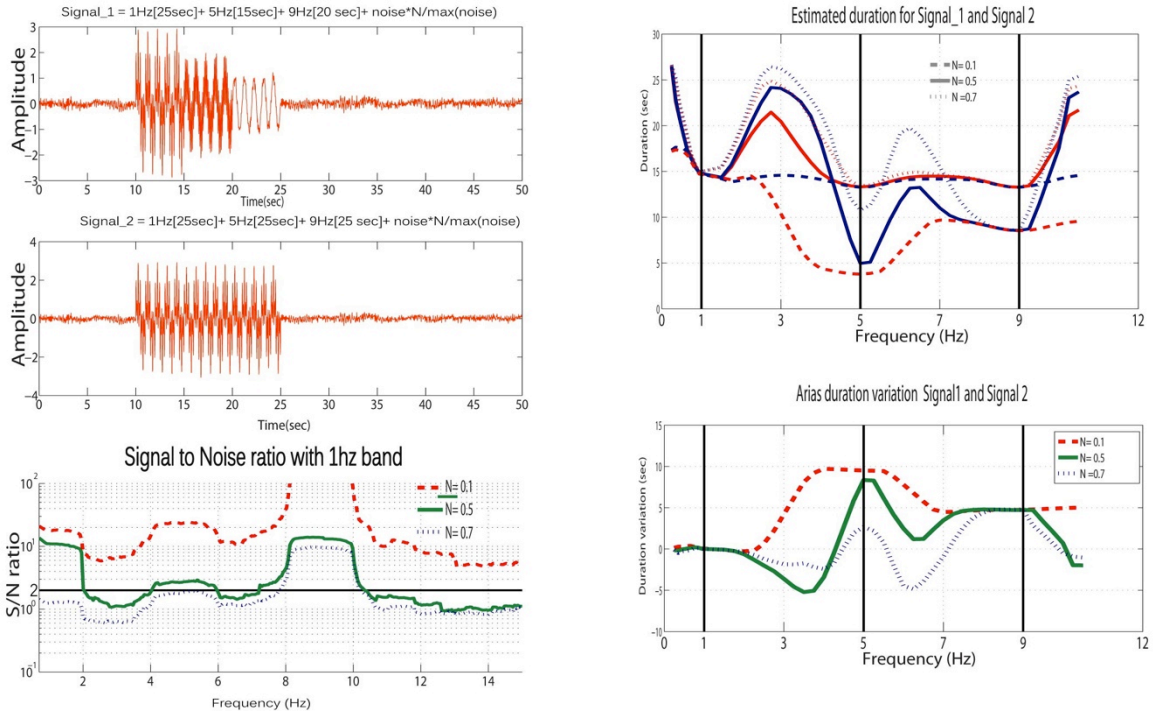

Figure 4.4: Arias filtered duration estimation for summation of sinusoid waves. N – is normalization factor for added noise. The signal in blue has a S/N ratio lower then 3 for frequency 5 and the duration difference is underestimated .

4.4.2 Application to recorded events.

I selected the NS component for an event recorded at the site 11 (epicentral distance of 408 km, magnitude 4.5 ML). In order to test the stability of the method using different time windows length, I select 7 windows between 20 seconds to 200 seconds length for the NS components of both sites (figure 4.5). Arias "filtered duration" and its difference between rock and sedimentary sites are calculated for each time window. Then the duration lengthening is observed at frequencies of 3 to 5 Hz using any windows length between 30 to 200 seconds but the results are stabilized only for windows of 80 seconds or longer (figure 4.5 d). This procedure to estimation the duration different shows that the estimated duration varies with the length of the selected window but the duration difference is relatively stable if the length of window cover the main part of the S or coda wave recorded at the amplified site (sedimentary in our case). Nevertheless, a much longer window does not affect the results, therefore, a choice of a length of about 1 to 2 times the duration of the longest signal is recommended if no new signal appears during this time.

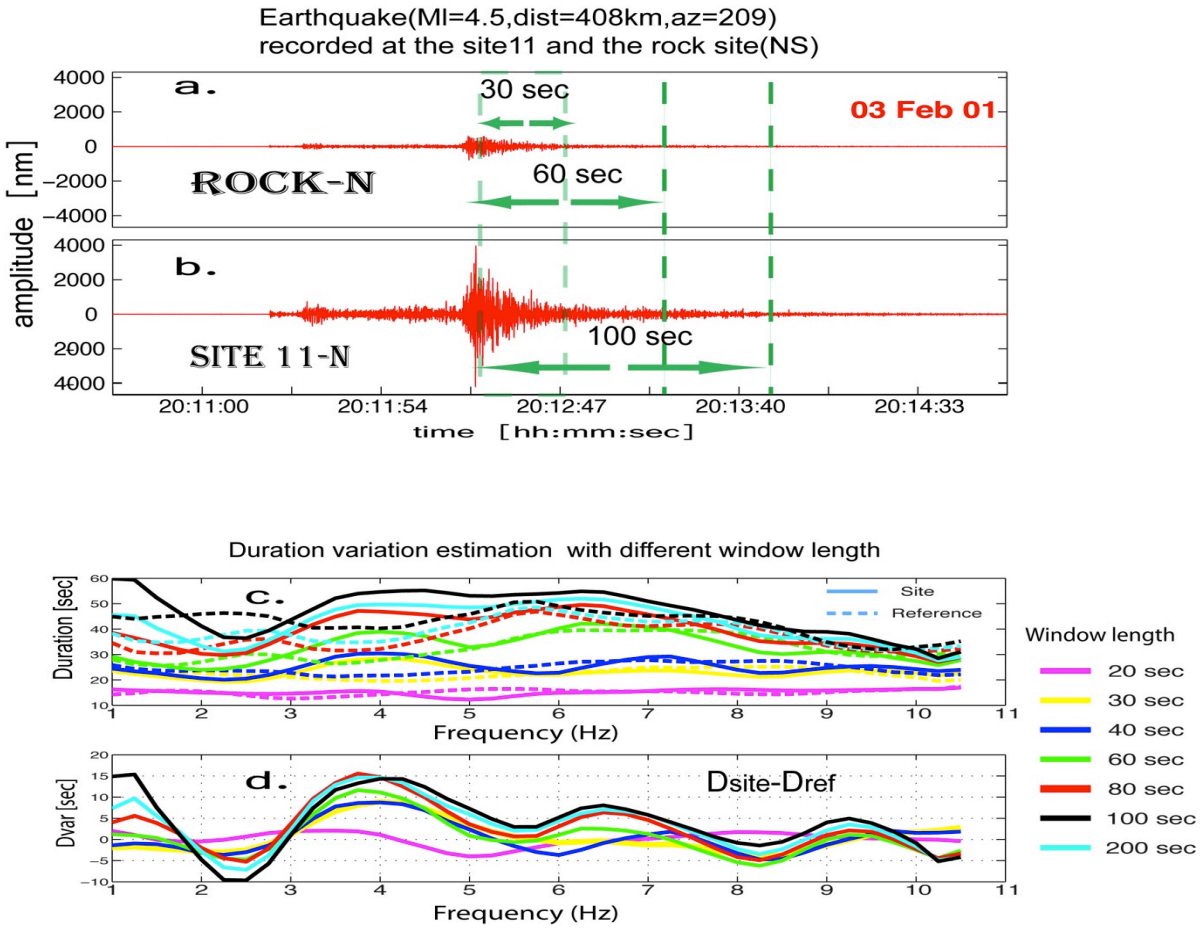

Figure 4.5: The duration variation measurement processes: - a and b are the signal recorded at the site 11 and at the reference site. c -is the measured duration at the site and at the reference point for various length of time window. d -shows the duration difference between site 11 and reference site for different windows length.

4.5 Procedure to measure the absolute duration ratio

It is not the global duration of the ground shaking that interest us but the duration of a certain level of it. Therefore I will measure absolute duration using the same amplitude level on the waveforms recorded at rock and sedimentary sites. In most cases, at Ulaanbaatar basin, the recorded events at sedimentary sites have amplitudes of 2 to 5 times higher than at the reference site. But at the sedimentary site, before the S phase or even P phase, we observe sometimes a noise level amplified in respect to the rock site. Then, this noise level at the sedimentary site can be very high, or even higher, in comparison to the maximum amplitude of this "weak motion

event" recorded at the rock site (figure 4.7). This noise level is also observed after the S-waves coda, which does not allow to estimating a lengthening at a certain level. Therefore, this makes sometimes difficult to estimate the absolute duration using the same level of signal on sedimentary and reference sites using weak motion records.

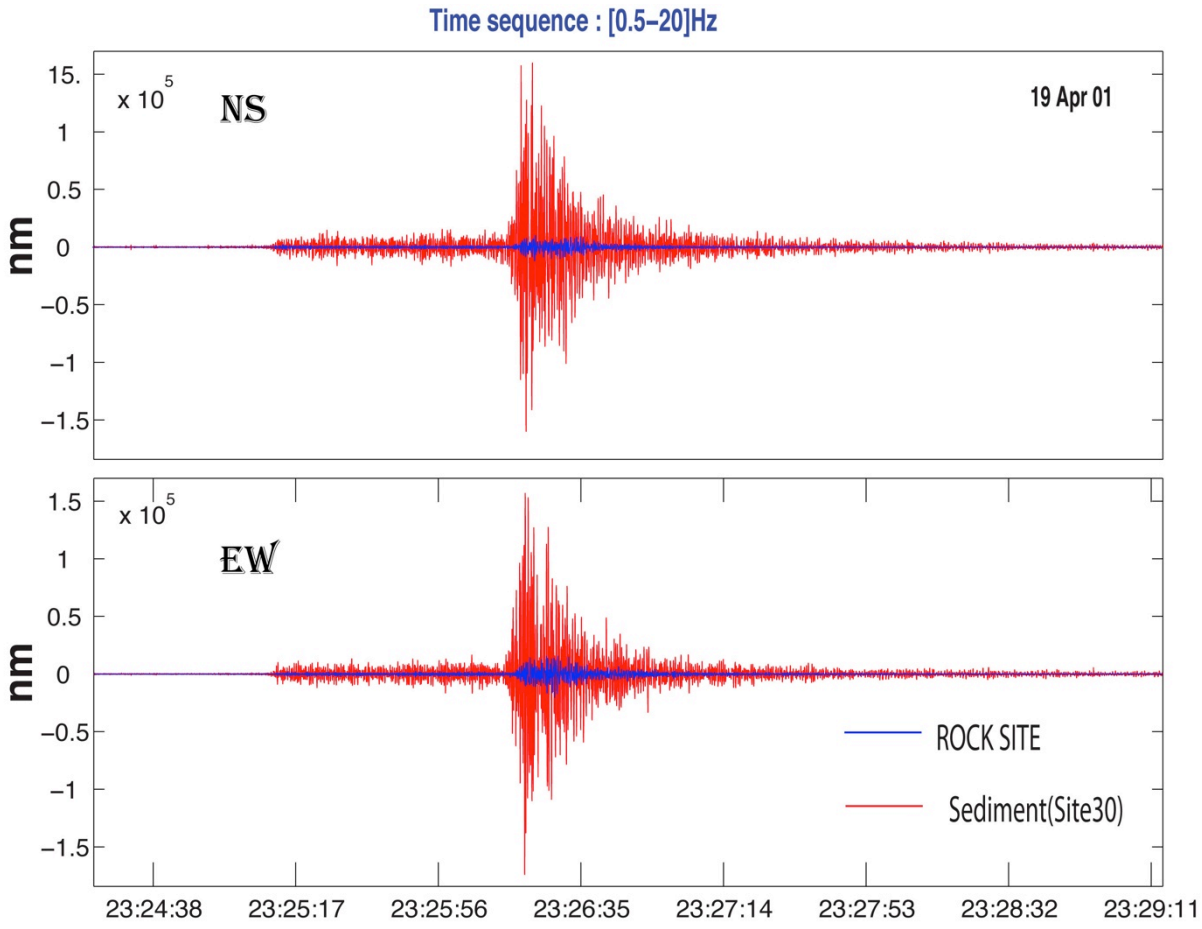

Figure 4.7: Seismic event recorded at the sedimentary site 30 and the reference rock site. The noise level at site 30 before S arrival is of the same order then the S signal level at the rock site.

Therefore I defined the ***absolute duration ratio using the coda-waves decay:*** For that, I fit a curve to the S coda-waves decay on the envelope of the signal in log scale, at site and reference. The absolute duration is taken, at a given level of amplitude of the envelope, between the beginning of the S phase and the decay curve.

To explain the procedure step by step, I take the example of the event "31" (Table 4.1) recorded at site 11 (figure 4.9). The epicentre was at 408 km from the station and magnitude 4.7 ML .

1. First I obtain narrow band signals using zero phase Butterworth filters. The central frequency of the band is assumed to correspond to the band frequency.
2. The envelope of the signal is calculated by taking the absolute value of the analytic signal. For that I applied Hilbert transform and then I applied a 0.2 Hz (this 0.2 Hz depend on event and analysis window length) low pass Butterworth zero phase filter (figure 4.9b).
3. I fit a curve at the decay part of the signals for both records, at sedimentary and reference sites (figure 4.9c). The figure 4.9 d presents the example of 9 filtered signals.
4. I consider the common amplitude range of the two fitted curves as illustrated by the shadow zone in figure 4.8. Then I take the middle of this amplitude range for both curve and plot the time on the both fitted curves (red and blue circles). In this case, the rock site absolute duration is 70 seconds, and the sedimentary site absolute duration is 150 seconds considering the beginning time at 100 seconds (0 is the P arrival time).
5. Then I calculate an absolute duration ratio and a lengthening duration. For this example at the frequency of 4.5 Hz, the ratio is 150/70=2.14 and the lengthening is 80 seconds .

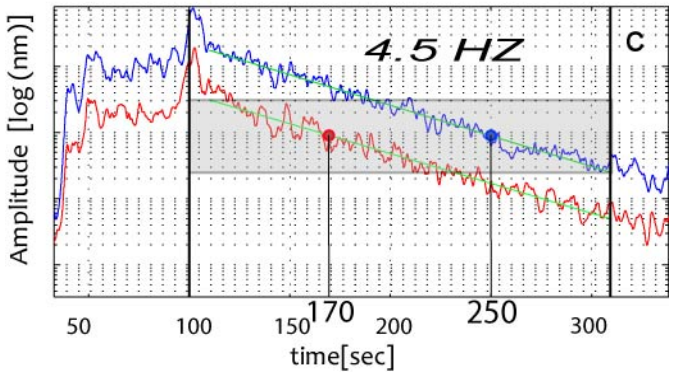

Figure 4.8: Amplitude range useful for absolute duration procedure for the filtered signal at 4.5 Hz (band of 4 to 5 Hz). The shadow zone is the common amplitude range of the decay on rock and sedimentary sites.

6. All the procedure is made automatically, using a script written on Matlab, for 6 different time windows length with a uniform step between them. For example (figure 4.10), I select a signal window of 94 seconds after the S wave arrival and for the analysis I calculated the

durations using 15, 31, 47 … 94 seconds time window. Then I obtain a fitted curve for each analysis window length and for each frequency band signal. Considering the obtained fitted curves and the envelop, I select manually the most reliable results (figure 4.10). I consider that it is not possible to apply directly a specific analysis time window because the optimum one varies with the frequencies and the noise level.

Test on the windows length of the signal used for the calculation.

I tested the impact of the window length for the duration calculation. It is starting at S wave arrival onset (at 100 seconds on figure 4.9b and 4.9 c) until a length of 200 seconds with steps of 20 seconds (Figure 4.9f).

The first 2 windows (20 and 40 seconds) were too short to determine the duration difference because, within these time windows, the minimum amplitude of the fitted curve at the sedimentary site is higher than the maximum amplitude of the fitted curve at the reference point. Above 60 seconds window length, we can easy determine the duration ratio for most of the frequencies bands. Then the duration ratio is quite stable except for frequencies lower than 2Hz for which the variation is plus or minus 0.2 for this event (Figure 4.9f). But for some sites, especially sites that have low SNR as for the event 4 at station UB9, this duration ratio is not stable despite the duration ratio shape is similar for different window analysis length. (Figure 4.10)

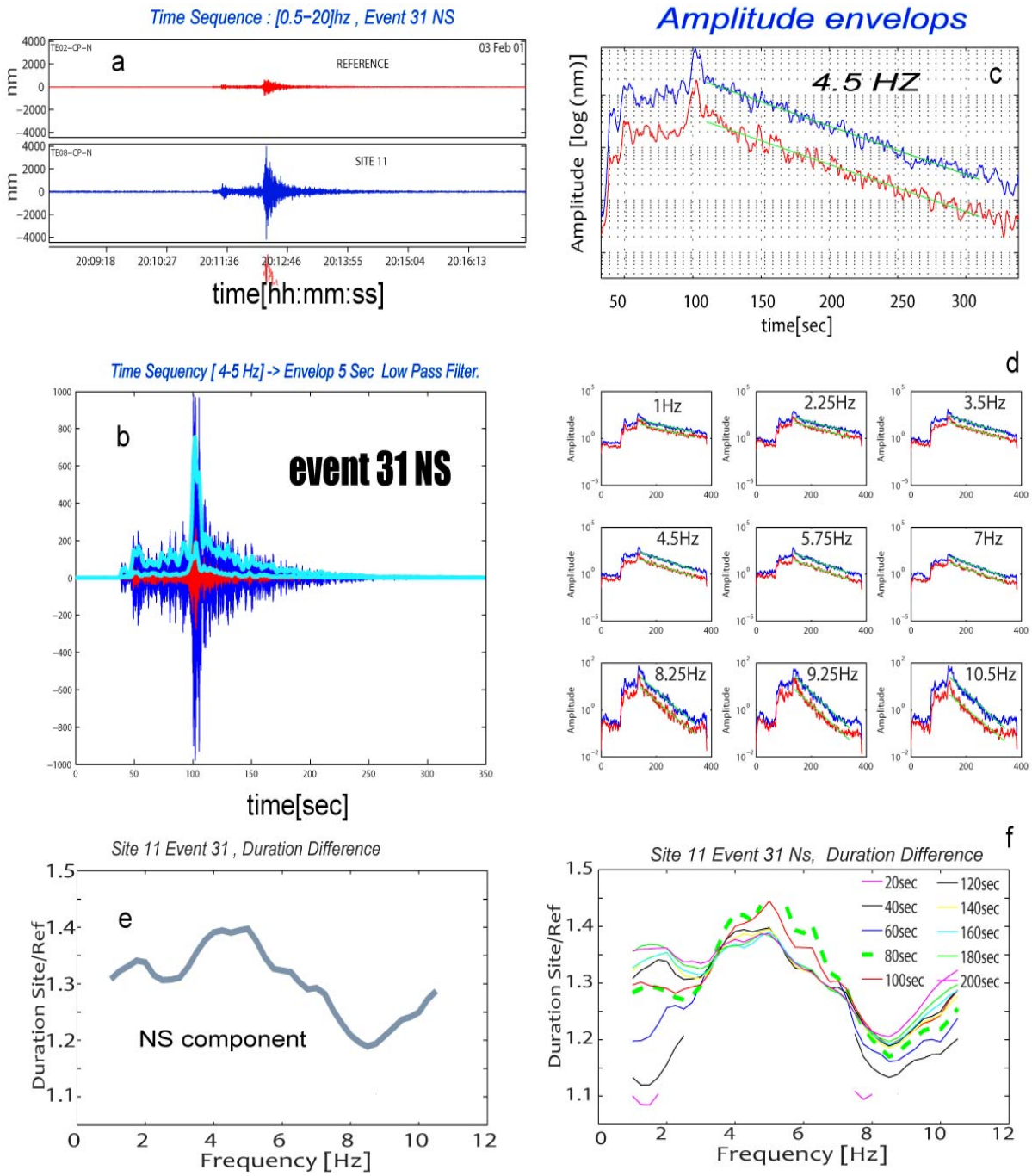

Figure 4.9: Absolute duration measurement procedure at site 11 and event 31. "a"=recorded signal, "b"=envelop of the signal, "c" = fitted curve with S coda-wave envelop "d"=same as "c" for different frequencies band, "e"= duration ratio (sediment/rock) relative to frequency, "f"= same as "e" but for different signal windows length for the analysis.

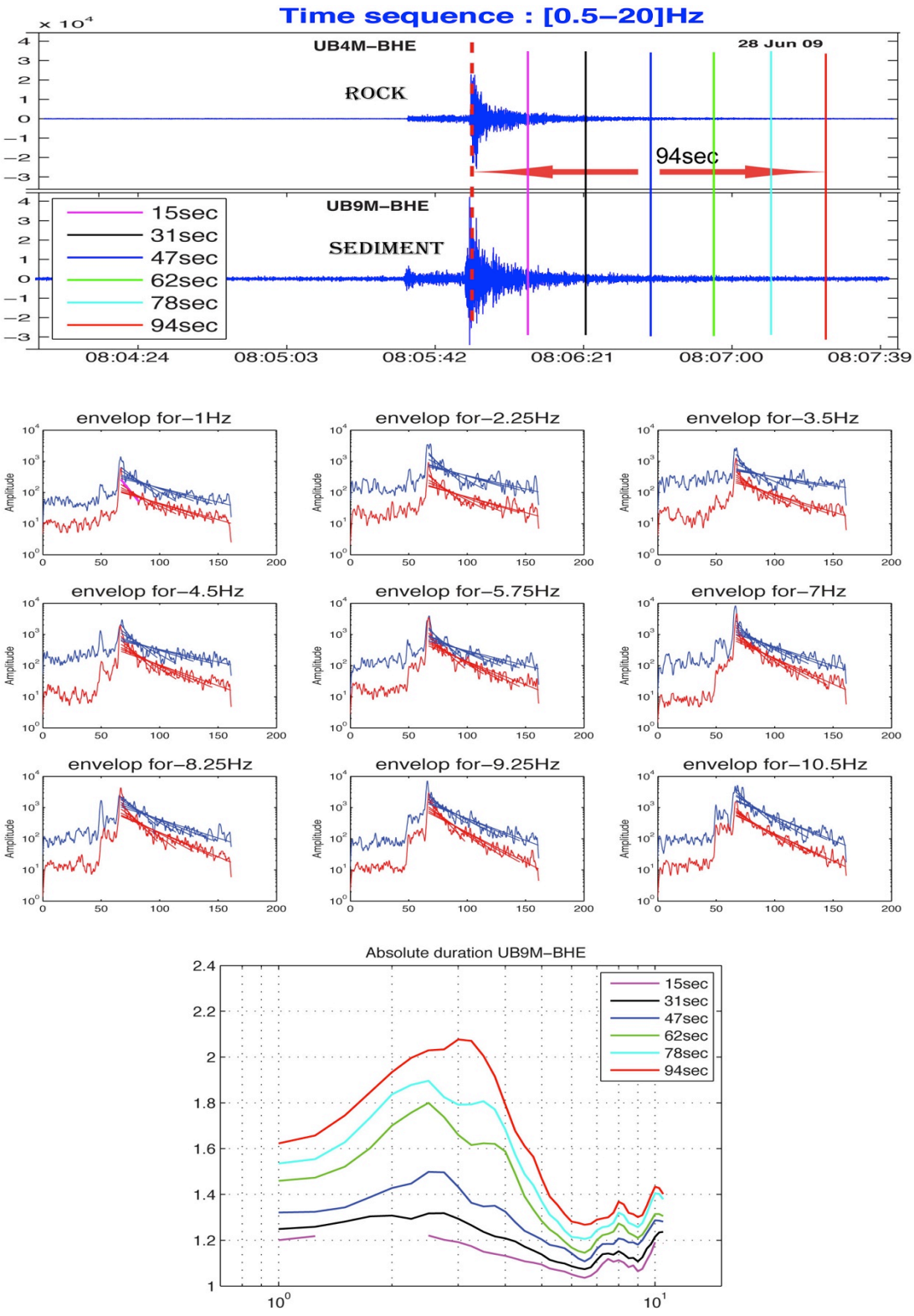

Figure 4.10: Duration estimation process using different time window at site UB9, event 4.

4.6 Result and discussion

4.6.1 Arias duration

The "Arias duration method" is applied for sites when the average of SNR (signal noise ratio) is above 3 for all the frequency range of our interest. Indeed, during the analysis I observed, when a record at a site has low SNR at only certain frequencies, that Arias duration is overestimated even for "good looking" waveforms. The reason is that when the event signal is decaying with time; the noisy part of the signal is still present. Then, the duration with 95% of the energy of the seismogram increases. This effect is strongly observed at site 29 and at site UB9 that are close to the Power plant IV generating high noise at 10Hz.

The results of ***Arias duration*** estimation for different sites were represented in table 5.1. With this method, I calculated duration difference (sedimentary minus rock sites) between -1 to 8 seconds for the horizontal component and between -1 to 11 seconds for vertical components. For each site I determined the average duration difference (Column "Dura. diff-H" and "Dura. diff-Z"). The longest duration differences were observed at sites 6, 17 and 15 (8 seconds). But at site 3 that is located at the middle of the basin, I did not observe duration variation on the horizontal component.

The figure 4.11 (left side) represents the duration difference versus the thickness of sediments under the sites. The average of the duration lengthening of all sites is 2.8 seconds for horizontal component and 4.7 seconds for vertical component.

For the case of the site UB9, I analysed 12 events that occurred at a distance betwenn 100 to 800 km with magnitude from 3 to 4 ML. The duration difference for the horizontal component is -2 to 4 seconds and -1 to 11 seconds for vertical components (figure 4.10).

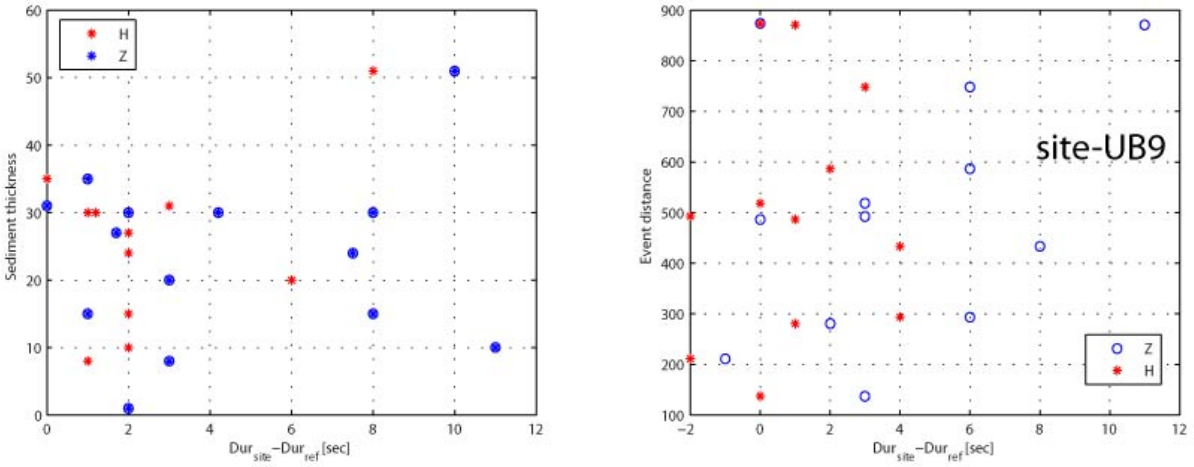

Figure 4.11. Duration difference calculated with respect to reference sites. The differences are shown against estimated site sediment thickness (left-hand). Duration difference estimated at site UB9 for 12 different events against its epicentre distance (right-hand)

At UB9 site, for events 13 and 18, we observe a duration shortening. This can be due to the duration estimation procedure itself. For example, if the high frequencies are amplified due to site amplification, then the high frequencies dominate in the whole waveform. After normalized we will estimate this high frequency duration. But if waveform recorded a rock site has more lower frequency content then decay will be longer. This difference can be reflecting for this Arias duration estimation procedure.

To clarify the idea, I used simple signals generated by the summation of sinusoids (Figure 4.4.) . First sinusoids have frequencies of 1, 5 and 9 Hz and with durations of 25, 15 and 20 seconds respectively. Second signal is assuming same as first signal but amplified 3 times at 5 Hz. This shows that the duration length calculated by this method for the amplified signal is shorter than non-amplified signal.

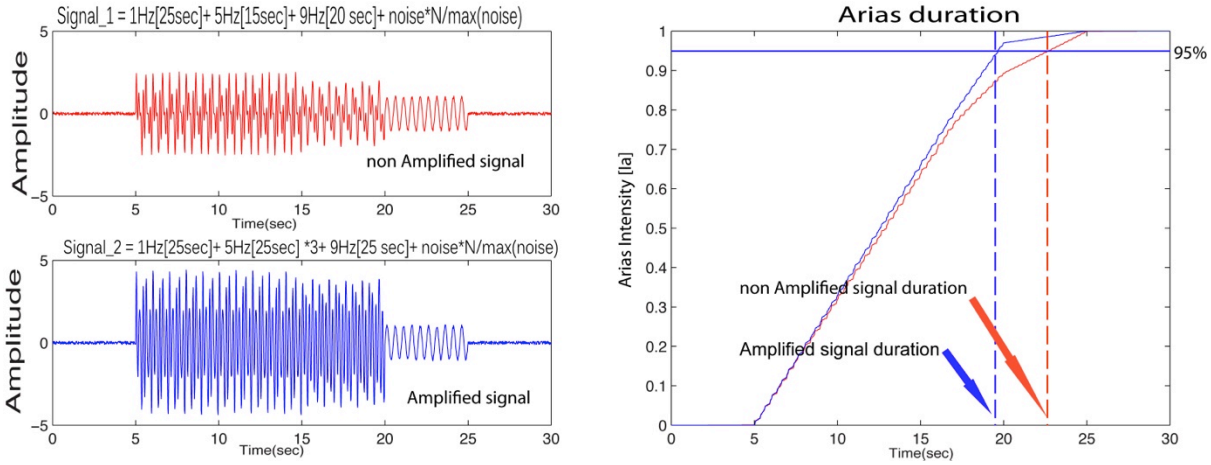

Figure 4.12: Illustration of apparent shortening duration, using Arias duration, due to particular frequency amplification using simple sinusoids.

Wit this method I observed that the Z component has higher lengthening than horizontal component. This can be explained as the Z component is less amplified than horizontal component (see figure 4.12) and it contents more surface wave.

If we compare the obtained duration lengthening at Ulaanbaatar basin with those obtained at Santiago basin (1.5 to 2.3 times lengthening) determined by the same Arias duration method, [Pilz et al. 2009], we see that the lengthening at Ulaanbaatar it is much smaller. They are several possible explanations, some are related to the geophysical process, other are related to the method: 1) Ulaanbaatar basin is a more shallow and open basin that does not induce signal lengthening or only small lengthening deduce from this method, 2) for this analysis, I used weak motions that have probably not sufficient energy to generate surface wave which are, for many authors, the main reason for the duration lengthening of the ground motion. 3) The Arias duration is representing the duration of the 90% of the main motion; therefore if the lengthening is related to a small part of the "energy", the Arias duration will not be sensitive to it.

4.6.2 Arias frequency dependent:

I observed small differences between recorded weak motion at sedimentary basin and rock sites using arias duration difference. Nevertheless, it is possibly that the ground motion is lengthened at certain frequencies.

Therefore I calculated the duration difference with the ***Arias duration on filtered records*** on the same data. First I applied it on the 12 events recorded at the site UB9. The duration differences by frequency calculated were not stable event to event (figure 4.13 right side). On the same events, I calculated the Standard Spectral Ratio (Horizontal component) using UB4 station as reference for rock (left side of figure 4.13). They are no relation between the stable amplified frequency observed with SSR (2 to 3Hz) and the frequencies having the longest duration increase (5 to 8Hz) with this method.

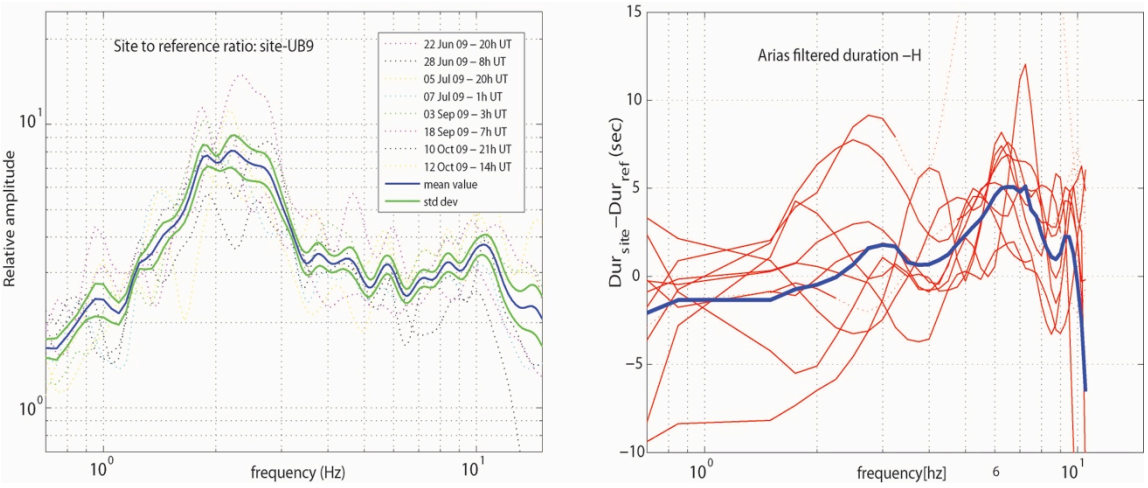

Figure 4.13: SSR between site UB9 (sediment) and site UB4 (rock) for the 12 recorded events. Right side: Arias duration difference versus frequency at site UB9 for the 12 recorded events.

I applied the same procedure on the other sites with measured weak motion. The sites were grouped into two classes; one is for the sites lying on 1 to 15 m of sediments (class 1-15 m) and the other for the sites lying on 20 to 35 m of sediments (class 20-35 m). For class 1-15 m, the duration variation is within a range of about plus or minus 5 seconds for all frequencies, and for

class 20-35 m the duration lengthening up to 15 seconds for certain frequencies (figure 4.14). The value considered at each site is the average between various records.

For UB9 site (figure 4.13 right), the most stable lengthened frequencies are between 5 to 8 Hz for most of the events with a duration lengthening between 2 to 10 seconds. This lengthened frequency was more or less observed at all sites. Nevertheless, it seems that it is at lower frequency for thickest parts (class 20-35 m). The lengthening duration is more important for class 20-35 m (up to 12 seconds) then for class 1-15 m (up to 8 seconds but most of time lower). Unfortunately, the records at stations on the thickets part of the basin have low SNR that makes difficult to estimate the Arias duration.

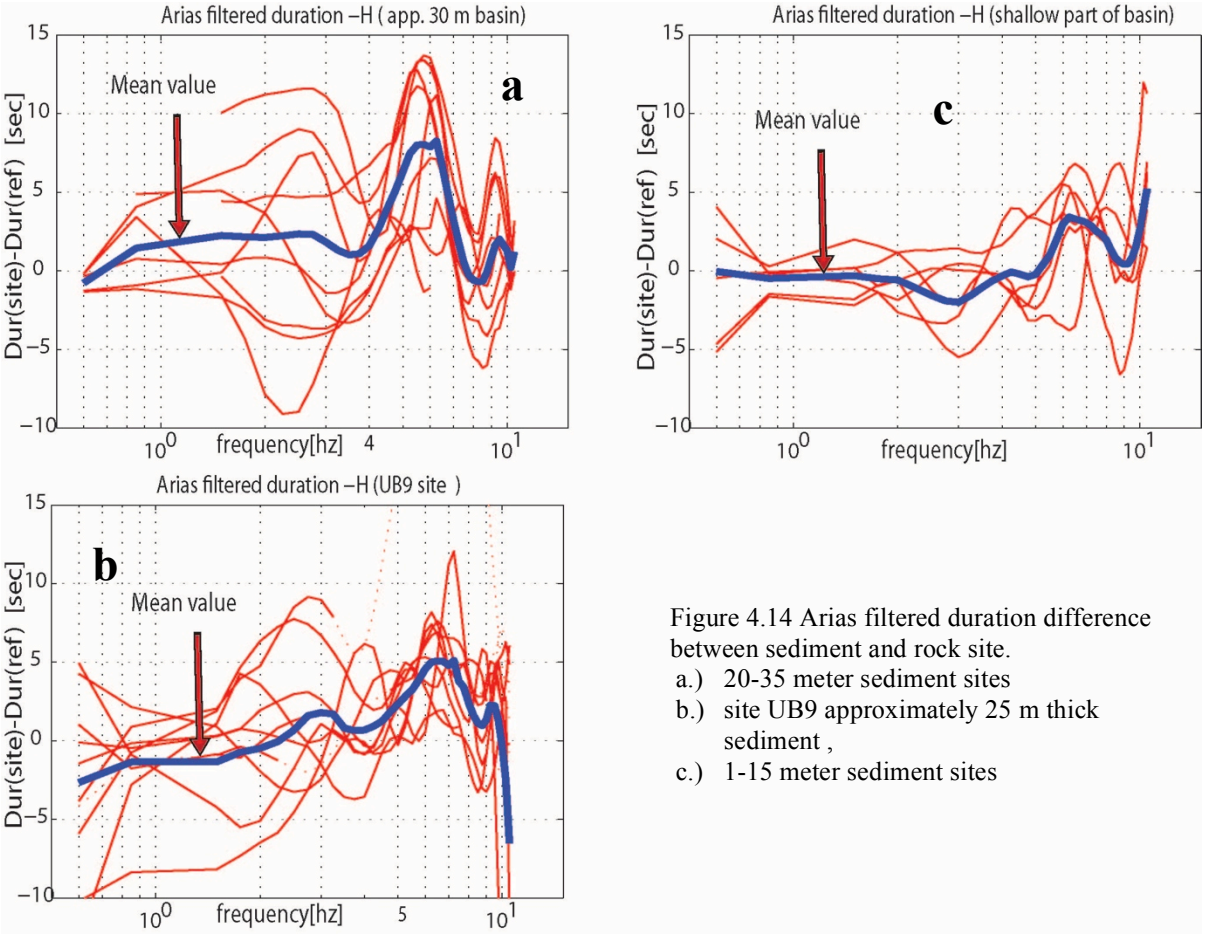

Figure 4.14 Arias filtered duration difference between sediment and rock site.
a.) 20-35 meter sediment sites
b.) site UB9 approximately 25 m thick sediment ,
c.) 1-15 meter sediment sites

4.6.3 Comparison of the duration, using Arias frequency dependent duration, between 2D modelling and field records.

The 2D spectral element method [Mariotti, 2007] was applied to model the seismic waves through the Ulaanbaatar basin (see chapter 3). At the top of the sediment layer, we putted 30 virtual stations with a distance between them of 1 km. I calculated the arias filtered duration difference using the simulated waveforms. The results are compared with the observation obtained at sites near to the cross section area. The duration estimated by the 2D simulation is compared with sites 3, 15, 29, 30 and UB9 (figure 4.15). Before interpreting the results, we should consider the following limitations: 1) the 2D simulation used waves that propagate only along the cross section plane, 2) the observed sites were not exactly on the cross section, 3) the simulation used a simplified 2D basin model. Nevertheless, the comparison shows us that, with the Arias frequency dependent duration method, the observed and simulated signals have an increasing duration at similar frequencies and a lengthening of the same order.

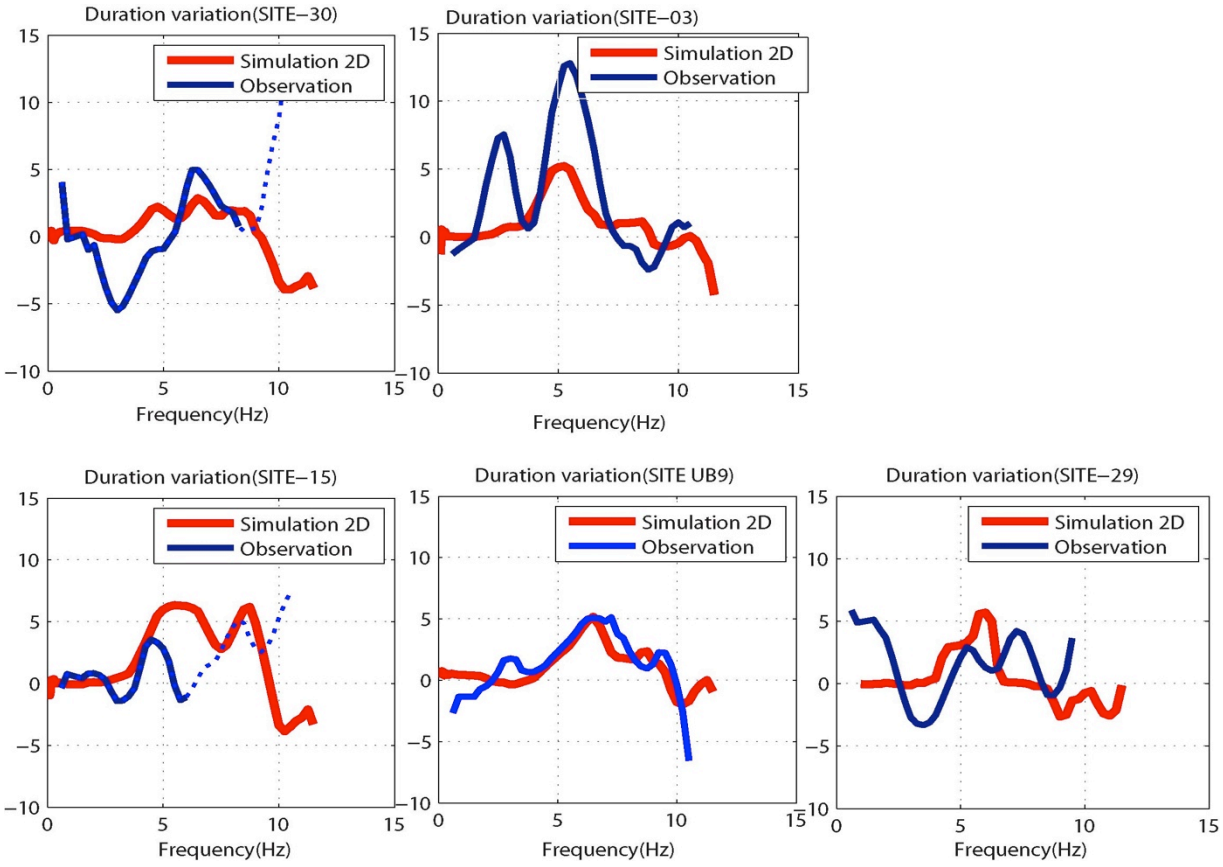

Figure 4.15: Comparison of the duration variation deduce from 2D simulation and observed data (Arias frequency dependence duration).

We can then assume that the durations estimated with the 2D simulations can represent the lengthened frequencies of the basin, at the cross section area. Then, these simulated waveforms, at each kilometre along the cross section, give us the possibility to generate a map of the duration variation, in respect to rock site (figure 4.16.). In the simulation, the class 20-35 m corresponds with the cross section distance of 4 to 7 km and 23 to 31 km (figure 4.16: x-axis). As we saw in previous part, we obtain from this simulation, at site on 30 meter thick sediment, a duration lengthening of about 5 to 7 seconds at frequencies around 4 to 7 Hz, similar to those observed on field records.

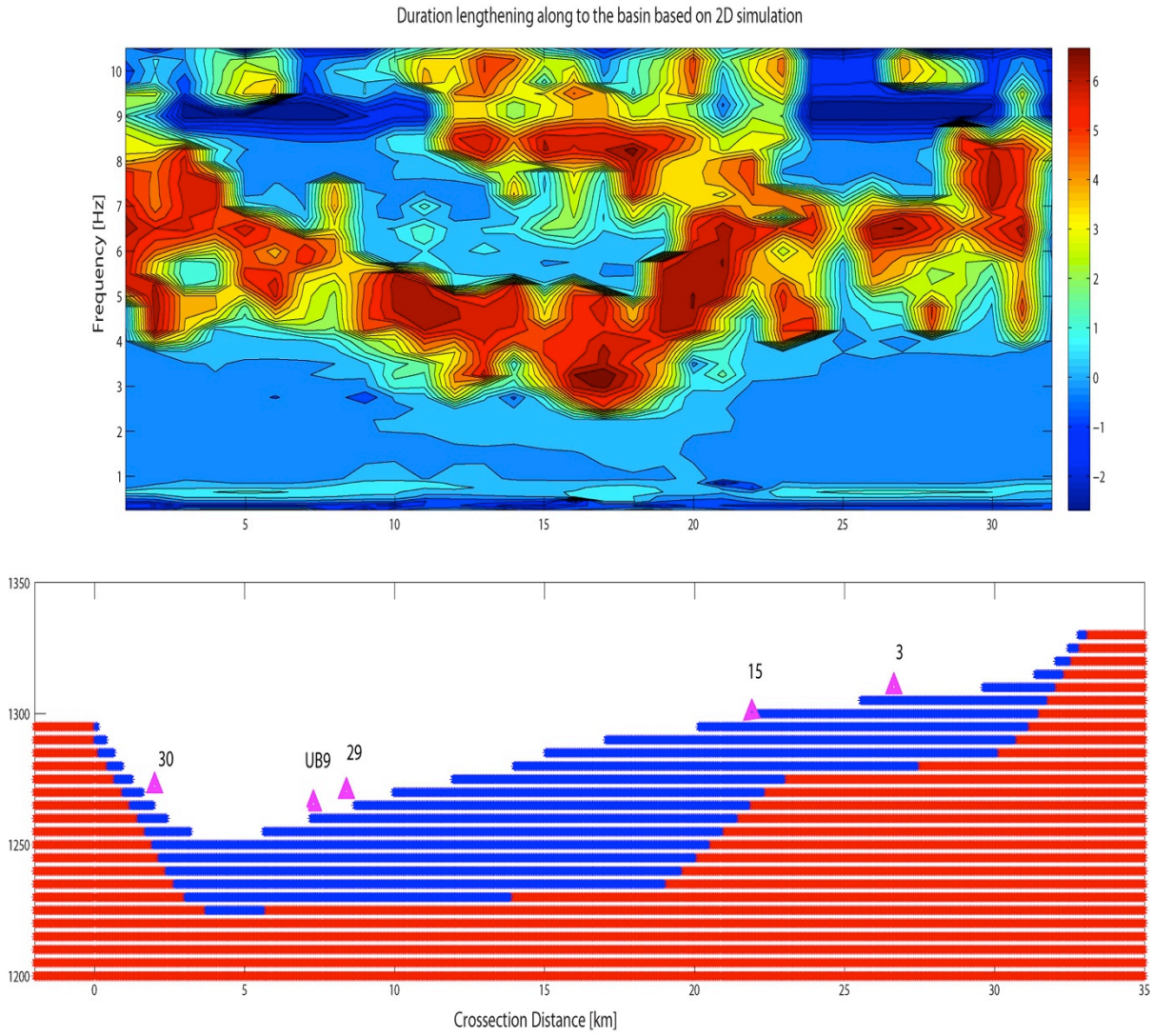

Figure 4.16: Duration lengthening along the cross section area using arias filtered duration.
For both graphs, X axis is the distance along the cross section. Top graph, Y axis represents the frequency and the colour contours represents the duration difference between rock and site in seconds. Bottom graph, Y axis is the altitude, blue colour is the sediment and red colour is the bedrock. Triangles are real stations located near the cross section.

4.6.4 Absolute duration ratio

The procedure to calculate the absolute duration ratio is applied for each component separately. The estimated duration ratio for the 12 events recorded at the site UB9 and the SSR is presented in figure 4.17 (UB4 as rock reference site).

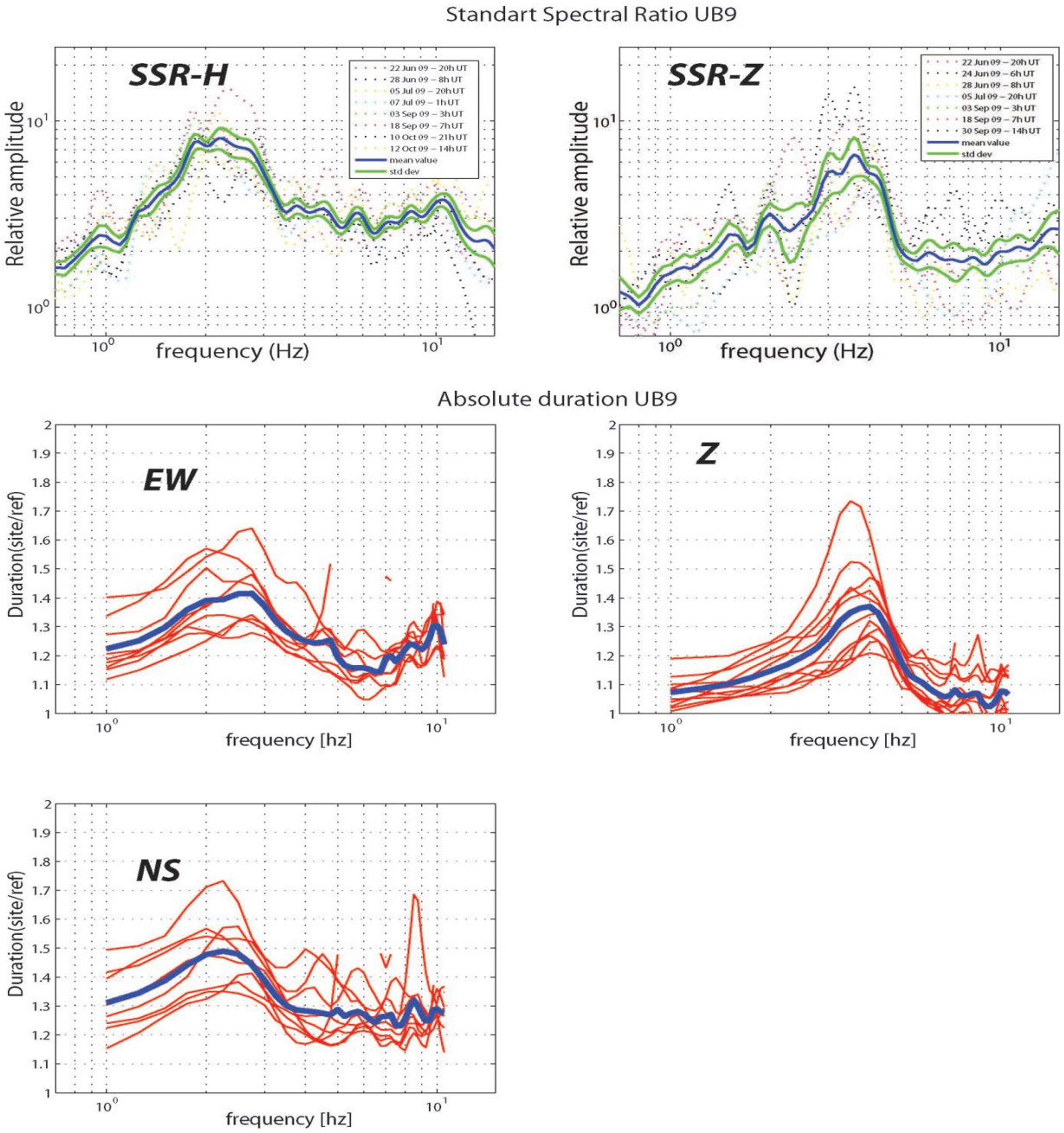

Figure 4.17: Top: SSR of UB9 site respect to UB4 for H(EW+NS) and Z components. Bottom: Absolute duration ratio measurement result UB9 site for EW, NS and Z components.

The results show that curves of absolute duration ratio with frequency give very similar shapes than with SSR shape for both vertical and horizontal components. The analysis of several events

recorded at a single site (UB9) shows that the duration ratio between sediment and rock sites have a general shape of lengthening (or most lengthened frequencies) very similar for the various events despite they are small local variability.

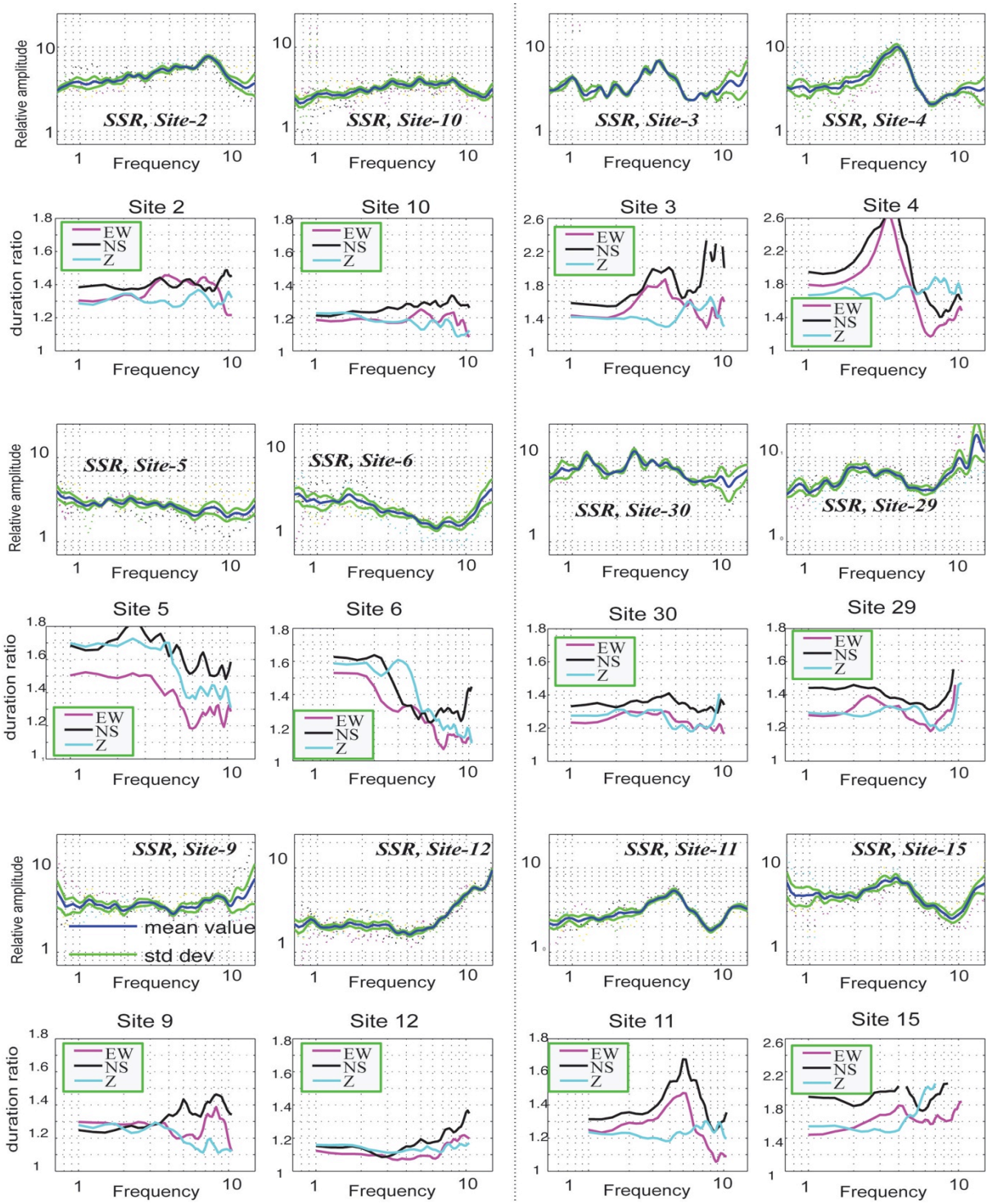

Figure 4.18: Absolute duration ratio measurement results of different sites for EW, NS and Z components and it's comparison with SSR of horizontal components.

Using same events and same stations (sediment and rock respectively at UB9 and UB4) the SSR of horizontal components are compared with the duration ratio. They have a very good correlation (figure 4.18). We observe also that horizontal components are always more lengthened than vertical components. This means that duration lengthening of weak motion at Ulaanbaatar basin is mainly due to its amplification factor (same frequency and more important for horizontal component). The ratio value is between 1.4 to 1.8 for most sites, then the average lengthening is about 40% with a variation up to 80%. .

The duration ratio has been calculated using 40 to 100 seconds window length. The duration ratio is more important for short windows and seems to be stabilized for longer one with a value of about 1.4 (left side figure 4.19). The windows length has an impact on the result and, as previously explained, it has to be optimized.

On the other hand, when the sediment thickness is increasing the duration ratio value is increasing with value up to 2 (right-side, figure 4.19.)

These results show that, probably, the duration lengthening is mainly connected to the site amplification itself (1D), at least for weak motion.

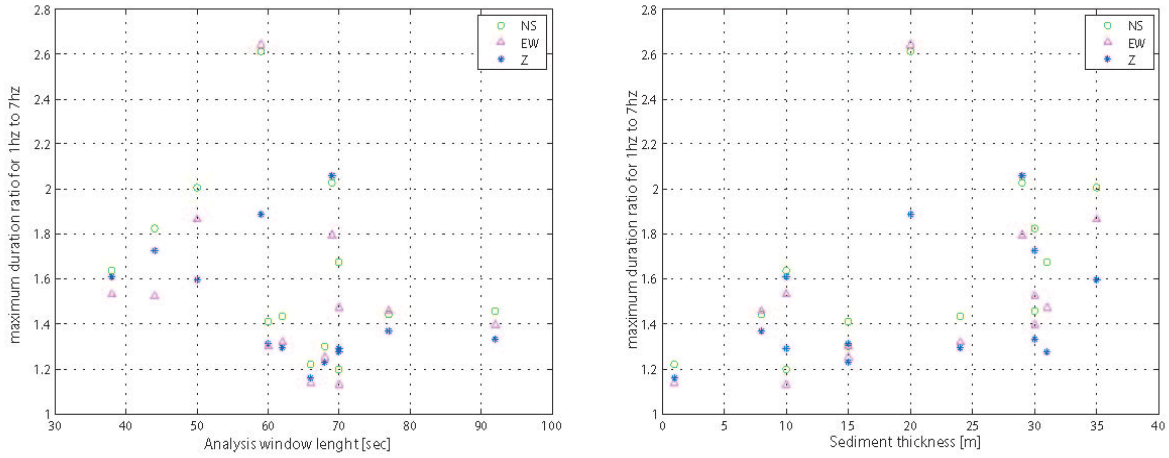

Figure 4.19: Left-side: Maximum duration ratio value versus window length used for calculation. Right-side: maximum duration ratio versus the sediment thickness of the site.

From figure 4.18, we can observe that the NS component has, at most of the sites, a longer duration ratio than the EW component. Then a question raise, does it means that, at Ulaanbaatar basins, the NS component of seismic wave has always stronger lengthening than the EW component? Therefore I calculated the SSR ratio and absolute duration for all events recorded at the UB9 sites, for each horizontal component (figure 4.20). The SSR ratio for individual components shows that NS component has always higher amplification than EW components.

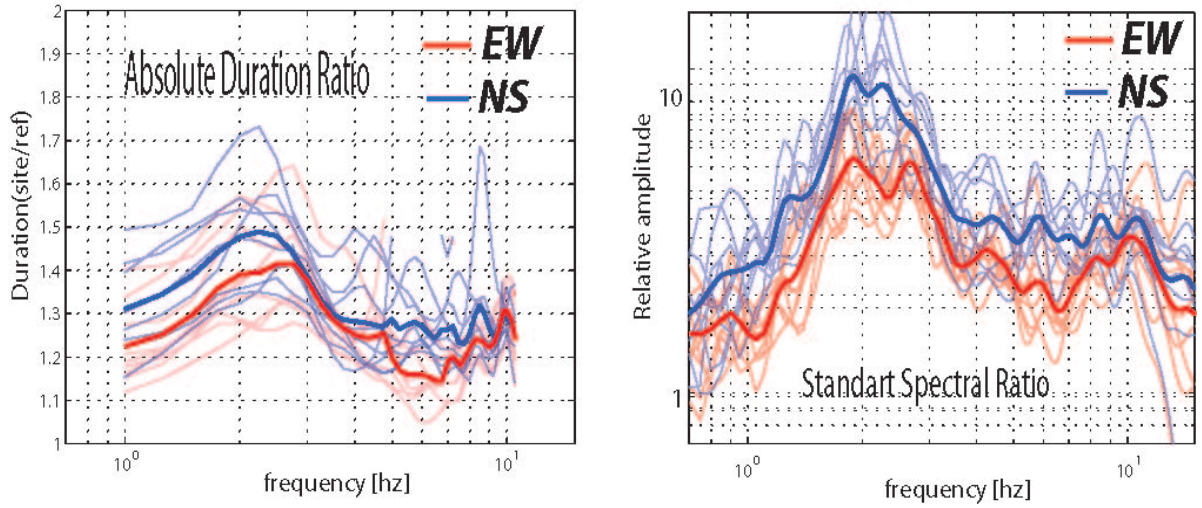

Figure 4.20: UB9 site: Absolute duration results for NS and EW components and its mean value (left-side). Standard spectral ratios for NS and EW components and its mean value for the same 12 events (right-side)

This kind of amplification difference cannot be directly related to 1D effects. Then, probably, this is due to polarization effects of the surface wave generated by the edge of the basin. Joyner (2000) made the following consistent assumption. Basin waves are polarized predominantly in the direction parallel (Love waves) and normal (Rayleigh waves) to the edge of the basin. As the Ulaanbaatar basin is along an EW direction, the NS direction predominating surface waves could be Rayleigh waves.

Consequently, ***with arias duration***, I observed only small duration lengthening. This could be due to several reasons. First I used weak motion records for all analysis that have

probably not sufficient energy to generate observable surface wave or trapped waves with that method.

With Arias filtered signal I observed small duration lengthening (5 to 10 seconds) at areas on 20 to 35 meter of sediment. This lengthening was quite in good agreement with 2D numerical simulation obtained for a cross section along the main trend of Ulaanbaatar basin. The amplified frequencies were different from the duration lengthening frequencies. They are then related not to 1D effect but 2D or possible 3D effects.

At the end, I observed clear duration lengthening, due to amplification factor, using ***Absolute frequency dependent duration*** measurement technique. With this method, I observed that the NS component shows in most cases longer lengthening that the EW component. For UB9 site, I observed 2 different frequency ranges lengthening. The first frequency was the same with the most amplified frequency and the second was close to the frequency lengthened observed with Arias filtered duration but with very small lengthening. The Absolute duration lengthening show that the duration is extending by a factor of 1.2 to 1.8 except at site 4 where the observed duration is extended up to 2.6 times at around 3-4 Hz.

In conclusion, the estimation of the duration depends strongly on the method used. The arias intensity duration method is not adapted for weak motions data. The Arias filtered duration gives interesting information on the lengthened frequency but does not describe clearly duration variation using weak motion data. At the end, the absolute duration method, which I developed using coda-waves, gives the best results with our weak motion data. We observe then a duration increase between 20 to 80% and locally up to 160% at particular frequencies . These results are important for the seismic hazard assessment of Ulaanbaatar and for the risk mitigation.

CHAPTER 5: Conclusions

5. CONCLUSIONS

The purpose of this thesis is the estimation of the characteristics of site effects generated by the sedimentary basin of Ulaanbaatar, capital of Mongolia. An explicit aim of the study is to progress as far as possible using ambient noise and weak motion records to estimate the site effects of an urban area in point of view of amplification, amplified frequency and ground motion duration.

For the analysis in this thesis, I used weak motion signal recorded at 32 sites and ambient noise recorded at 104 sites with a limited number of stations (maximum 8 in same time). For the weak motion records, the seismic stations were deployed during 1 to 2 weeks at each site in order to detect several seismic events. We could record at each site 1 to 3 events but, due to high seismic noise level in the urban area, several events could not be used as the signal noise ratio was below 3 at some frequencies. For ambient noise measurements, the seismic stations were deployed between 30 minutes to 2 hours at each site.

Some sites were strongly disturbed by local noise. Therefore, an analysis was made to compare, using various ambient noise level, the impact of the noise on the HV spectral ratio and the reliability of the results. The study of the diurnal variation of the HV spectral ratio of ambient noise shows that, for site effect studies, the ambient noise measurements should be done during the quiet hours of a day, when man-made noise within the urban environment does not exceed a desirable level. Also local strong sources can have an important impact on HV results especially if low frequency is observed.

When we use the recorded seismic signals, weak motion, the HV and SSR analysis give the same amplified frequencies but different amplification factor. The obtained amplified frequency is independent from the used methods (HV and SSR). For the

amplification factor, we can only use SSR and the observed amplification factor of the basin is in the range 3 to 10 on weak motion. The extrapolation to strong motion is still under question and was not simulated in this work.

The HV polarization analysis, on ambient noise records, shows that the same HV peaks are observed at all azimuths but with different amplitudes. On the other hand, I show that the amplified frequency bands, observed with HV ratio, are polarized. Diurnal analysis of HV spectral ratio shows that the amplified frequency, obtained from HV ratio, is polarized in a specific direction during several hours but polarization direction vary during a day especially during night time near the Power plant IV. A polarization is observed at 10 Hz near the Power plant IV that generated seismic noise. Despite we had only limited number of data and observations, it seems that near strong source of seismic noise, the amplified peak of ambient noise is polarized perpendicular to the direction of the noise source.

During my thesis, I built a GIS database for the Ulaanbaatar basins physical and geometrical properties including the existing gravity data, seismic profiles and drilling information. Based on this database, I produced the first 3D digital geometric model of the Ulaanbaatar basin for the interface between bedrock and sedimentary deposits.

I determined 3 S-wave velocities profiles along the basin using the array technique. I calculated amplified frequencies over all the basin, with shake91 and input parameters coming from the 3D model (for local thickness) and the velocities profiles (average shear wave velocity measured locally). I generated then a map of amplified frequencies, which is in good agreement with the frequencies obtained from the HV ratio observations except on Noegen clay and locally at the east and west borders of the basin. This misfit could be due to the velocity structure used not adapted for these sites. Therefore, in the future, it is necessary to improve the basin geometry and the velocity information by adding array measurements in the basin and collecting more reliable geological and geophysical information.

2D seismic wave simulation was applied along to main trend of the basin using a 2D version of Mak3D code. This 2D simulation can explain wide observed peak where the basin interface between sediments deposits and bedrock is dipping. But, at this step of the simulation, the amplified frequencies were estimated at higher frequency than the HV observed frequencies. This could be due to several reasons. Firstly, attenuation of the basin is poorly known, also recorded sites were not laying exactly on the cross section used for the simulation. Another reason is the misestimating of the interface geometry for the cross section itself (not enough information on the basin, resolution of simulation with a grid of 5

meters, which could create 1 Hz shift for the amplified frequency). This 2D simulation is prolongated to a 3D case as a part of continuous collaboration between RCAG, CEA-DASE and EOST.

Moreover, I evaluate the duration difference, for weak motion records, between rock and sedimentary site. I used an approach based on the envelop of different frequency bands obtained by filtered signals (using absolute level of amplitude power). The observed lengthening reached locally 160%. Also it is observed that the NS component has a more important duration lengthening than the EW component for all my observations that cannot be explained by only a 1D effect knowing that the basin of Ulaanbaatar is mainly oriented EW.

We can observe a lengthening duration, using normalized Arias intensity, due to other basin effects then 1D. We observe locally, by this approach, lengthening between 5 to 13 seconds for 40 to 80 seconds weak motion signals. The lengthened frequency is always higher than the amplified frequency. The obtained lengthening is has good fitting compared with the 2D simulations.

The duration lengthening, observed on weak motion records at Ulaanbaatar basin, is mainly due to 1D amplification.

This whole work allows me to propose a zoning of the site effects, induced by the basin of Ulaanbaatar, which is essential for the seismic hazard assessment and its consideration for the risk mitigation of the capital of Mongolia. (Figure 5.1)

This work was possible thanks to equipment provided by CEA-DASE and fruitful collaboration between RCAG, EOST and CEA-DASE.

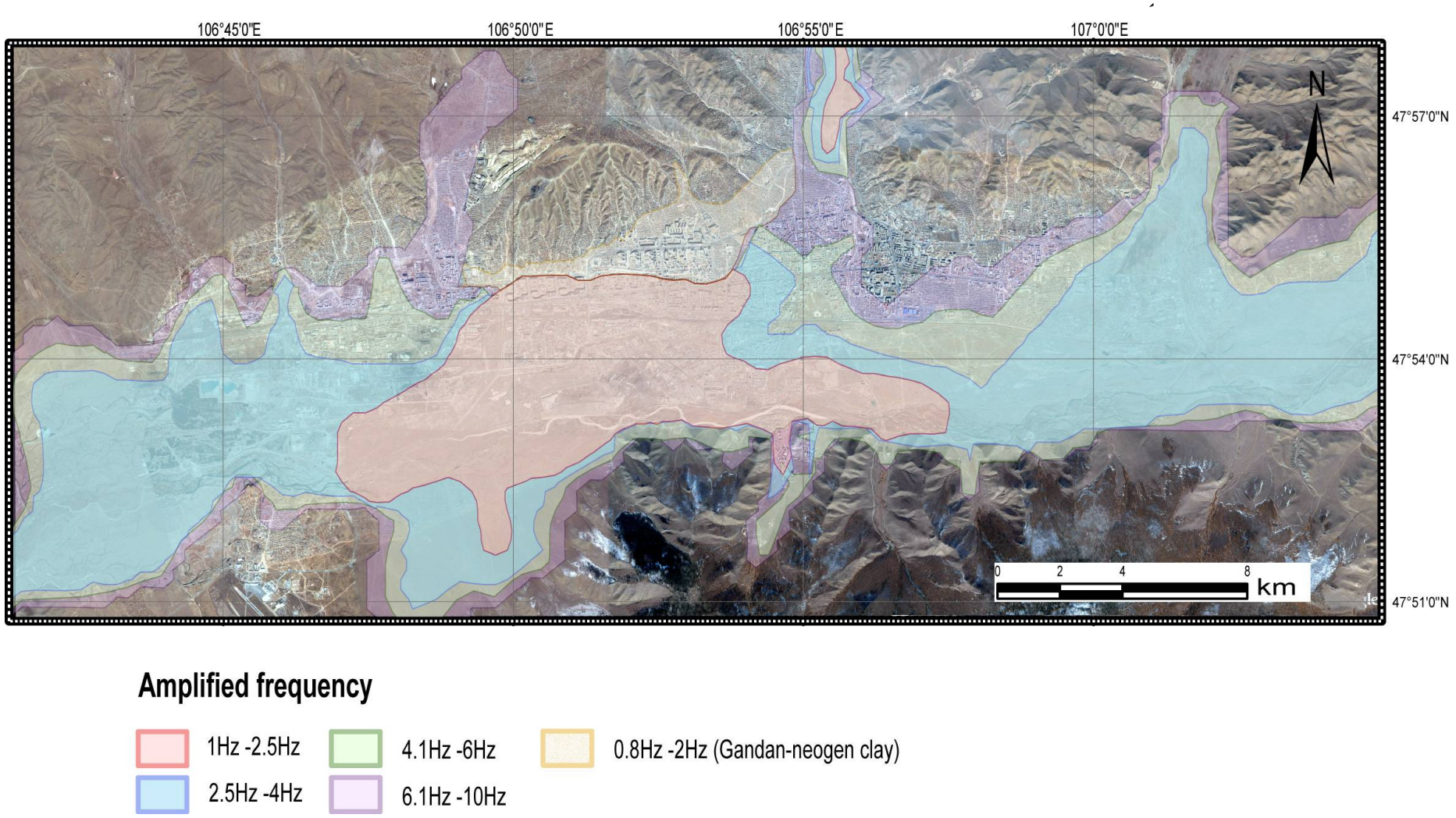

Figure 5.1: Amplified frequency zoning map for Ulaanbaatar basin

APPENDIX

APPENDIX A

HV AND SSR RATIO COMPARISON RESULTS FOR WEAK MOTION RECORDED SITES.

During field measurement time 32 sites were deployed seismic stations for 1-3 weeks. We recorded weak motion at 29 of them. At each site were applied HV and SSR ratio. HV ratio was applied using noise measured period and also using weak motions. The obtained results at each site for HV noise, HV event and SSR are represented in figures A1 to A5. Few sites, despite they were measured over long time, did not record clearly events and I could then only apply HV noise spectral ratio technique, the results are represented down side of the figure A-5. For sites with short time measurements I applied HV noise spectral ratios which are represented in the figures A6 to A10. The result of microtremor HV spectral ratio analysis (HV noise) is summarized in the Table A.1. For HV noise ratio analysis, I classified the microtremor records at each site with it's maximum amplitude level and signal distortion level.

Distortion level low: signal has low amplitude up to 500 nm and in the time sequence there is not clear spike or very few making easy to select period of time for HV noise ratio analysis.

Distortion level middle: signal has amplitude up to 1000 nm and in the time sequence there is clear visible of local noise and few spike making that HV noise ratio analysis always include some part of spikes.

Distortion level high: In the time sequence there is clear visible local noise and many spikes and during all the measurements period the signal seems perturbed with local noise that make difficult to select portion of signal for HV noise analysis.

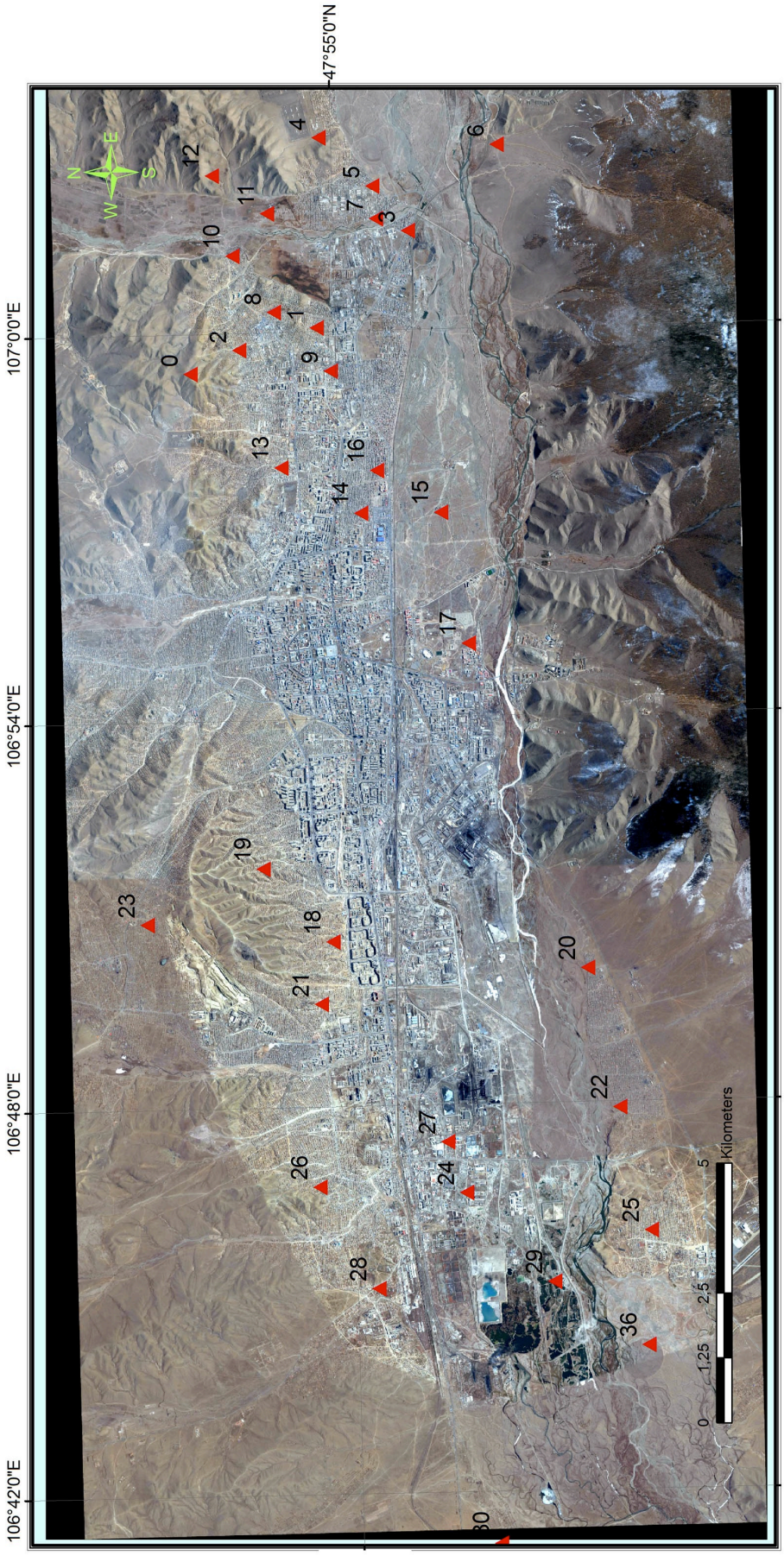

Figure A.1: Long time deployed stations position.

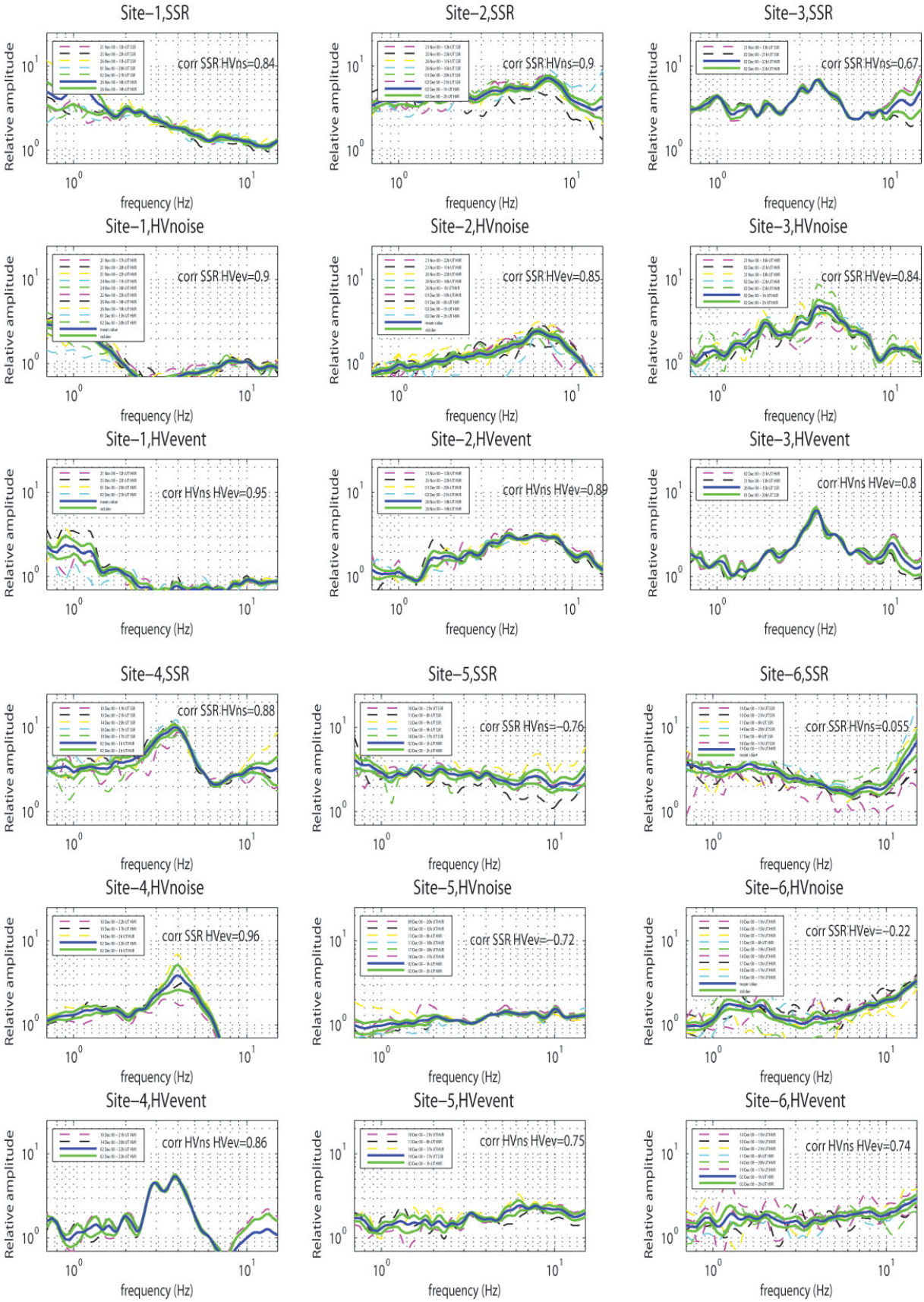

Figure A.2: HV noise, HV event and SSR ratio for each site with recording over long period of time.

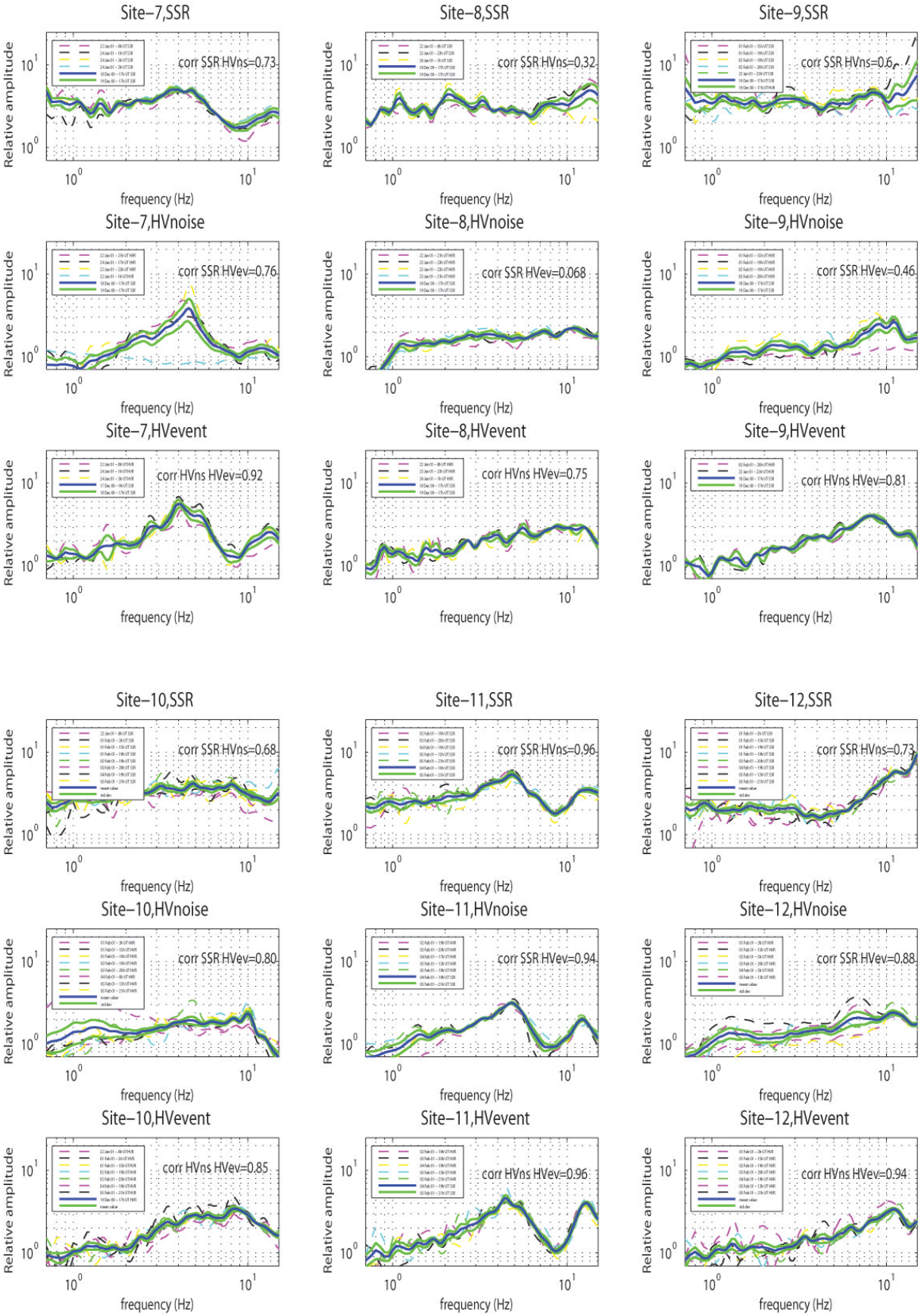

Figure A.3: HV noise, HV event and SSR ratio for each site with recording over long period of time.

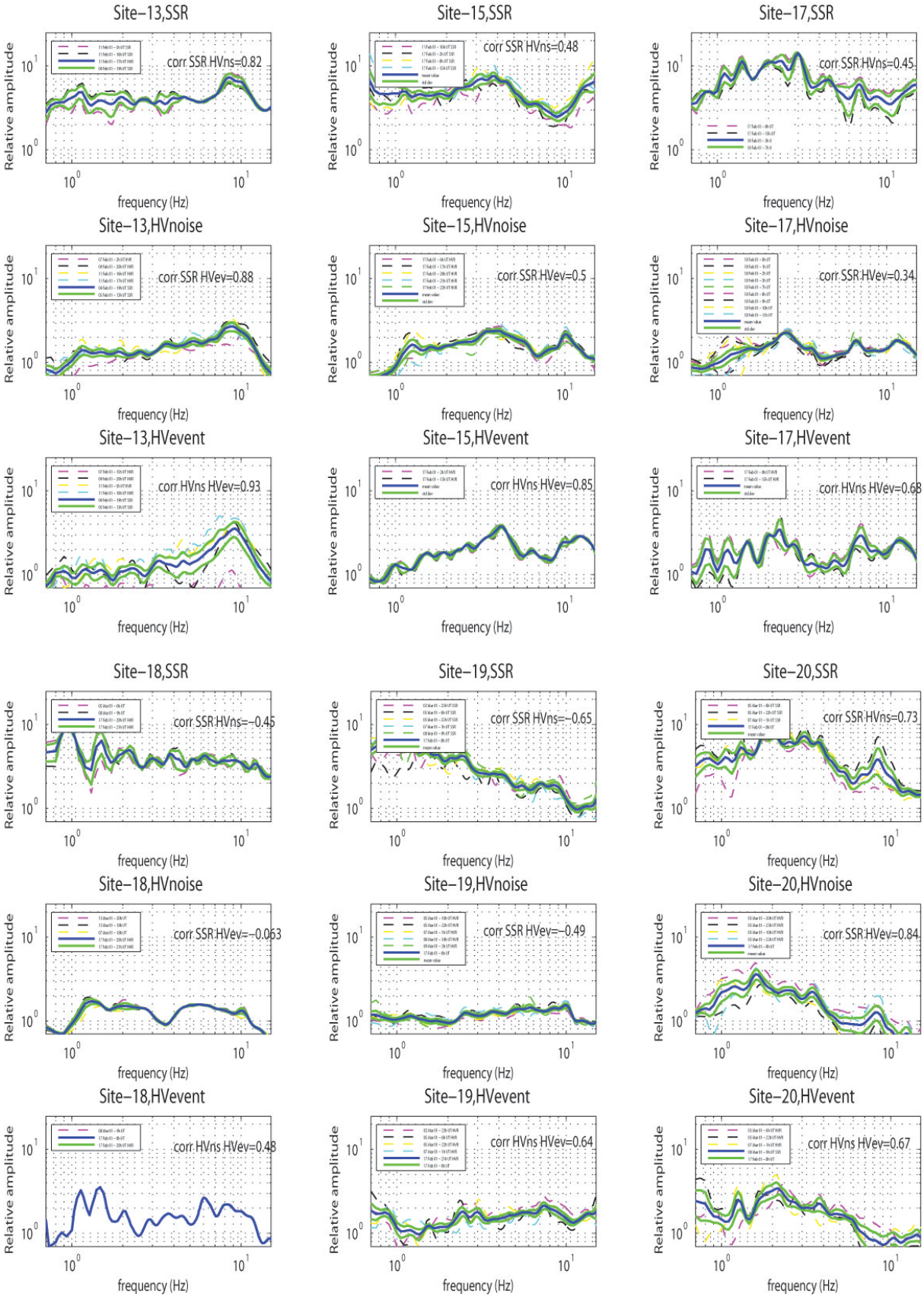

Figure A.4: HV noise, HV event and SSR ratio for each site with recording over long period of time.

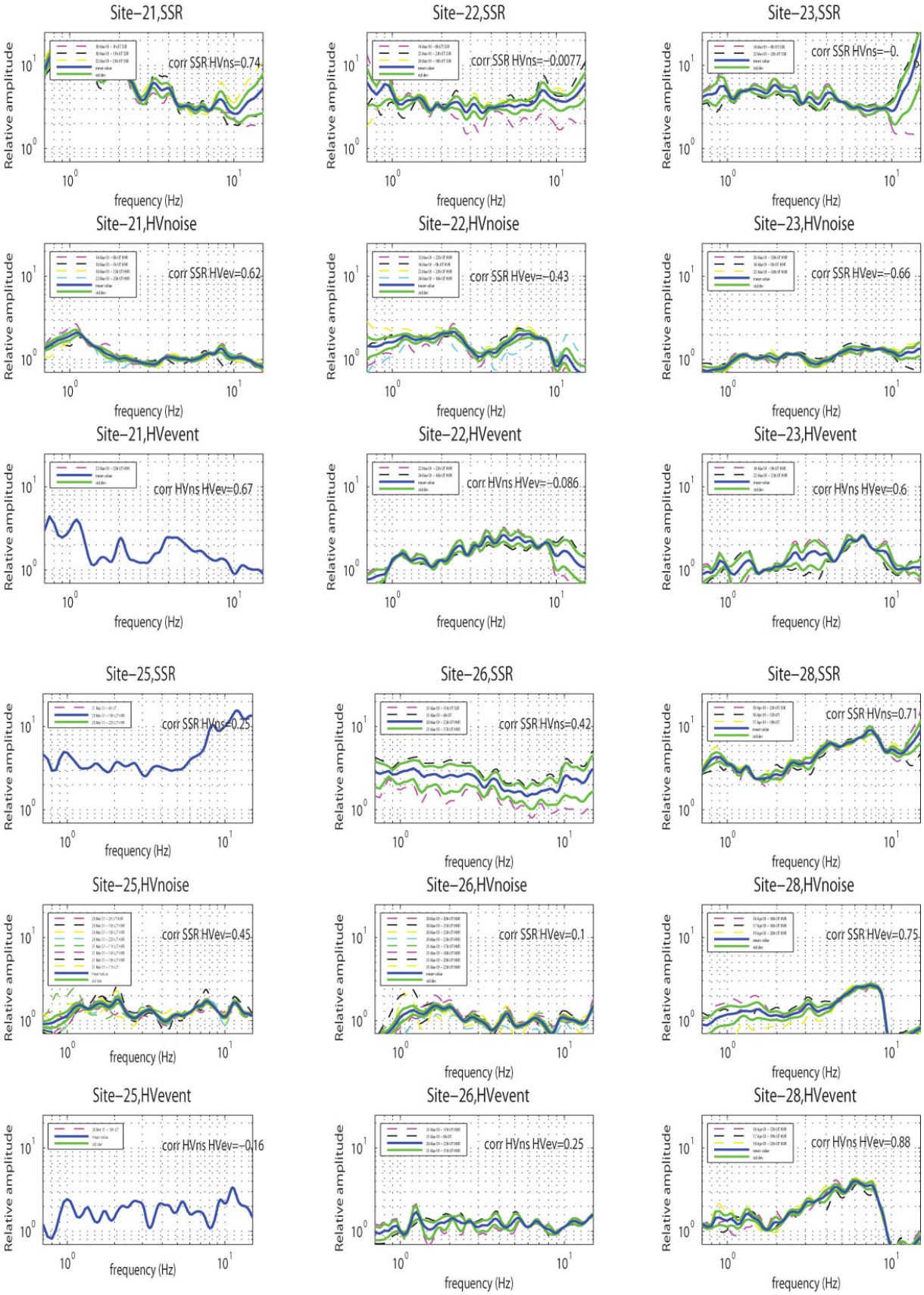

Figure A.5: HV noise, HV event and SSR ratio for each site with recording over long period of time.

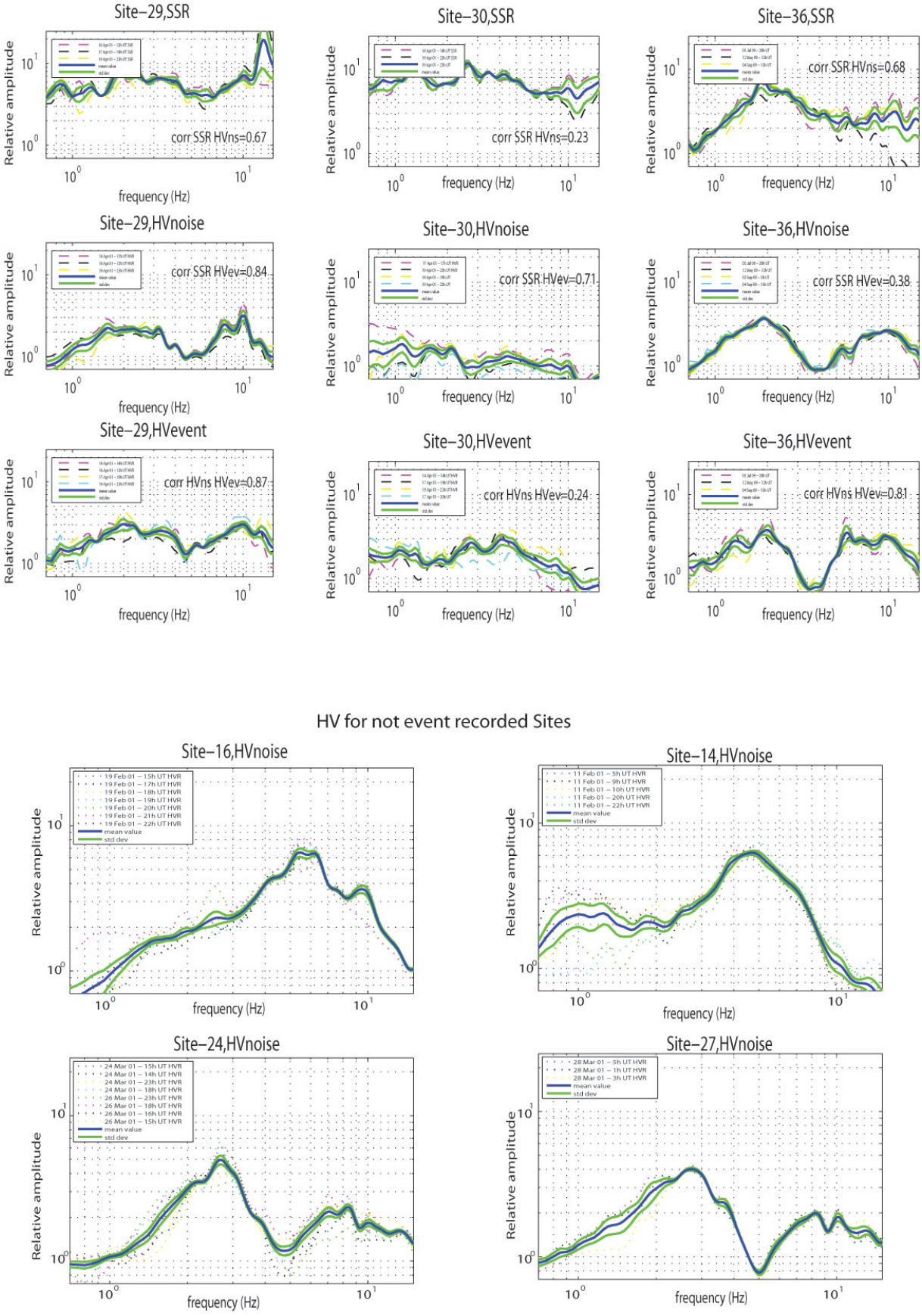

Figure A.6: HV noise, HV event and SSR ratio for each site with recording over long period of time. Down part shows HV noise ratio for site with unusable event records.

Result of HV analysis for short time microtremor recorded sites

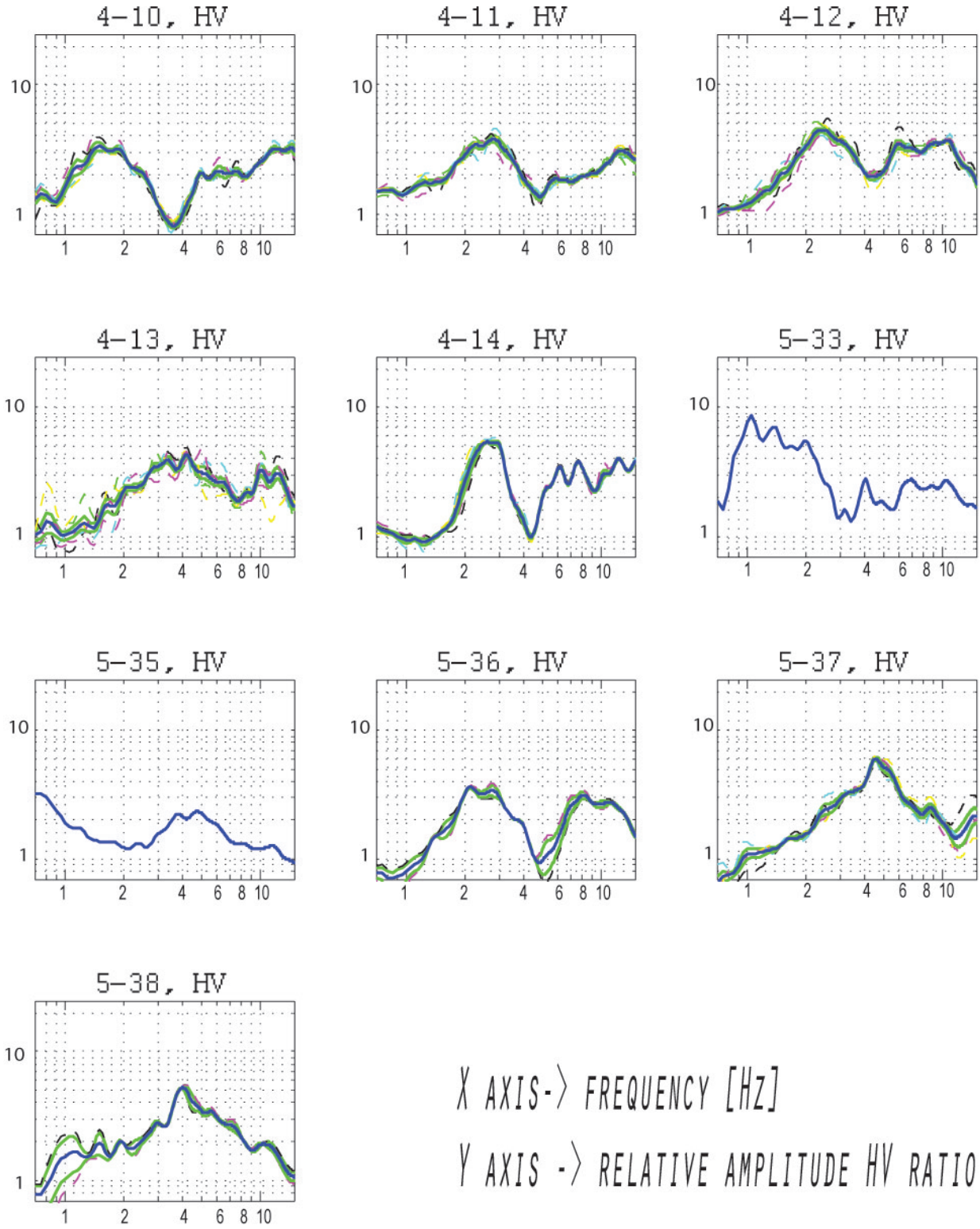

Figure A.7: HV noise ratio analysis for each site with recording over short period of time

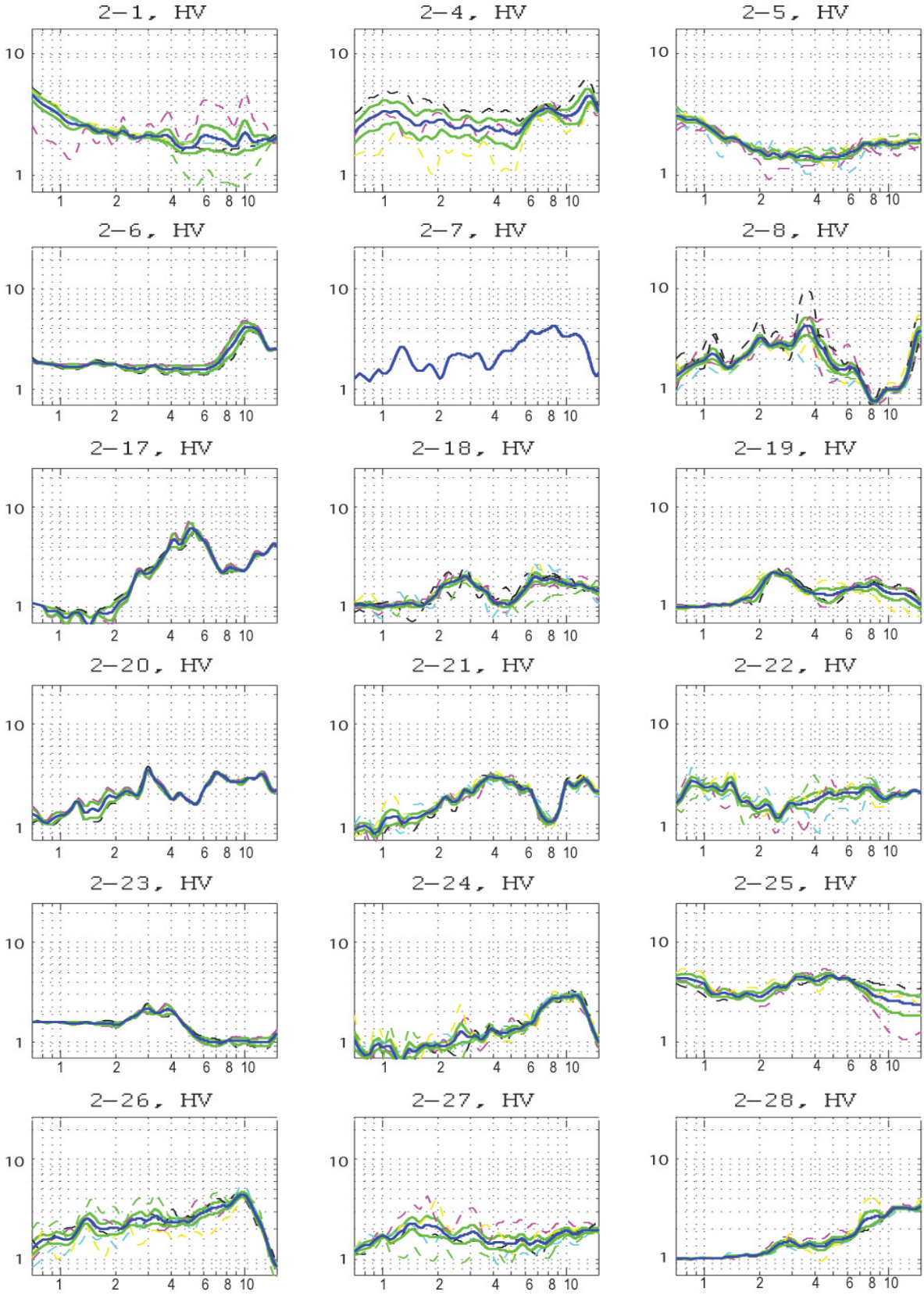

Figure A.8: HV noise ratio analysis for each site with recording over short period of time

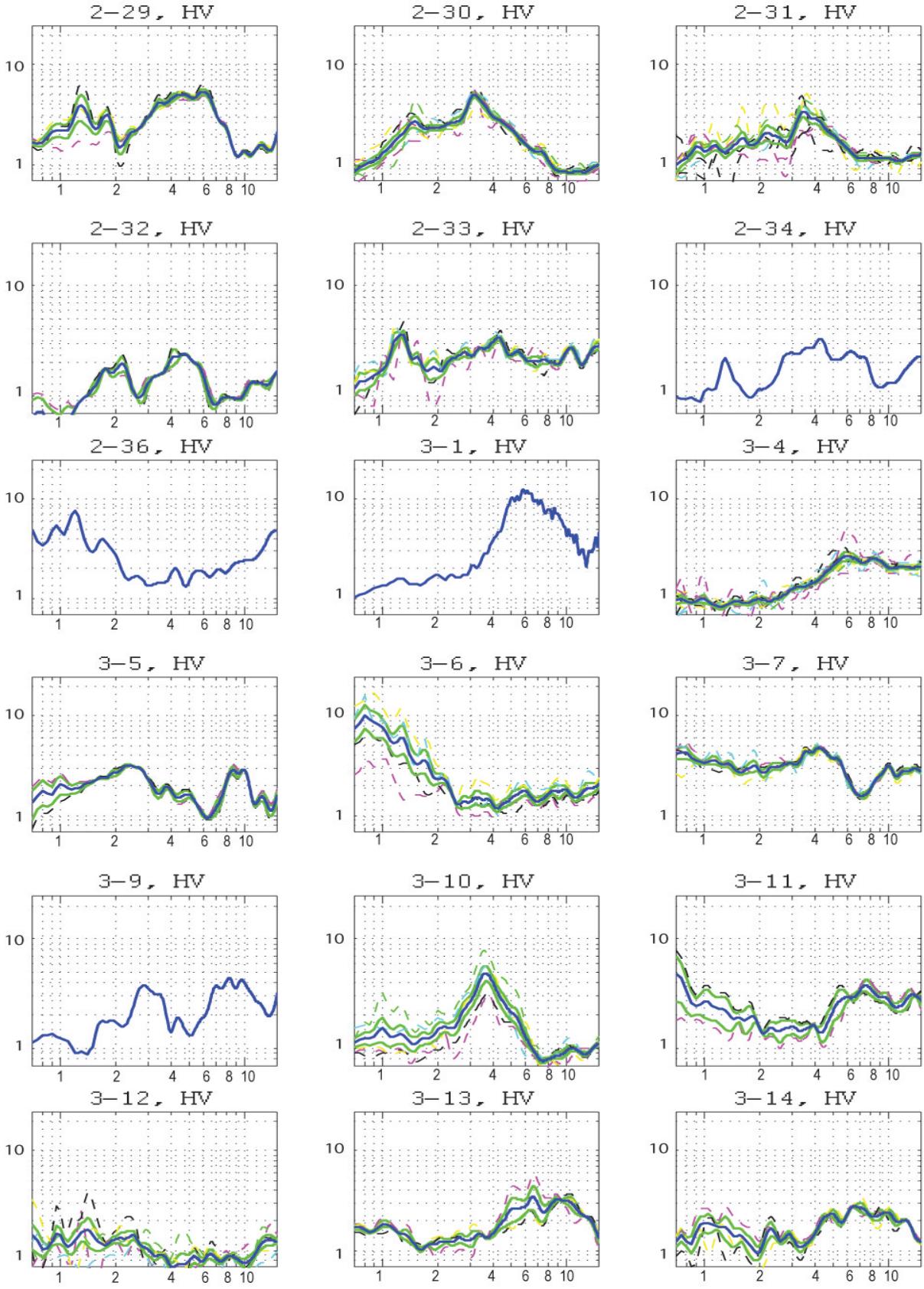

Figure A.9: HV noise ratio analysis for each site with recording over short period of time

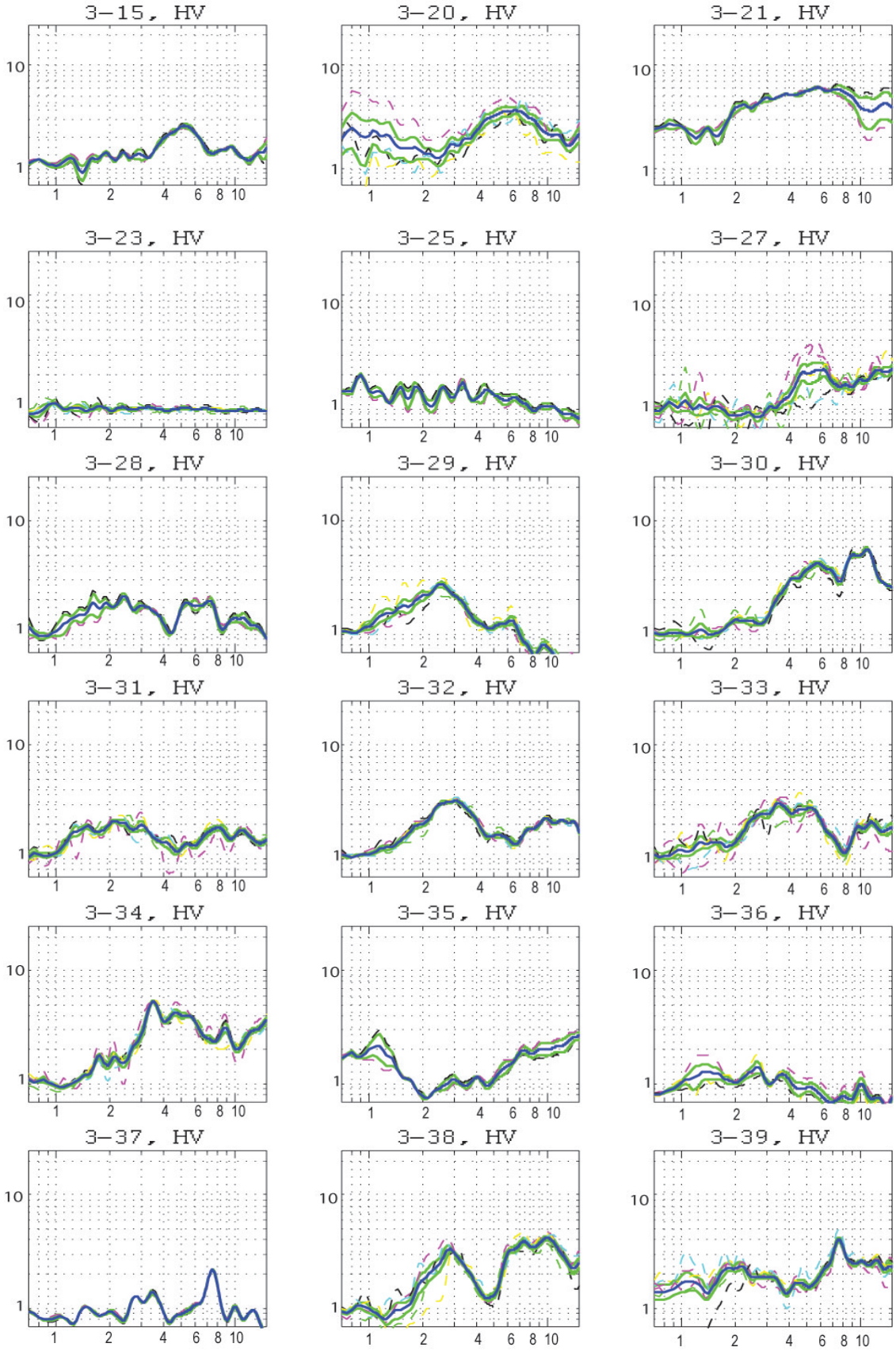

Figure A.10: HV noise ratio analysis for each site with recording over short period of time

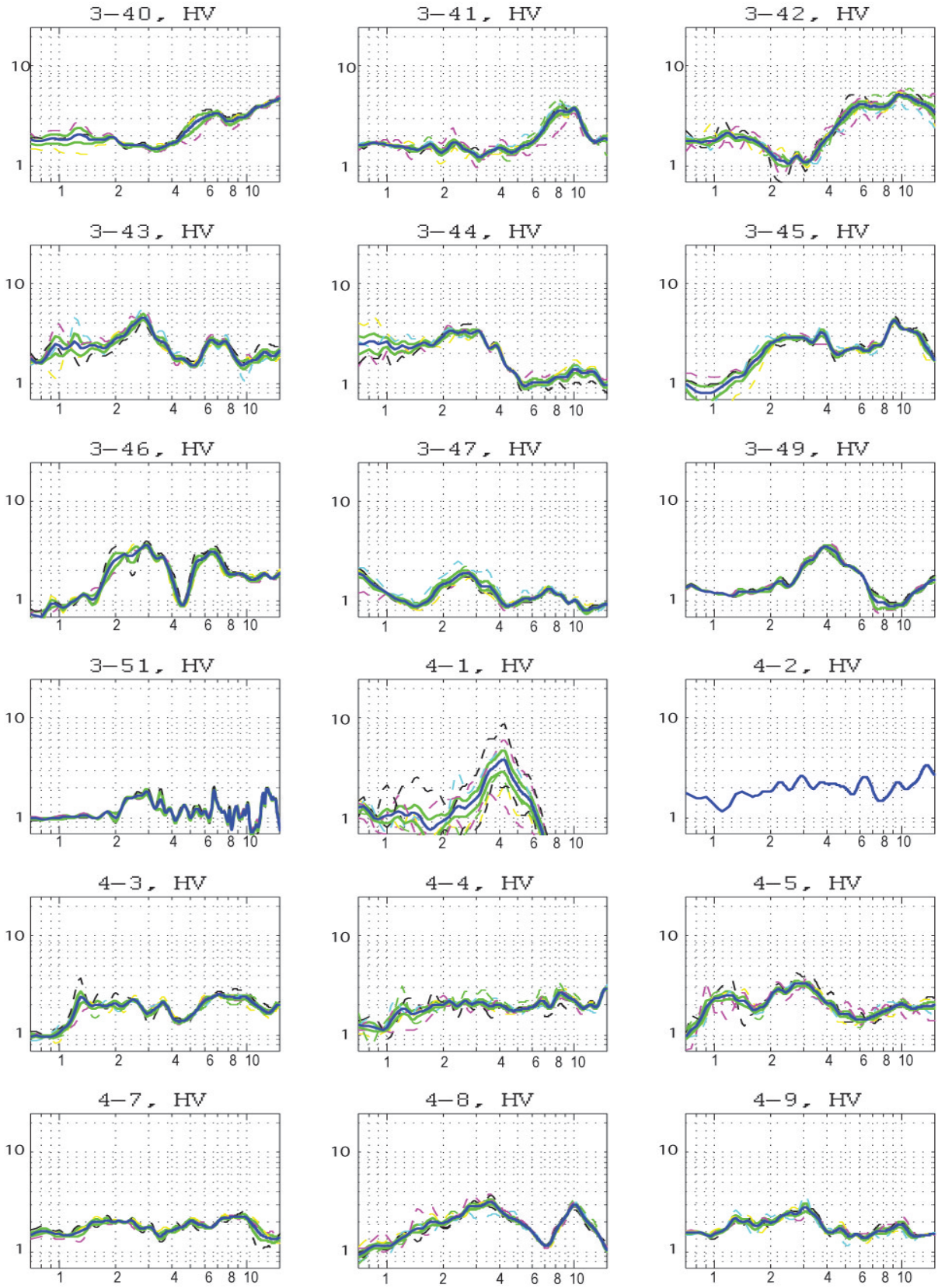

Figure A.11: HV noise ratio analysis for each site with recording over short period of time

Table A.1. Microtremor measurement sites and their HV characteristics

N- number (name) of site; **ALT**- altitude of site, **Lat**-latitude; **Lon**-longitude; **STA**- station number used for database; **Dur**- duration of station deployed time; **Fr** – amplified frequency peak or "band" of HV ratio, **Fr_av**- average of amplified frequencies, value used for plotting in GIS; **Amp** – average maximum amplitude of microtremor; **Distort**- local noise distortion level of microtremor record,

N	ALT	LAT	LON	STA	Dur (min)	Fr [Hz]	Fr_av [Hz]	class	Amp	Distort
2-01	1240	47.85370	106.73538	11	97	--	--	C	400	high
2-02	1370	47.94342	107.16212	10	65	--	--	C	1000	high
2-03	1340	47.93073	107.16128	11	87	7-10	8	B	3000	high
2-04	1370	47.93578	107.14293	10	75	8	8.00	B	300	high
2-05	1390	47.93435	107.13885	1	56	--	9.50	C	50	middle
2-06	1340	47.92422	107.13113	10	86	09-12	10.00	A	500	middle
2-07	1345	47.92305	107.12653	1	70	06-10	8.00	A	200	middle
2-08	1370	47.92883	107.08340	1	81	3-4	3.50	A	50	low
2-09	1350	47.91792	107.05067	11	116	--	--	C	4000	high
2-10	1380	47.93247	107.08497	6	65	--	--	C	1000	high
2-11	1330	47.89008	107.08260	10	55	--	--	C	1500	high
2-12	1310	47.90433	107.00137	10	100	--	--	C	2000	high
2-13	1300	47.89390	106.99810	7	148	--	--		0	nodata
2-14	1310	47.89643	106.99783	1	131	--	--	C	1000	high
2-15	1300	47.89642	107.00405	6	112	--	--	C	5000	high
2-16	1310	47.89373	107.00362	10	59	--	--	C	1000	high
2-17	1290	47.90435	106.93418	1	16	4-7	5.00	B	400	middle
2-18	1277	47.89627	106.97913	10	30	2-4	2.50	B	50	low
2-19	1299	47.90173	106.99082	10	30	2-3	2.50	A	40	low
2-20	1285	47.90240	106.97827	10	30	2.5-4	3.00	A	100	low
2-21	1256	47.90348	106.94908	10	27	3-5	4.00	A	100	low
2-22	1223	47.89498	106.68578	1	36	--	--	B	100	middle
2-23	1240	47.87928	106.68822	6	29	3-4	3.50	B	150	high
2-24	1370	47.85552	106.83775	6	20	7-12	8.00	B	100	low
2-25	1350	47.85192	106.82092	1	57	3-7	6.00	B	500	high
2-26	1370	47.93088	107.01183	1	40	8-11	9.00	B	100	low

2-27	1400	47.93653	107.00062	1	43	--	--	C	100	low
2-28	1340	47.92465	106.98240	1	44	--	--	C	100	high
2-29	1300	47.91348	106.91840	1	45	4-6	4.00	A	300	high
2-30	1246	47.90933	106.97708	11	109	2.8-3.5	3.20	A	50	low
2-31	1289	47.91833	106.97028	11	35	2.8-3.5	3.50	A	100	low
2-32	1286	47.90408	107.01345	11	7	2, 4-5	4.50	A	200	low
2-33	1264	47.92227	106.91527	11	10	1.5, 3.5-4.5	4.10	A	300	middle
2-34	0	47.91444	106.90195	11	53	3-5	4.20	A	200	low
2-36	1275	47.91505	106.82455	7		1.3	1.20	B	200	high
3-01	1282	47.90333	107.07300	1	90	3-10	6.00	B	500	high
3-02	1280	47.91147	107.07010	1	77	--	--		0	nodata
3-03	1280	47.91258	107.07958	1	14		--		0	nodata
3-04	1290	47.91430	107.07847	1	100	5-9	6.00	B	50	low
3-05	1250	47.88012	106.77720	6	125	2-3, 8-9	2.50	A	200	low
3-06	1300	47.87127	106.77137	6	120	--	--		100	low
3-07	1260	47.88077	106.76255	11	137	3-5	4.00	B	400	low
3-08	1250	47.87643	106.73293	6	122	8-10	9.00	A	1000	high
3-09	1250	47.88287	106.69785	6	93	2.5-3.5	3.00	A	1000	high
3-10	1340	47.92478	107.08708	10	95	3-4	3.50	A	50	middle
3-11	1387	47.92111	107.13223	6	131	6-9	7.50	A	50	middle
3-12	1312	47.91263	107.12665	6	152	--	--	A	400	high
3-13	1277	47.91635	107.12543	11	112	5-10	7.00	B	400	high
3-14	1320	47.90997	107.11147	6	102	5-10	7.00	B	200	middle
3-15	1307	47.91345	107.10305	11	58	4.5-6	5.30	A	400	high
3-16	1331	47.90770	107.09902	6	140	--	--	C	2000	high
3-17	1320	47.91073	107.09543	11	126	--	--	C	3000	high
3-18	1320	47.91342	107.09167	11	88	--	--	C	2000	high
3-19	1310	47.90893	107.08903	6	60	--	--	C	2000	high
3-20	1310	47.91365	107.07123	7	28	5-8	6.00	B	200	middle
3-21	1310	47.90855	107.06795	6	70	3-8	6.00	B	200	middle
3-22	1310	47.91148	107.06045	6	108	5	6.00	C	1200	high
3-23	1320	47.90062	107.06755	11	63	--	--	C	1	no_amp
3-24	1279	47.90008	107.05194	11	114	5	5.00	C	4000	high
3-25	1277	47.90722	107.04806	7	91	--	--	D	200	middle
3-26	1277	47.90444	107.04861	11	71	7	7.00	B	3000	high

3-27	1300	47.90017	107.02117	6	26	4.5-7	4.90	B	900	high
3-28	1300	47.89558	107.00640	6	33	2-3,	2.50	B	200	low
3-29	1310	47.89368	107.00307	6	23	2-3	2.50	A	150	low
3-30	1300	47.89565	106.95988	6	32	4-7 ,9-11	6.00	B	200	low
3-31	1300	47.89053	106.96420	1	40	1.5-3	2.50	A	100	low
3-32	1290	47.89922	106.94660	1	40	2-4	3.00	A	100	low
3-33	1280	47.90245	106.93147	1	15	3-6	3.50	A	500	low
3-34	1280	47.90393	106.91992	1	9	3-6	3.50	B	900	low
3-35	1209	47.89493	106.69758	1	83	--	--	C	200	middle
3-36	1198	47.89358	106.71440	7	33	--	--	C	100	middle
3-37	1162	47.89182	106.72340	7	41	7.5	7.50	B	400	middle
3-38	1226	47.89122	106.73362	7	21	2.8,6-10	2.80	A	200	middle
3-39	1240	47.87865	106.69775	6	33	7,5	7.50	B	200	middle
3-40	1250	47.88432	106.70368	6	30	6-7	7.00	B	100	middle
3-41	1240	47.88213	106.71048	6	30	7-10	8.00	A	100	high
3-42	1250	47.88725	106.72757	6	36	5-10	7.00	B	200	middle
3-43	1250	47.89752	106.74393	6	33	2,5-3,7	2.80	B	400	middle
3-44	1250	47.88460	106.75977	6	37	2-4	2.50	B	100	low
3-45	1250	47.87887	106.77155	6	27	2-4	3.00	B	200	low
3-46	1250	47.88353	106.77845	6	18	2-4,7	3.00	A	200	low
3-47	1330	47.86253	106.83373	1	58	2-3	2.50	B	100	low
3-48	1300	47.85545	106.81050	6	30	--	--	C	1200	high
3-49	1390	47.86845	106.90837	7	26	4	4.00	A	40	middle
3-50	1350	47.87527	106.90935	7	30	--	--	B	200	high
3-51	1270	47.88760	106.83638	7	22	3	3.00	B	400	middle
3-52	1320	47.89642	107.08073	10	62	--	--	C	10000	high
4-01	1290	47.89545	106.93045	11	120	4	4.00	A	100	low
4-02	1280	47.88808	106.83980	11	145	2-5	3.00	B	800	high
4-03	1240	47.89127	106.95165	60	30	1-3,6-10	2.50	B	50	low
4-04	1276	47.89483	106.95213	1	31	2-4,8-9	2.50	B	100	low
4-05	1290	47.89227	106.94362	6	40	2-4,8-9	2.90	A	200	middle
4-06	1256	47.89005	106.95825	1	33	--	--			nodata
4-07	1290	47.88997	106.94413	6	40	1.8-	2.00	B	100	middle

						3.5,6-8				
4-08	1232	47.89928	106.92268	1	31	2.8-4	3.50	A	100	low
4-09	1290	47.89393	106.93000	6	29	3	3.00	A	100	low
4-10	1280	47.89087	106.92443	1	31	1-2	1.80	A	100	low
4-11	1280	47.88947	106.90212	6	15	2-3.2	2.40	A	250	low
4-12	1263	47.89073	106.89787	1	23	2-3	2.20	A	1000	low
4-13	1260	47.87805	106.79337	6	15	3-4.5	3.80	A	400	low
4-14	1270	47.88337	106.79713	1	10	2-3.4	2.50	A	1000	low
5-33	1280	47.90115	106.89176	2		1-2	--	B	1000	high
5-34	1272	47.90727	106.87508	0		--	--	C	2000	high
5-35	1272	47.92039	106.87090	0		3-5	5.00	A	900	high
5-36	1263	47.888772	106.78166				2.20	A		low
5-37		47.899723	107.02423				4.50	A		low
5-38		47.905176	106.91320				4.00	A		low

APPENDIX B

ESTIMATION OF THE FREQUENCY DEPENDENT DURATION USING GROUP VELOCITY DELAY TIME.

One of my goals was to evaluate the duration extension of the ground motion at Ulaanbaatar sedimentary basin. Beauval and Bard [2001] and Beauval et al. [2003] used a method that was firstly introduced by Sawada [1998] for seismic site effect studies. The method uses the group delay time difference between events recorded at sedimentary and rock sites. Taking the Fourier transform S(ω) of the time history s(t) yields the amplitude spectrum A(ω) and phase spectrum φ(ω)

$$S(\omega) = \frac{1}{2\pi}\int_{-\infty}^{\infty} s(t)e^{-i\omega t}dt = A(\omega)e^{-i\varphi(\omega)} \qquad \text{(B.1)}$$

The gradient of the phase φ(ω) contains information on the arrival time of the energy as a function of frequencies. In order to retrieve phase gradient, the phase must be first unwrapped, then differentiated with respect to frequency (ω) . The obtained quantity has a time dimension and it is defined as the group delay time (T_{gr}).

$$T_{gr}(\omega) = \frac{d\varphi(\omega)}{d\omega} \qquad \text{(B.2)}$$

Unwrapping the phase is not easy to do. Then I used a way to compute phase derivative that does not require unwrapping the phase (Boore, 2003).

S(ω) - Fourier transform of time history s(t),

St(ω) –Fourier transform of time history s(t)*t, then

$$\frac{d\varphi}{d\omega} = 2\pi\left[R(S)R(St) + I(S)I(St)\right]/\,A^2 \qquad \text{(B.3)}$$

Here R(S), I(S) - real and imaginary part of S(ω), R(St),

I(St)-real and imaginary part of St(ω).

This calculated Group delay is unstable, therefore a smoothing is applied using $W_A(\omega,\omega_0)$ function that take into account the signal Fourier amplitude.

Average spectrum $\mu_{Tgr}(\omega)$ and variance spectrum $\sigma_{Tgr}^2(\omega)$ of Tgr is defined as follows:

$$\mu_{Tgr}(\omega_0) = \frac{1}{S}\int_0^{\infty} W_A(\omega;\omega_0)T_{gr}(\omega)d\omega \qquad \text{(B.4)}$$

$$\sigma_{Tgr}{}^{2}(\omega_0) = \frac{1}{S}\int_0^{\infty} W_A(\omega,\omega_0)(Tgr(\omega) - \mu_{Tgr}(\omega_0))^2\, d\omega \qquad \text{(B.5)}$$

where

$$W_A(\omega,\omega_0) = W(\omega,\omega_0)\frac{A(\omega)}{\mu_A(\omega)} \qquad \text{(B.6)}$$

$$S = \int_0^{\infty} W_A(\omega,\omega_0)d\omega \text{ and } \mu_A(\omega_0) = \frac{\int_0^{\infty} W(\omega,\omega_0)A(\omega)d\omega}{\int_0^{\infty} W(\omega,\omega_0)d\omega} \qquad \text{(B.7)}$$

The smoothing function $W(\omega,\omega_0)$ that I used was a Konno and Omachi [1998] window with b=40. I developed a script in Matlab to compute this group delay time. Then I tested the script on a simple signal made of summation of three truncated sinusoids as Beauval (2003) did. Sinusoids was created adding 0.5, 1 and 5 Hz mono frequency signals and with duration of 7, 2 and 3 sec respectively (Figure B.1). I got similar result those Beauval et al., (2003) in their analysis.

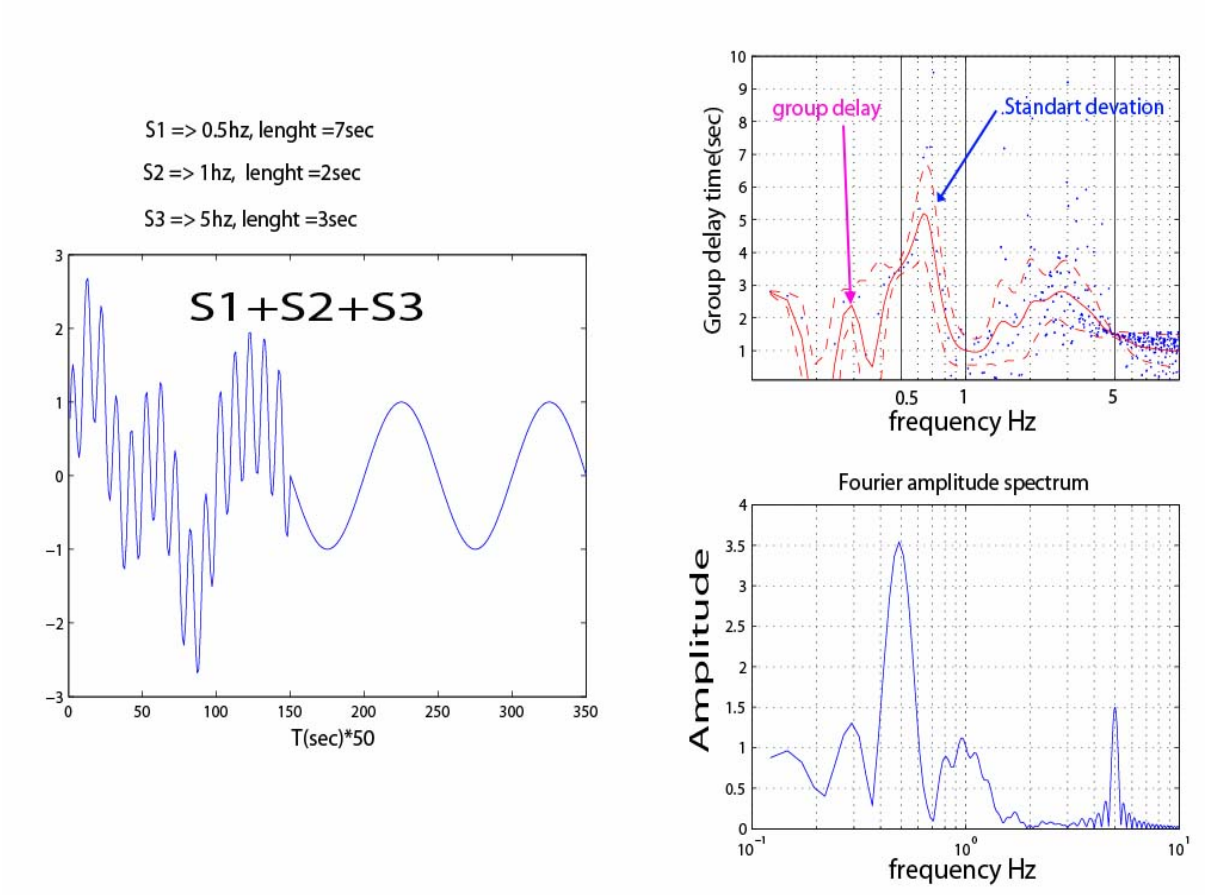

Figure B.1: Test of the Group delay calculation using a simple summation of sinusoid waves.

At Ulaanbaatar basin, the group delay time, for ground motion duration differences, was tested for several sites using weak motion records. Considering the amplified frequencies by the basin and the instrumental response of our station, I calculated this group delay time between 1 to 10 Hz. Therefore, outside of this ranges, my calculated group delay values have no significant meaning. In the figure B.2 shown one of signal that used for this analysis which recorded at site36 and rock site.. Green part of waveforms is used for group delay calculation.

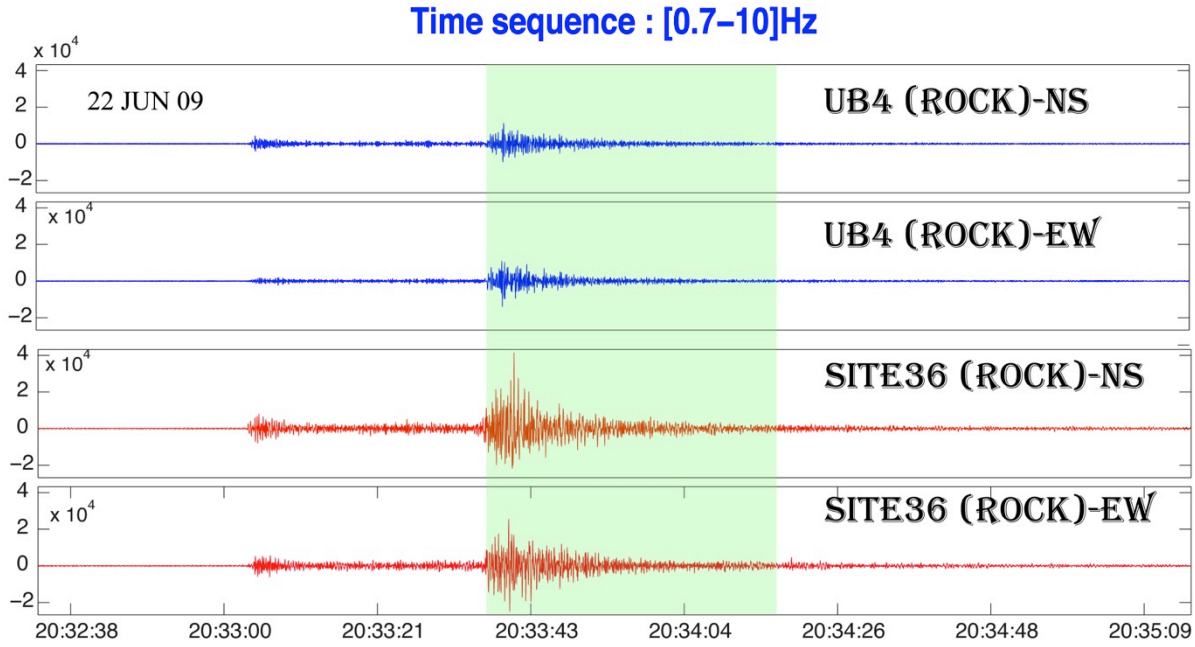

Figure B.2: Event waveform that used for group delay analysis. Green shadow part of waveform were used for group delay analysis

The figure B.3 presents the group delay time difference calculation on weak motion recorded at several sedimentary sites. At the site 36 (correspond also to the site UB9), for 3 different weak motion records, the results are non consistent. We observe that the value of Group delay difference varies between these events within a range of ± 5 seconds for specific frequencies. Therefore, I inferred that the weak motions recorded at Ulaanbaatar basin did not have clear duration lengthening by using group delay time.

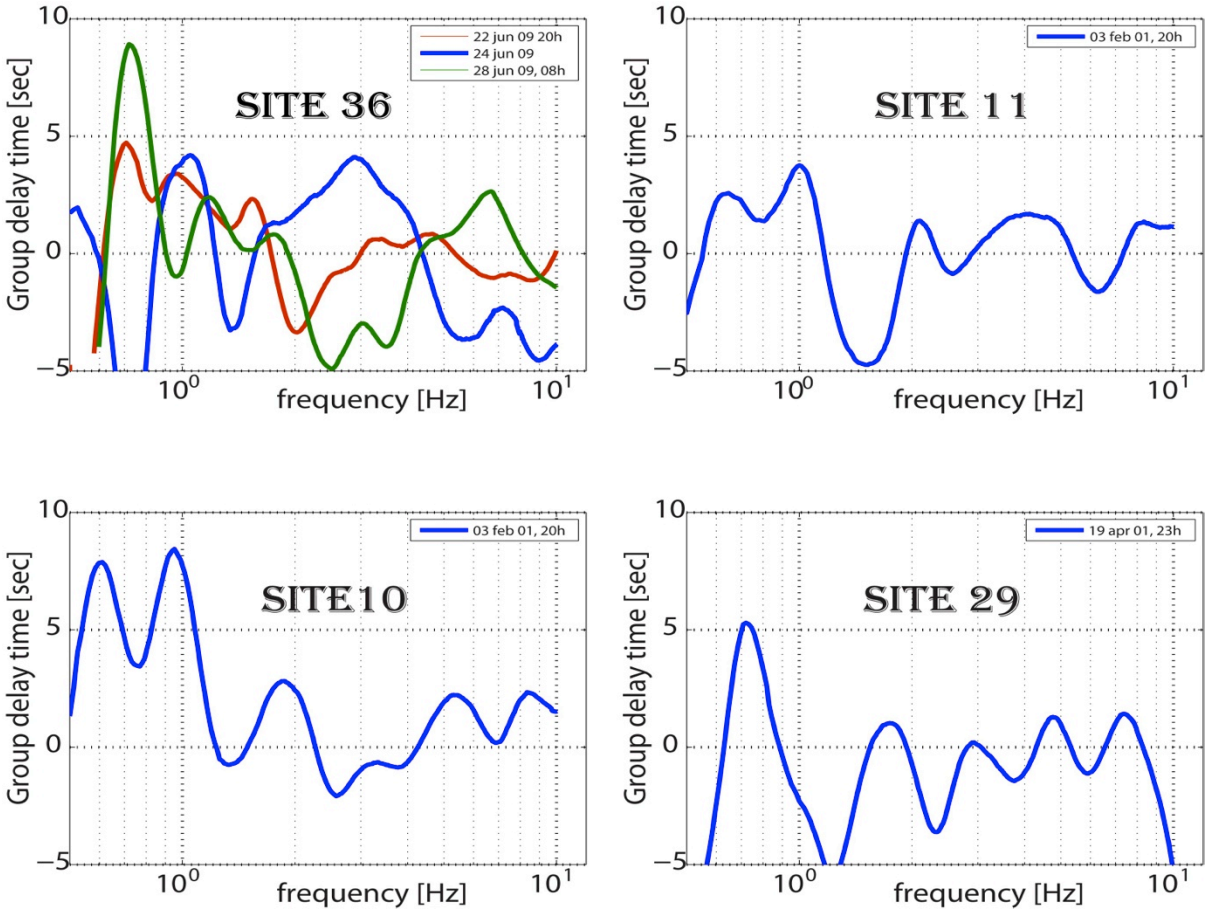

Figure B.3: Calculation of the group delay time difference at several sedimentary sites with respect to reference (rock) site.

APPENDIX C

USED PROGRAM AND SCRIPTS FOR THIS THESIS .

Most of the analysis in this thesis was performed using MATLAB scripts that I continuously developed on the initial DASE software, (Based on Infrasound software developed by Alexis Le Pichon CEA/DASE) which is optimized for DASE records format. My programming under MATLAB, outside the experience I go from it, allowed me to control all processing (no black box) and to develop easily any specific characteristic needed for my research during my PhD. I was cross-checked my developed scripts (SiteEffect) when it was possible to perform other existing free software for the same purpose. As an example, the Figure C.1 represented HV noise and HV event analysis results performed either using GEOPSY or SiteEffect programs.

The main software I used are.

Geopsy (UJF/LGIT), Shake91 (Berkeley), Mka3D (CEA) software. Geopsy was used especially for FK array analysis.

Also, for building the GIS database, which was fed with the data and the results, and create various mapping (event, basin, etc.) I used extensively GIS software.

Here I included list of my developed scripts and it's brief description for future usage.

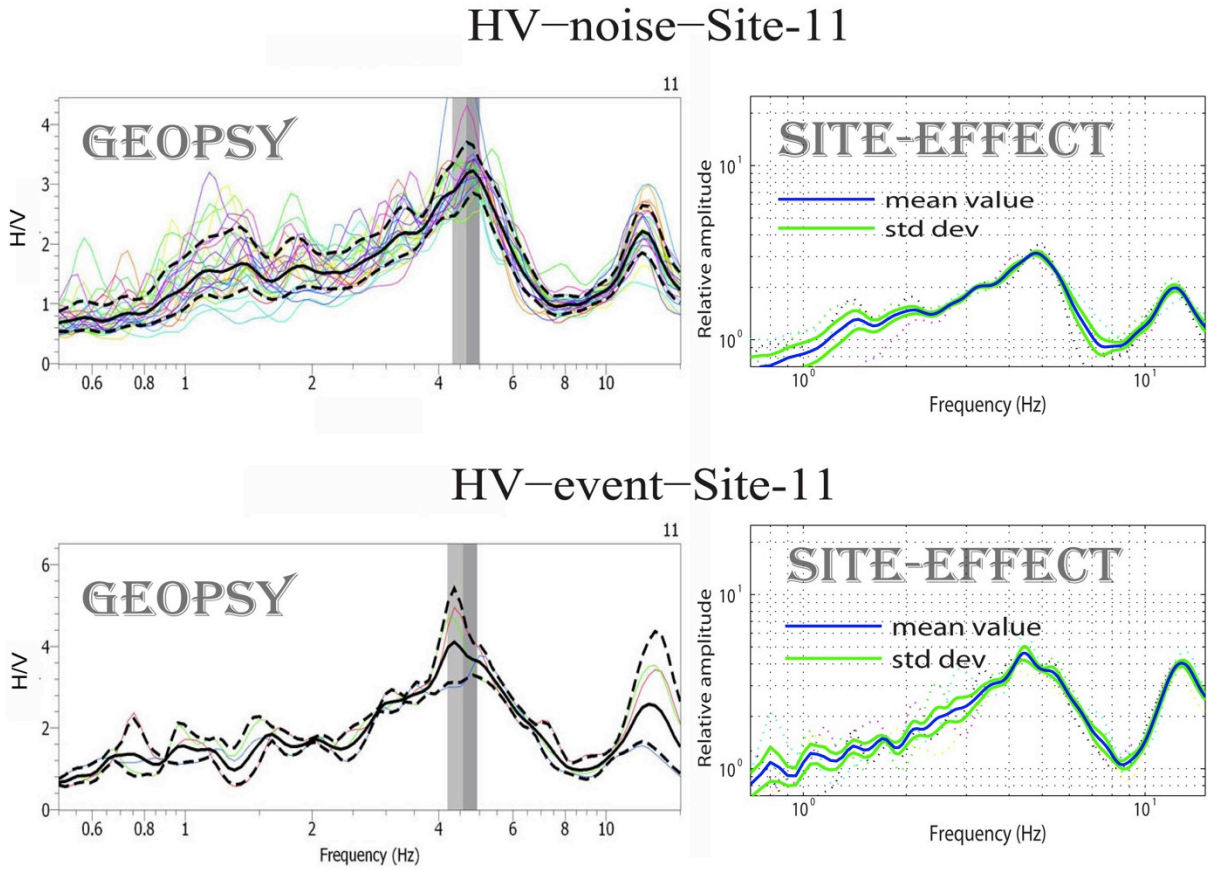

Figure C.1: Comparison of HV event and HV noise analysis using either GEOPSY or Site Effect.

Arias- Calculate Arias duration difference between a studied site and reference site

Arias-fil- Calculate Arias filtered duration difference between a studied site and reference site

Arias-fil-azim Calculate frequency dependent Arias duration variation with azimuth and plot azimuth versus frequency graph with contour of arias duration difference

Deconv- remove instrument response (for FONYX format: Mark -4C, CMG-40)

Dur-abs- Calculate absolute duration difference between site and reference

Dur-plot- plot estimated durations and calculate average and standard deviation of duration curves.

Energy-plot- calculate energy of signal for each narrow bands using spectrogram,

Envelop- evaluate envelop of signal using Hilbert transform and zero phase digital filter

Group-delay- Calculate group delay difference time between site and reference (As mentioned)

Naka-HV- Calculate HV ratio for 3 component signal (Konno-Omachi smoothing, 90% overlaping, Fourier spectrum)

Naka_azim- calculate HV ratio's azimuth variation (input EW and NS component)

Nakaplot– plot calculated HV ratios and it's mean value and standard deviation.

Omachi_win- smoothing with Konno-Omachi window.

Plot-poliz- plot compass of amplified frequency from azimuth calculated figure file.

Save-Arias- Save Arias duration result as a text file.

SNR_calc – estimate Signal Noise Ratio

Save-SNR- Save SNR or HV spectral ratio results in 2 columns text file

Sonogram– calculate sonogram of site respect to reference site and draw sonogram

StR- calculate Standard Spectral Ratio

Peakseek-find peaks from spectral ratio for given frequency interval

Shake_m –graphical interface for input Shake91.

Shake_out- read and display output files Shake91.

Shake_out_basin -apply shake for all nodes of a map grid.

Unit_conv- convert weight, length between metric and US systems. Used for Shake input

Interp+basin- Interpolate basin shape using altitude, latitude and longitude information included input shape (GIS) formatted lines and points

Tif2coord- convertgeoreferenced tiff to lat, long and altitude column text file

Plot_rec_sim2- plot simulation waveforms from Mka3D results and interface for HV, SSR and Arias duration for simulation result.

Crossection- Create cross section from 3D basin model.

BIBLOGRAPHY

Arias, A. (1970), "A Measure of Earthquake Intensity", in Seismic Design for Nuclear Power Plants (R.J. Hansen, ed), MIT Press, Cambridge,MA, 438-483.

Arvisbaatar, H., H. Dugaraa, and L. Batjargal (1991), "Ulaanbaatar basin structure " Gravimeter work report, Ulaanbaatar.

Andrews, D. J. (Ed.) (1986), Objective determination of source parameters and similarity of earthquake of different size, 259-268 pp., American Geophysical Union Washingoton D.C.

Baljinnyam, I., A. Bayasgalan, B. A. Borisov, A. Cisternas, M. G. Dem'yanovich, L. Ganbaatar, V. M. Kochetkov, R. A. Kurushin, P. Molnar, H. Philip, and Y. Y. Vashchilov (1993), Ruptures of major earthquakes and active deformation in Mongolia and its surroundings, Geological Society of America, Memoir 81.

Bard, P.-Y., and M. Bouchon (1980), The seismic response of sediment-filled valleys. Part1. The case of Incident SH waves Bulletin of the Seismological Society of America, 70(4), 1263-1286.

Bard, P.-Y., and M. Bouchon (1980), The seismic response of sediment-filled valleys. part2. The case of incident P and SV waves, Bulletin of the Seismological Society of America, 70(5), 1921-1941.

Beauval, C., and P.-Y. Bard (2001), Quantification of the Frequency Dependent Lengthening of the Duration of Seismic Ground Motion, in Relation with the Local Geology: Application to the Euro-Seistest paper presented at EGS XXVI General Assembly Nice, France.

Beauval, C., P.-Y. Bard, P. Moczo, and J. Kristek (2003), Quantification of Frequency-Dependent Lengthening of Seismic Ground-Motion Duration due to Local Geology: Applications to the Volvi Area(Greece) Bulletin of the Seismological Society of America, 93(1), 371-385.

Bindi, D., S. Parolai, F. Cara, G. D. Giulio, G. Ferretti, L. Luzi, G. Monachesi, F. Pacor, and A. Rovelli (2009), Site Amplifications Observed in the Gubbio Basin, Central Italy: Hints for Lateral Propagation Effects, Bulletin of the Seismological Society of America, 99(2A), 741-760.

Bonilla, L. F., J. H. Steidl, G. T. Lindley, A. G. Tumarkin, and R. J.Archuleta (1997), Site amplification in the San Fernando Valley, California : Variability of site-effect estimation using the S-wave, coda, and H/V methods Bulletin of the Seismological Society of America, 87, 710-730.

Bonnefoy-Claudet, S., C. Cornou, P.-Y. Bard, F. Cotton, P. Moczo, J. Kristek, and D. Fah (2006), H/V ratio: a tool for site effects evaluation. Results from 1-D noise simulations.Geophysical Journal International, 167(2), 827-837.

Bonnefoy-Claudet, S., F. Cotton, and P.-Y. Bard (2006), The nature of noise wavefield and it's applications for site effects studies A literature review, Earth-Science Reviews 79, 205-227.

Bonnefoy-Claudet, S., S. Baize, S. Bonnefoy-Claudet, S. e. Baize, L. F. Bonilla, C. Berge-Thierry, C. Pasten, J. Campos, P. Volant, and R. Verdugo (2009), Site effect evaluation in the basin of Santiago de Chile using ambient noise measurements, Geophysical Journal International, 176, 925-937.

Boomer, J. J., and A. Martinez-Pereira (1999), The effective duration of strong ground motion, Journal of Earthquake Engineering, 3(2), 127-172.

Boore, D. M. (2003)., Phase Derivatives and Simulation of Strong Ground Motions, Bulletin of the Seismological Society of America, 93(3), 1132-1143.

Borcherdt, R. D. (1970), Effect local geology on ground motion near San Francisco Bay, Bulletin of the Seismological Society of America, 60, 29-81.

Capon, J. (1969)., High Resolution Frequency-Wavenumber Spectrum Analysis, Proceedings of the IEEE, 57(8), 1408-1419.

Cornou, C., and P.-Y. Bard (2003), Site-to-bedrock over 1D transfer function ratio: An indicator of the proportion of edge-generated surface waves?, Geophysical Research letters, 30(9), 1453.

Chatelain, J.-L., B. Guillier, F. Cara, A.-M. Duval, K. A. ·, P.-Y. Bard, and T. W. S. team (2007), Evaluation of the influence of experimental conditions on H/V results from ambient noise recordings, Bulletin of Earthquake Engineering, 6, 33-74.

Dugarmaa, T., A.Schlupp ., RCAG team, (2006) Seismic Hazard Assessment of Ulaanbaatar , Capital of MONGOLIA, Project report for Ulaanbaatar administration.

Drouet, S., P. Triantafyllidis, A. Savvaidis, and N. Theodulidis (2008), Comparison of Site-Effects Estimation Methods Using the Lefkas, Greece, 2003 Earthquake Aftershocks, Bulletin of the Seismological Society of America, 98(5), 2349-2363

Dzurick, V. I., A. I. Kluchevskii, S. P. Serebrenikov, B. M. Demiyanovich, T. Batsaikhan, G. Bayaraa, and (2009), Seismicity and seismic hazard zoning of Mongolian region, Earth's Crust Institute, Irkutsk

Faccioli, E., M. Vanini, and L. Frassine (2002), "Complex" site effects in eaqrthquake ground motion, including topography, in 12th European Conference on Earthquake Engineering, edited, Elsevier Science Ltd

Fäh, D., F. Kind, and D. Giardini (2001), A theoretical investigation of average H/V ratios, Geophysical Journal International, 145(2), 535-549.

Field, E. H., and K. H.Jakob (1995), A comparison and test of various site response estimation techniques, including three that are not reference site dependent, Bulletin of the Seismological Society of America, 85, 1127-1143.

Hartzell, S., A. Leeds, A. Frankel, and J. Michael (1996), Site response for urban Los Angeles using aftershock of the Northridge earthquake., Bulletin of the Seismological Society of America, 86, S168-S192.

Hartzell, S., S. Harmsen, R. A. Williams, D. Carver, Arthur Frankel, G. Choy, P.-C. Liu, R. C. Jachens, T. M. Brocher, and C. M. Wentworth (2006), Modeling and Validation of a 3D Velocity Structure for the Santa Clara Valley, California, for Seismic-Wave Simulations, Bulletin of the Seismological Society of America, 96, 1851-1881.

Haskell, N. A. (1953), The dispersion of surface waves on multi layered media, Bulletin of the Seismological Society of America, 43, 17-34.

Herak, M. (2008), ModelHVSR-A MATLAB-tool to model horizontal-to-vertical spectral ratio of ambient noise Computers & Geosciences, 34(11), 1514-1526.

Husid, L. R. (1969), Caracteristicas de terremotos. analisis general., In Revista del IDIEM 8, 21-42.

Horike, M. (1985), Inversion of phase velocity of long- period microtremors to the S- wave velocity structure down to the basement in urbanized areas, Journal Physics Earth, 33, 59-96.

Horike, M., B. Zhao, and H. Kawase (2001), Comparison of Site Response Characteristics Inferred from Microtremors and Earthquake Shear Waves, Bulletin of the Seismological Society of America, 91(6), 1526-1536.

Idriss, I. M., and I. J. Sun (1992), Shake91, A computer program for conducting equivalent linear seismic response analysis of horizontal layered soil deposits, edited, University California.

JICA (Japan Meteorological Agency), (1995), The Study on Water Supply System in Ulaanbaatar and Surroundings, Ulaanbaatar.

Joyner, W. B. (2000), Strong Motion from Surface Waves in Deep Sedimentary Basins, Bulletin of the Seismological Society of America, 90, S95-S112.

Koketsu, K., H. Miyake, Afnimar, and Y. Tanaka (2009), A proposal for a standard procedure of modelling 3-D velocity structures and its application to the Tokyo metropolitan area, Japan, Tectonophysics, 472, 290-300.

Konno, K., and T. Ohmachi (1998), Ground-motion characteristics estimated from spectral ratio between horizontal and vertical components of microtremor. Bulletin of the Seismological Society of America, 88, 228-241.

Lebrun, B., A.-M. Duval, P.-Y. Bard, O. Monge, M. Bour, S. Vidal, and H. Fabriol (2004), Seismic Microzonation: A Comparison between Geotechnical and Seismological Approaches in Pointe-à-Pitre (French West Indies) Bulletin of Earthquake Engineering, 2(1), 27-50.

Lermo, J., and F. J. Chávez-García (1993), Site effect evaluation using spectral ratios with only one station, Bulletin of the Seismological Society of America, 83(5), 1574-1594.

Lermo, J., and F. J. Chávez-García (1994), Are Microtremor Useful in Site Response Evaluation ?, Bulletin of the Seismological Society of America, 84(5), 1350-1364.

Mariotti, C. (2007), Lamb's problem with the lattice model Mka3D, Geophysical Journal International, 171, 857-864.

Medvedev, S. V. (1962), Engineering seismology Gosstroiizdat, Moscow.

Medvedev, C. B. (1971), Seismic zoning Ulaanbaatar, NAUKA, Moscow.

Molnar, S., and J. F. Cassidy (2006), A comparison of Site Response Techniques Using Weak-Motion Earthquakes and Microtremors, Earthquake Spectra, 22(1), 169-188.

Molnar, S., J. F. Cassidy, P. A. Monahan, T. Onur, C. Ventura, and A. Rosenberger (2007), Earthquake site response studies using microtremor measurements in southwest British

Columbia MEASUREMENTS IN SOUTHWESTERN BRITISH COLUMBIA, Ninth Canadian Conference on Earthquake Engineering Ottawa, Ontario, Canada, 410-419.

Mora, M. M., L. Philippe, D. Jacques, B. Pierre-Yves, M. Jean-Philippe, E. A. Guillermo, and L. Carlos (2001), Study of seismic site effect using H/V spectral ratios at Arenal Volcano, Costa Rica, Geophysical Research letters, Vol.28, 2991-2994.

Montejo, L. A., and M. J.Kowalsky (2008), Estimation of Frequency-Dependent Strong Motion Duration Via Wavelets and Its Influence on Nonlinear Seismic Response, Computer-Aided Civil and Infrastructure Engineering, 23, 253-264.

Munkhuu, U., M. Adiya, B. Batkhuu, O. Sebe, A. Schlupp, S. Usnikh, and D. Sodnomsambuu (2010), The Emeelt active faults, revealed by the outbreakof microseismicity and its impact on the PSHA of Ulaanbaatar, capital of Mongolia, in ESC, edited, Montpellier, France

Nakamura, Y. (1989), A method of dynamics characteristics estimations of subsurface using microtremors on the ground surface, Quarterly report of Railway Technical Research Institute, 30, 25-33.

Nogoshi, M., and T. Igarashi (1971), On the amplitude characteristics of microtremor (Part 2), Journal of the Seismological Society of Japan, 24, 26-40.

Novikova, E. I., and M. D. Trifunac (1993), Duration of strong earthquake ground motion: physical basis and empirical equations 265 pages pp, University of Southern California Department of Civil Engineering Los Angeles, California.

Ohrnberger, M., E. Schissele, C. c. Cornou, M. Wathelet, A. Savvaidis, F. Scherbaum, D. Jongmans, and F. Kind (2004), Microtremor Array Measurements For Site Effect Investigations: Comparison Of Analysis Methods For Field Data Crosschecked By Simulated Wavefieldsin 13th World Conference on Earthquake Engineering, edited, p. 14, Vancouver, B.C., Canada.

Ozel, O., E. Cranswick, M. Meremonte, M. Erdik, and E. Safak (2002), Site Effects in Avcilar, West of Istanbul, Turkey, from Strong- and Weak-Motion Data, Bulletin of the Seismological Society of America, 499-508(92).

Parolai, S., and P. Y. Bard (2003), Evaluation of site effect by means of Joint Analysis of Sonogram and Standard Spectral Ratio (JASSSR), Journal of Seismology, 7, 479-492.

Parolai, S., D. Bindi, M. Baumbach, H. Grosser, C. Milkereit, S. Karakisa, and S. Zu¨nbu¨l (2004), Comparison of Different Site Response Estimation Techniques Using Aftershocks of the 1999 Izmit Earthquake, Bulletin of the Seismological Society of America, 94(3), 1096-1108.

Parolai, S., F. Cara, D. Bindi, and F. Pacor (2009), Empirical site-specific response-spectra correction factors for the Gubbio basin (Central Italy). , Soil Dynamics and Earthquake Engineering, 29(3), 546-552.

Pilz, M., S. Parolai, F. Leyton, J. Campos, and J. Zschau (2009), A comparison of site response techniques using earthquake data and ambient seismic noise analysis in the large urban areas of Santiago de Chile, Geophysical Journal International, 178, 713-728.

Riepl, J., P.-Y. BARD, D. Hatzfeld, C. Papaioannou, and S. Nechtschein (1998), Detailed Evaluation of Site-Response Estimation Methods across and along the Sedimentary

Valley of Volvi (EURO-SEISTES), Bulletin of the Seismological Society of America, 88(2), 488-502.

Satoh, T., H. Kawase, and S. i. Matsushima (2001), Difference Between Site Characteristics Obtained From Microtremors, S-waves, P-Waves, and Codas, Bulletin of the Seismological Society of America, 91(2), 313-334.

Sawada, S. (1998), Phase characteristics on the site amplification of layered ground with irregular interface, The Effects of Surface geology on Seismic Motion,Irikura K.,,KudoK &Sasatani .T., (eds), 1009-1014.

Schlupp, A. (1996), Neotectonic of western Mongolia using field, seismological and remote sensing data. , Université Louis Pasteur de Strasbourg, Strasbourg.

Semblat, J. F., M. Kham, E. Parara, P. Y. Bard, K.Pitilakis, K.Makra, and D.Raptakis, (2005), Seismic wave amplification: Basin geometry vs. soil layering, Soil Dynamics and Earthquake Engineering, 25, 529-538.

SESAME (2004), Guidelines For The Implementation Of The H/V Spectral Ratio Technique On Ambient Vibrations Measurements, Processing And Interpretation, 62 pp.

Singh, S. K., E. Mena, and R. Castro (1988), Some Aspect of Source Characteristic of the 19 September 1985 Michoacán earthquake and ground motion amplification in and near Mexico city from strong motion data, Bulletin of the Seismological Society of America, 78(2), 451-477.

SteidlJ.H , A. G.Tumarkin, and R. J. Archuleta (Devember, 1996), What is a Reference Site?, Bulletin of the Seismological Society of America, 86(6), 1733-1748.

Tapponnier, P., and P. Molnar (1979), Active faulting and Cenozoic tectonics of the Tien Shan, Mongolia and Baykal regions, Journal of Geophysical Research, 84(B7), 3425-3459.

Tokimatsu, K. (1997), Geotechnical site characterization using surface waves Earthquake Geotechnical Engineering, Ishihara (ed.) 1997 Balkema, Rotterdam, 1333-1368.

Trifunac, M. D., and A. G. Brady (1975), A study on the duration of strong earthquake ground motion Bulletin of the Seismological Society of America, 65, 581-626.

Wathelet, M. (2005), Array recordings of ambient vibrations: surface-wave inversion. Liège University (Belgium), Ph.D. thesis, 177.

Wathelet, M., D. Jongmans, M. Ohrnberger, and S. Bonefoy-Claudet (2008), Array performances for ambient vibrations on a shallow structure and consequences over Vs inversion, Journal of Seismology, 12, 1-19.

Yamanaka, H. (1998), Geophysical explorations of sedimentary structures and their characterization, in The effects of surface geology on seismic motion, edited by K. Irikura, et al., pp. 15-33, Rotterdam, Balkema.

Yamanaka, H. (2003), Effect of Surface geology on seismic motion, , IISEE lecture note, 1,2.

Résumé

Les principales failles actives près de la capitale de la Mongolie, Ulaanbaatar avec environ 1.2 M d'habitants, sont à moins de 20 km et pourraient produire des séismes avec des magnitudes jusqu'à 7.5. La ville est construite sur un bassin sédimentaire, d'une épaisseur jusqu'à 100 mètres, qui peut générer des effets de site. Pour quantifier leur impact sur l'amplitude et la durée du mouvement du sol, selon la fréquence, j'utilise des mesures de mouvements faibles, à 32sites, et de bruit de fond, à 104 sites. Pour cela, j'ai appliqué les rapports spectraux « horizontal sur vertical » (HV) et « site sédimentaire sur rocher » (SSR). L'analyse de la fiabilité des résultats montre que l'amplitude du rapport HV varie en fonction du niveau du bruit de fond et que lorsqu'on est en présence d'une source de bruit particulière la fréquence amplifiée se polarise perpendiculairement à la direction de cette source.

Une structure de vitesse du bassin, évaluée à partir de 3 mesures en réseaux, et un modèle numérique 3D du bassin m'ont permis de produire des simulations 1D et 2D. La fréquence amplifiée (HV) est bien expliquée par la simulation 1D mais la forme du pic (SSR) se corrèle mieux avec la simulation 2D.

L'extension de la durée de signal induite par le bassin a été étudiée à partir de méthodes basées sur l'Intensité d'Arias et l'analyse fréquence-temps. A certains sites du basin, la durée augmente entre 20 et 160%. L'augmentation principale de la durée du mouvement du sol est due à l'amplification 1D, une partie étant à relier à des effets 2D à 3D. Nous avons cependant besoin de mouvements plus forts pour observer et étudier des effets 2D ou 3D.

Finalement, je propose une carte de la fréquence amplifiée qui est essentielle pour l'évaluation de l'aléa sismique d'Ulaanbaatar.